論文 / 著書情報
Article / Book Information

題目(和文)	
Title(English)	1.5--1.6 μm Wavelength GaInAsP/InP Injection Lasers
著者(和文)	荒井滋久
Author(English)	SHIGEHISA ARAI
出典(和文)	学位:工学博士, 学位授与機関:東京工業大学, 報告番号:甲第1370号, 授与年月日:1982年3月26日, 学位の種別:課程博士, 審査員:
Citation(English)	Degree:Doctor of Engineering, Conferring organization: , Report number:甲第1370号, Conferred date:1982/3/26, Degree Type:Course doctor, Examiner:
学位種別(和文)	博士論文
Type(English)	Doctoral Thesis

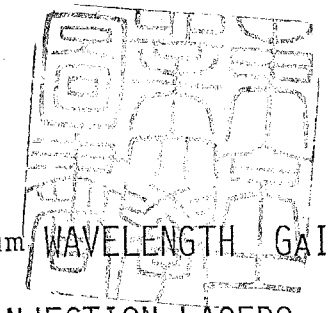

1.5--1.6 μm WAVELENGTH GaInAsP/InP INJECTION LASERS

Directed by
Professor YASUHARU SUEMATSU

Presented by
SHIGEHISA ARAI
Department of Electronics,
Doctoral course in
Graduate school of Science
and Engineering,
Tokyo Institute of Technology

CONTENTS

ABSTRACT

This thesis deals with 1.5-1.6μm wavelength GaInAsP/InP semiconductor lasers as light sources for the long distance optical fiber communication. For this purpose, the light source should operate in 1.5-1.6μm wavelength region with a narrow spectral width under high speed modulation.

A new structure GaInAsP/InP double heterostructure (DH) laser by the use of an additional anti-melt-back (AMB) layer is proposed to overcome the meltback problem which has been often experienced in a liquid phase epitaxial growth of GaInAsP/InP DH wafers with the emitting wavelength of 1.5-1.6μm.

In order to realize a low threshold current density GaInAsP/InP lasers with the AMB layer, the affects of the AMB layer on the threshold current density were evaluated for the new structure lasers and the conditions of the AMB layer are given.

Crystal growth conditions for the lattice-matched GaInAsP on (100) InP substrate are given for the wavelength range of 1.1-1.65μm by a two-phase solution technique. On the basis of this study, GaInAsP/InP lasers in such a wide wavelength region have been realized. Especially in the wavelength of longer than 1.5μm, a new structure GaInAsP/InP DH laser with the AMB layer has been realized and room temperature continuous wave (CW) operation has been achieved.

A buried heterostructure (BH) GaInAsP/InP DH laser emitting 1.6μm has been demonstrated by the use of a new

fabrication process. Its low threshold current room temperature CW operation has been achieved.

A GaInAsP/InP buried heterostructure distributed Bragg reflector integrated twin guide (BH-DBR-ITG) laser has been fabricated for the purpose of obtaining stable single mode operation under high speed direct modulation at 1.5-1.6μm wavelength. Low threshold current and a narrow spectral width operations under high speed direct modulation have been achieved.

Temperature dependence of the lasing wavelength of a DBR laser is calculated theoretically and the direction towards the improvement is suggested.

To summarize this study, the superiority of the 1.5-1.6μm wavelength GaInAsP/InP BH-DBR laser as a light source for the practical long distance optical fiber communication has been given.

CHAPTER 1 INTRODUCTION

Progresses of science and technology have created huge amounts of knowledge and things in this century such as an airplane, an atomic power, a transistor, a laser, etc. And these new things changed the circumstance of human beings, for example, airplanes carried us to very far place even to the behind of the earth in a day and gave us so many beautiful sceneries and new experiences which enlarged our world of mind. Invention of the transistor was one of the most important events in this century. Because of it, many new electronic products were made and our life style was affected by it and following inventions. These inventions made our life rich, and at the same time, demands for fast informations become larger as can be seen in the popularization of telephone, television set, and computers. This tendency will continue hereafter and communication technique should be improved extensively.

1.1 Optical fiber communication and the light sources

In earlier times, communication was done by use of visual or sound signal code because the propagation velocity of the light and the sound was very large. However, the transmission capacity of these communications was very small due to a poor response time of the man who took a role of a transmitter and a receiver. Then electric and electronic devices took place of the man, and the capacity of transmission line has been utilized effectively. Nowadays, a new communication technique using an optical fiber as a transmission line has grown up

because of several excellent features of it, such as a low transmission loss, a wide transmission bandwidth, a light weight, a wealth of material, no affection by an electromagnetic induction. Simultaneously, great efforts have been poured into the research of the transmitter and the receiver, mainly in semiconductor devices because of superiorities of compact size, high efficiency, and possibilities of an easy combination with an electric circuit and of a highly densed integration. A combination of these optical fibers and the semiconductor devices will give the highest capacity communication system with the lowest transmission loss.

(1) Appearance of ultra low-loss optical fiber

The origin of optical fiber communication was in the suggestion by Kao and Hockhem in 1966[1]. However, the transmission loss of an optical fiber was too large for the practical use, great efforts had been paid to reduce it and resulted in realization of an ultimately low-loss optical fiber with the transmission loss of 0.2dB/Km at the wavelength of 1.5-1.6μm [20]. The history of transmission loss of the optical fiber has been leading the study of the optical fiber communication system such as a semiconductor laser diode(LD) and a light emitting diode(LED) as a light source, and a photodiode(PD) and an Avalanche photodiode(APD) as an optical receiver. The remarkable point in the history was that the loss of the optical fiber was clarified to be caused by an absorption of remaining OH radicals and that the lower transmission loss would be obtained in a longer wavelength region

after the reduction of OH content untill the infra-red fundamental absorption loss begins to dominate. This was predicted by Keck, Maurer, and Schultz in 1973 [4] after some experimental results reported before by Kapron, Keck, and Maurer [2], Keck, Schultz, and Zimar [3], and by Cohen, Kaiser, MacChesney, O'Connor, and Presby [5]. According to this prediction, a new technique for the preparation of optical fiber called the modified chemical vapor deposition(MCVD) was introduced and resulted in realization of the loss of 2dB/Km at the wavelength of 1.05μm in 1974 by MacChesney, O'Connor, and Simpson [6][7]. Remarkable loss reduction was achieved at the wavelength of 1.2μm with the loss of 0.5dB/Km in 1976 by Horiguchi and Osanai [8]. This event was a real trigger for opening the study of long distance optical fiber communication system in the meaning of that semiconductor materials for the light source and the light detectors had been studied to match to the loss minimum wavelength region of 1.2-1.3μm. Efforts to reduce the loss of a fiber had been continued to study the effect of doped materials in silica [9] and reduction of OH content of a fiber [10]. As a result, an ultimately low-loss of 0.2dB/Km at the wavelength of 1.55μm was achieved with a single-mode fiber in 1979 by Miya, Terunuma, Hosaka, and Miyashita [20]. This event encouraged us to study the longer wavelength light sources and light detectors which operated with the wavelength around 1.5-1.6μm. The history of reduction of a optical fiber loss is shown in Fig.1-1. On the other hand, a new fabrication technique of an optical fiber called vertical axis deposition(VAD) method had been studied and considerable

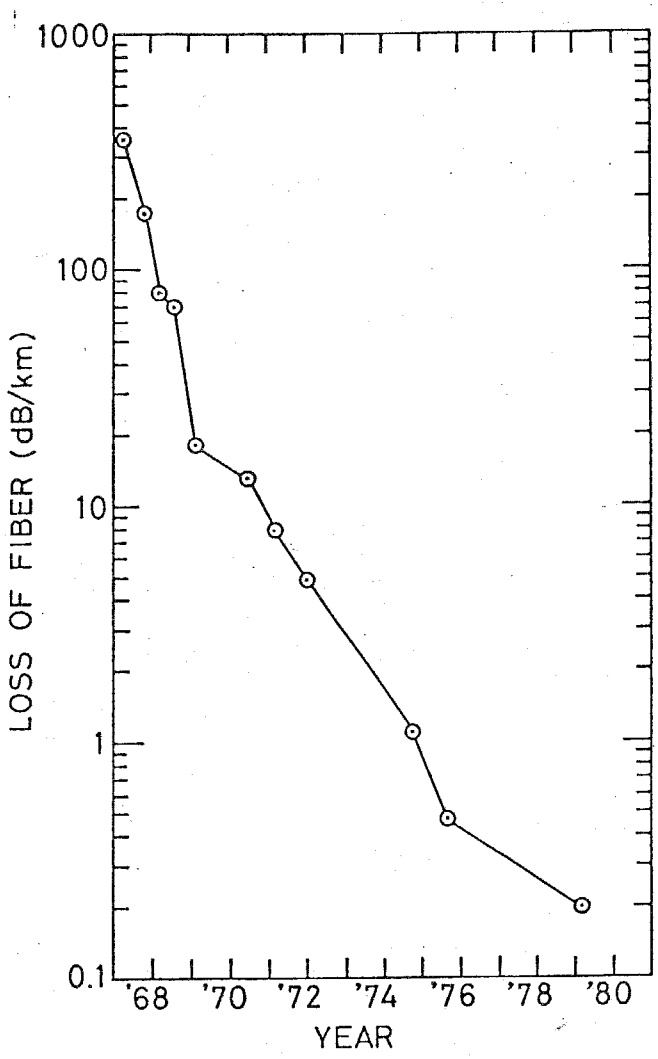

Fig.1-1 Historical change of the transmission loss of a optical fiber.

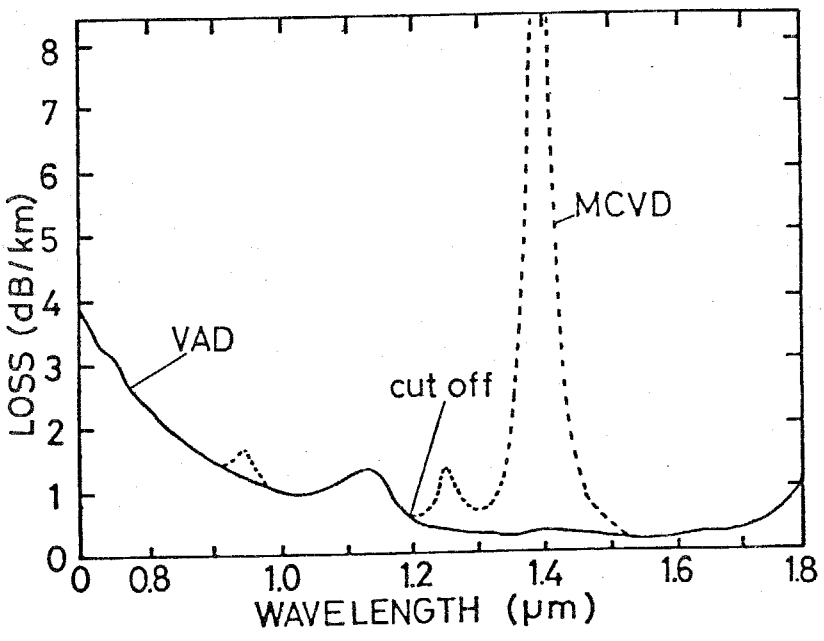

Fig.1-2
The transmission loss characteristics of optical fibers fabricated by MCVD method and by VAD method, after ref.[22].

elimination of OH was achieved by an introduction of gas of $GeCl_4$ during SiO_2 soot forming [11]-[13]. Comparison of the transmission loss property as a function of the transmission wavelength is shown in Fig.1-2. This VAD method was very effective from the view points not only of OH elimination but also of a continuous fabrication of 100Km long fiber with a total loss of 30dB and of a wide band multi-mode fiber because the central dip of refractive index profile in the core was eliminated. However, the product of transmission bandwidth and transmission distance of a multi-mode fiber is limited to very small by a modal dispersion [14] compared with a single-mode fiber [15], only less than 7GHzKm had been obtained although the VAD method was used [16]-[18]. Therefore a long distance optical fiber communication should be achieved by use of a single-mode fiber and a multi-mode fiber would be used for a relatively short distance communication systems such like a linkage between central processing unit and the terminal unit of a computer, and for a relatively small transmission bandwidth communication systems such like a local telephone line and a cable television (CATV) system. In these cases, there is no significant limitation to the light source specification, lasers and LEDs of both AlGaAs/GaAs and GaInAsP/InP materials can be available for them.

(2) Long distance optical fiber communication

For long distance optical fiber communication, problems on an optical fiber are mainly limited to a low transmission loss of a single-mode fiber and a material dispersion

characteristic of it. Reduction of transmission loss was performed as the same manner with a multi-mode fiber [8] and the first announcement was made in 1977 by Kawachi, Kawana, and Miyashita at the minimum loss wavelength of 1.27μm. After the apperance of the ultimately low-loss single-mode fiber at the wavelength of 1.55μm [20][21], complete elimination of fiber loss peak at the wavelength around 1.4μm was achieved by VAD method [11] and the residual OH absorption loss of 0.1dB/Km at the wavelength of 1.39μm was obtained in 1981 by Tomaru, Yasu, Kawachi, and Edahiro [22]. From the viewpoint of a fiber loss, a bending loss and a splicing loss should be involved to be discussed. Bending loss of optical fiber was calculated theoretically for both multi-mode fibers and single-mode fibers and concluded that it was not significant when the curvature of the bend was larger than several cm [36]-[39]. The splicing loss influences severely on the total transmission loss of fibers especially at the low-loss wavelength region. Fusion splice was used for single-mode fibers [40], and fairly well splice loss value of 0.1dB per splice was obtained at the wavelength of 1.3μm in 1981 by Toda, Watanabe, Ogai, and Seikai [41]. These losses limit the ultimate transmission distance, in other words the repeater spacing, in cooperation with the performance of the light detectors. However, the dispersion problem of the optical fiber is severer than those losses because not only the repeater spacing but also the transmission bandwidth are limited by it.

The dispersion of group delay in the optical fiber τ consists of the modal dispersion τ_m due to the delay time

among the propagating modes, the material dispersion τ_n due to the difference of refractive index with the wavelength, and the structural dispersion τ_v due to the effects of geometrical structure to the group delay time. The transmission bandwidth B of the optical fiber is given by

$$B=1/\tau \tag{1-1}$$

where $$\tau=\{\tau_m^2+(\tau_n+\tau_v)^2\}^{1/2} \tag{1-2}$$

For single-mode fibers, the modal dispersion τ_m is very small because the propagating modes are only two which are polarized perpendicular to each other. Thus τ_m is normally neglected except at the zero-dispersion wavelength [24]. Then eq.(1-2) could be rewritten to

$$\tau=\tau_n+\tau_v \ . \tag{1-3}$$

In the wavelength region around 1.3μm, the signs of τ_n and τ_v of a typical silica single-mode fiber are opposite, then three dispersions cancel out which results in zero dispersion. Figure 1-3 shows an example of measured dispersions as a function of the wavelength for Ge-doped single-mode fiber with the refractive index difference between the core and cladding of 0.2 percent and the cut-off wavelength of 1.1μm [25]. The wavelength dependence of τ_n and τ_v can be controlled by changing the refractive index difference and the geometrical structure. Several research groups tried to get the zero-dispersion wavelength at around 1.55μm region in order to get an ultimately low-loss property together with an ultra wide bandwidth property [26]-[34]. However, it resulted in not only a shift of the zero-dispersion wavelength but also the increase of the transmission loss due to the increase of impurity

concentration of GeO_2 which was used to change the refractive index of the core.[35]. The transmission loss characteristics is shown in Fig.1-4 with a parameter of the refractive index difference between the core and the cladding.[23]. Therefore the optical fiber communication system using single-mode fibers can be divided to two kinds of systems. One is relatively long distance transmission system using laser diodes as light sources at the wavelength of 1.3μm(at around the zero-dispersion wavelength), and the other is ultra long distance transmission system using special laser diodes as light sources at the wavelength of 1.5-1.6μm(at the minimum transmission loss wavelength). For these long distance optical fiber communication systems, only one kind of a single-mode fiber is preferable from the aspects of a mass production, an installation, and a maintenance.

From above mentioned points, the light sources for the ultra long distance transmission system are required to have a narrow spectral width property even in high frequency direct modulation. The dispersion τ is given by eq.(1-4) using the chromatic dispersion $\bar{\tau}$ of the single-mode fiber per unit spectral width of the light source $\Delta\lambda_s$ per unit distance L,

$$\tau=\bar{\tau}\Delta\lambda_s L \qquad (1-4)$$

When the spectral width of the light source under the modulation $\Delta\lambda_s$ is larger than that of the corresponding modulation bandwidth of $\Delta\lambda_{mod}=2B\lambda^2/c$, the transmission bandwidth B is limited by $\Delta\lambda_s$ and rewritten as follows using eqs. (1-1) and (1-4),

$$B=1/(\bar{\tau}\Delta\lambda_s L) \qquad (1-5)$$

B is inversely proportional to the transmission distance L. When the spectral width of the light source under the modulation $\Delta\lambda_s$ is smaller than that of the corresponding bandwidth $\Delta\lambda_{mod}$, the transmission bandwidth B is limited by $\Delta\lambda_{mod}$ and given by,

$$B=1/(\bar{\tau}\Delta\lambda_{mod}L)=\{c/(2\lambda^2\bar{\tau}L)\}^{1/2} \qquad (1-6)$$

In this case, B is inversely proportional to the square root of the transmission distance and gives the theoretical limit of the transmission bandwidth of a single-mode fiber. The spectral width $\Delta\lambda_{mod}$ is 0.016nm for B=1GHz at the wavelength of 1.55μm. Usually semiconductor laser diodes are directly modulated with the frequency up to a few GHz, the spectral broadening due to the longitudinal lasing mode increase is observed for the Fabry-Perot type lasers composed by two facet mirrors [283]. The value of the spectral broadening of conventional Fabry-Perot typa lasers was measured to be approximately 10nm for GaInAsP/InP material at the wavelength of 1.6μm and 2nm for AlGaAs/GaAs material at the wavelength of 0.84μm [289]. Thus the bandwidth-distance product of a single-mode fiber transmission system using a conventional laser at the wavelength of 1.6μm is calculated to be BL=6.25GHzKm supposing the chromatic dispersion $\bar{\tau}$ to be 20psec/nm/Km. This value is almost comparable to that of a multi-mode fiber and the merit of a single-mode fiber is not available in this situation. Therefore a single longitudinal mode operation during the high frequency modulation is required to the light source for the long distance optical fiber communication system at the wavelength of 1.5-1.6μm. This is an essential point for the 1.5-1.6μm

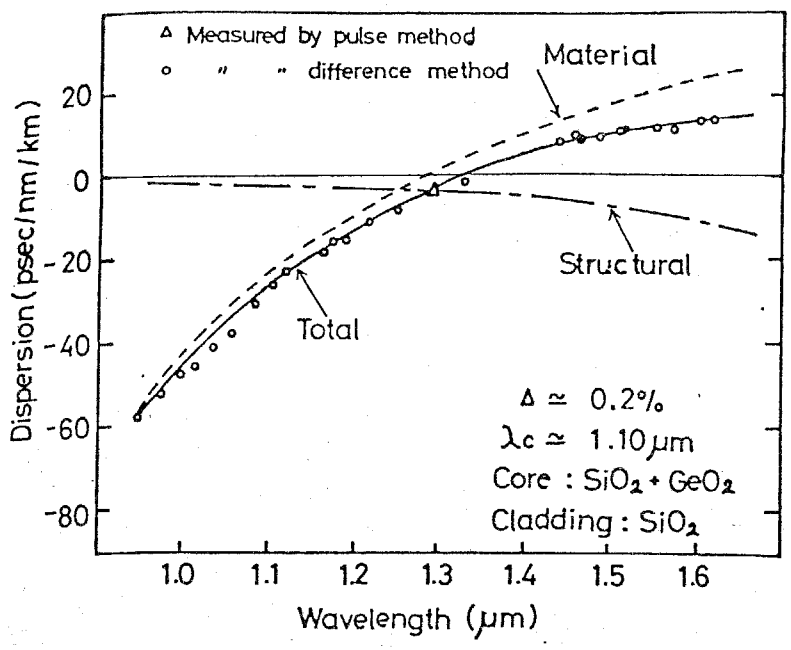

Fig.1-3

Dispersions of a typical single-mode fiber with the refractive index difference of 0.2% and the cut-off wavelength of 1.1μm, after ref.[25]. Measurements were made for the pulse delay method and the difference method.

Fig.1-4 Calculated transmission loss characteristics of a silica single-mode fiber doped with GeO_2, after ref.[23]. The refractive index difference Δ increases with the content of GeO_2. The main mechanism of the loss are the Rayleigh scattering and the fundamental absorption of silica.

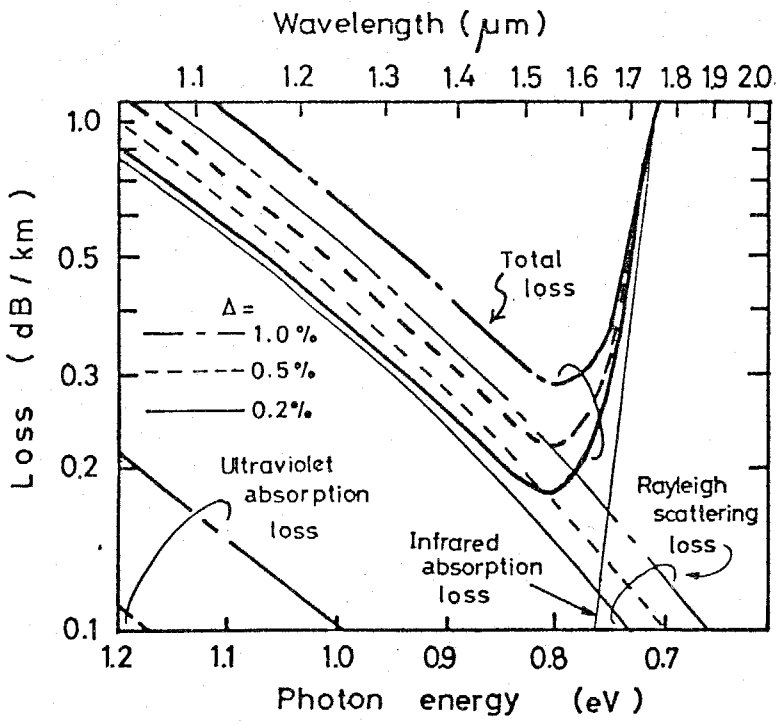

Calculated loss characteristics of GeO_2 doped single mode fibers

wavelength lasers and gives the background of this thesis.

When the light source for the ultra long distance optical fiber communication satisfying above mentioned conditions was realized, the transmission distance would be actually dominated by a performance of a light detector, namely the signal noise ratio(SNR). The SNR of a PIN photodiode is given by,

$$SNR(PIN)=\frac{\bar{I}_p^2}{2e(I_p+I_d)B+4kTB/Re} \qquad (1-7)$$

where $I_p=(e/h\nu)\eta_p P_{opt}$ (η_p:quantum efficiency, P_{opt}:incoming optical power) is the photocurrent, e is the electronic charge, B is the effective bandwidth of the optical channel, and Re is the equivalent input resistance of the amplifier.

In the case of an Avalanche photodiode(APD), an excess noise is generated by the avalanche multiplication process and given by [56]-[58],

$$F=M\{1-(1-k)(M-1)^2/M^2\} \qquad (1-8)$$

where M is the avalanche gain, k is the ionization coefficient ratio of holes to electrons, assuming $k=\beta/\alpha<1$. In case of $\beta/\alpha>1$, k is replaced by 1/k. Then the SNR of an APD is given by,

$$SNR(APD)=\frac{\bar{I}_p^2}{2eB(I_p+I_d)F+2eB\bar{I}_p/M^2+4kTB/(ReM^2)} \qquad (1-9)$$

From eqs.(1-8) and (1-9), smaller value of k leads to smaller excess noise F and to larger SNR of an APD. For both kinds of light detectors, the dark current is an essential factor to limit the SNR.

Previous works on the light detectors for the long distance optical communication were made intensively by using GaInAsP quaternary system materials [59]-[116], Ge material [117]-[123], AlGaAsSb quaternary system materials [124]-[129], and $Hg_{0.3}Cd_{0.7}Te$ [131]. Specific points of these detectors are summarized and listed in Table I. For the materials of Ge and $Ga_{0.47}In_{0.53}As$, the dark current is relatively high compared with that of Si due to the smaller bandgap and tunneling current [108]-[110]. The value k of these materials are very large compared with that of Si, thus the SNR can not be improved significantly in contrast with the well established Si APD in short wavelength system. However, some new technological improvements to obtain smaller value of k were recently suggested and reported. One is the discovery of a resonant impact ionization effectzdue to impact ionization initiated by holes from the split-off valence band, and the value k of more than 20 was obtained in 1981 by Hildebrand, Kuebart, Benz, and Pilkuhn [128]. This effect was measured on GaAlSb APDs and would be applied to the material which has the same bandgap energy as the spin orbit splitting energy. The other was the invention of a new structure APD with the graded bandgap reported in 1981 by Cappaso, Tsang, and Hutchinson [130]. Assuming that p-type side has a wider bandgap, the ionization of an electron is accelerated due to the reduction of apparent barrier height, at the same time the ionization of a hole is suppressed due to the increase of it. Therefore a large value k of 10 was obtained for AlGaAs APDs fabricated by a molecular beam epitaxy. This method is considered to be applicable to

Table I. Quaternary materials lattice matched to substrates and related optical materials for the light detector application.

Material	$Ga_xIn_{1-x}As_yP_{1-y}$ /Inp	$Ga_{.47}In_{.53}As$ /InP	$Ga_{.27}In_{.73}As_{.40}P_{.60}$ /InP	$Hg_{0.3}Cd_{0.7}Te$	$Al_xGa_{1-x}As_ySb_{1-y}$ /GaSb	Ge	Si
Energy gap E_g (eV)	1.35-0.75	0.75	0.95	0.92	1.24-0.73	0.72	1.1
Energy gap Wavelength λ (μm)	0.92-1.67	1.67	1.30	1.35	1.0-1.7	1.72	1.1
Mobility μ (cm^2/Vs) e h	3200-8500 70- 180	8500 180	5000 80			3900 1900	1300 500
Effective mass m_e^*/m_o	0.08-0.04 (λ=0.92-1.67μm)	0.034-0.041	0.045-0.055			0.08	0.19
Dark current I_d (nA) [area:$4\times10^3\mu m^2$]	10^{-2}-$_a\times10^{-1}$	10^{-1}	10^{-2}	60	10^2	10	10^{-4}
Ionization rate k (β/α or α/β)	0.2-0.3	0.25	0.25	$\beta>\alpha$ 0.03	$\beta>\alpha$ 0.05-0.5	$\beta>\alpha$ 0.5	0.02
Absolute Sensitivity (A/W)	0.6-0.8	0.8	0.6	0.6	(0.6)	0.85	
Melting point of Substrate (°C)	1070				712	958	1412
Hardness of Substrate (Knoop)	535				450		1150
Reference	[59]-[116]			[131]	[124]-[129]	[117]-[123]	[132]

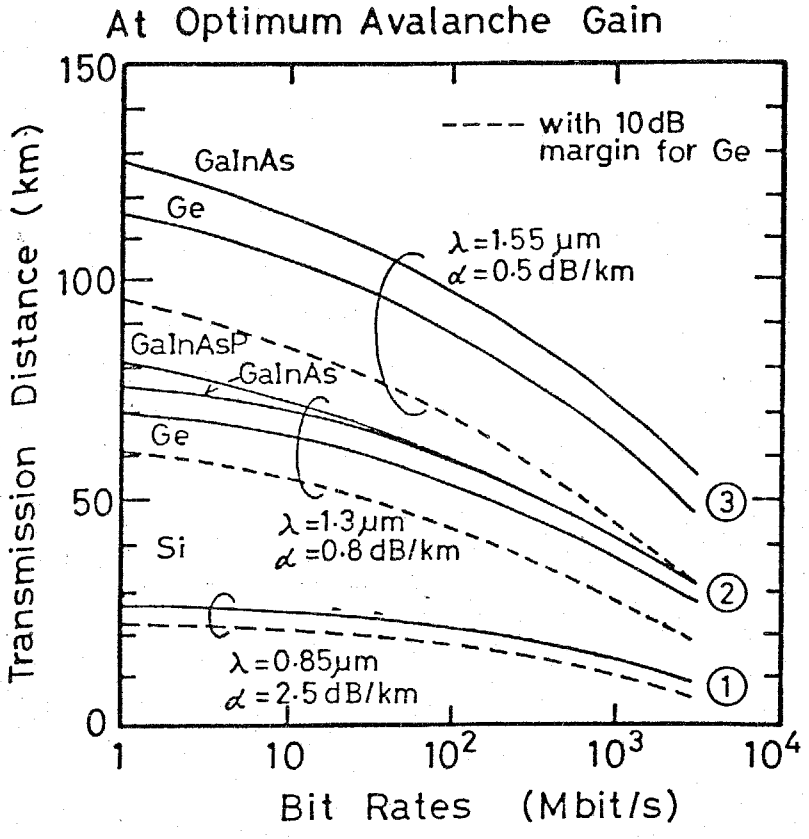

Fig.1-5 Transmission distance without a repeater as a function of bit rates for different detectors set at the optimum avalanche gains, after refs.[132][133].

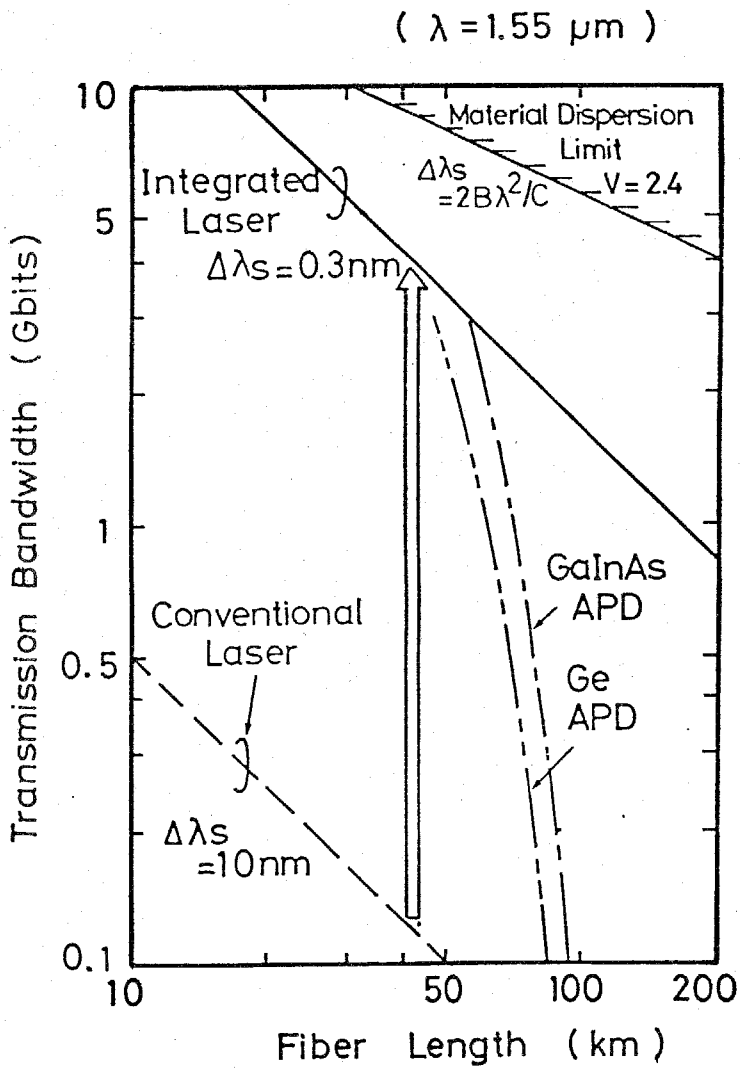

Fig.1-6 The transmission bandwidth B as a function of the transmission distance L, drawn with a parameter of the spectral width $\Delta\lambda_s$ of the light source for solid lines and from the detector performance in Fig.1-5 for the dashed line.

other materials and the possibility of the low noise APDs for 1.5-1.6μm wavelength region remains still now.

Figure 1-5 shows the transmission distance without a repeater as a function of bit rates for different detectors set at the optimum avalanche gain [132][133]. Broken lines correspond to Ge APD with the system margin of 10dB. The transmission loss is assumed to be α=2.5dB/Km for the wavelength of λ=1.3μm, and α=0.5dB/Km for λ=1.55μm. The input power of -6dBm is assumed. From this figure, the transmission distance without a repeater of 72Km is obtained for the wavelength of 1.55μm and the modulation bit rates of 1Gbit/sec. Then the transmission bandwidth-the transmission distance product of 72GHzKm is approximately enough at present for the single-mode optical fiber communication. It corresponds to the spectral width of the light source of $\Delta\lambda_s$=0.69nm. Figure 1-6 shows the transmission bandwidth B as a function of the transmission distance L. Solid lines were drawn from eqs.(1-5) and (1-6) with a parameter of the spectral width $\Delta\lambda_s$ of the light source, the broken lines were drawn from the aspect of the detector performance. The spectral width of the light source of 0.3nm should be required for the present single-mode optical fiber communications.

In a future single-mode optical fiber system such as a heterodyne detection system or a wavelength division multiplexing system, the requirements for the light source and the optical fiber will be severer. As for the single-mode optical fiber, polarization control of the light output from it is

very severe. To overcome this problem, two kinds of approaches have been done till now. One is a polarization control system using electro-magnetic and electro-optical devices [42]-[45]. The other one is a development of a single polarization optical fiber [46]-[55]. The transmission loss of 0.62dB/Km at the wavelength of 1.52μm was obtained for this fiber with asymmetrical strain bireferingence in 1981 by Hosaka, Okamoto, Miya, Sasaki, and Edahiro [54]. These fibers are preferable to be used for the high capacity optical communication system with not so long distance because it has relatively high transmission loss. In this case, the required spectral width of the light source will be mainly dominated by the density of a wavelength division multiplexing, the limit of the density of the ultimate wavelength division multiplexing system is given by the corresponding modulation bandwidth $\Delta\lambda_{mod}$. Therefore the great efforts for the narrower spectral width should be paid to realize the future ultra high capacity optical fiber communication.

1.2 1μm wavelength region semiconductor lasers

Developments of the light sources for the optical fiber communication have been achieved in accordance with the loss reduction of the optical fiber. Semiconductor lasers were considered to be the most suitable as the light sources for that purpose from their merits of (1) small size, (2) ease of pumping by current injection, (3) high efficiency, (4) capability of high frequency direct modulation, (5) long life, and (6) possibility of integration with other electronic devices

monolithically. The LEDs were considered to be also applicable for the short distance optical fiber communications with a relatively low transmission bandwidth due to a poor efficiency, a narrow modulation bandwidth, and a very wide spectral width compared with those of the semiconductor lasers.

The first reports on semiconductor lasers were done with GaAs homojunction structure by Hall, Fenner, Kingsley, Soltys, and Carlson of GE [134], Nathan, Dumke, Burns, Dill, and Lasher of IBM [135], and Quist, Keyes, Krag, Lax, McWhorter, Rediker, and Zeiger of MIT [136], at the nearly same time in 1962. However, these laser diodes were operated only at the liquid nitrogen temperature because of no confinement structure for injected carriers and the light wave. To reduce the threshold current for higher temperature operation, double hetero-junction structure injection laser was proposed by Kroemer in 1963 [137]. But his idea was not carried out soon since his idea lacked in a selection of the materials and the crystal growth technique. Remarkable suggestion to get the hetero-junction structure laser was a concept of a lattice matching between two different bandgap semiconductor crystals, that was reported by Rupprecht, Woodall, and Pettit in 1967 [138]. They reported about $Ga_{1-x}Al_xAs$ LEDs at room temperature grown by liquid phase epitaxy and clarified that the lattice constant of $Ga_{1-x}Al_xAs$ was almost the same as that of GaAs as a substrate, and got a stimulated emission from GaAlAs diode soon in 1967 [139]. After that, the reduction of the threshold current was achieved by demonstrating Kroemer's idea with the introduction of liquid phase epitaxial growth technique for GaAlAs crystal,

and resulted in the room temperature continuous wave(CW) operation in 1970 by Hayashi, Panish, Foy, and Sumski [140]. This event opened the first optical communication field for 0.8-0.9μm wavelength region in accordance with the reduction of the loss of an optical fiber down to 20dB/Km [2].

The semiconductor lasers of the longer wavelength more than 1μm had become required to suit the lower loss optical fibers as mentioned in section 1.1. In the early years of 1970s, 1μm wavelength operations of the lasers of $In_xGa_{1-x}As/In_yGa_{1-y}P$ on GaAs substrates were achieved by use of a vapor phase epitaxial growth technique [144]-[148], and of $GaAs_{1-x}Sb_x/Al_yGa_{1-y}As_{1-x}Sb_x$ on GaAs substrates by a liquid phase epitaxial technique [151]-[155]. However, the CW operation of these lasers were obtained in 1976 [147][152], at this time the CW operation of $Ga_yIn_{1-y}As_xP_{1-x}$/InP quaternary system laser was achieved by Hsieh, Rossi, and Donnelly [164], and the remarkable loss reduction of the optical fiber was achieved in the wavelength of 1.3μm by Horiguchi and Osanai [8].

In the beginning of this work in 1977, we faced the problem on the selection of a material which should be the best for the low-loss optical fiber communications. After considerations that the laser material could be grown lattice matched to the substrate and the corresponding wavelength should be more than 1.3μm (since the minimum loss wavelength of the optical fiber was estimated to be shifted to the longer side with the continuous efforts for the reduction of OH content in it), only two candidates were picked up among the III-V semiconduc-

tor compounds. Figure 1-7 shows the variation of the bandgap and the lattice constant with composition for various III-V semiconductor compounds given by Sasaki, Nishiuma, and Takeda [143]. The solid lines and dashed lines indicate the bandgap for a direct transition and an indirect transition regions, respectively. From this figure, several groups of III-V semiconductor compounds lattice matched to the substrates were picked up and summarized in Fig.1-8 with their corresponding wavelength and the basic parameters of the binary compound substrates. The candidates for the low-loss optical fiber communication seemed to be GaInAsP quaternary material on InP substrate and AlGaAsSb quaternary material on GaSb substrate. Then the GaInAsP/InP system was chosen from the following merits in comparison with the AlGaAsSb/GaSb system.

[1] Free from the formation of tenancious oxides by an introduction of Al, which leads to reliable and easier crystal growth by a liquid phase epitaxy.

[2] The substrate InP has a wider bandgap than that of the GaInAsP crystal, so that cladding layers for an optical and an injected carrier confinements can be formed by InP, which leads to easier crystal growth of a double heterostructure. Figure 1-9 shows the lattice constant and the bandgap of III-V semiconductor compounds by the elements of (Ga, In, Al)(As, P, Sb) [141].

[3] The hardness of the substrate InP is larger than that of GaSb, which is preferable for practical use.

[4] The melting point of the substrate InP is higher than that of GaSb, which might lead to relatively larger

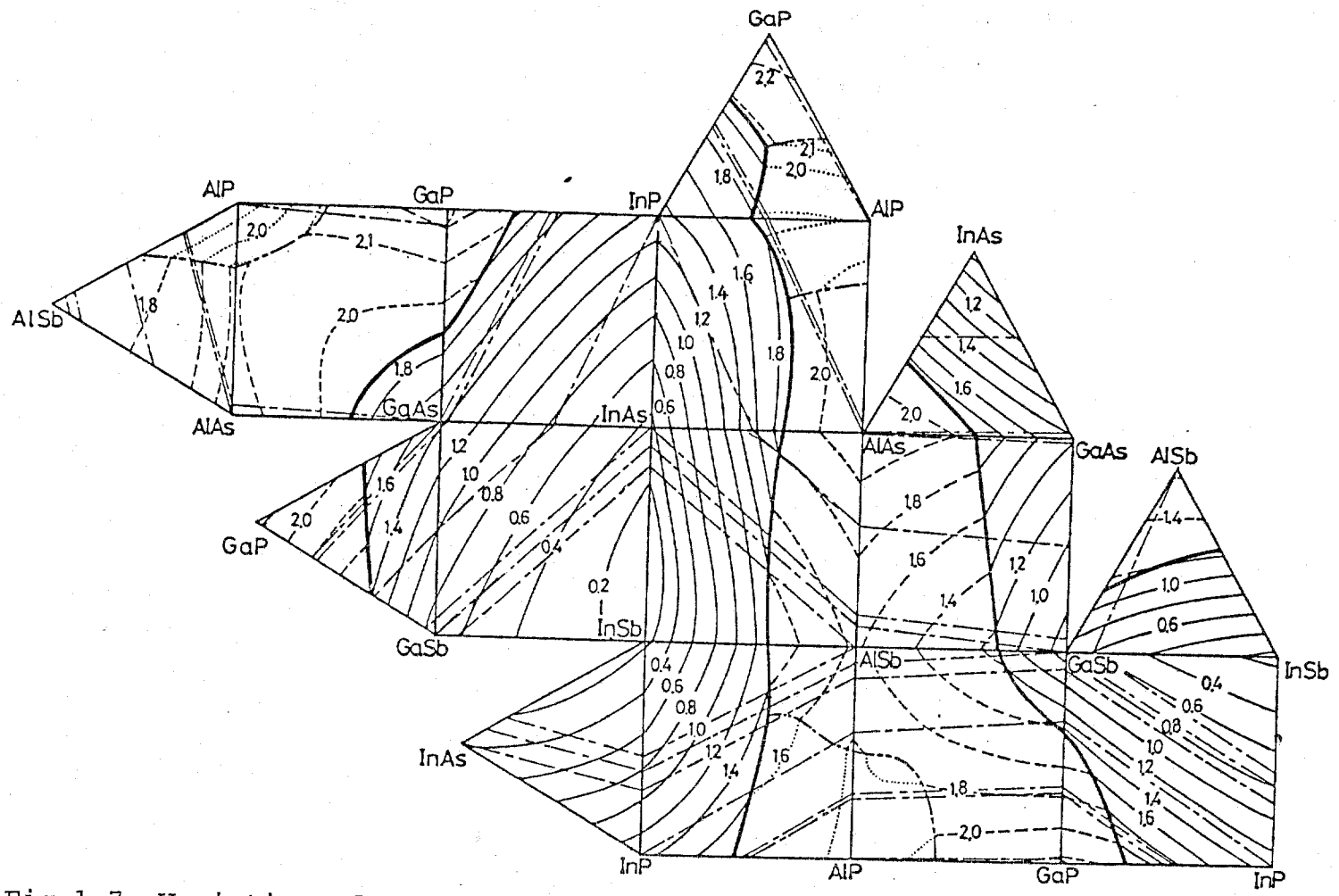

Fig.1-7 Variation of the bandgap and the lattice constant with the composition for various III-V semiconductor compounds. Solid lines and dashed lines indicate a direct transition and an indirect transition regions.

Long Wavelength Materials

Active Material	Substrate Mater.	Melt.P. (°c)	Hardness (Knoop)
GaInAsP	InP	1070	535
	GaAs	1238	750
GaInSbP	InP	1070	535
	GaSb	712	450
GaInAsSb	InAs	943	381
	GaSb	712	450
AlGaAsSb	GaSb	712	450
InAsSbP	InAs	943	381
AlGaAs	GaAs	1238	750

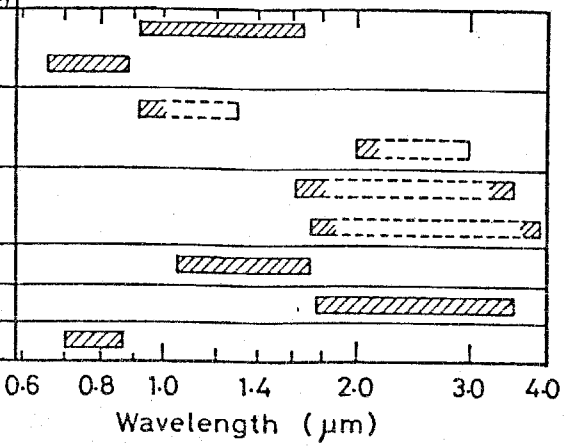

Fig.1-8 III-V semiconductor compounds materials lattice matched to the substrates and their available wavelength.

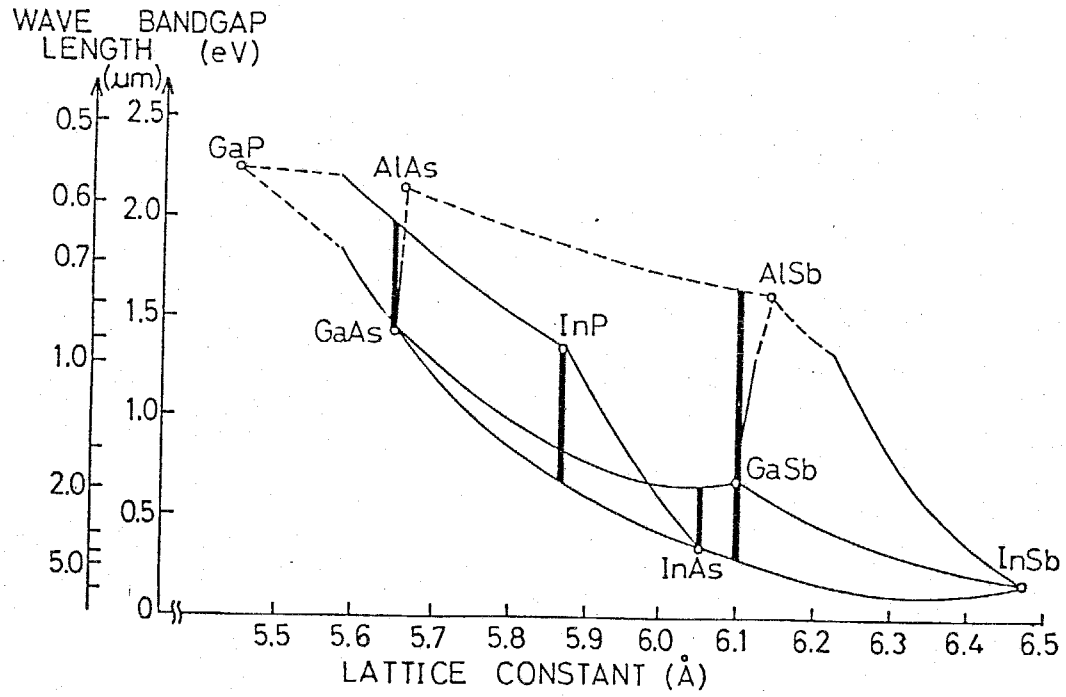

Fig.1-9 Lattice constant and the bandgap of III-V semiconductor compounds by (Ga,In,Al)(As,P,Sb) elements. Solid lines and dashed lines correspond to a direct and an indirect transition regions, respectively.

tolerance of the crystal growth temperature by a liquid phase epitaxy.

The current of that time was on GaInAsP quaternary system and we could not get any successful information about AlGaAsSb quaternary system. The successful reports of AlGaAsSb/GaSb double heterostructure lasers have been done recently with the operation wavelength of 1.5-1.8μm region [143][156][157]. Other material semiconductor lasers for the wavelength from 1 to several μm were investigated in these three years [158]-[161].

1.3 Progresses in research of GaInAsP/InP lasers

The appearance of GaInAsP quaternary semiconductor compound on an InP substrate has its origin in the theoretical study on the bandgap and the lattice constant of GaInAsP crystal, which was reported in 1974 by Moon, Antypas, and James [320]. They clarified the relation between the alloy composition and the bandgap or the lattice constant of GaInAsP crystal by use of Vegard's law, and suggested the capability of the long wavelength semiconductor laser for the optical fiber communication. The first achievement of GaInAsP/InP laser was reported in 1975 by Bogatov, Dolginov, Eliseev, Milvidskii, Sverdlov, and Shevchenko [162]. Success in the room temperature CW operation of this laser with the wavelength of 1.1μm was reported soon in 1976 by Hsieh, Rossi, and Donnelly [164]. After the big event in the optical fiber, the lasers with the operation wavelength of 1.3μm was aimed and achieved in 1977 by Yamamoto, Sakai, Akiba, and Suematsu [167]. The (100) oriented substrate

was used from this year, considering several advantages of (1) easy forming of a laser cavity by cleavage, (2) feasibility of a device fabrication on the analogy of AlGaAs/GaAs lasers which were fabricated with the (100) oriented substrate, and (3) relatively insensitive growth on misoriented surface. The success of GaInAsP laser on the (100) oriented substrate changed the trend of that on the (111)B oriented substrate and led out of following various kinds of stripe lasers.

After 1977, the number of reports about GaInAsP/InP lasers has been increasing year by year, because the life time of this laser was assumed to be fairly long from the earlier reports of the life time of more than 4000hour and 10000hour for the lasers grown by a vapor phase epitaxy and by a liquid phase epitaxy, respectively [181][191]. A lot of stripe structure lasers have been fabricated in order to get high reliability such as a stable transverse single mode operation and a low operation current, those by a buried heterostructure (BH), a mesa substrate buried heterostructure(MSB), a rib waveguide structure(RW), a self aligned structure(SA), a ridge waveguide structure(RidgeW), a buried crescent structure(BC), a planar convex waveguide structure(PCW), a terraced substrate structure(TS), a planar buried heterostructure(PBH), a current confined mesa substrate buried heterostructure(CCM), a separated multi-layer structure(SML), an embeded mesa stripe structure(EMS), a V-shape grooved substrate buried hetero-structure(VGSB), a shottky barrier defined structure, and a lens-like strip waveguide structure(LLSW).

The longer wavelength GaInAsP/InP lasers were investigated

from relatively early time before the appearance of the ultimately low-loss optical fiber [166][171][174][176][179][180]. The room temperature CW operation of 1.5-1.6μm wavelength laser was achieved for the first time in July of 1979 by use of an anti-melt-back layer structure by Akiba, Sakai, Matsushima, and Yamamoto [184]. Within a month after that, Kawaguchi, Takahei, Toyoshima, Nagai, and Iwane of NTT and we obtained the room temperature CW operations successively. The reduction of the threshold current under room temperature CW operation of the longer wavelength GaInAsP/InP laser was achieved in the beginning of 1980 together with a transverse single mode operation by introducing the buried heterostructure, by Nagai, Noguchi, Takahei, Toyoshima, and Iwane [208] and by us [212][215]. However, there still remained a big problem of the dynamic spectral width which means the spectral width under direct modulation. In conventional semiconductor lasers which have Fabry-perot type cavity and facet mirrors, the spectral broadening due to the mode hopping and mode competition was observed under high frequency direct modulation even for the lasers which had built-in index step for the transverse mode stabilization. Sakakibara, Furuya, Utaka, and Suematsu reported the single longitudinal mode operation under high-speed direct modulation in GaInAsP/InP distributed Bragg reflector integrated twin guide(DBR-ITG) laser with the operation wavelength of 1.3μm [287]. Therefore the operation wavelength of the DBR-ITG laser was shifted to 1.5-1.6μm region [216] and the effective DBR-ITG lasers with the buried heterostructure were obtained in 1981 by Utaka,

Kobayashi, and Suematsu [243]. However the threshold current of those BH-DBR-ITG lasers were so high compared with a conventional Fabry-Perot type laser, and the spectral property of them under high frequency direct modulation was not so well known. Much effort was required to improve them and resulted in the low threshold current operation and simultaneously the narrow dynamic spectral width of less than 0.3nm with the modulation frequency up to 3GHz, which is described in Chapter 6 of this thesis [259]. After that, such narrow dynamic spectral width and the room temperature CW operations were also achieved in GaInAsP/InP distributed feedback(DFB) lasers at nearly the same time in October of 1981 by NTT group and KDD group [261][262].

Other remarkable historical points in the progresses of GaInAsP/InP lasers were the developments of the crystal growth techniques, such as a vapor phase epitaxy(VPE) and a metal organic chemical vapor deposition(MO-CVD), and of etched mirror lasers. The VPE and MO-CVD techniques have several attractive merits compared with the LPE technique, such as (1) suitability for mass production because of their simple growth process and of the capability for a large size wafer growth, (2) fine control of a layer thickness because of the larger dynamic range in the growth speed, which enables us to grow an ultra thin film devices, namely a quantum well structure laser and a super lattice device. The room temperature CW operations of VPE grown GaInAsP/InP lasers were obtained with the wavelength of 1.25-1.65μm [181][207][215][217][218]. MO-CVD grown GaInAsP/InP laser was reported in

1980, for the first time, by Hirtz, Duchemin, Hirtz, DeCremoux, Pearsall, and Bonnet [213], and was also operated under the room temperature CW condition with the wavelength of 1.23μm in 1981 [250].

The etched mirror GaInAsP/InP laser was reported in 1980 by Iga and Miller [210], which aimed to make not only an very short cavity laser but also make a batch process of lasers on a wafer possible. The room temperature CW operation of this laser was achieved in 1980 by Iga and Miller with the wavelength of 1.3μm [225].

The history of researches of GaInAsP/InP lasers was summarized and listed in Table A in Appendix.

The lifetime of a GaInAsP/InP laser was estimated to be far longer than that of an AlGaAs/GaAs laser though the dislocation density of the substrate InP was much higher than that of GaAs [291][292], besides the limit power of the optical damage to the facets of the GaInAsP/InP laser was found to be several times greater than that of the AlGaAs/GaAs laser [290]. Therefore the reliability of the GaInAsP/InP laser could be better than any other laser at a present time and will be improved for the practical use. Only the problem of the GaInAsP/InP laser is a temperature dependence of the threshold current, which will be discussed later in Chapter 5.

The light emitting diodes(LED) were also investigated intensively for the short distance optical fiber communication with a low transmission bandwidth [263]-[282]. The extrapolated half lifetime in excess of 10^9hour was estimated at the ambient temperature of 60°C in 1981 by Yamakoshi, Abe, Wada, Kamiya,

and Sakurai [280], which led to the practical use for CATV and the local communication system, etc.

1.4 Purpose and contents of this thesis

This thesis gives investigations on the 1.5-1.6μm long wavelength GaInAsP/InP semiconductor lasers especially for the light source of ultimately low-loss optical fiber communications. Reliable 1.5-1.6μm wavelength GaInAsP/InP lasers were achieved by an introduction of newly proposed anti-melt-back layer. Narrow dynamic spectral width required for the long distance optical fiber communication was obtained with BH-DBR-ITG laser.

In this thesis, Chapter 1 devotes to the introduction with emphasis on the requirements of the light source for the long distance and high capacity optical fiber communication.

In Chapter 2, the basis of 1.5-1.6μm wavelength GaInAsP/InP lasers with an anti-melt-back layer is discussed. The temperature dependences of the threshold current and the lasing wavelength of DBR lasers are discussed to improve the DBR lasers.

In Chapter 3, the crystal growth conditions of lattice matched GaInAsP/InP lasers by the LPE technique are given experimentally for almost complete wavelength region of 1.1-1.65μm.

In Chapter 4, the lasing properties of GaInAsP/InP lasers for the various wavelength are given, such as threshold current density, temperature dependences of the threshold current and the lasing wavelength, and so on.

In Chapter 5, fabrication process and the lasing properties of buried heterostructure lasers of 1.6μm wavelength region are given. The temperature dependences of the threshold current and the differential quantum efficiency were measured and analized.

In Chapter 6, fabrication process and the lasing properties of buried heterostructure distributed Bragg reflector integrated twin guide(BH-DBR-ITG) lasers of 1.5-1.6μm wavelength region are given. Dynamic spectral width measurements under high frequency direct modulation up to 3GHz are given.

Chapter 7 is devoted to the conclusions.

CHAPTER 2 BASIS OF 1.5-1.6 μm WAVELENGTH GaInAsP/InP DOUBLE HETEROSTRUCTURE (DH) LASERS

2.1 Introduction

In the study of 1.5-1.6μm wavelength GaInAsP/InP lasers, a meltback of the active layer during the growth of InP cladding layer was the severest problem for a low threshold current density operation. A new structure with an additional "anti-melt-back (AMB)" layer was proposed and introduced for the first time to overcome it. Another problem of the 1.5-1.6 μm wavelength laser was to get a narrow spectral width under high speed direct modulation. It was overcome by an introduction of the distributed Bragg reflector(DBR) structure.

In this chapter, the threshold current density of the newly proposed GaInAsP/InP double heterostructure(DH) laser with the wavelength of 1.5-1.6μm is discussed from the viewpoint of the carrier confinement, the optical confinement, and the first order gain. The temperature dependences of the lasing wavelength and the threshold current density of a DBR laser is also calculated taking account of the refractive index variation due to injected carriers.

2.2 Carrier confinement

In the conventional GaInAsP/InP DH lasers with the wavelength less than 1.5μm, a symmetric three layer structure was used, where the GaInAsP active layer was sandwiched by both n and p type InP cladding layers as shown in Fig.2-1(a). However in the 1.5-1.6μm long wavelength GaInAsP/InP lasers,

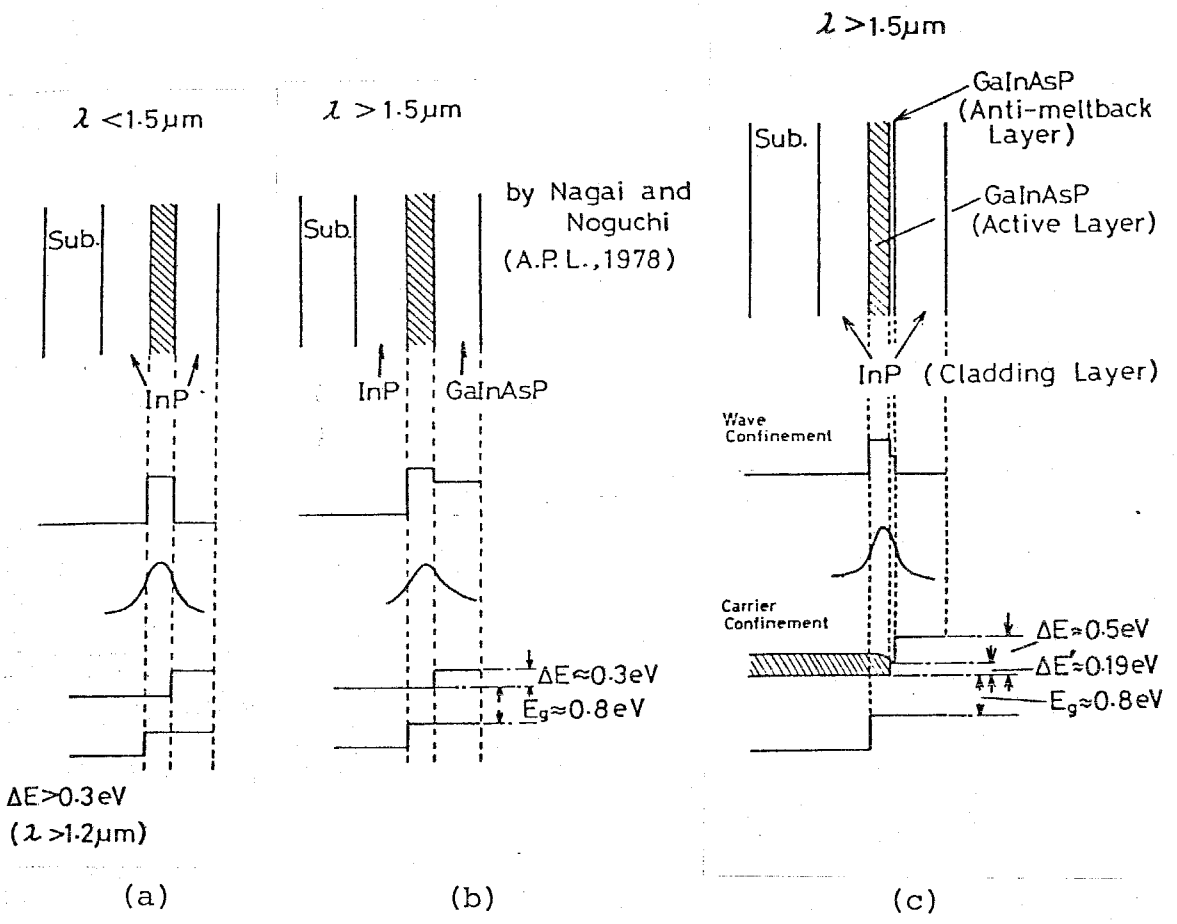

Fig.2-1 (a) Energy band diagram of the conventional three layer structure for $\lambda<1.5\mu m$.
(b) Energy band diagram of the asymmetric three layer structure for $\lambda>1.5\mu m$.
(c) Energy band diagram of the four layer structure for $\lambda>1.5\mu m$.

the active layer was easily melted back during the growth of p type InP cladding layer in the liquid phase epitaxial growth, GaInAsP of higher bandgap than the active layer was used as a cladding layer to overcome it at the sacrifice of a low threshold current density operation with a lack of the hetero-junction barrier as shown in Fig.2-1(b). Therefore a four layer structure GaInAsP laser was proposed to give an enough barrier height by InP cladding layer with inserting a GaInAsP thin layer (the bandgap is larger than that of the active layer) between the active layer and the cladding layer as shown in Fig.2-1(c). This GaInAsP layer was named "anti-melt-back(AMB)" layer.

The leakage current due to unconfined carriers is considered in this section according to the manner presented by Casey [339]. The carrier density injected to p type active layer N_c is expressed as,

$$N_c = \frac{(2m_c^* kT)^{3/2}}{2\pi^2\hbar^3} \int_0^\infty \frac{E^{1/2}\, dE}{1+\exp\{(E-E_{EC})/kT\}} \qquad (2\text{-}1)$$

where m_c^* is the effective mass of an electron, k and $\hbar=h/2\pi$ are the Boltzmann and Planck constants, T is the absolute temperature, E_{FC} and E are the quasi Fermi level of injected electrons and an energy level both from the bottom of the conduction band. The carrier density N_p which contributes to the leak across the p-p heterojunction is expressed as,

$$N_p = \frac{(2m_c^* kT)^{3/2}}{2\pi^2\hbar^3} \int_{\Delta E_c}^\infty \frac{E^{1/2}\, dE}{1+\exp\{(E-E_{FC})/kT\}} \qquad (2\text{-}2)$$

where ΔE_c is the effective barrier height as shown in Fig.2-2 and is given as follows,

$$\Delta E_c=\Delta E_g-\{(E_{FV}-E_{V2})-(E_{FV}-E_{V1})\} \qquad (2-3)$$

where ΔE_g is a bandgap difference between the active layer and the cladding layer, E_{FV} is the quasi Fermi level of holes, E_{V1} and E_{V2} are the top energy levels of the valence bands in the active and the cladding layers.

When the field is taken as zero and only the diffusion current is taken into account, the minority carrier density in p type cladding region $N_p(x)$ is given,

$$N_p(x)=C_1\exp(-x/L_n)+C_2\exp(x/L_n) \qquad (2-4)$$

where x is a position from the p-p heterojunction, L_n is a diffusion length of the electron. The arbitary constants are evaluated by the boundary conditions. At x=0, $N_p(0)$ should be N_p given by eq.(2-2). And it goes to zero at the ohmic contact located at a distance W away from x=0. Then, eq.(2-4) becomes,

$$N_p(x)=\frac{\exp\{(W-x)/L_n\}-\exp\{-(W-x)/L_n\}}{\exp(W/L_n)-\exp(-W/L_n)}N_p \ . \qquad (2-5)$$

The diffusion current density J_n is given by $-eD_n dN/dx$ at x=0,

$$J_n=\frac{eD_nN_p}{L_n\tanh(W/L_n)} \qquad (2-6)$$

where D_n is a diffusion coefficient of the electrons in p type cladding region.

The diffusion current density due to holes can be derived in a similar way,

$$J_p = \frac{eD_p N_n}{L_p \tanh(W'/L_p)} \qquad (2\text{-}7)$$

however, it is much smaller than J_n because of large value of W' and small values of L_p, D_p, and N_n.

Assuming that the threshold carrier density is $2X10^{18}cm^{-3}$ to $3X10^{18}cm^{-3}$ and the impurity levels in both active and cladding layers are the same, E_{FC} is calculated from eq.(2-1), and N_p is given by eq.(2-2) putting the E_{FC} and $\Delta E_c = \Delta E_g$. Figure 2-3 shows the leakage current density J_n due to the drift current across the p-p heterojunction as a function of ΔE_g, where $m_c^* = 0.043m_0$ (for $\lambda_g = 1.6\mu m$) [293]-[295], $D_n = 75cm^2/sec$, $L_n = 5\mu m$, and $W = 2\mu m$ were used. Here D_n was taken as constant for each composition of quaternary cladding layer, whereas D_n increases with the decrease of the bandgap of the cladding layer in proportional to the electron mobility. Therefore, J_n calculated here gives the lower limit of the leak current. for the low threshold current density operation as low as $1\text{-}2KA/cm^2$, the barrier height ΔE_c of more than 0.3eV can be required.

In the four layer structure as shown in Fig.2-4, the leakage current density due to the diffusion current is estimated to be less than $1A/cm^2$ because of higher effective barrier height of $\Delta E_c \sim 0.5eV$. An excess current density is caused by the recombinations in the AMB layer and is given,

$$J_{AMB} = ed'N_{AMB}/\tau' \qquad (2\text{-}8)$$

where d' and τ' are the thickness of the AMB layer and the carrier life time in it. N_{AMB} can be expressed in a similar

way as eq.(2-2),

$$N_{AMB}=\frac{(2m_c^* kT)^{3/2}}{2\pi^2\hbar^3}\int_{\Delta E_c'}^{\infty}\frac{E^{1/2}\,dE}{1+\exp\{(E-E_{FC})/kT\}} \qquad (2\text{-}9)$$

where $\Delta E_c'$ is the barrier height between the active layer and the AMB layer. At high injection carrier density, the carrier life time was experimentally found to be inversely proportional to the injection carrier density [340], and is given,

$$1/\tau=B_{eff}N \qquad (2\text{-}10)$$

where B_{eff} is the effective recombination constant and was estimated to be $1\text{-}2X10^{-10}cm^3/sec$ for 1.6μm wavelength GaInAsP /InP lasers. Using eq.(2-10), eq.(2-8) can be rewritten,

$$J_{AMB}/d'=eB_{eff}N_{AMB}^2 \qquad (2\text{-}11)$$

Figure 2-5 shows the normalized carrier density J_{AMB}/d' as a function of the effective barrier height $\Delta E_c'$, where B_{eff} was taken as $8X10^{-11}cm^3/sec$ [316]. The normalized threshold current density of the conventional three layer structure is written,

$$J_{th}/d=eB_{eff}N_{th}^2 \qquad (2\text{-}12)$$

where d is the active layer thickness, N_{th} and J_{th} are the threshold carrier density and threshold current density. For 1.3-1.5μm wavelength GaInAsP/InP DH lasers of the conventional three layer structures, J_{th}/d of approximately $5KA/cm^2/\mu m$ was obtained and N_{th} was estimated to be $2X10^{18}cm^{-3}$ from it. As can be seen in Fig.2-5, when the effective barrier height $\Delta E_c'$ of more than 0.1eV was obtained, the excess of the J_{th}/d would be only less than 20 percent even if the AMB layer thickness

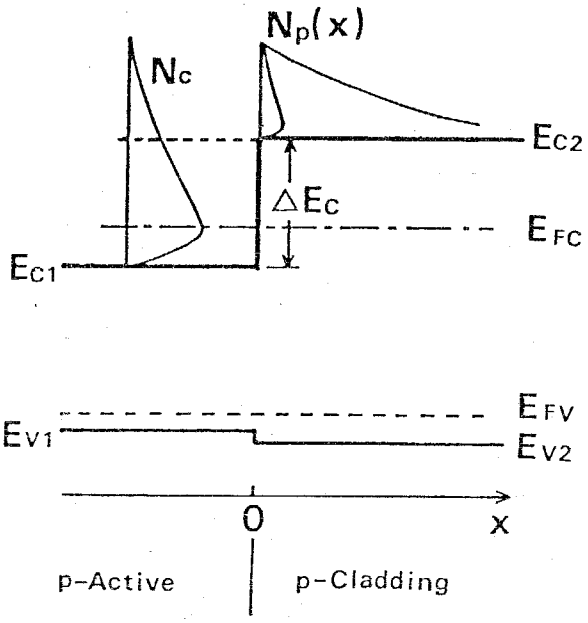

Fig.2-2

The p-P heterojunction energy band diagram for an N-p-P double hetero-structure at high excitation.

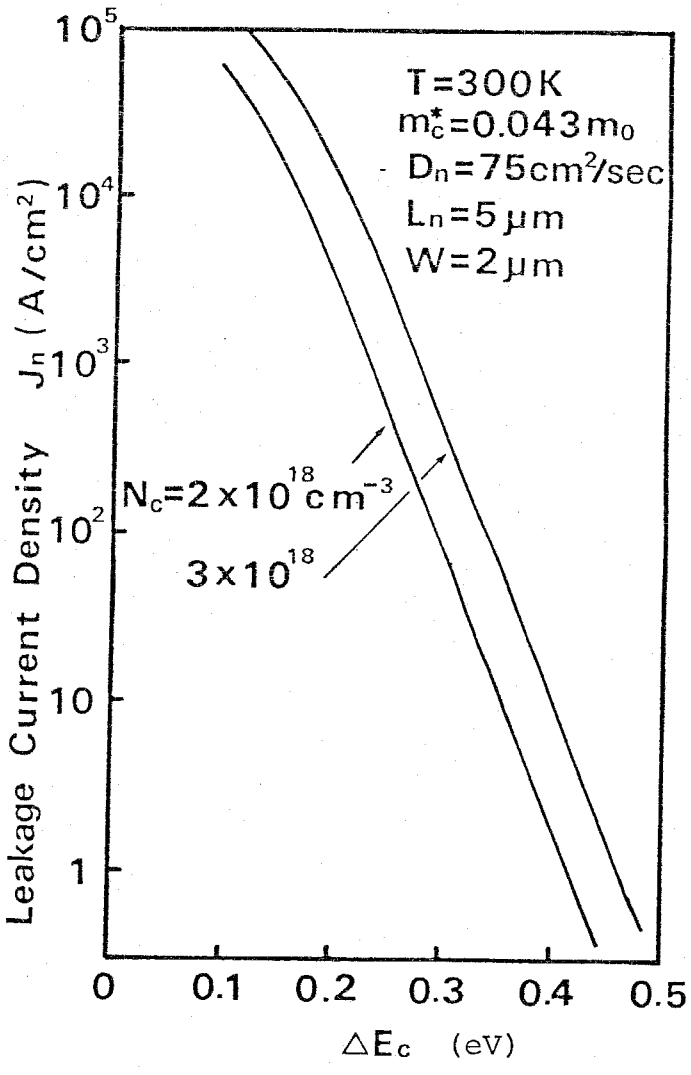

Fig.2-3

Calculated leakage current density at T=300K as a function of the barrier height between the active and the cladding layers.

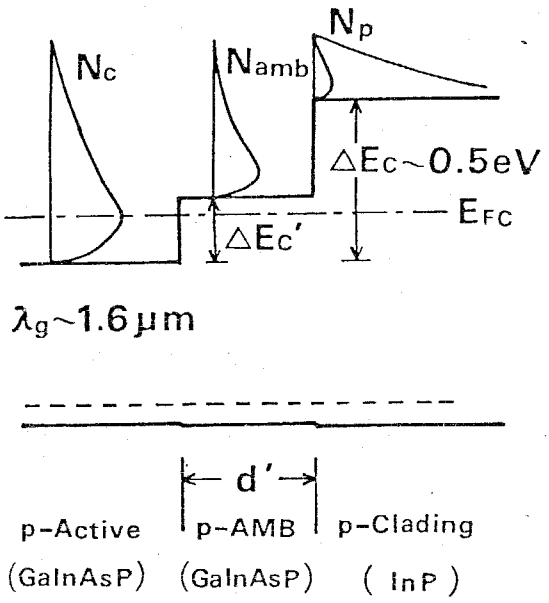

Fig.2-4

The p-P heterojunction energy band diagram of the four layer structure GaInAsP/InP laser.

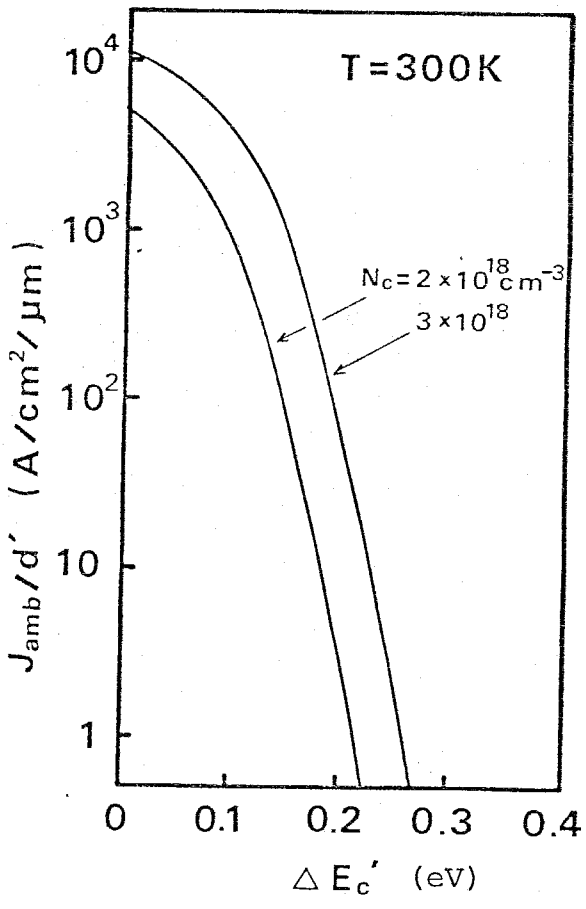

Fig.2-5

Calculated normalized current density J_{AMB}/d' at T=300K as a function of the effective barrier height $\Delta E_c'$.

was comparsble to the active layer thickness. From eqs.(2-11) and (2-12), the observable normalized threshold current density J_{obs}/d is given,

$$J_{obs}/d=eB_{eff}\{N_{th}^2+(d'/d)N_{AMB}^2\} \qquad (2\text{-}13)$$

2.3 Optical confinement

The optical confinement factor ξ of the active layer affects to the threshold carrier density, thus the effect on ξ by the insertion of the AMB layer is estimated in this section. The refractive index profile used in this calculation is shown in Fig.2-6. The electric field distribution for guided TE mode is given as follows,

$$E_y(x)=\begin{cases} A_1\exp\{\kappa_1(x+d)\} & -d>x>-\infty \\ A_2\cos(\gamma_2 x)+A_3\sin(\gamma_2 x) & 0>x>-d \\ A_4\cos(\gamma_3 x)+A_5\sin(\gamma_3 x) & d'>x>0 \\ A_6\exp\{-\kappa_4(x-d')\} & \infty>x>d' \end{cases} \qquad (2\text{-}14)$$

where $A_2=A_1\{\cos(\gamma_2 d)+(\kappa_1/\gamma_2)\sin(\gamma_2 d)\}$

$A_3=A_1\{-\sin(\gamma_2 d)+(\kappa_1/\gamma_2)\cos(\gamma_2 d)\}$

$A_4=A_2$

$A_5=A_3(\gamma_2/\gamma_3)$

$A_6=A_2\cos(\gamma_3 d')+A_3(\gamma_2/\gamma_3)\sin(\gamma_3 d')$

$\kappa_i=\kappa_0(n_{eq}^2-n_i^2)^{1/2}$

$\gamma_j=\kappa_0(n_j^2-n_{eq}^2)^{1/2}$

$\kappa_0=2\pi/\lambda$

n_{eq} denotes the equivalent refractive index of the guided mode which leads to the propagation constant as $\beta=2\pi n_{eq}/\lambda$.

The eigen value equation is given from eq.(2-14),

$$\tan(\gamma_3 d') = -\frac{(\kappa_1+\kappa_4)\cos(\gamma_2 d)+(\frac{\kappa_1\kappa_4}{\gamma_2}-\gamma_2)\sin(\gamma_2 d)}{(\frac{\kappa_1\kappa_4}{\gamma_3}-\gamma_3)\cos(\gamma_2 d)-(\frac{\kappa_1\gamma_3}{\gamma_2}+\frac{\kappa_4\gamma_2}{\gamma_3})\sin(\gamma_2 d)} \qquad (2\text{-}15)$$

The optical confinement factor ξ of the active layer is written,

$$\xi=\int_{-d}^{0} E_y^2\,dx \Big/ \int_{-\infty}^{\infty} E_y^2\,dx \qquad (2\text{-}16)$$

From eqs.(2-14)-(2-16), ξ was calculated and the results are shown in Fig.2-7 as a function of the active layer thickness d with a parameter of the AMB layer thickness d', where the refractive indices of $n_1=n_4=3.1618$, $n_2=3.5349(\lambda_g=1.62\mu m)$, $n_3=3.3979(\lambda_{AMB}=1.35\mu m)$ were used. As can be seen in Fig.2-7, the value of ξ hardly changes when the AMB layer thickness is only about 0.1μm.

Figure 2-8 shows the equivalent refractive index n_{eq} as a function of the active layer thickness. From this n_{eq}, the maximum guide width W_{max} for transverse single mode of the rectangular waveguide is calculated by the analogy of slab waveguide as,

$$W_{max}=\lambda/\{2(n_{eq}^2-n_1^2)^{1/2}\} \qquad (2\text{-}17)$$

where n_1 is the refractive index of InP and n_{eq} is given by eq.(2-15). Figure 2-9 shows the W_{max} as a function of the active layer thickness and the AMB layer thickness.

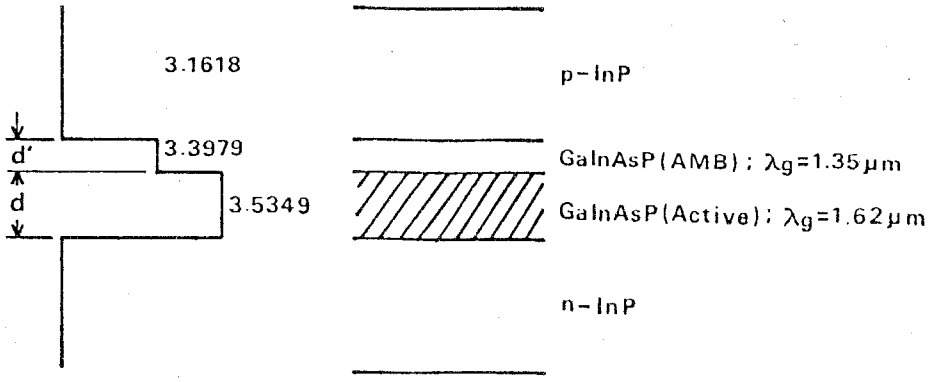

Fig.2-6 Refractive index profile of the four layer structure GaInAsP/InP laser.

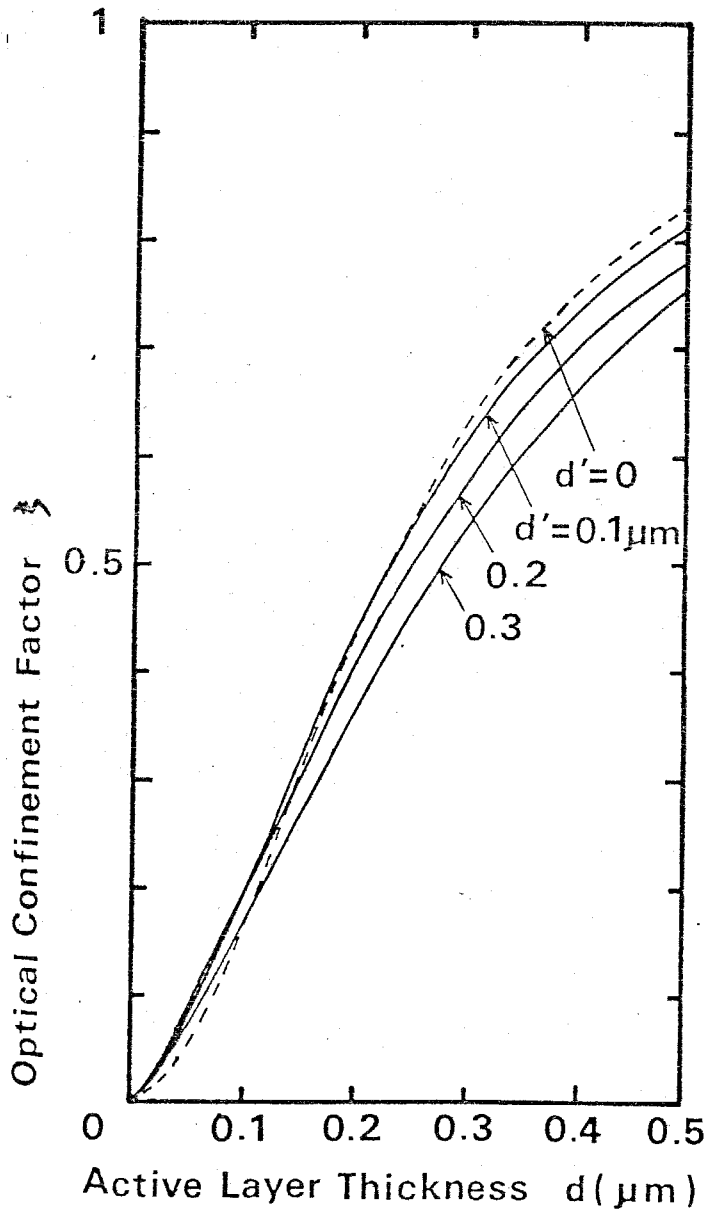

Fig.2-7

Optical confinement factor ξ of the active layer as a function of the active layer thickness and the AMB layer thickness.

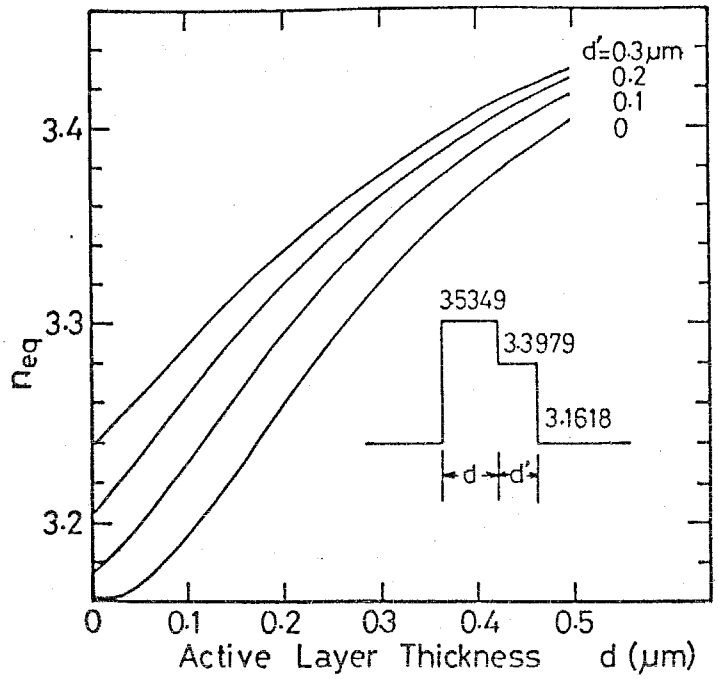

Fig.2-8 Equivalent refractive index of the four layer structure as a function of the active layer thickness and the AMB layer thickness.

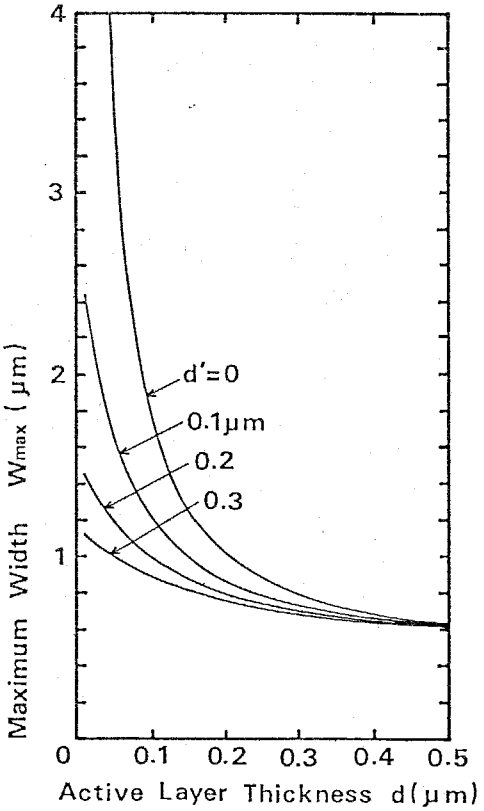

Fig.2-9

The maximum guide width W_{max} as a function of the active layer thickness and the AMB layer thickness.

2.4 Threshold current density

The threshold current density of semiconductor lasers is defined by the gain, the loss, and the carrier life time.

First, the linear gain with the assumptions of the parabolic state density, the Fermi-Dirac distribution function, and the momentum conservation(k-selection rule) was obtained for the 1.6μm wavelength GaInAsP active region according to the theory presented by Yamada and Suematsu [341].

The linear gain $\alpha^{(1)}$ of a lightly doped laser medium is written as ,

$$\alpha^{(1)}=(\mu/\varepsilon)^{1/2}\omega<M>^2\int_{W_G}^{\infty}\frac{g_{CV}(f_C-f_V)}{(\bar{n}\omega-W_{CV})^2+(\bar{n}/\tau_{in})^2}\cdot\frac{h}{\tau_{in}}dW_{CV} \quad (2\text{-}18)$$

where $g_{CV}=[\{2m_C^*m_V^*/(m_C^*+m_V^*)\}^{3/2}/(2\pi^2h^3)](W_{CV}-W_G)^{1/2}$

$$f_C=[1+\exp[\{(W_{CV}-W_G)m_V^*/(m_C^*+m_V^*)-(E_{FC}-W_G)\}/kT]]^{-1}$$

$$f_V=[1+\exp[\{-(W_{CV}-W_G)m_C^*/(m_C^*+m_V^*)-E_{FV}\}/kT]]^{-1}$$

μ and ε are the permeability and dielectric constant, ω is angular frequency of the light, <M> is the expectation value of the dipole moment, τ_{in} is the relaxation time of the dipole moment, m_C^*, m_V^*, and E_{FC}, E_{FV} are effective masses and quasi Fermi levels of the electrons and holes respectively, and W_G is the bandgap energy. The energies in these equations are measured from the top of the valence band as shown in Fig.2-10.

Assuming a lightly p-doped laser medium, E_{FC} and E_{FV} are determined by the following equations,

$$N = \frac{(2m_C^*)^{3/2}}{2\pi^2\hbar^3}\int_0^\infty \frac{W_C^{1/2}\, dW_C}{1+\exp\{(W_C-E_{FC}+W_G)/kT\}} \qquad (2\text{-}19)$$

$$P = N + P_0$$

$$= \frac{(2m_V^*)^{3/2}}{2\pi^2\hbar^3}\int_0^\infty \frac{W_V^{1/2}\, dW_V}{1+\exp\{(W_V-E_{FV})/kT\}} \qquad (2\text{-}20)$$

where N is the injected electron density, P is the total hole density while P_0 is that thermally generated from acceptors. P_0 is assumed to be almost equal to the acceptor concentration of $1X10^{17}cm^{-3}$ at room temperature.

To calculate $\alpha^{(1)}$ from eq.(2-18), the measured results for m_C^* and interpolated values from those of binary compounds for m_V^* were used [294].

Figure 2-11 shows an example of the calculated results of the bandgap wavelength of 1.6μm, where $m_C^*=0.043m_0$, $m_V^*=0.62m_0$, and $\tau_{in}=1.0X10^{-13}$sec(intraband relaxation time) were used. The peak value of the gain spectrum is shown in Fig.2-12 as a function of an injected carrier density with the various values of τ_{in}.

From the results in Fig.2-12, the peak gain $\alpha_p^{(1)}$ can be approximately given by,

$$\alpha_p^{(1)} \simeq A_0(N-N_G) = A_0N - \alpha_{in} \qquad (2\text{-}21)$$

where A_0 is the gradient of $\alpha_p^{(1)}$ versus N, N_G is the injected carrier density at which the peak gain is equal to zero, and $\alpha_{in}=A_0N_G$ is so called "biased loss of the laser medium".

The temperature dependence of the normalized peak gain as a function of N is shown in Fig.2-13 for λ_g=1.6μm. As can be

seen, approximation by eq.(2-21) is valid under most conditions. A_0 increases with decreasing temperature while N_G decreases. This is caused by the concentration of carriers into a narrower energy region at lower temperatures due to the change of the Fermi distribution function.

At threshold the peak gain $\alpha_p^{(1)}$ is equal to the total loss in the laser cavity, i.e.,

$$\xi\alpha_{th}^{(1)} = \alpha_{loss} = \xi\alpha_{ac}+(1-\xi)\alpha_{ex}+\ln(1/R)/\ell \qquad (2\text{-}22)$$

where $\alpha_{th}^{(1)}$ is $\alpha_p^{(1)}$ at threshold, α_{loss} is the total loss in the laser, ξ is the optical confinement factor of the active region, α_{ac} and α_{ex} are the losses in the active region and in the cladding region respectively, ℓ is the cavity length, and R is the reflectivity of the end mirrors.

In four layer structure lasers with the AMB layer, eq.(2-22) may be written as,

$$\xi\alpha_{th}^{(1)}=\xi\alpha_{ac}+\xi'\alpha_{AMB}+(1-\xi-\xi')\alpha_{ex}+\ln(1/R)/\ell \qquad (2\text{-}23)$$

where ξ' and α_{AMB} are the optical confinement factor and the loss of the AMB layer.

Combining eqs.(2-21) and (2-23), the threshold carrier density N_{th} can be written,

$$N_{th}=\{\alpha_{in}+\alpha_{ac}+\alpha_{AMB}(\xi'/\xi)+\alpha_{ex}(1-\xi-\xi')/\xi+\ln(1/R)/\ell/\xi/\}A_0 . \qquad (2\text{-}24)$$

The relation between N and the current density J is

$$J=edN/\tau_T \qquad (2\text{-}25)$$

where d is the thickness of the active layer and τ_T is the total carrier life time which may be separated into radiative

and non-radiative parts. From experimental results, the carrier life time was inverse proportional to the injected carrier density as defined in eq.(2-10). Equation (2-10) can be rewritten as follows,

$$\tau_T=1/\{B_{eff}(N+P_0)\}\simeq 1/(B_{eff}N)=\tau_{T0}N_0/N \qquad (2\text{-}26)$$

where τ_{T0} is a certain value of τ_T at a certain fixed value of N.

From eqs.(2-21), (2-25), and (2-26), the peak gain can be written,

$$\alpha_p^{(1)}=A_1(J/d)^{1/2}-\alpha_{in} \qquad (2\text{-}27)$$

where $$A_1=A_0/(eB_{eff})^{1/2}=A_0(\tau_{T0}N_0/e)^{1/2} \qquad (2\text{-}28)$$

The calculated results are shown in Fig.2-14.

Combining eqs.(2-24)-(2-26) and (2-28), the threshold current density can be written,

$$J_{th}=d/A_1^2\{\alpha_{total}+\ln(1/R)/\ell/\xi\}^2 \qquad (2\text{-}29)$$

where $$\alpha_{total}=\alpha_{in}+\alpha_{ac}+\alpha_{AMB}(\xi'/\xi)+\alpha_{ex}(1-\xi-\xi')/\xi \quad . \qquad (2\text{-}30)$$

When the bandgap difference between the active and the AMB layers was taken as more than 0.1eV, α_{AMB} would be as same as α_{ex}. Thus the excess carrier density due to the insertion of the AMB layer is negligible from the viewpoints of the optical confinement and the loss. The excess of the threshold current density is only given by the recombination current in the AMB layer as discussed in section 2.2.

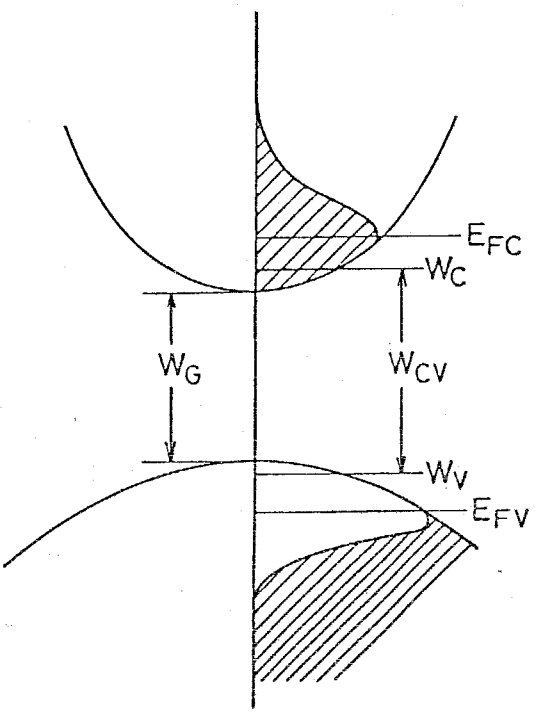

Fig.2-10

Schematic diagram of highly injected carriers. Parabolic band and the Fermi-Dirac distribution were assumed.

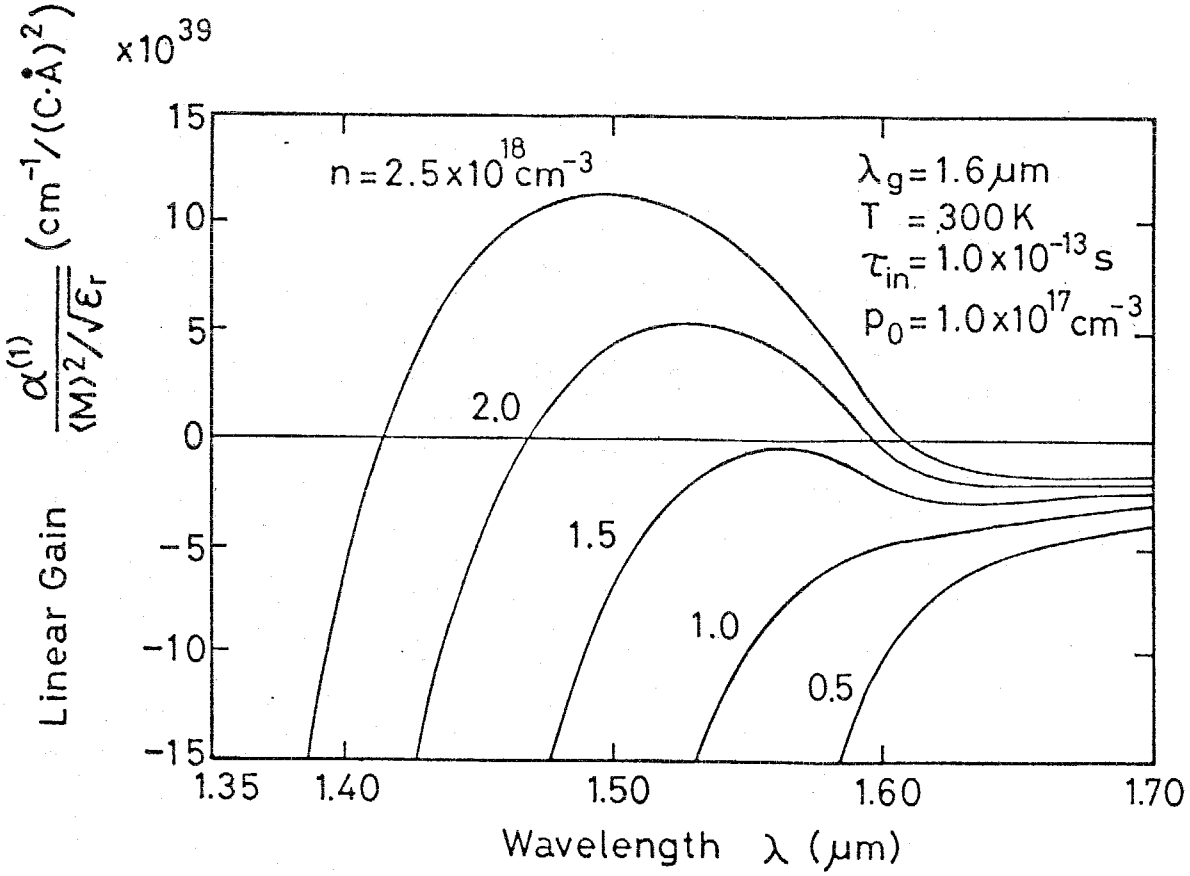

Fig.2-11 Normalized linear gain spectra with the various injected carrier density for the bandgap wavelength of 1.6μm.

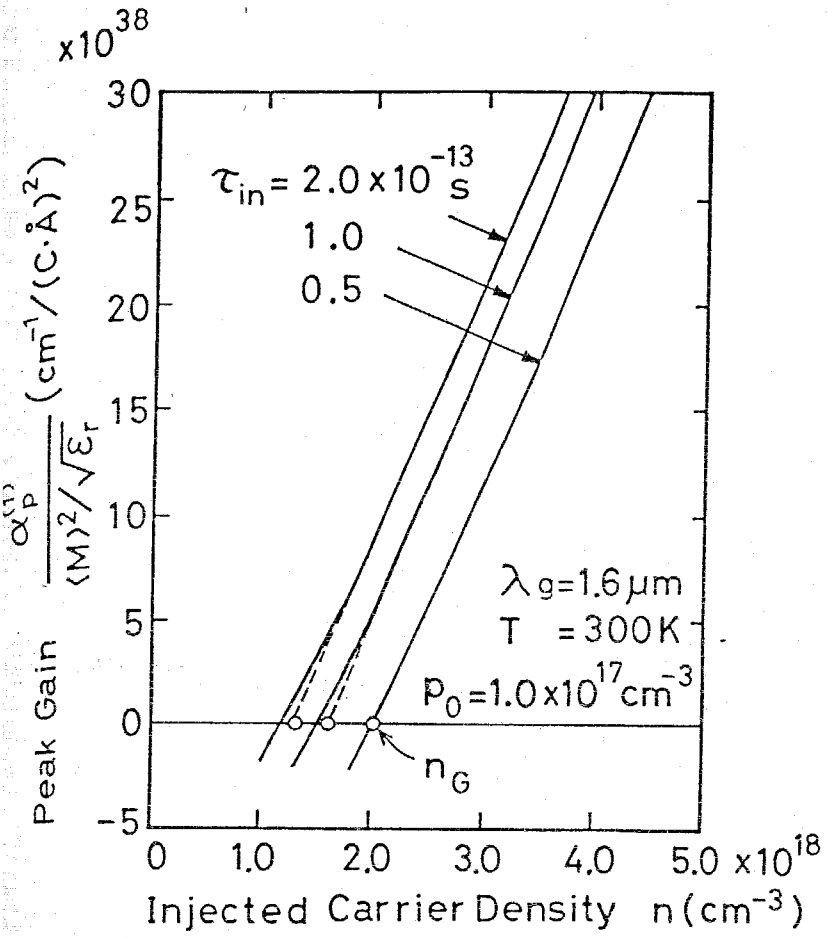

Fig.2-12

Theoretical peak gain as a function of an injected carrier density with a parameter of the intrabavd relaxation time for the bandgap wavelength of 1.6μm.

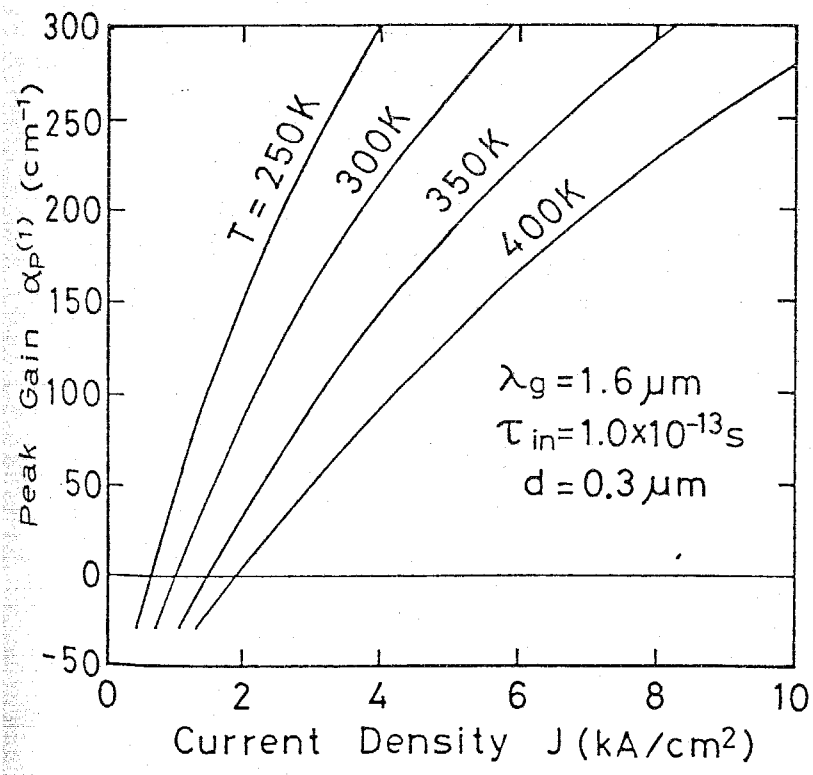

Fig.2-13

Theoretical peak gain as a function of an injected carrier density at various temperatures for the bandgap wavelength of 1.6μm.

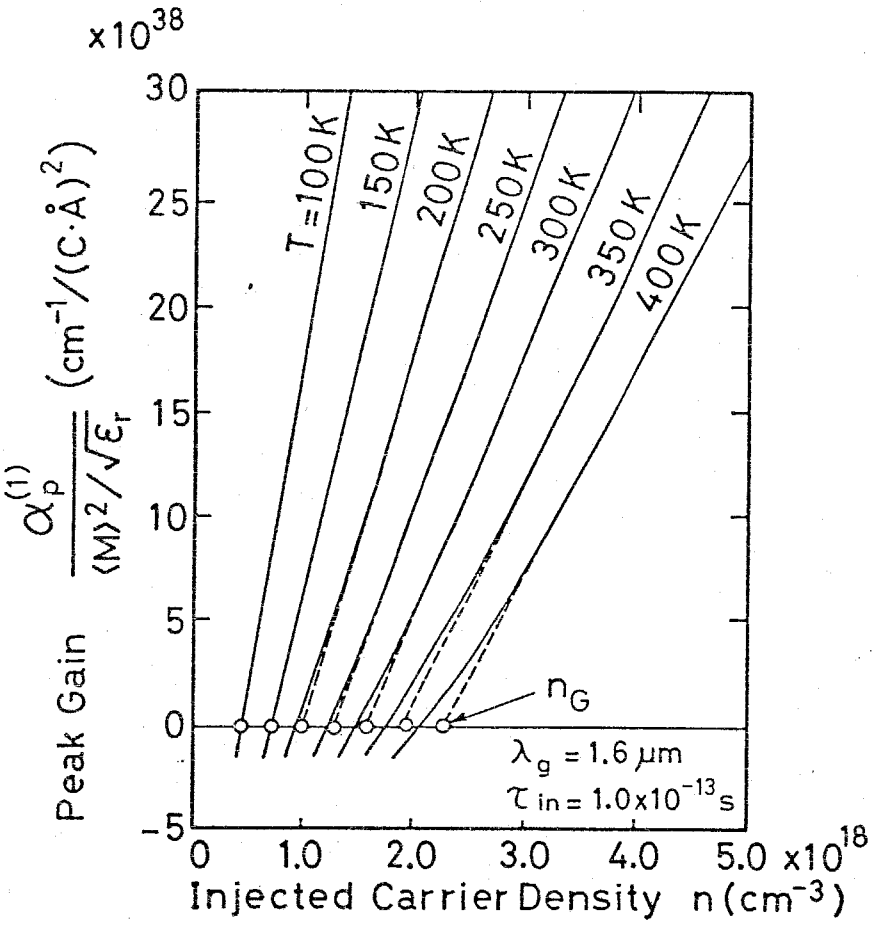

Fig.2-14 Theoretical peak gain as a function of an injection current density for the bandgap wavelength of 1.6μm.

2.5 Temperature dependence of lasing wavelength of Distributed Bragg Reflector (DBR) laser

For a narrow spectral width operation under high speed direct modulation, a distributed Bragg reflector (DBR) laser is one of the attractive devices. The fabrication processes and the lasing properties of the BH-DBR-ITG lasers are detailed in chapter 6. The importance of the DBR laser is a temperature dependence of the lasing wavelength because the single wavelength operation condition depends on the wavelength shift due to the change of the temperature.

In this section, the temperature dependence of the lasing wavelength of the DBR laser is discussed taking account of the refractive index variation due to the injected carriers. The temperature range of single mode operation is also given.

The model used for the calculation is schematically shown in Fig.2-15. In this figure, L_i and ℓ are the lengths of the DBR regions and the active region, respectively. n_{eq} and $\overline{n_{eq}}$ are the equivalent refractive indices of the DBR and active regions, respectively.

The reflectivity of the DBR at the end of the active region is written,

$$r_i=\kappa/\{-(\Delta\beta-j\alpha)+j\gamma\coth(\gamma L_i)\}$$
$$\equiv|r_i|\exp(-j\phi_i) \qquad (2\text{-}31)$$

where κ is the coupling constant between the incident and the reflected waves, α is the loss of the DBR region due to the free carrier absorption and scattering, $\gamma^2=\kappa^2+(\alpha+j\Delta\beta)^2$, $\Delta\beta$ is deviation from Bragg condition given by,

$$\Delta\beta=\beta-\beta_0=2\pi n_{eq}/\lambda-p\pi/\Lambda \qquad (2\text{-}32)$$

Λ is the pitch of the corrugations and p=1 is for the first order corrugations.

Using the complex reflectivies of DBRs' given by eq.(2-31), the threshold condition of a DBR laser is written,

$$|r_1||r_2|\exp\{j(-\phi_1-\phi_2-2\bar{\beta}\ell)\}\exp(\xi g_{th}-\alpha)\ell=1 \qquad (2\text{-}33)$$

where $\bar{\beta}=2\pi\overline{n_{eq}}/\lambda$, g_{th}, and α are the propagation constant in the active region, gain, and the loss of the cavity. The lasing wavelength condition is given by,

$$2\bar{\beta}\ell+\phi_1+\phi_2=2m\pi \qquad (m:\text{integer}) \qquad (2\text{-}34)$$

Assuming that the variation of the phase of the reflected wave ϕ_i is proportional to the deviation from Bragg condition $\Delta\beta$ and the proportional constant is defined as,

$$\left.\frac{\partial\phi_i}{\partial(\Delta\beta)}\right|_{\Delta\beta=0} \equiv 2L_{eff,i} \qquad (2\text{-}35)$$

where L_{eff} is so called the effective length of DBR region. Then the mode separation λ_{sep} of the DBR laser is written as,

$$\lambda_{sep}=\frac{\lambda^2}{2\{\ell\overline{n_{eff}}+(L_{eff1}+L_{eff2})n_{eff}\}} \qquad (2\text{-}36)$$

where $\overline{n_{eff}}=\overline{n_{eq}}-\lambda\frac{\partial\overline{n_{eq}}}{\partial\lambda}$, $n_{eff}=n_{eq}-\lambda\frac{\partial n_{eq}}{\partial\lambda}$, L_{eff1}, L_{eff2} are for DBR regions 1 and 2 as shown in Fig.2-15. Figure 2-16 shows the calculated results of L_{eff} as a function of the length of the DBR region with parameters of κL and α.

When the lasing condition of eq.(2-34) is satisfied at the temperature T, the increase of the temperature ΔT causes the increase of $\Delta\lambda$, $\Delta\overline{n_{eq}}$, Δn_{eq}, and $\Delta\phi_i$. Then the lasing wavelength condition is written as,

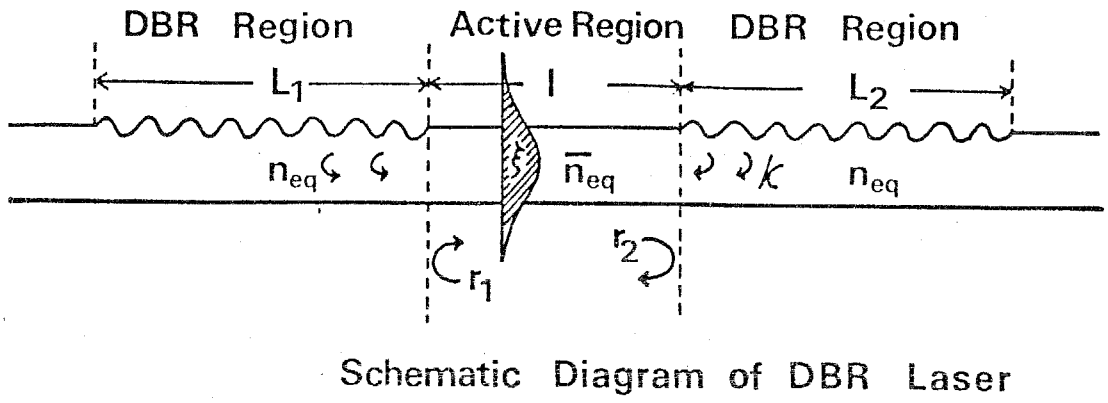

Fig.2-15 Schematic diagram of DBR laser used for the calculation.

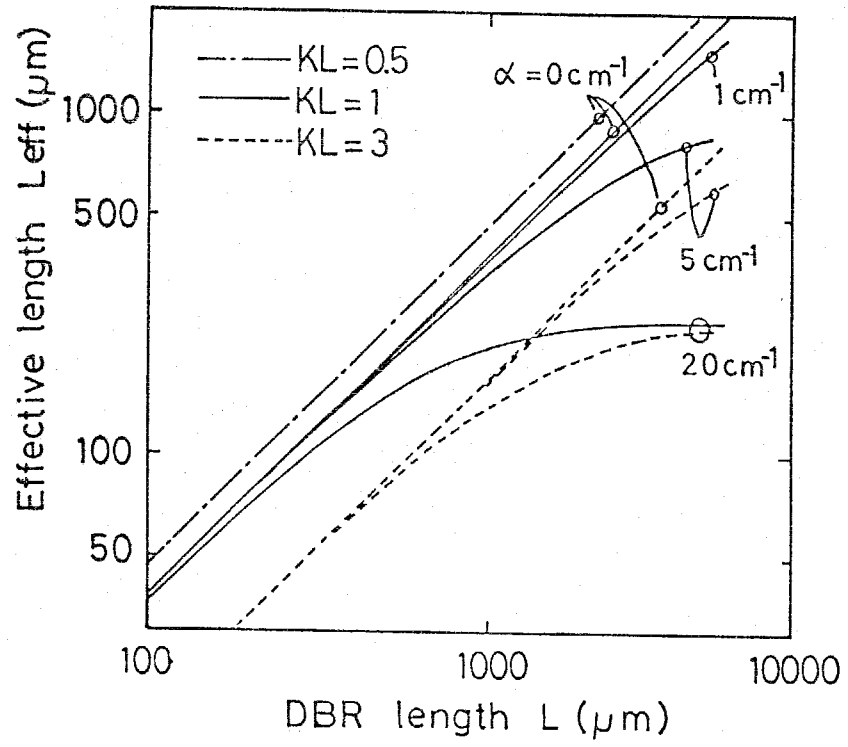

Fig.2-16 Calculated effective length of DBR region as a function of the DBR region length and κL.

$$4\pi(\overline{n_{eq}}+\Delta\overline{n_{eq}})\ell/(\lambda+\Delta\lambda)+(\phi_1+\Delta\phi_1)+(\phi_2+\Delta\phi_2)=2m\pi \qquad (2\text{-}37)$$

where $$\Delta\overline{n_{eq}}=\frac{\partial\overline{n_{eq}}}{\partial T}\Delta T+\frac{\partial\overline{n_{eq}}}{\partial\lambda}\Delta\lambda$$

$$\Delta\phi_i=\frac{\partial\phi_i}{\partial n_{eq}}\frac{\partial n_{eq}}{\partial T}\Delta T+\frac{\partial\phi_i}{\partial\lambda}\Delta\lambda \ .$$

Using eqs.(2-34) and (2-37), the differential coefficient of the lasing wavelength to the temperature is given by,

$$\frac{d\lambda}{dT}=\lambda\frac{\ell\frac{\partial\overline{n_{eq}}}{\partial T}+(L_{eff1}+L_{eff2})\frac{\partial n_{eq}}{\partial T}}{\ell\overline{n_{eff}}+(L_{eff1}+L_{eff2})n_{eff}} \qquad (2\text{-}38)$$

As can be seen, the variation of the lasing wavelength is expressed by the averaged equivalent refractive index variation due to temperature variation. The equivalent refractive index of the active region n_{eq} varies with the injected carriers [298][299], it is rewritten as,

$$\overline{n_{eq}}=\overline{n_{eq0}}+\xi\frac{\partial\overline{n}}{\partial N}N \qquad (2\text{-}39)$$

where $\overline{n_{eq0}}$ is the equivalent refractive index of the active region without carrier injection, $\overline{n}$ is a refractive index of the active layer, ξ and N are the optical confinement factor of the active layer and the injected carrier density. From the experimental results of the temperature dependence of the lasing wavelength of DBR lasers, $\frac{\partial n_{eq}}{\partial T}$ was estimated to be approximately $3\times10^{-4}deg^{-1}$ [243]. $\frac{\partial\overline{n}}{\partial N}$ was estimated to be $-7\sim-10\times10^{-21}cm^3$ from the measurement of 1.6μm wavelength BH laser [340]. Threshold carrier density variation due to the temperature variation is estimated to be approximately $3\times10^{16}cm^{-3}deg^{-1}$ taking account of the temperature dependence

of the threshold current density and the carrier life time. Thus the effect of the injected carriers on the temperature dependence of the equivalent refractive index should be taken account. Then putting the eq.(2-39) into eq.(2-38),

$$\frac{d\lambda}{dT}=\lambda\frac{\ell\left(\frac{\partial\overline{n_{eq0}}}{\partial T}+\xi\frac{\partial\overline{n}}{\partial N}\cdot\frac{dN_{th}}{dT}\right)+(L_{eff1}+L_{eff2})\frac{\partial n_{eq}}{\partial T}}{\ell\overline{n_{eff}}+(L_{eff1}+L_{eff2})n_{eff}} \qquad (2\text{-}40)$$

where N_{th} is a threshold carrier density. The temperature dependence of the threshold carrier density can be derived from the eq.(2-33) and the following assumptions.

Assumption (1) The gain profile is parabolic for the axis of wavelength and written as,

$$g_{th}=aN_{th}-b-c'(\lambda-\lambda_0)^2 \qquad (2\text{-}41)$$

where λ_0 is the peak gain wavelength, c' is a constant, a and b are the constants corresponding to A_0 and α_{in} in eq.(2-21), respectively.

Assum.(2) Temperature dependence of the threshold carrier density at $\lambda=\lambda_0$ is expressed by an exponential function from the analogy of that of the threshold current density and written as,

$$N_{th}(\lambda=\lambda_0)=N_{th0}\exp\{T/(2T_0)\} \qquad (2\text{-}42)$$

where T_0 is the temperature coefficient of the threshold current density as given by,

$$J_{th}=J_{th0}\exp(T/T_0) \ .$$

Assum.(3) The loss due to DBR mirror is approximated as parabolic function in the main lobe near the Bragg wavelength. For a symmetric structure DBR laser,

the mirror loss is written by,

$$\ln|(1/r)|^2=R_B\{1+d(\lambda-\lambda_B)^2\} \qquad (2\text{-}43)$$

where λ_B is the Bragg wavelength, R_B is the mirror loss at $\lambda=\lambda_B$, d is a fitting parameter. In the case of $\kappa L<1$, R_B and d can be expressed as,

$$R_B \simeq 2\ln\{\coth(\kappa L)\} \qquad (2\text{-}44)$$

$$d\simeq \frac{\ln[1+\{\coth(\kappa L/\sqrt{2})\}^2]-2\ln\{\coth(\kappa L)\}-\ln 2}{\kappa^2\{\lambda_B^2/(2\pi n_{eq})\}^2\ln\{\coth(\kappa L)\}} \qquad (2\text{-}45)$$

where the loss of the DBR region α denoted in the eq.(2-31) was neglected.

Then the threshold condition for the symmetric structure DBR laser is expressed by using eqs.(2-31) and (2-43),

$$\xi g_{th}=\xi\alpha_{ac}+(1-\xi)\alpha_{ex}+R_B\{1+d(\lambda-\lambda_B)^2\}/\ell \qquad (2\text{-}46)$$

The threshold carrier density can be obtained from eqs.(2-41), (2-42), and (2-46),

$$N_{th}=N_{th0}\exp\{T/(2T_0)\}+\{c'(\lambda-\lambda_0)^2+R_B d(\lambda-\lambda_B)^2/(\xi\ell)\}/a \qquad (2\text{-}47)$$

Differentiating eq.(2-47) by the temperature with assuming that a, b, c', d, R_B, ξ, and ℓ are independent of the temperature,

$$\frac{dN_{th}}{dT}=A\frac{d\lambda}{dT}-B\frac{d\lambda_0}{dT}-C\frac{d\lambda_B}{dT}+D \qquad (2\text{-}48)$$

where

$$A=2\{c'(\lambda-\lambda_B)+R_B d(\lambda-\lambda_B)/(\xi\ell)\}/a$$

$$B=2c'(\lambda-\lambda_0)/a$$

$$C=2R_B d(\lambda-\lambda_B)/(\xi\ell a)$$

$$D=N_{th0}/(2T_0)\exp\{T/(2T_0)\} \quad .$$

$\frac{d\lambda_0}{dT}$ was considered to be constant from the experimental results shown in chapter 4. $\frac{d\lambda_B}{dT}$ is given by,

$$\frac{d\lambda_B}{dT}=\frac{\lambda_B}{n_{eff}}\cdot\frac{\partial n_{eg}}{\partial T} \qquad (2\text{-}49)$$

Combining the eqs.(2-40) and (2-48), the temperature dependences of the threshold carrier density and the lasing wavelength can be obtained by an iterative calculation method.

When $\frac{dN_{th}}{dT}$ is positive, $\frac{d\lambda}{dT}$ is always smaller than $\frac{d\lambda_B}{dT}$ and the lasing mode goes to the shorter wavelength side with increasing the temperature in relation to the Bragg wavelength. Then the lasing mode jumps to the next mode at the wavelength of $\lambda_B-\lambda\simeq\lambda_{sep}/2$. The conceptional diagram of the movements of the lasing mode , Bragg wavelength, and the peak gain wavelength is shown in Fig.2-17. Figure 2-18 shows the conceptional diagram of the lasing wavelength as a function of the temperature. For the conventional structure laser, the lasing mode jumps to the next mode with a small increase of the temperature of $T_s\simeq\lambda_{sep}/(\frac{d\lambda_0}{dT})$, which is approximately 2deg for 1.6μm wavelength GaInAsP/InP laser with λ_{sep}=1nm.

Assuming that the lasing wavelength λ is just the Bragg wavelength at the temperature of 300K, the differential coefficient $\frac{d\lambda}{dT}$ is calculated from eqs.(2-40) and (2-48) as a function of the gain peak deviation from the Bragg wavelength as shown in Fig.2-19(a). $\frac{d\lambda}{dT}$ varies with the temperature due to the variation of the gain peak wavelength deviation $\lambda_0-\lambda_B$. However, the single mode operation temperature range T_s can be roughly evaluated by the following equation,

$$T_s \simeq \lambda_{sep} / \left(\frac{d\lambda_B}{dT} - \frac{d\lambda}{dT}\right) \qquad (2\text{-}50)$$

and the results are shown in Fig.2-19(b). As can be seen, the reduction of the threshold carrier density leads to large T_s at the fixed values of ℓ and ξ.

Eq.(2-50) can be approximately rewritten,

$$T_s \simeq \frac{\lambda_B}{2\ell\xi\left(-\frac{\partial \bar{n}}{\partial N}\right)\left\{\frac{N_{th0}}{2T_0}\exp\left(\frac{T}{2T_0}\right) - \frac{2c'}{a}(\lambda_B - \lambda_0)\frac{d\lambda_0}{dT}\right\}} \qquad (2\text{-}51)$$

From the eq.(2-51), the reductions of ℓ and ξ are effective to increase T_s. They correspond to the increase of λ_{sep} and the suppression of the refractive index variation due to injected carriers, respectively. Combining the eqs.(2-12), (2-40), and (2-48), the temperature dependences of the threshold current density and the lasing wavelength were calculated iteratively. Wide temperature range of single mode operation of more than 100deg can be obtained by the reduction of the active region length as shown in Fig.2-20. Figure 2-21 shows an example of the temperature dependences of the threshold current density and the lasing wavelength with ℓ=100μm and ξ=0.22.

This kind of mode jump is particular for a DBR laser which consists of an active and a passive regions, not for a DFB laser which consists of only an active region. Thus the wavelength tuning mechanism by use of an electro-optic effect is required for a DBR laser.

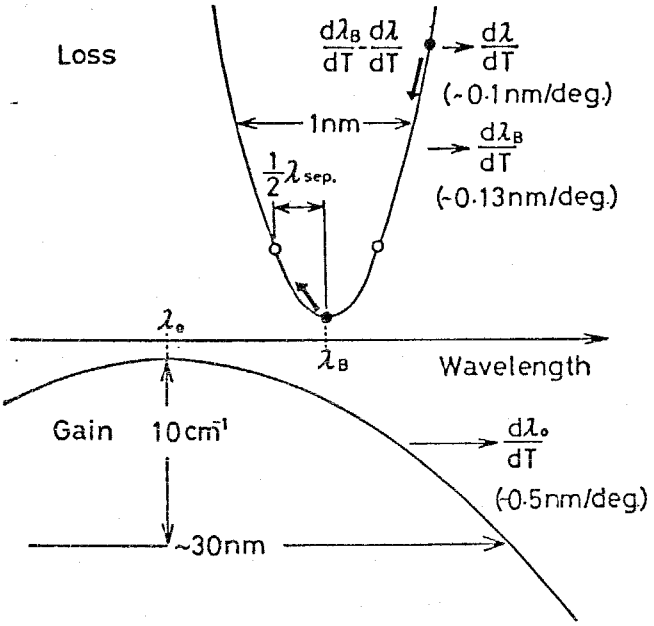

Fig.2-17 Conceptional diagram of the monements of the lasing mode, the Bragg wavelength, and the gain peak wavelength with increasing the temperature.

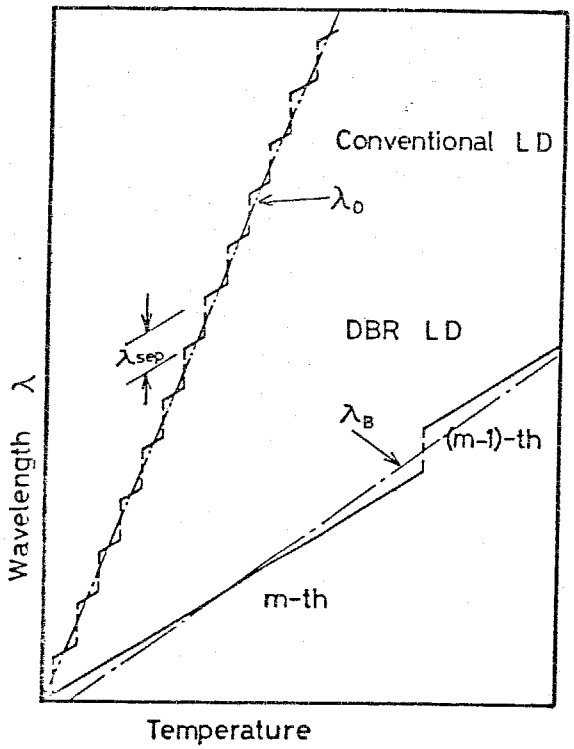

Fig.2-18
Conceptional diagram of the lasing wavelength as a function of the temperature.

(a)

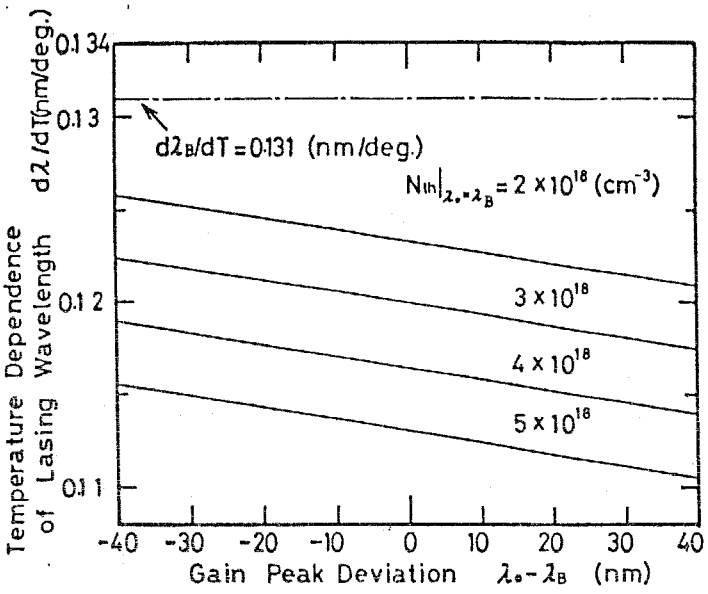

(b)

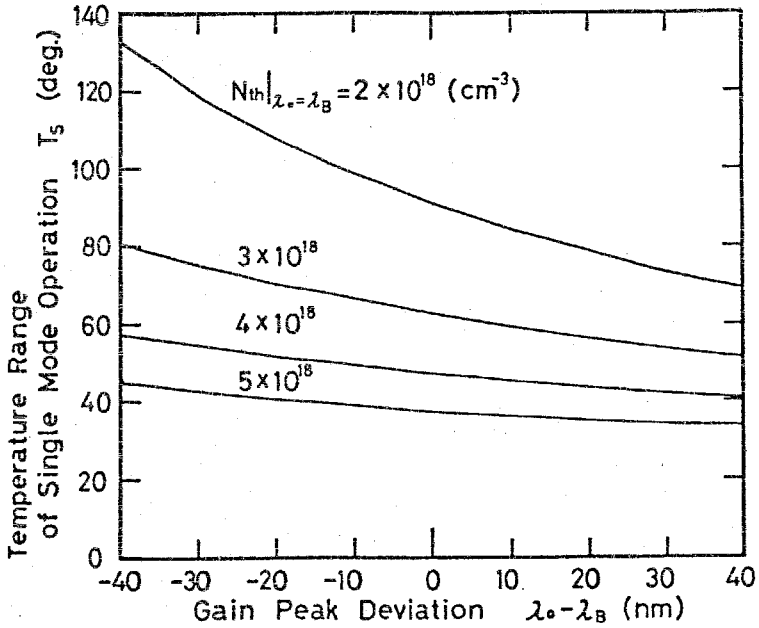

Fig.2-19 (a) Temperature dependence of the lasing wavelength as a function of the gain peak deviation from Bragg wavelength. Used parameters are ℓ=300μm, $L_1=L_2$=250μm, L_{eff}=100μm, κL=1, $\overline{n_{eq}}$=3.2960, n_{eq}=3.2630, $\overline{n_{eff}}$=3.6960, n_{eff}=3.6630, $\frac{\partial \overline{n_{eq}}}{\partial T}=\frac{\partial n_{eq}}{\partial T}=3\times10^{-4}\,deg^{-1}$, λ_B=1.6μm, ξ=0.22, $\frac{\partial \bar{n}}{\partial N}=-7.2\times10^{-21}\,cm^{-3}$, $a=1.80\times10^{-16}\,cm^2$, $c'=3.52\times10^4\,cm^{-1}\mu m^{-2}$, $\frac{d\lambda_0}{dT}$=0.5nm/deg, T_0=60K, and T=300K.

(b) Single mode operation temperature range as a function of the gain peak deviation.

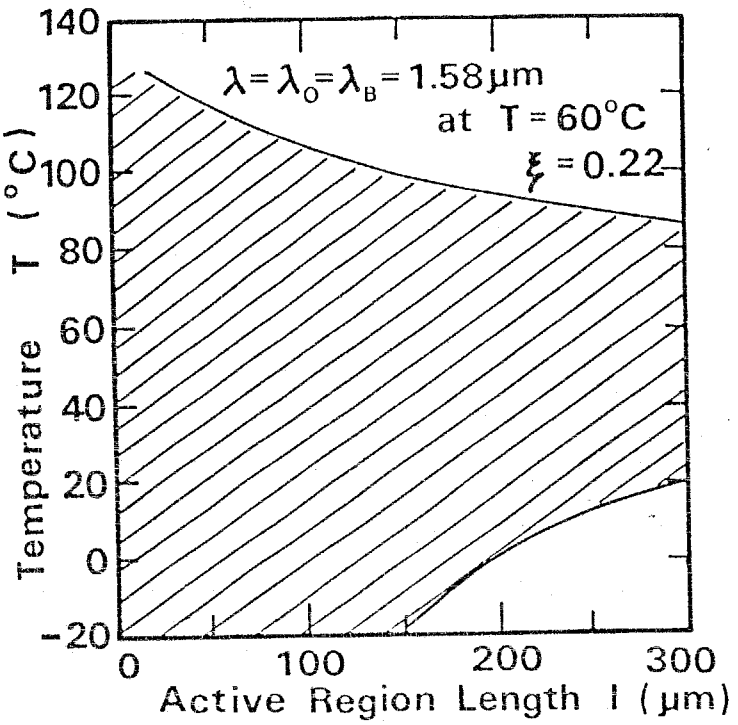

Fig.2-20 Single mode operation temperature region indicated by hatched area of a DBR laser as a function of the active region length. Used parameters are as same as those in Fig.2-19.

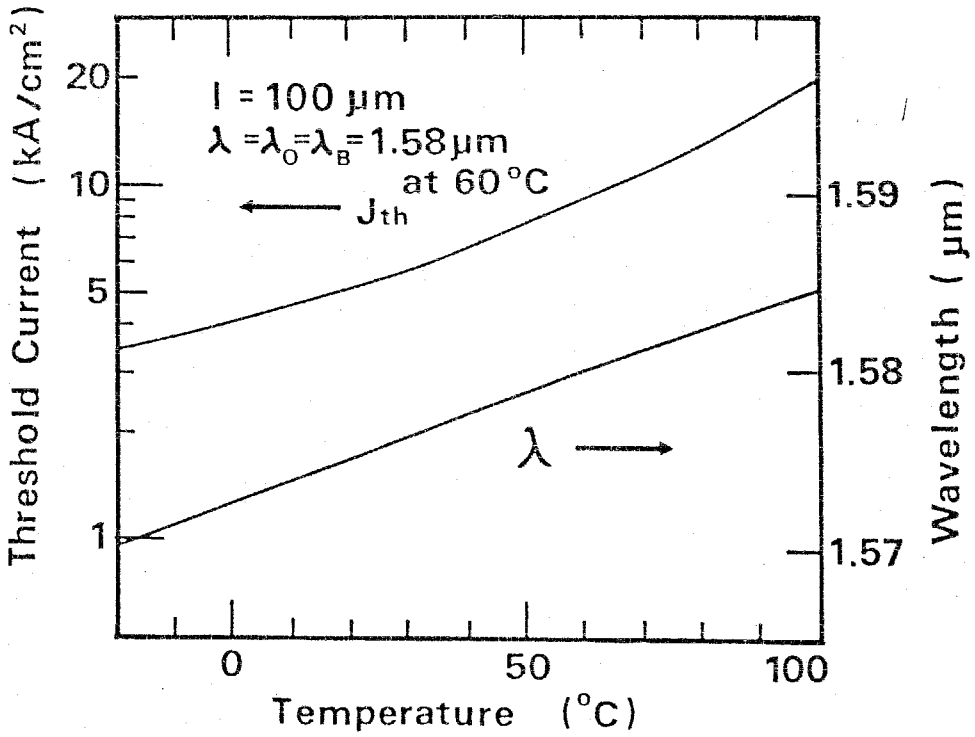

Fig.2-21 An example of the temperature dependences of the lasing wavelength and the threshold current density.

2.6 Conclusion

The threshold current density of the four layer structure GaInAsP/InP double heterostructure laser with an additional anti-melt-back(AMB) layer was discussed theoretically from the viewpoints of the carrier confinement and the optical confinement. The excess of threshold current density due to the insertion of the AMB layer is caused mainly by the recombination current in the AMB layer and it was found to be negligible when the effective barrier height between the active layer and the AMB layer was more than 0.1eV and the thickness of the AMB layer was less than 0.3μm.

The temperature dependences of the lasing wavelength and the threshold current density of DBR laser were theoretically discussed taking account of refractive index variation due to the injected carriers. Single mode operation temperature range can be increased more than 100deg by the reductions of the active region length and the optical confinement factor of the active layer.

CHAPTER 3 GROWTH CONDITION OF GaInAsP/InP CRYSTAL

3.1 Introduction

It is an essential to get a lattice matched GaInAsP crystal on the substrate InP for an efficient light emitting devices such as a semiconductor laser. In case of an AlGaAs/GaAs double heterostructure laser, the lattice mismatch of less than 0.05 percent can be kept for ordinary used wavelength, which gave far easier way to get a high performance. However, the difficulty and the tireness in getting the growth condition for a lattice matched GaInAsP crystal should be cancelled out by taking account of the advantages which GaInAsP quaternary crystal has inherently. GaInAsP/InP lasers can be operate with the wavelength region of 0.92-1.67 μm by choosing the appropriate compositions while the complete lattice match is maintained.

In this chapter, the growth process and the conditions for the lattice matched GaInAsP/InP DH lasers over the almost complete wavelength range of 1.11-1.65μm are given. The two phase solution technique and the substrate of (100) oriented InP were used.

3.2 Lattice constant and bandgap of GaInAsP crystal

The lattice constant a_0 and the bandgap of $Ga_yIn_{1-y}As_xP_{1-x}$ quaternary crystal was calculated by Moon, Antypas, and James in 1974 for the first time with an extrapolation according to Vegard's law [320]. They derived the equations for a_0 and Eg as a function of the compositions of x and y from the lattice

constants and the bandgaps of the four constituent ternaries. In 1978, Nahory, Pollack, and Johnston derived the same kind equations from those of the four constituent binaries of InP, GaAS, InAs, and GaP, and demonstrated the Vegard's law [331].

Derived equations for the lattice constant a_0(A) and the bandgap Eg(eV) are as follows,

$$a_0(x,y)=5.8696-0.4184x+0.1894y+0.0130xy \qquad (3\text{-}1)$$

$$Eg(x,y)=1.35+0.668x-1.17y+0.758x^2+0.18y^2 -0.069xy-0.322x^2y+0.03xy^2 \qquad (3\text{-}2)$$

From eq.(3-1), the relation between x and y is given for any GaInAsP crystal lattice matched to InP crystal by substituting $a_0(x,y)=5.8696$. Therefore the bandgap of the quaternary crystal lattice matched to InP crystal is defined by one of the compositions of x and y. The bandgap for the quaternary crystal lattice matched to InP was empirically given by following equation [331],

$$Eg(y)=1.35-0.72y+0.12y^2 \qquad (3\text{-}3)$$

The contour map of the lattice constant and the bandgap as a function of the alloy compositions is shown in Fig.3-1. The lattice constant of the four constituent binaries are listed in Table 3-1.

Table 3-1 The lattice constants of the four constituent binaries.

Material	Lattice constant(A)
InP	5.8696
GaAs	5.6536
InAs	6.0560
GaP	5.4512

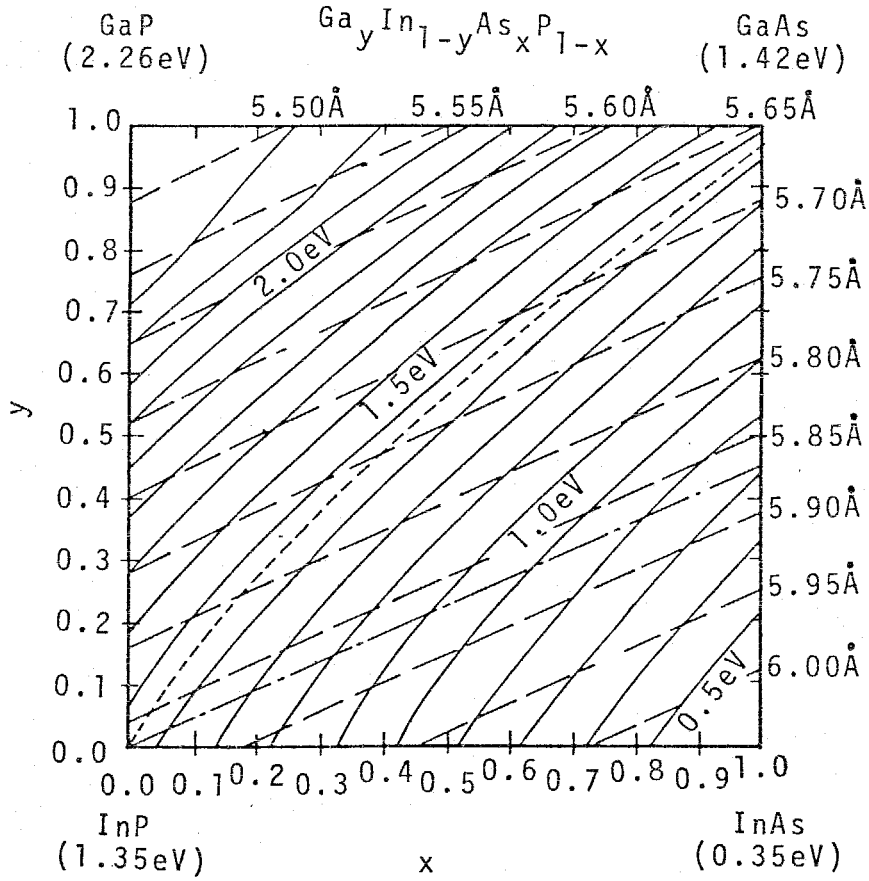

Fig.3-1 The contour map of the lattice constant and the bandgap as a function of alloy compositions of x and y for $Ga_yIn_{1-y}As_xP_{1-x}$.

3.3 Liquid phase epitaxial growth technique

For the study of GaInAsP/InP lasers, the liquid phase epitaxial(LPE) growth technique was employed with a conventional horizontal type electric furnace. In this growth process, the solutes are first disolved into the solvent at the high temperature, then the substrate crystal is shifted into and touched with the solution with cooling the temperature gradually or step by step.

In the growth of GaInAsP crystal, the solvent of Indium, the solutes of InP,GaAs, and InAs were used because the contour line of the lattice constant of InP lies on the triangle area surrounded by those three constituent binaries. The dopants of Zn and Te were mainly used for p and n type regions because they are more reliable compared with other dopants of Cd and Be for p type and Sn, Ge, and Si for n type. The growth temperature is limited from 580°C to 750°C because the thermal damage due to the decomposition of InP substrate becomes severe at 750°C and the growth instability due to the low solubility of P comes out at 580°C [335][336].

There are typically four kinds of LPE growth techniques, namely, the equilibrium-cooling growth technique, the super-cooling growth technique, the step-cooling growth technique, and the two-phase solution super-cooling technique [321]. In the growth of GaInAsP quaternary system, the setting of growth parameters are complicated, because we have to determine the growth temperature, the super-cooling temperature, and the distribution coefficients of Ga, As, and P in the Indium melt. Thus, in the beginning of this research, it was very difficult

to grow, at will, a given composition of GaInAsP crystal, so that we have to use the two-phase solution technique for the growth of GaInAsP/InP DH wafer. Using this technique under a consistent growth process, we could eliminate one parameter, namely, the distribution coefficient of P. Because in this technique the source crystal of InP can be loaded in excess amount to saturate the Ga-As-In solution, so that it is not necessary to control or change the amount of InP when the other components are varied. A detail report was given by Pollack, Nahory, DeWinter, and Ballman concerning this two-phase solution technique used for the growth of GaInAsP lattice matched to (100) InP [328]. We have also reported it separately [180]. As the details of both experiments were different from each other, our results are compared with theirs in section 3.4.

In this section, the apparatus of LPE growth for this study, the preparation of growth materials, and the growth process are described.

(1) LPE apparatus

Two groups of LPE apparatus were used in this study, that is, a combination of LPE furnace A and the carbon boat A and the other combination of those B. First the two LPE furnaces are explained with the help of the illustrations as shown in Figs.3-2 and 3-3. The apparatus consists of the electric furnace with an accurate temperature controller and the processor for cooling control, an evacuation system, a hydrogen purifier, a nitrogen filled box, and a quartz

reaction tube penetrated into the furnace. The horizontal sliding type carbon boat is located at the center of the furnace which consists of three zone block heaters. The temperature flatness along the sliding direction of 0.05°C within 20cm long growth region can be obtained by adjusting the temperature controllers. As shown in Fig.3-3, the furnace B has a moving mechanism, the faster cooling after the growth is capable and leads to the reduction of a thermal damage due to the decomposition of InP. It also has a high vacuum turbo molecular pump for the reduction of the residual impurities by a high temperature baking(800-900°C) under a high vacuum of 10^{-6}Torr. The specifications of these apparatus are listed in Table 3-2.

Table 3-2 Specifications of two LPE apparatus A and B.

Apparatus		A	B
Electric furnace	Length Width Height	75cm 45cm 40cm	120cm 45cm 40cm
Reaction tube (Quartz)	Length Diameter Thickness	1400mm 70mm 3mm	1500mm 70mm 3mm
Evacuation system		Rotary pump	Rotary pump Turbo molecular pump
Vacuum degree	(Torr)	10^{-3}	10^{-7}
Temperature range	(°C)	400-1000	400-1300
Raising or cooling rate	(°C/min)	0-9.9	0-9.9
(Accuracy)	(°C/min)	0.01	0.01

(a)

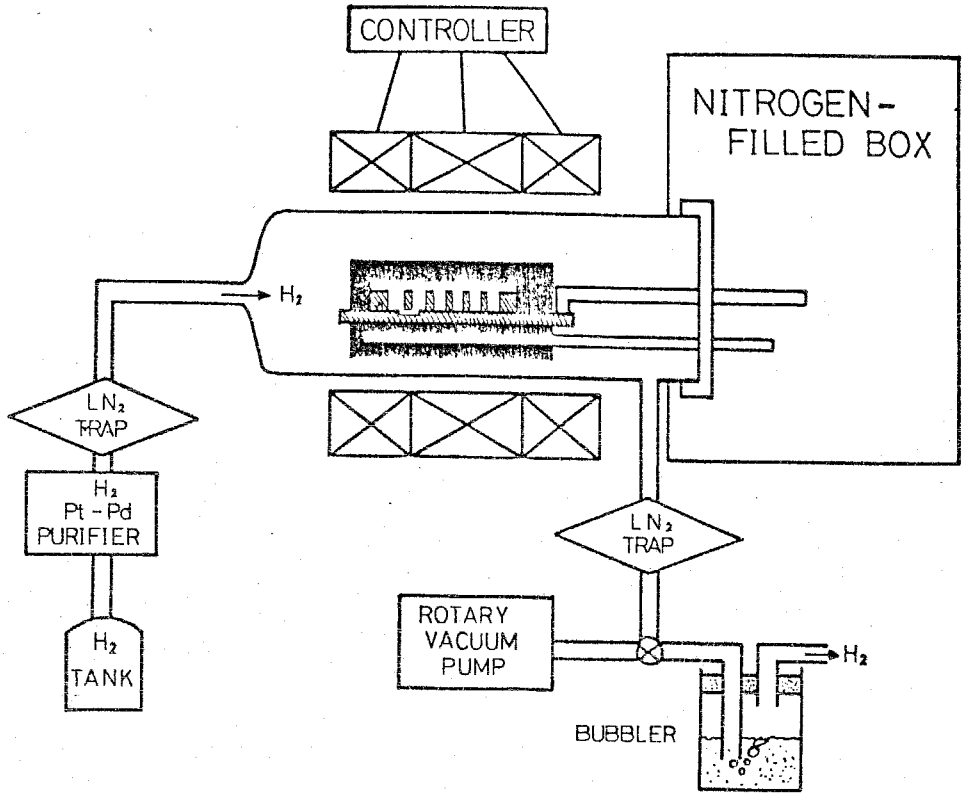

(b)

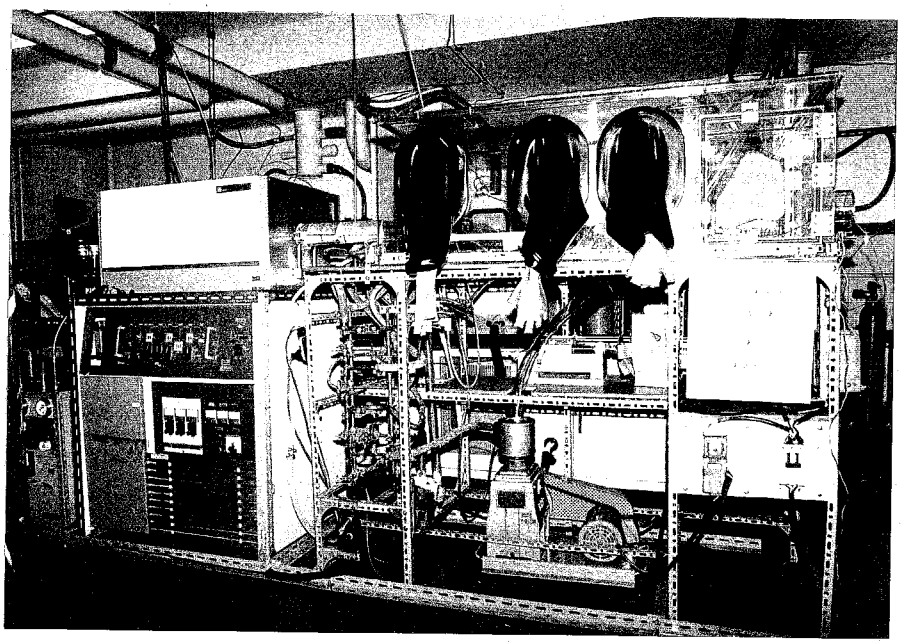

Fig.3-2 (a) Schematic diagram of the LPE apparatus A, and (b) Photograph of its outside view.

(a)

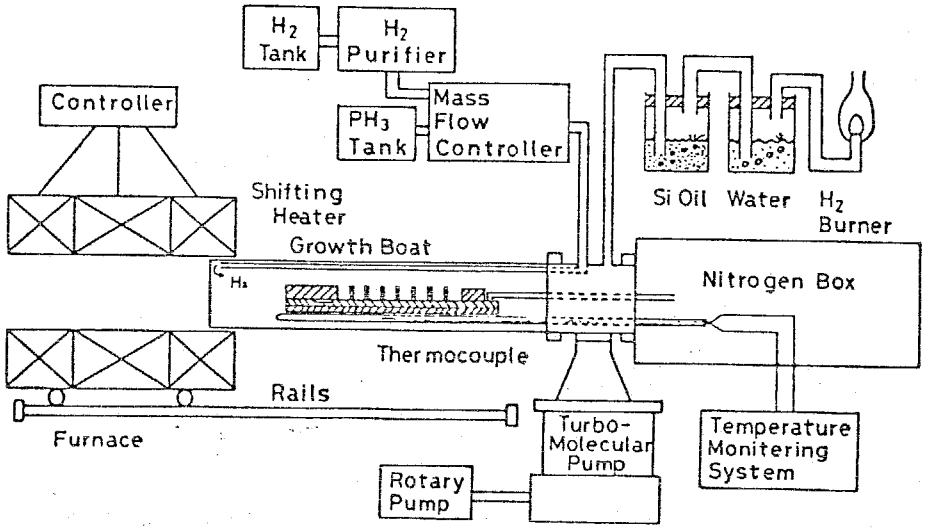

(b)

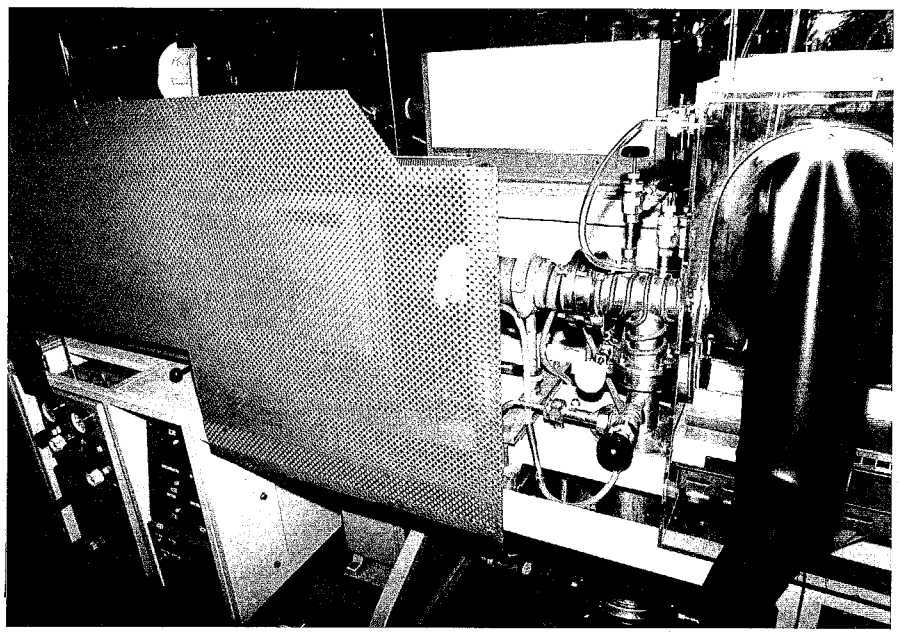

Fig.3-3 (a) Schematic diagram of the LPE apparatus B, and (b) Photograph of its outside view.

The two types of the horizontal sliding boat made of high purity graphite were used for this study as shown in Figs.3-4 and 3-5. The boat A was used with the furnace A in the early term, mainly for the study of the growth conditions of lattice matching. The boat B was used with the furnace B for the growth of larger size wafer which made the fabrication of the integrated twin guide lasers and the buried heterostructure lasers much easier. These boats basically consisted of four parts, namely, (a) the solution holder, (b) the substrate holder, (c) the chassis, and (d) the screws used to contact the solution holder and the substrate holder tightly in order to prevent the solution from carrying over. In the boat B, a large well was opened to set a cover of InP just on the substrate in order to prevent the thermal decomposition of it, which was an useful way for the regrowth of the etched and shaped wafer. The specifications of these boats are listed in Table 3-3.

Table 3-3 Specifications of two growth boats A and B.

		A	B
Solution holder	Length Width Thickness Bin size	119mm 42mm 10mm 7mmX7mm (7pieces)	176mm 50mm 8mm 12mmX20mm (10pieces)
Substrate holder	Length Width Thickness Channel size depth	231mm 22mm 5mm 7mmX9mm 0.4mm	360mm 31mm 3mm 12mmX22mm 0.4mm
Chassis	Length Width Thickness	225mm 42mm 16mm	350mm 50mm 10mm

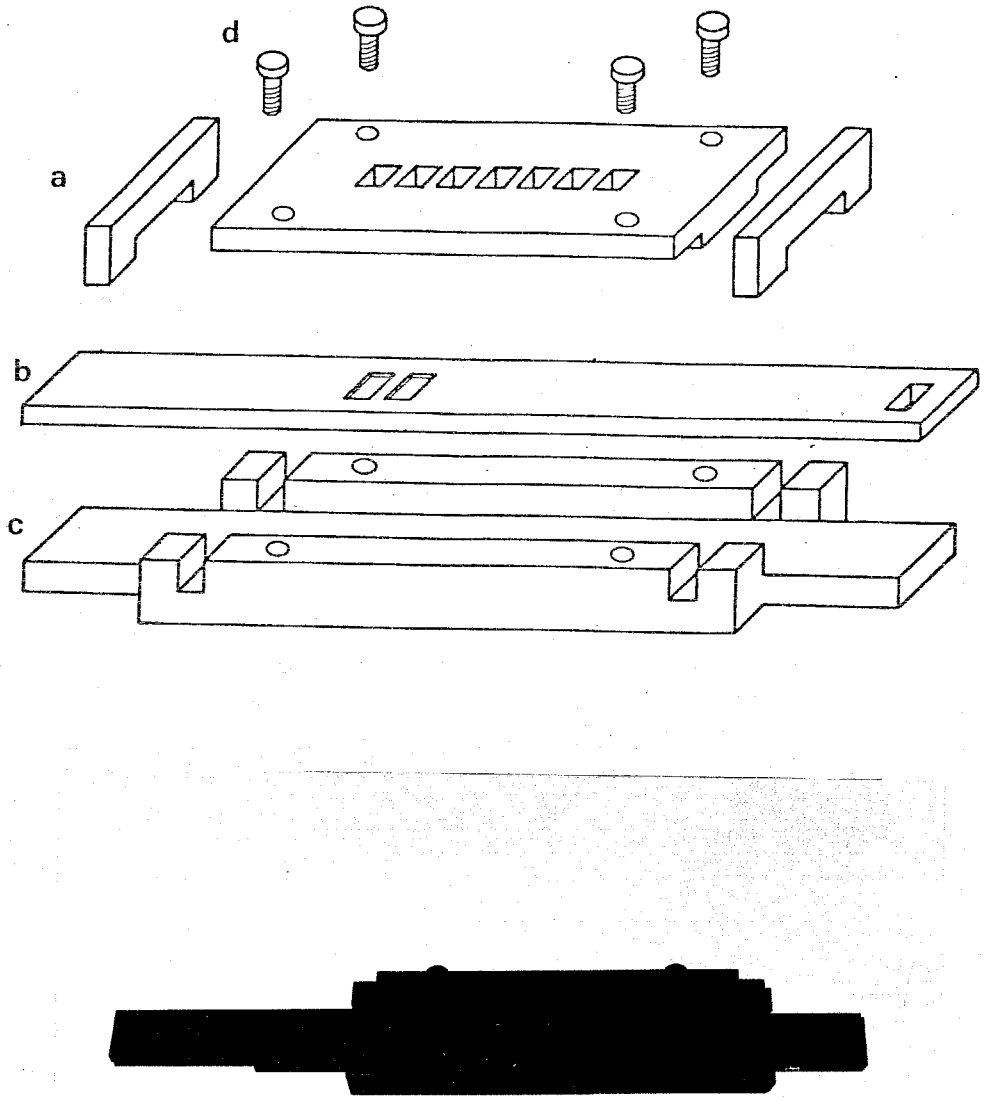

Fig.3-4 Schematic diagram and the photograph of the growth boat A, which consists of (a)the solution holder, (b)the substrate holder, (c)the chasis, and (d)the screws.

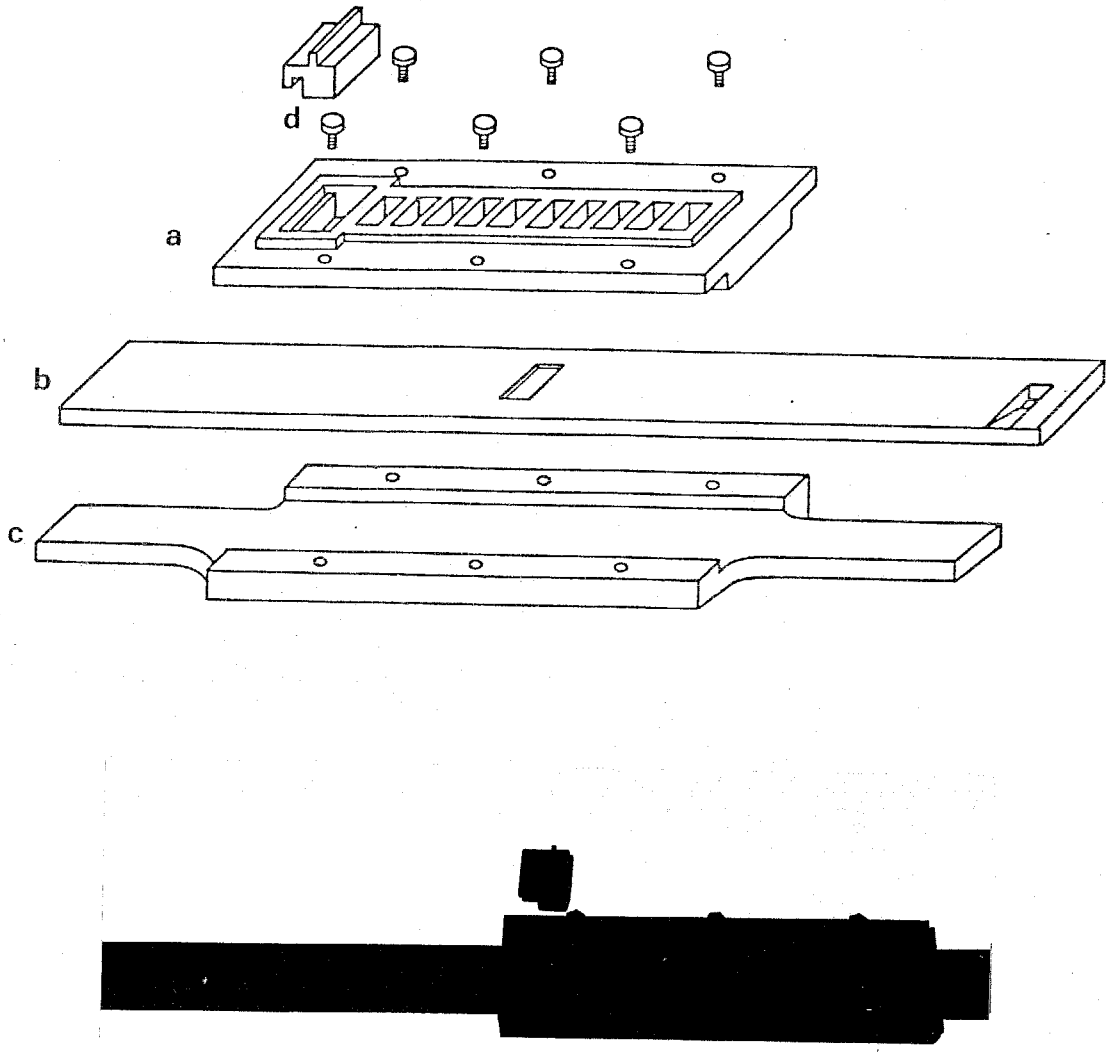

Fig.3-5 Schematic diagram and the photograph of the growth boat B, which consists of (a)the solution holder, (b)the substrate holder, (c)the chasis, and (d)the screws.

Before the use, a new boat was treated by following procedures.

[1] All the parts of the boat were cleaned in pure water using ultrasonic cleaner. The pure water was changed with the interval of 30min cleaning until the water did not become cloudy with carbon radicals(3-4 times).

[2] They were dried in natural air with a drying lamp after blowing the water drops away.

[3] They were baked for about 4hour in high vacuum of 10^{-6} Torr with the temperature of 900°C.

[4] They were baked for 1-3 days in hydrogen atmosphere with the temperature of 900°C.

[5] After the construction, Indium was loaded into each bin, then the baking was continued with the same way as in [4].

[6] Baked Indium was taken out, then the boat underwent to the growth. When the Indium contacted tightly with the boat, the solute of InP was put into the melt.

In the use of the furnace A, the procedure [3] was avoided.

(2) Preparation of growth materials

In preparation of the growth, the substrate InP, the source crystals InP, GaAs, and InAs were cleaned by ultrasonic cleaner in methyl alcohol, trichloroethylene, and methyl alcohol again for 5, 10, and 5min, respectively. Then the substrate, the source crystals, the solvent Indium, and the dopants were etched as follows.

[1] The substrate InP was treated with the solution of $H_2O+3H_2SO_4$(95 percent)$+H_2O_2$(35 percent) at 70-90°C

for about 20sec in order to prevent it from the generation of uneveness after the following etching by Br-methanol. The etching was stopped by flashing the beaker several times with pure water. Then the beaker was flashed with methanol.

[2] The solvents of 6n grade Indium were etched by HNO_3 (60 percent) for 3min. Electronic grade HNO_3 should be diluted with the same volume of pure water to suppress the furious reaction. Then etching was stopped by the same manner as in [1].

[3] The substrate and the source crystals were etched with 0.3 percent Br-methanol for 2min. The etching was stopped by flashing tha beaker several timea with methanol. In the case of the etching of the substrate, appropriate etching time was used for the thickness of each substrate. Then the etching was stopped by methanol thoroughly.

[4] The dopant alloys of In-Zn and In-Te were etched with diluted HNO_3 (30 percent) for 30sec. It was stopped by the same manner as in [1].

After above mentioned etchings, the substrate, the source crystals, the solvents of Indium, and the dopant alloys were cleaned by methanol and preserved in high purity grade methanol. Then they were dried in natural air by use of a drying lamp, and put on glass spoons. Figure 3-6 shows the photographs of (a) small glass ladles used for ultrasonic cleaning of the source crystals and the substrate and (b) glass spoons used to carry the growth materials into the

(a)

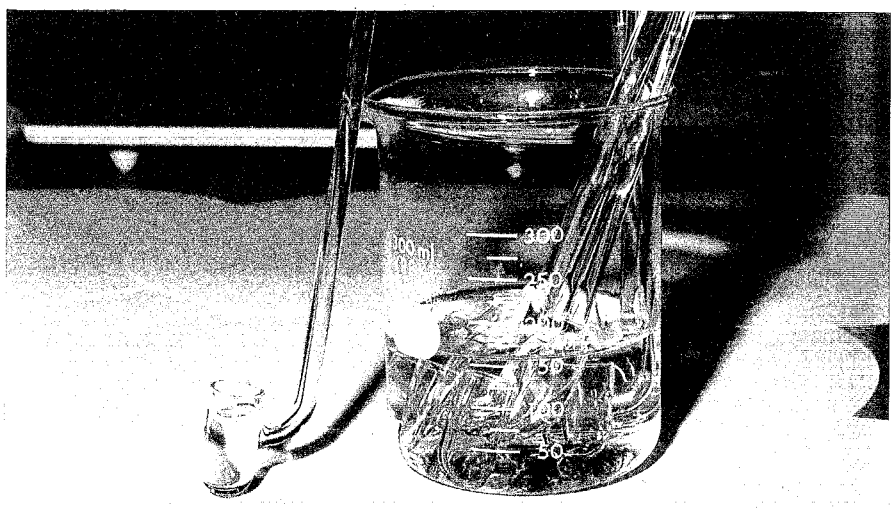

(b)

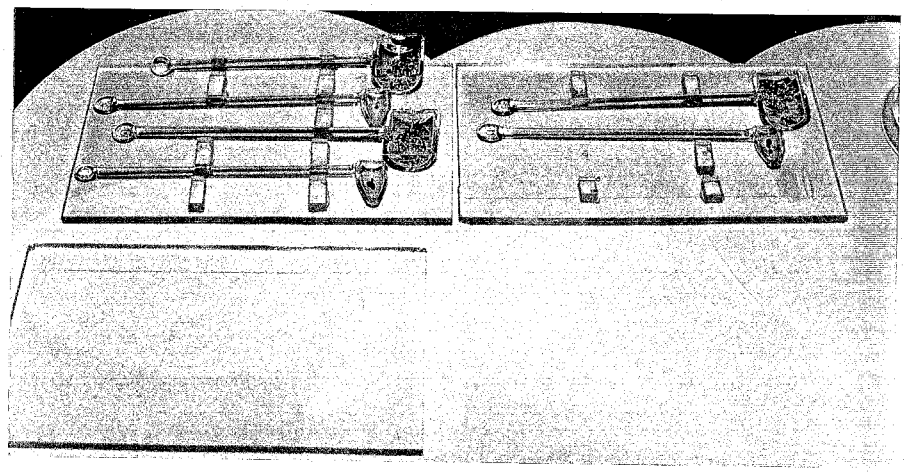

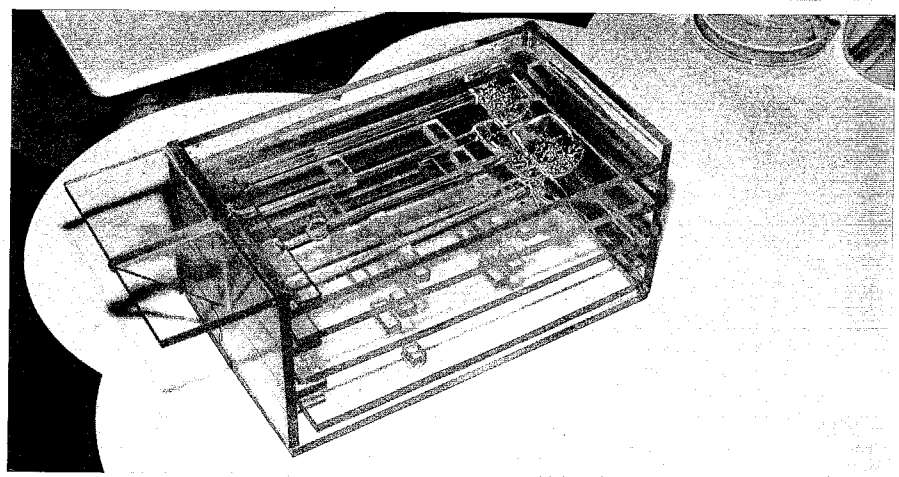

Fig.3-6 Photographs of (a) glass ladles used for ultrasonic cleaning and (b) glass spoons to carry the source materials.

Fig.3-7

(a) Donor concentration of InP as a function of the atomic fraction of Te in Indium, after ref. [337].

(a)

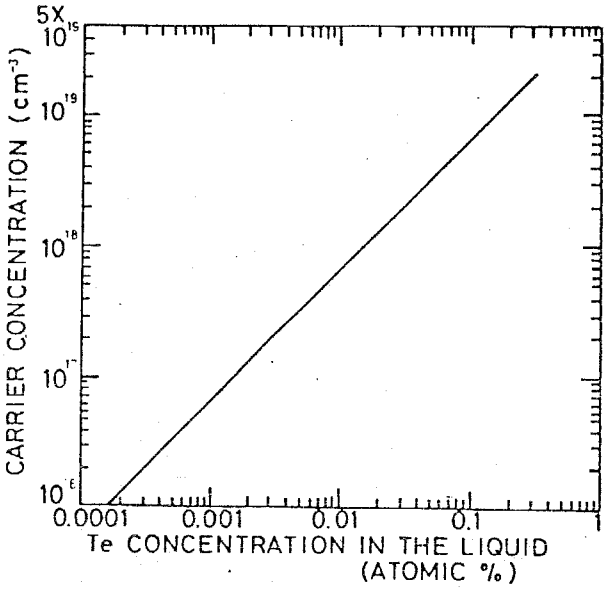

(b) Acceptor concentration of InP as a function of the atomic fraction of Zn in Indium indicated by dashed line after ref.[337], and measured acceptor concentration of the GaInAsP active region using In-Zn alloy indicated by solid line after ref.[338].

(b)

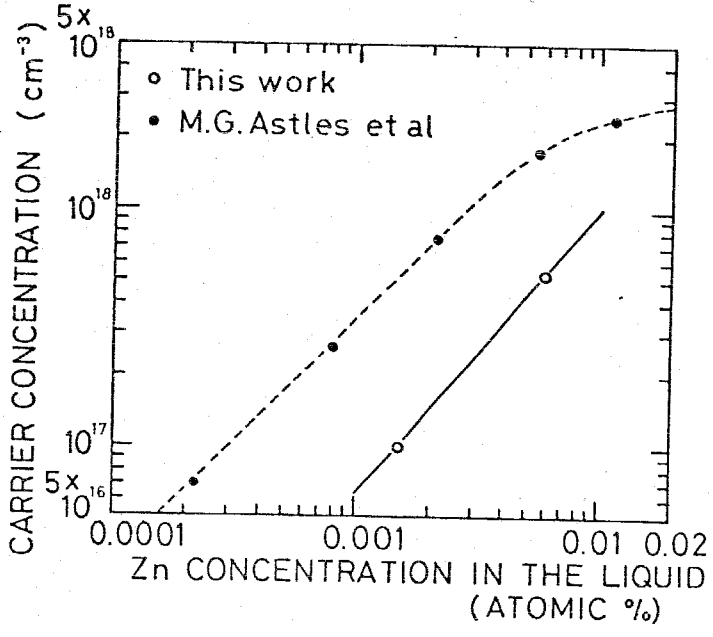

nitrogen box.

In the earlier study of the growth, 5n's or 6n's pure Te and Zn were used as the n and p type dopants, respectively. These dopants have fairly high distribution coefficients. Then the dopant alloys of In-Te and In-Zn were prepared by dissolving the dopants into Indium under the same condition as the wafer growth, that is, after keeping the temperature 670°C for 40min it was cooled down with a cooling rate of 0.8°C/min for 50min and the furnace was moved out.

Other dopant materials Sn and Cd were also tried but their distribution coefficients were much low,which made us afraid of the affection to the growth conditions. Not only that Cd has high vapor pressure at the temperature of 670°C, it sublimated from the solution and congealed to the cool region of reaction tube such like soot.

The donor and acceptor concentrations as a function of the atomic fractions of Te and Zn in Indium are shown in Fig.3-7 (a) and (b), respectively [327]. In Fig.3-7(b), the acceptor concentration measured by C-V characteristic method of the grown wafers using 1 percent (weight) In-Zn alloy is shown as a reference, after Rosental, Itaya, and Suematsu [328].

(3) Growth process

After cleaning and chemical etching, solution sources were loaded into graphite boat in nitrogen ambient gas in order to prevent the oxidation and to keep the loading area clean.

After the loading, the reaction tube was evacuated and

(a)

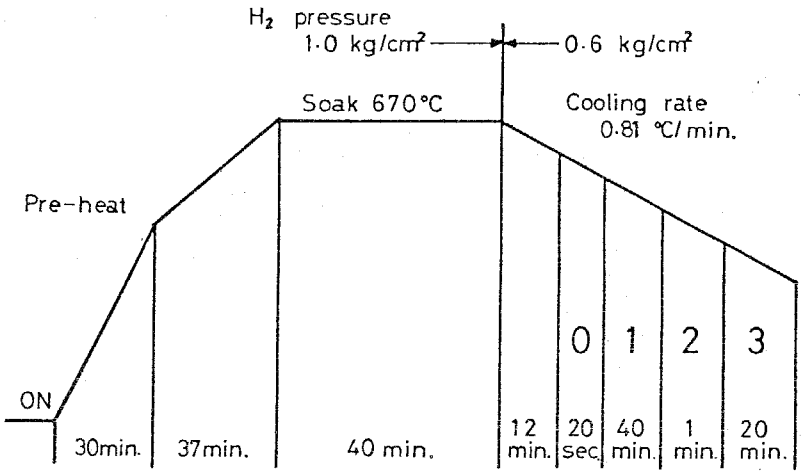

(b)

Two-phase Solution Technique

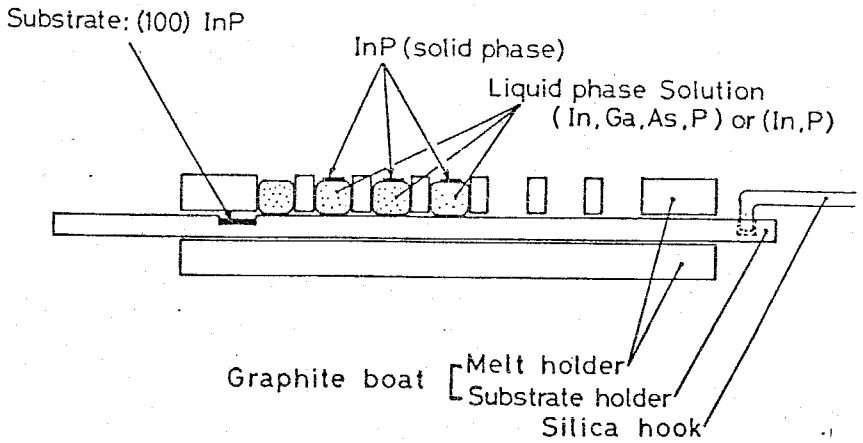

Fig.3-8 (a) An example of growth schedule used for the growth of the three layer structure laser.
(b) Conceptional diagram of the two-phase solution growth technique. Excess of InP source crystal is considered to be floating on Indium solvent during the growth.

flashed with Pd-purified hydrogen gas for 0.5-1hour. Then the DH wafer was grown with the schedule as shown in Fig.3-8. The temperature was raised rapidly to about 630°C in 30min, then slowly raised to the soak temperature of T_s=670°C in 37min, and held there for 40min to dissolve the source crystals into Indium. Then the temperature was lowered with the cooling rate of 0.81°C/min. When it came down to 663°C, the substrate was slid into pure Indium melt and held there for 10sec to remove the gas etched surface. By this procedure the substrate was melted back about 10μm depth. As the depth of melting back was larger at the edge of the substrate, that the first layer of n type InP was grown about 10μm thick to compensate the discrepancy of the substrate orientation caused by the melting back procedure. When the temperature came down to a fixed point of the growth temperature T_g, the substrate was slid into the solution for the growth of GaInAsP active layer. At last a cladding layer of p type InP was grown. However, as there was a problem of melting back of an active layer for longer wavelength lasers(λ>1.5μm), these longer wavelength lasers were realized by different configuration of DH wafer as detailed in section 3.6.

After the growth, Indium left over the substrate was removed by putting it into Hg and wiping off the surface with methanol. Then the grown wafer was applied to the measurement of a lattice matching.

3.4 Growth conditions of lattice matched GaInAsP/InP DH wafer

For the growth of heterostructure crystals it is very

important to get lattice matching between the crystals with different compositions, not only the crystal growth itself, but also from the viewpoint of highly efficient and reliable devices. The lattice mismatch of AlGaAs/GaAs DH structure was ordinary about 0.04-0.05 percent for the value x(Al content ratio) of 0.3-0.4, however highly efficient and reliable devices have been obtained even though such relatively large lattice mismatch exists. On the contrary in the $Ga_yIn_{1-y}As_xP_{1-y}$/InP DH system, complete lattice match can , in principle, be obtained in the wavelength range of 0.92-1.67μm by choosing the appropriate compositions of x and y [179][184][320][323]. So there is a possibility of more reliable devices in this quaternary system than the AlGaAs/GaAs system. In this section the growth conditions of lattice matched (100) GaInAsP/InP DH lasers in the range of 1.11-1.65 μm are given.

The lattice mismatch between GaInAsP quaternary layer and InP layer was evaluated by X-ray diffractometer measurements. In this measurement, the diffraction of Cu-Kα doublet radiation from the (400) plane was used, the lattice mismatch Δa/a (percent) was calculated from the diffracted peak shift angle Δθ (rad) of Cu-$K\alpha_1$ and is given by,

$$\Delta a/a=\Delta\theta\cot\theta \qquad (3\text{-}1)$$

Substituting θ=31.7(deg) into eq.(3-1), the lattice mismatch as a function of Δθ(min) was calculated as shown in Fig.3-9. For example, the diffraction pattern obtained by reflections of Cu-Kα doublet radiation from the (400) planes are shown in Fig.3-10. The estimated lattice mismatch resolution from the

resolution of the diffractometer was less than 0.02 percent in the best condition but usually less than 0.03 percent. As the lattice mismatch was usually within the resolution of our diffractometer, that we refer it only as within of 0.03 percent.

In the super-cooled solution technique, P or Ga fraction in liquid solution was changed in order to get the lattice match [322]. However, adopting the two-phase solution technique, the lattice match can be obtained by changing the As atom fraction.

Following discussion is limited mainly to the case of the two-phase solution technique. The growth solution consists of InP,GaAs, InAs, and In. If the amount of InP and GaAs can be fixed, only the As atom fraction could be controlled by varying the amount of InAs, because the atom fraction of In in the solution is very large compared with the other three elements. In these experiments with use of the LPE apparatus A and the boat A, 1 gram of Indium solvent was used and the amount of InP was fixed to be 10mg. Then the amount of InAs was changed for a given amount of GaAs, and the lattice mismatch of the grown wafer was measured. The lattice mismatch $\Delta a/a$ changed almost linearly with the As atom fraction in the two-phase solution at a given amount of GaAs, as shown in Fig. 3-11. In the same way, the lattice matching conditions of As atom fractions for various amounts of Ga atom fractions were determined experimentally.

Then the dependences of lasing wavelength on the growth temperature T_g and on the amounts of loaded source crystals

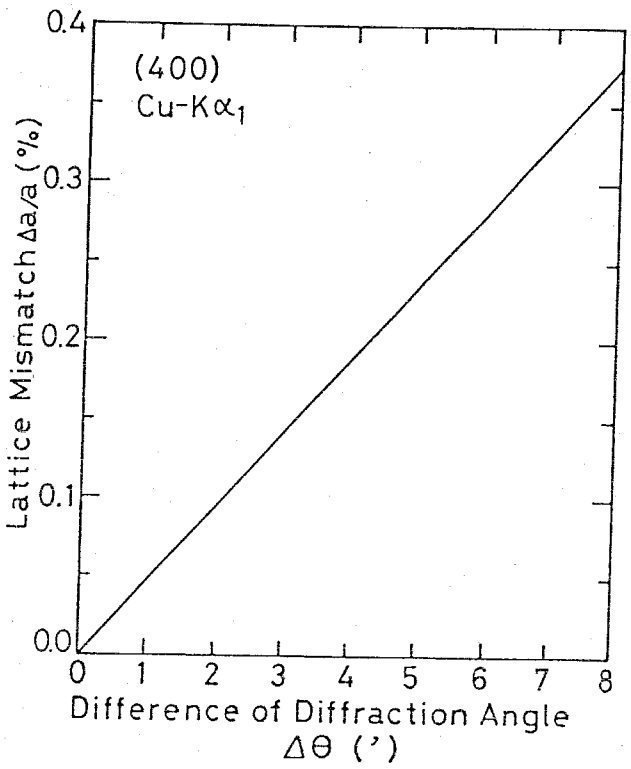

Fig.3-9

Lattice mismatch degree as a function of the diffraction angle difference between $K\alpha_1$ peaks of the GaInAsP and InP.

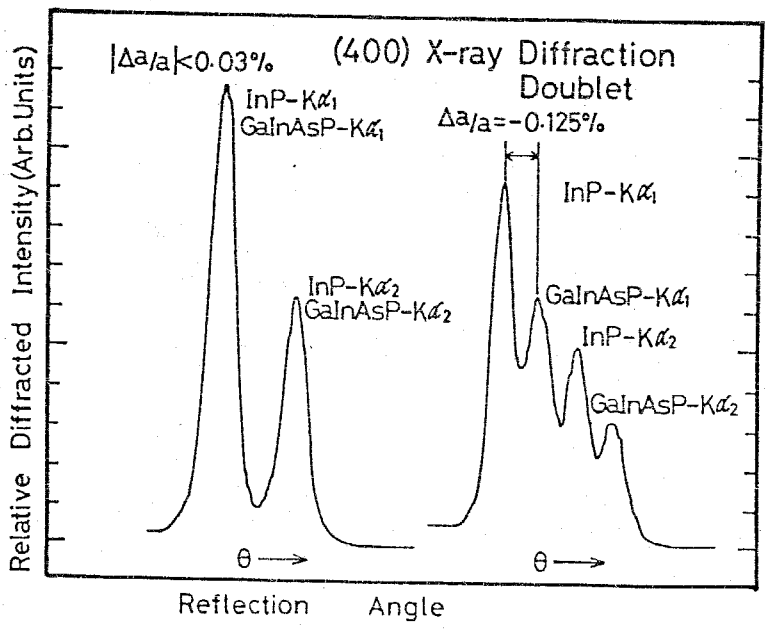

Fig.3-10 Examples of X-ray diffraction patterns of a lattice matched wafer with $\Delta a/a<0.03\%$ and a mismatched wafer with $\Delta a/a=-0.125\%$.

for the lattice matched GaInAsP crystal under the fixed soak temperature T_s were studied. The results are shown in Fig.3-12. The weight of GaAs or InAs for any composition of lattice matched GaInAsP grown on (100) InP can be directly read from Fig.3-12. It is remarkable that in the case of T_g=631°C the lasing wavelength varies linearly with the weight of GaAs in limited range from 1.25μm to 1.55μm. This tendency was also observed with T_g=623°C and the rate of lasing wavelength shift to the amount of the GaAs was 20(nm/mg). Lasing wavelength is so sensitive with the amount of GaAs, that GaAs was weighed quite accurately with an error of less than 1 percent. The lasing wavelength fluctuation of laser diodes cut out from the same wafer was typically about 20nm. So it is possible to obtain a laser emitting at any wavelength with setting error of less than 20nm using the two-phase solution technique. The gradient of the curve on InAs weight corresponds to severity of lattice match because lattice mismatch has a correlation to wavelength shift due to the change of solid composition [322][332]. There is another remarkable point in Fig.3-12: the lattice match is rather severe for the growth of DH wafer of longer wavelength compared with that of shorter one. The growth temperature dependence of lasing wavelength is also read from Fig.3-12. The data are translated, for simplicity, as shown in Fig.3-13, with a parameter of the amount of GaAs. In this figure, three data points (GaAs/In>2 weight percent) are consistent with the other two pairs of data linked by solid lines. The incremental wavelength-growth temperature ratio was $\Delta\lambda/\Delta T_g$=-4.5nm/deg and is in good agreement with

the value of -3.9nm/deg obtained by "step-cooling" technique [332]. When T_g was reduced from 631°C to 623°C with using the same composition of the solution, the lattice mismatch changed only less than 0.05 percent, but in the case of T_g=615°C the amount of InAs for lattice matched growth changed more significantly. From these results concerning lattice match, the two-phase solution technique for this quaternary system is considered to be more stable than the "step-cooling" technique in this limited temperature range. And the above mentioned significant change of the amount of InAs at T_g=615°C is considered to be caused by the nature of large super-cooling temperature [322]. Thus several pairs of Ga and As fractions in the different lasing wavelength were obtained under the temperature condition of (T_s, T_g)=(670°C, 631°C), as given in Table 3-3.

For comparison to other experiments published previously the solid compositions should be known. For this purpose, we simply assumed that the lasing wavelength λ corresponds to the bandgap energy E_g, and obtained it by following relation,

$$E_g(eV)=1.2398/\lambda\ (\mu m). \qquad (3-2)$$

This assumption leads to the error of less than 10 percent in accounting the solid compositions X and y of $Ga_yIn_{1-y}As_xP_{1-x}$. The lattice matched ternary $Ga_{0.47}In_{0.53}As$/InP laser was operated at λ=1.67μm [179][184], the difference between the bandgap wavelength λ_g=1.656μm of the lattice matched GaInAs on (100) oriented InP, which was measured from photoluminescence spectra by Pollack, Nahory, DeWinter, and Ballman [328], was only 15nm.

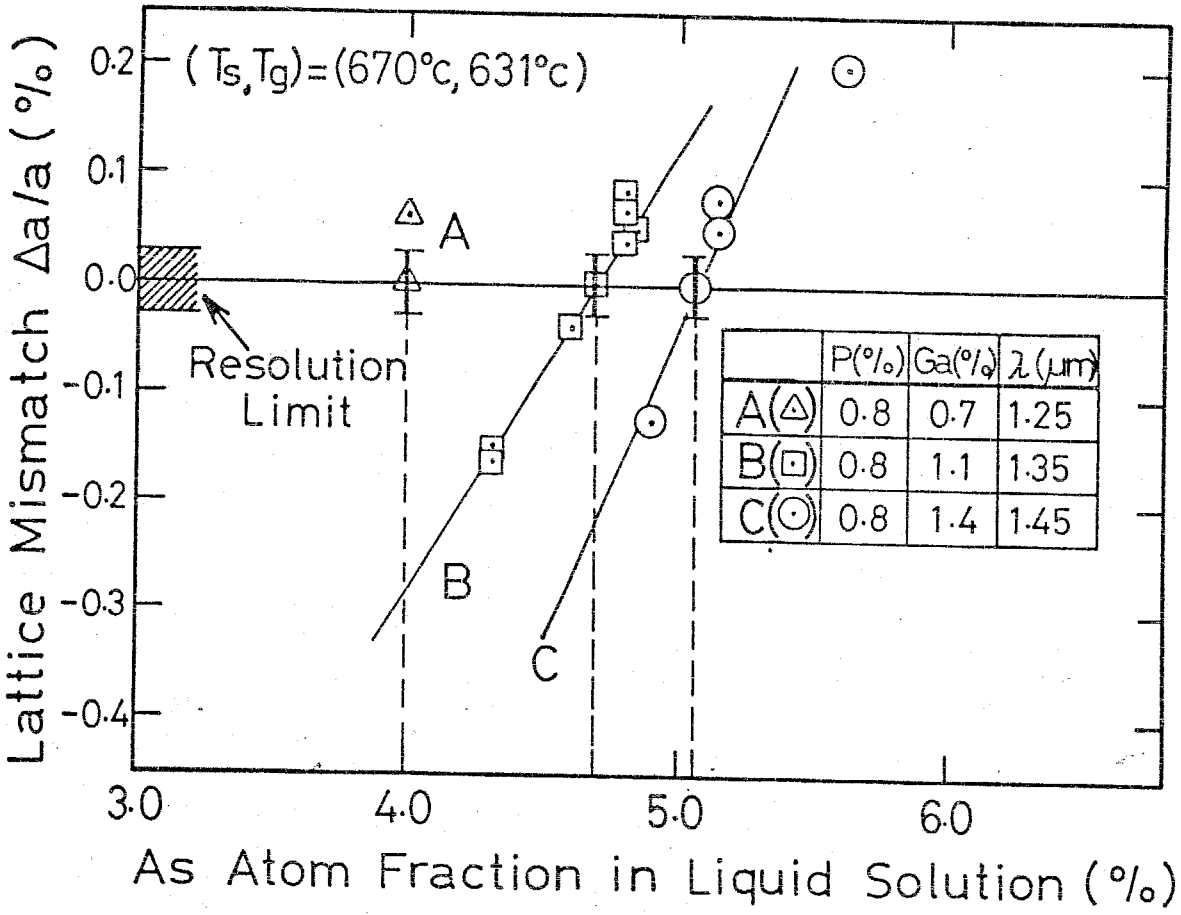

Fig.3-11 Lattice mismatch between the grown GaInAsP and InP crystals as a function of the atom fraction of As in the two-phase solution.

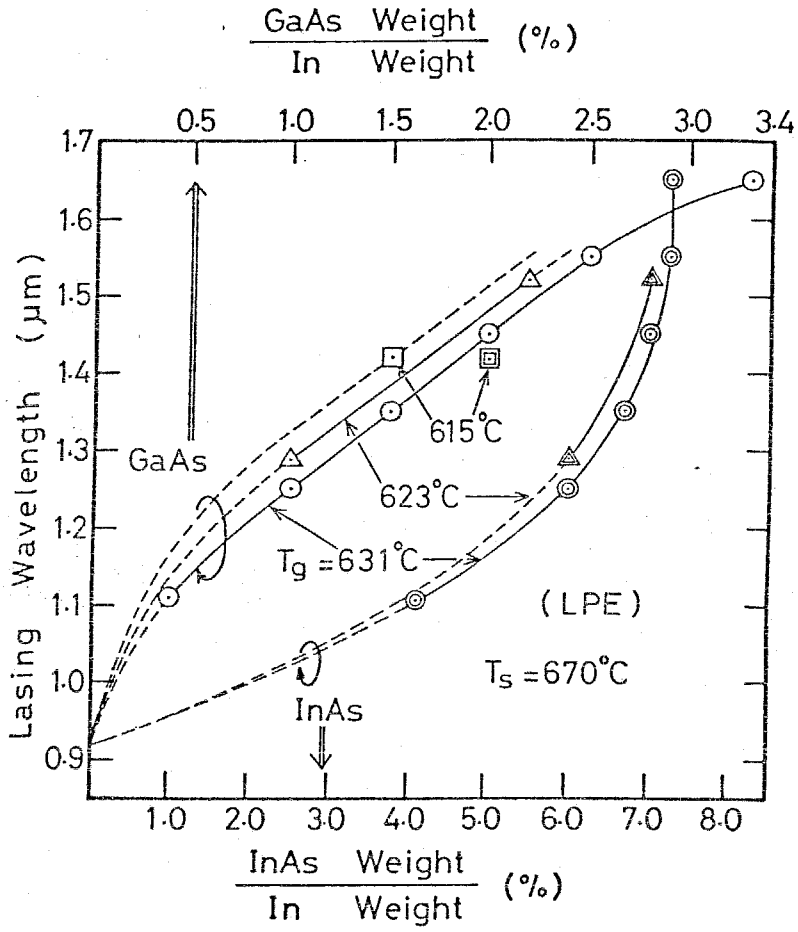

Fig.3-12

Proper amounts of GaAs and InAs crystals for lattice match as a function of the lasing wavelength.

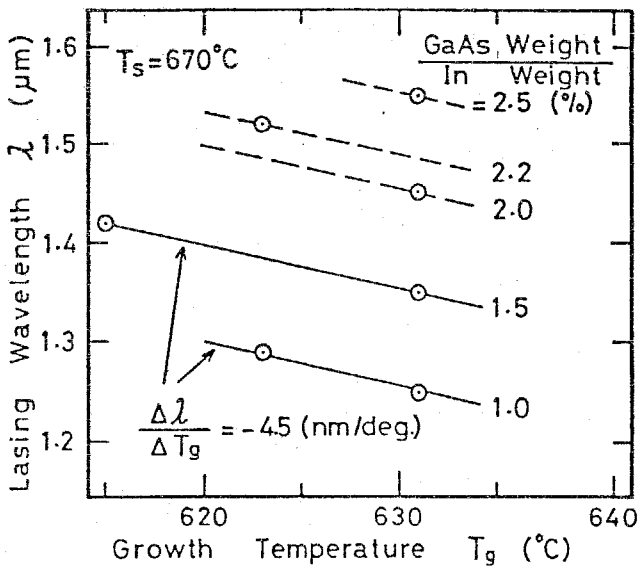

Fig.3-13

Growth temperature effect on the lasing wavelength with a parameter of GaAs amount loaded into the two-phase solution.

Using E_g determined from the lasing wavelength, the solid compositions x and y were estimated with a help of the Vegard's law deduced by Nahory, Pollack, and Johnston [331]. Figure 3-14 shows the As atom fraction in the two-phase solution and thus estimated solid compositions x and y versus Ga atom fraction in the two-phase solution for the growth of lattice matched GaInAsP on (100) oriented InP. In this figure, thus estimated values x and y are about 10-15 percent larger than those by Pollack et al [328], even though the relations of Ga and As fractions in the two-phase solution are almost coincident with each other. The discrepancy seems to be caused by the difference of temperature conditions of T_s and T_g. Even if the lasing wavelength is longer than the bandgap wavelength about 20nm at around λ_g=1.65μm, the difference of λ of here obtained data and λ_g of Pollack's data should be less than 40nm because the difference of T_g is only 4°C and $\Delta\lambda/\Delta T_g$=-4.5 nm/deg. But it was about 100nm and 50nm for λ=1.55μm and 1.35 μm, respectively. Then there are two chances which cause this discrepancy, one is the absolute temperature difference due to the difference of graphite boat structure, and the other is the difference of the amount of InP loaded in excess in the two-phase solution because the melt composition changes during the growth on floating InP. The curve of As atom fraction in the two-phase solution changes smoothly into a straight line as indicated by the dashed line as shown in Fig.3-14. The incline in this line ΔAs(a/o)/ΔGa(a/o) is almost unity. This means that the amount of InAs need not be changed in the straight line region, when the amount of GaAs was changed.

Table 3-3 Atom fractions of Ga and As in the two-phase solution for lattice match, the averaged lasing wavelength, and distribution coefficients of Ga and As.

Atom Fraction			Solid Composition		Distribution Coefficient	
Ga(a/o)	As(a/o)	λ(μm)	x	y	k_{Ga}	k_{As}
0.30	2.26	1.11	0.343	0.157	26.2	6.45
0.72	4.01	1.25	0.547	0.252	17.5	6.83
1.06	4.71	1.35	0.676	0.312	14.7	7.17
1.40	5.14	1.45	0.792	0.368	13.1	7.70
1.74	5.55	1.55	0.899	0.419	12.0	8.10
2.27	6.06	1.65	0.997	0.466	10.3	8.23

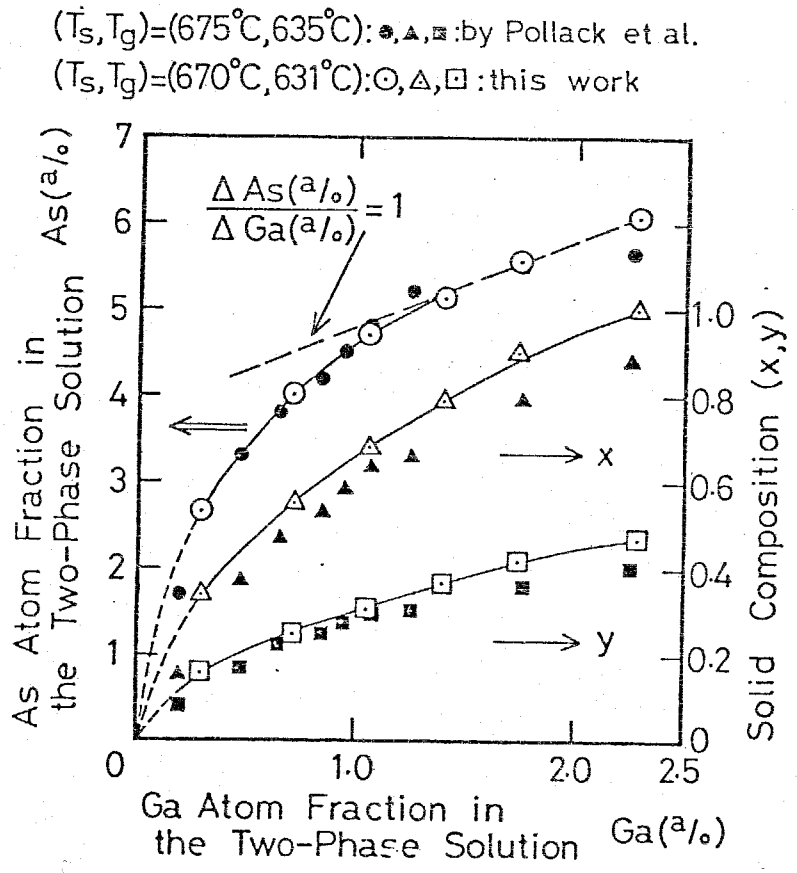

Fig.3-14 Arsenic atom fraction in the two-phase solution and solid compositions x and y for the lattice matched wafer as a function of Ga atom fraction in the solution.
Previously reported data are included for reference [328].

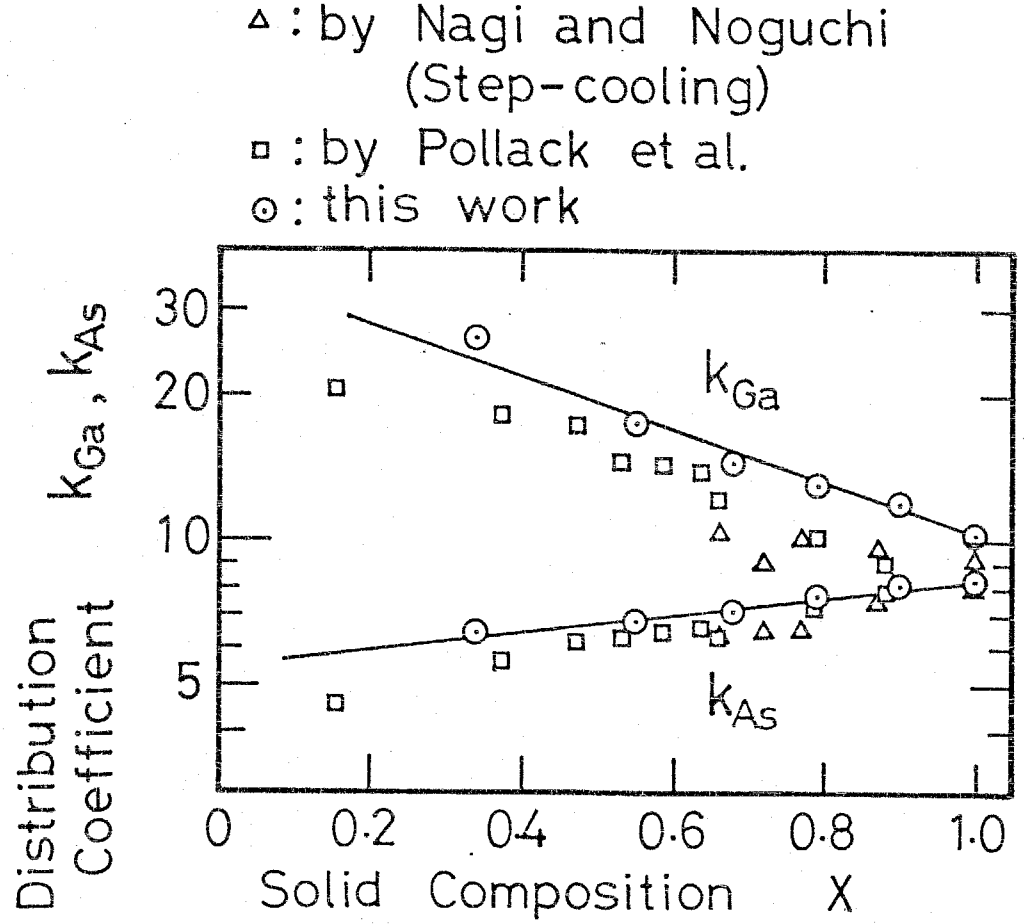

Fig.3-15 Distribution coefficients k_{Ga} and k_{As} as a function of solid composition x with two references [324][328]. Data point indicated by a triangle was calculated after ref.[324], and obtained by step-cooling technique.

The others were obtained by two-phase solution technique.

The distibution coefficients of Ga and As were calculated from following relations,

$$K_{Ga}=100y/2Ga(a/o), \qquad K_{As}=100x/2As(a/o). \quad (3\text{-}3)$$

These values are not exactly correct because the solution composition varies from the initially loaded composition due to the crystal growth on the surface of floating InP during the cooling time. In Fig.3-15, K_{Ga} and K_{As} are shown as a function of solid composition x, and in comparison, data obtained by Nagai and Noguchi for step-cooling technique under the conditions of T_g=637°C with the step-cool temperature of Δt=10°C are given [324].

The data obtained in this study are relatively larger at any composition value of x compared with other data, it is considered to be caused by lower growth temperature [325]. There were other reports about the distribution coefficients of Ga and As obtained by step-cooling technique with T_g=640°C and Δt=10°C for small range of x [325][327].

The thickness of the quaternary crystal layer was measured by means of a scanning electron microscope(SEM) after cleaving and etching the grown wafer with the solution of diluted KOH and $K_3Fe(CN)_6$. This etchant was prepared by following procedures.

[1] 5-7 grains of KOH(250mg) were dissolved in 4cc of warmed pure water(40°C).---solution A

[2] 250mg of $K_3Fe(CN)_6$ was dissolved in 4cc of warmed pure water(40°C)----------solution B

[3] Solutions A and B were mixed just before the usage.

This etchant etches much faster the GaInAsP layer than

InP layer, however the etching time of less than 10sec is enough to observe the thickness.

There are several reports about growth conditions of lattice matched GaInAsP on InP, but the dependence of the growth speed on the compositions of quaternary crystal was not previously reported. For more complicated functional devices (e.g., ITG laser), which need precise thickness control of each layer, it is important to know growth speed of various compositions of GaInAsP. Active layer thickness d of the DH wafer with a configuration of InP(n)/GaInAsP(undoped) /InP(p) is shown in Fig.3-16 as a function of growth time t with a parameter of lasing wavelength λ. But concerning the two data points of λ=1.05μm, we could not obtain a laser oscillation from the grown wafer so λ was estimated from the compositions of the two-phase solution using Fig.3-12. The active layer thickness d varied in proportion to $t^{0.7}$ for various wavelength lasers within an investigated time range. The growth speed increased with lasing wavelength due to larger amount of sources in the solution. So, the growth was considered to be done by supercooling and the initial cooling temperature was determined by the amount of sources in the solution [321]. Next we compared the growth speed of different growth temperatures T_g=615°C and 631°C, as shown in Fig.3-17. In this case, the same amount of GaAs was used but the amount of InAs was chnged to obtain lattice match as shown in Fig. 3-12. The slower growth speed can be obtained by lowering the growth temperature with the same cooling rate even if the wavelength of a laser is longer. However, in the range

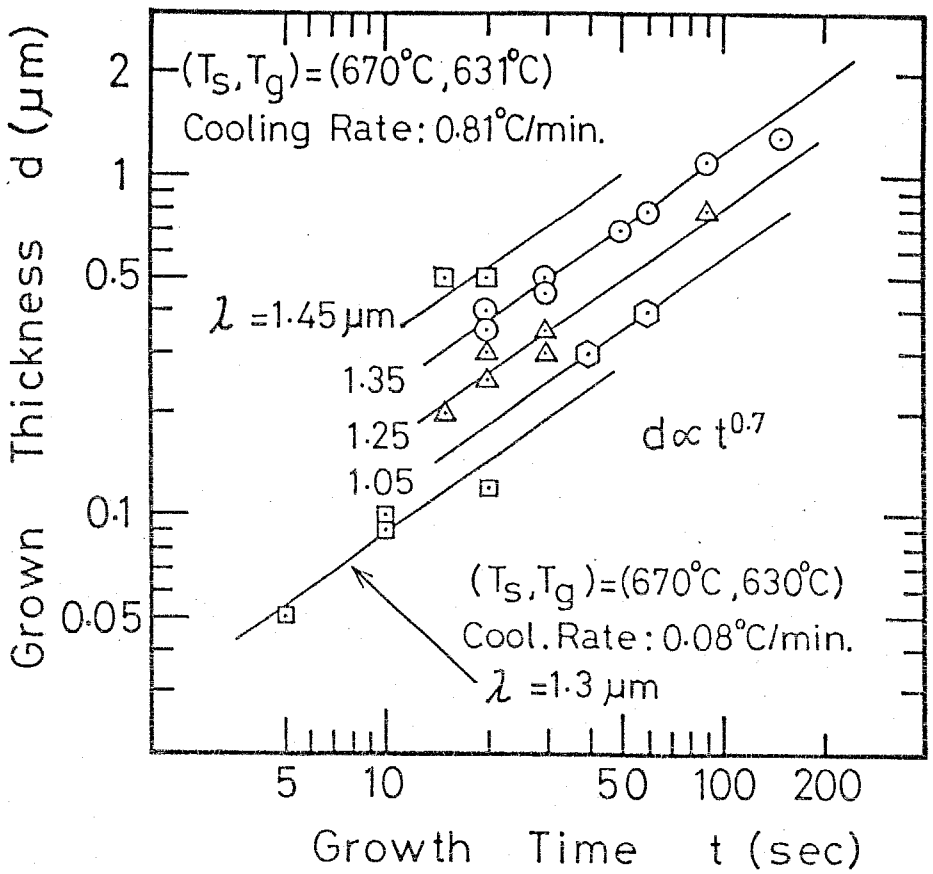

Fig.3-16 Active layer thickness as a function of growth time for the three layer structure DH wafer with a parameter of the lasing wavelength. Growth conditions (T_s, T_g, and a cooling rate) were fixed.

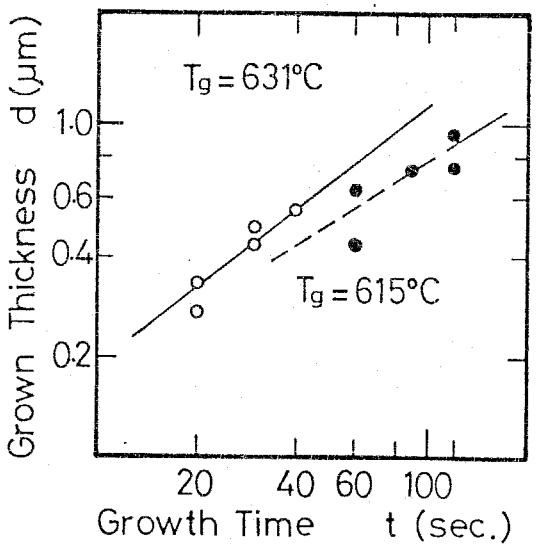

Fig.3-17

Active layer thickness as a function of growth time for the three layer structure DH wafer with a parameter of growth temperature T_g.

The composition of the solution was changed to get lattice match.

indicated by the dashed line for T_g=615°C, we could not obtain a flat active layer. Much slower growth speed was also obtained by lowering the cooling rate, typically 0.05μm/5sec at the cooling rate of 0.08°C/min, as will be described in the next session.

3.5 Comparison of the growth characteristics between the LPE apparatus A and B

The growth conditions for lattice matched GaInAsP crystal and the growth speed of it were also investigated by use of the LPE furnace B and the boat B with the various temperature conditions of (T_s, T_g)=(670°C, 630°C), (670°C, 615°C), and (630°C, 615°C). for all these cases, 5g of Indium was used to get the same thickness of the solution as used in the LPE apparatus A. 50mg and 37mg of InP source crystals were used for the cases of the soak temperature T_s of 670°C and 630°C, respectively.

The amounts of GaAs and InAs for lattice match are shown in Fig.3-18(a) and (b) as a function of the lasing wavelength with the data obtained by the LPE apparatus A mentioned in former session. The tendency in the lattice match conditions is almost as same as that of the former one, however the lasing wavelength was a few tens nm shorter in this investigation. This discrepancy is considered to be caused by the difference of impurity levels, the threshold condition, and of the growth solution condition, not by the difference of LPE furnace. Because the discrepancy was cancelled by introducing the same amounts of dopants and the same kind of boat B into the growth by the LPE furnace A.

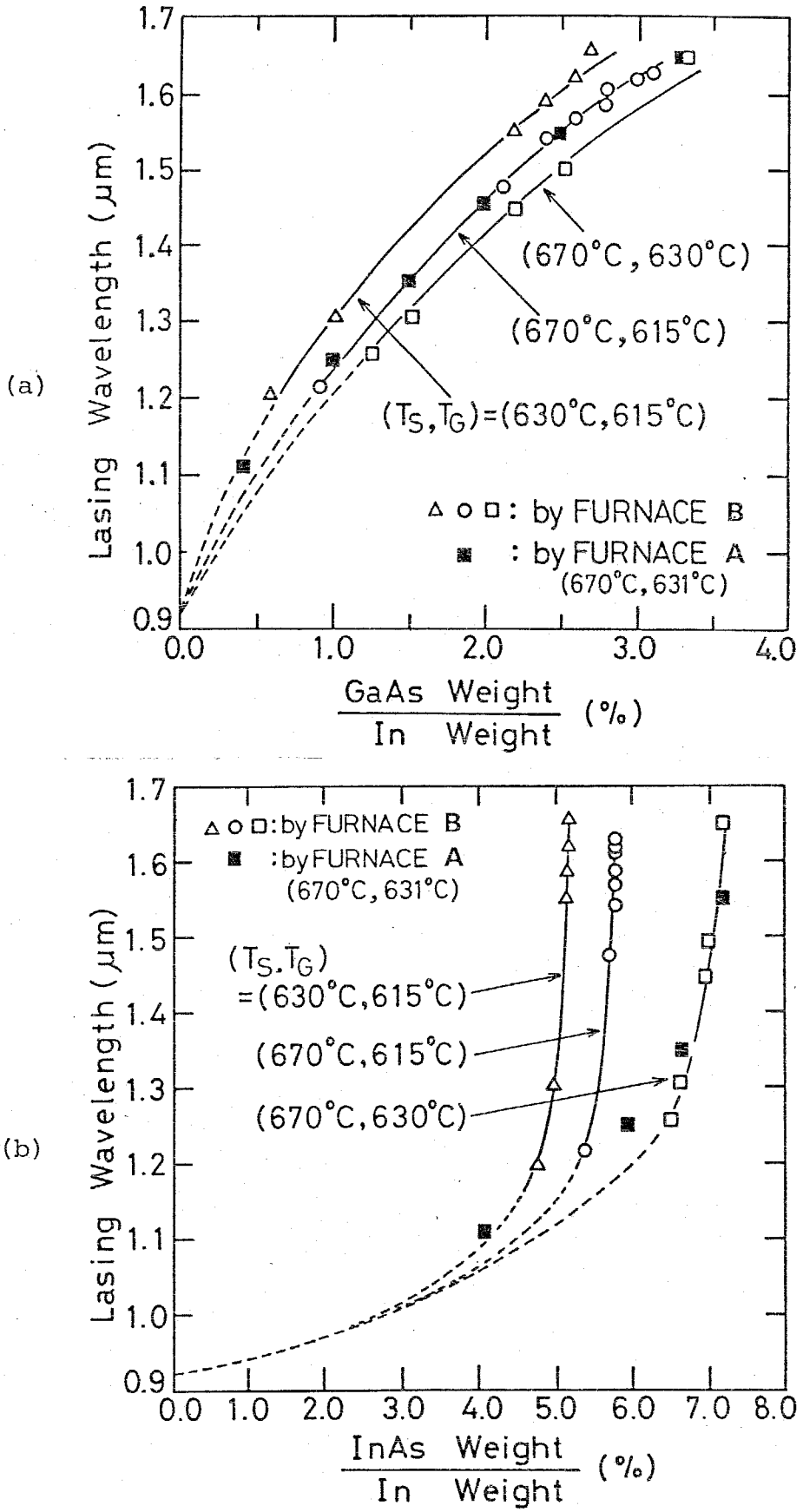

Fig.3-18 Proper amounts of (a) GaAs and (b) InAs for lattice match as a function of the lasing wavelength.

The growth speed of the longer wavelength GaInAsP crystal was larger as can be seen in Fig.3-16, the low growth temperature and the low cooling rate were necessary to control the layer thickness precisely in order to get the longer wavelength GaInAsP/InP ITG laser. Figure 3-19 shows the grown layer thickness of GaInAsP with the lasing wavelength of 1.62 μm as a function of the growth time. The lower growth speed was obtained for the lower growth temperature when the soak temperature was fixed at 670°C. However, it became much larger when the soak temperature was lowered to 630°C. These results were considered to be caused by the reduction of the initial cooling temperature during the cooling time before the growth of the quaternary layer.

3.6 Solution of meltback problem

It is very difficult to grow a longer wavelength GaInAsP/InP DH wafer, where an active layer of GaInAsP crystal is sandwiched by InP confining layers, because the quaternary layer of longer wavelength composition tends to dissolve into the solution of Indium and Phosphorus. This tendency seems to be stronger when the lasing wavelength is longer. This "melt-back" is caused by the difference between the liquid atomic fractions of P and As. The degree of super-cooling should be defined to the substrate, in other words, it changes with the substrate crystal even if the same solution was used. When the meltback occurs, the degree of super-cooling temperature can be considered to be negative. A solution for this problem is to increase the degree of super-cooling temperature for the

substrate of an As rich quaternary crystal.

From that reason, Nagai and Noguchi used the quaternary crystal with the corresponding wavelength of 1.05μm as a cladding layer to get DH lasers for the first time [174]. However the threshold current density of the lasers of this "quaternary cladding structure" was not sufficiently low compared with that of an ordinary symmetrical structure using InP cladding layers [176][180]. The cause of higher threshold was considered to be the lack of the barrier height of hetero interface between the active layer and the quaternary cladding layer. Then the cladding layer of InP was required to get a low threshold longer wavelength lasers. One of the solutions of it was an insertion of a quaternary layer between the active layer and InP cladding layer. This quaternary layer was used only to prevent the meltback not to confine the carriers, this is why it was named an "anti-melt-back(AMB) layer". Another solution was a reduction of the growth temperature to about 590°C [197]. However, the growth temperature can not be reduced at will, there is a limit wavelength of the laser grown by this way.

Using this AMB layer, $Ga_{0.47}In_{0.53}As$/InP DH lasers were obtained at the emission wavelength of 1.67μm. Figure 3-20 shows the X-ray diffraction pattern of this four-layer structure wafer. Complete lattice match was obtained with this structure. Figure 3-21 shows the SEM photograph of cross section of DH wafers of (a) ordinary three layer structure and (b) four layer structure with the AMB layer.

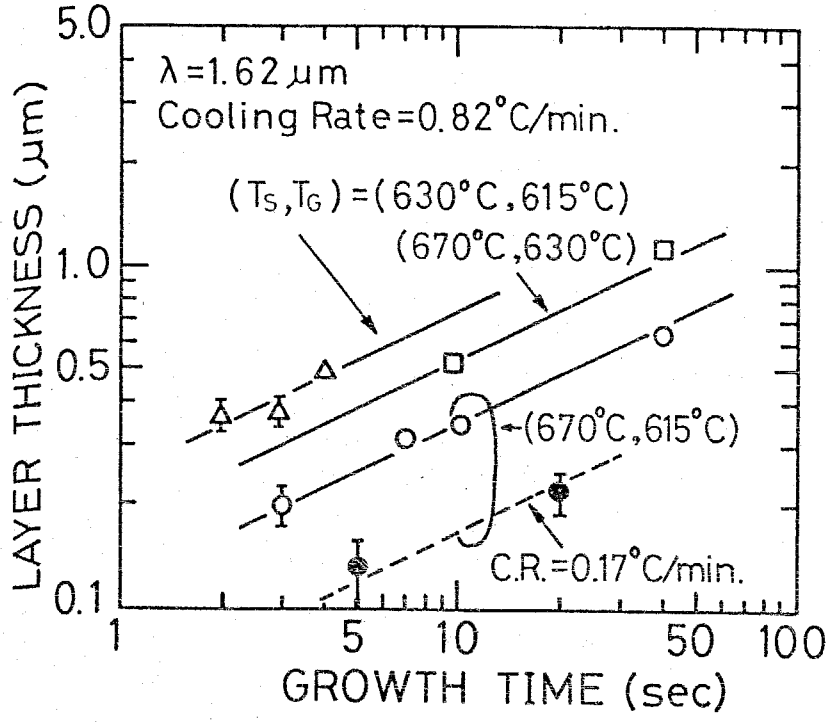

Fig.3-19

Active layer thickness as a function of growth time for the GaInAsP crystal of 1.62μm wavelength.

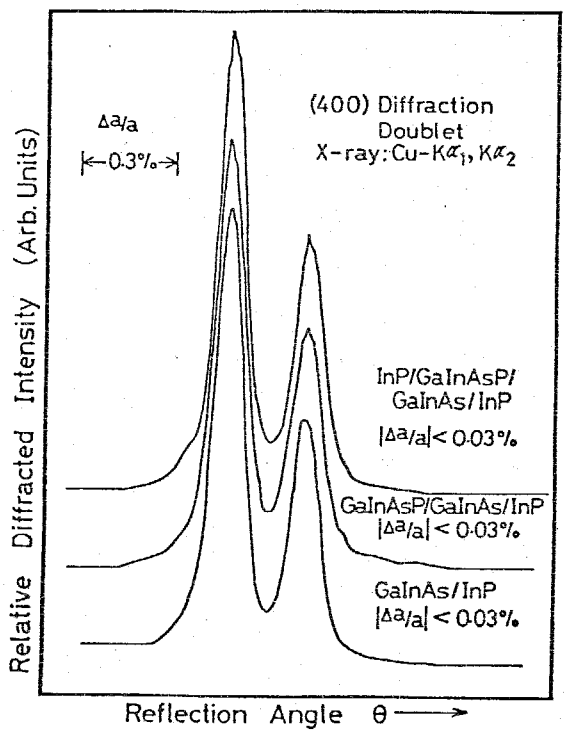

Fig.3-20

X-ray diffraction pattern of four layer structure DH wafer with the "anti-melt-back" layer.

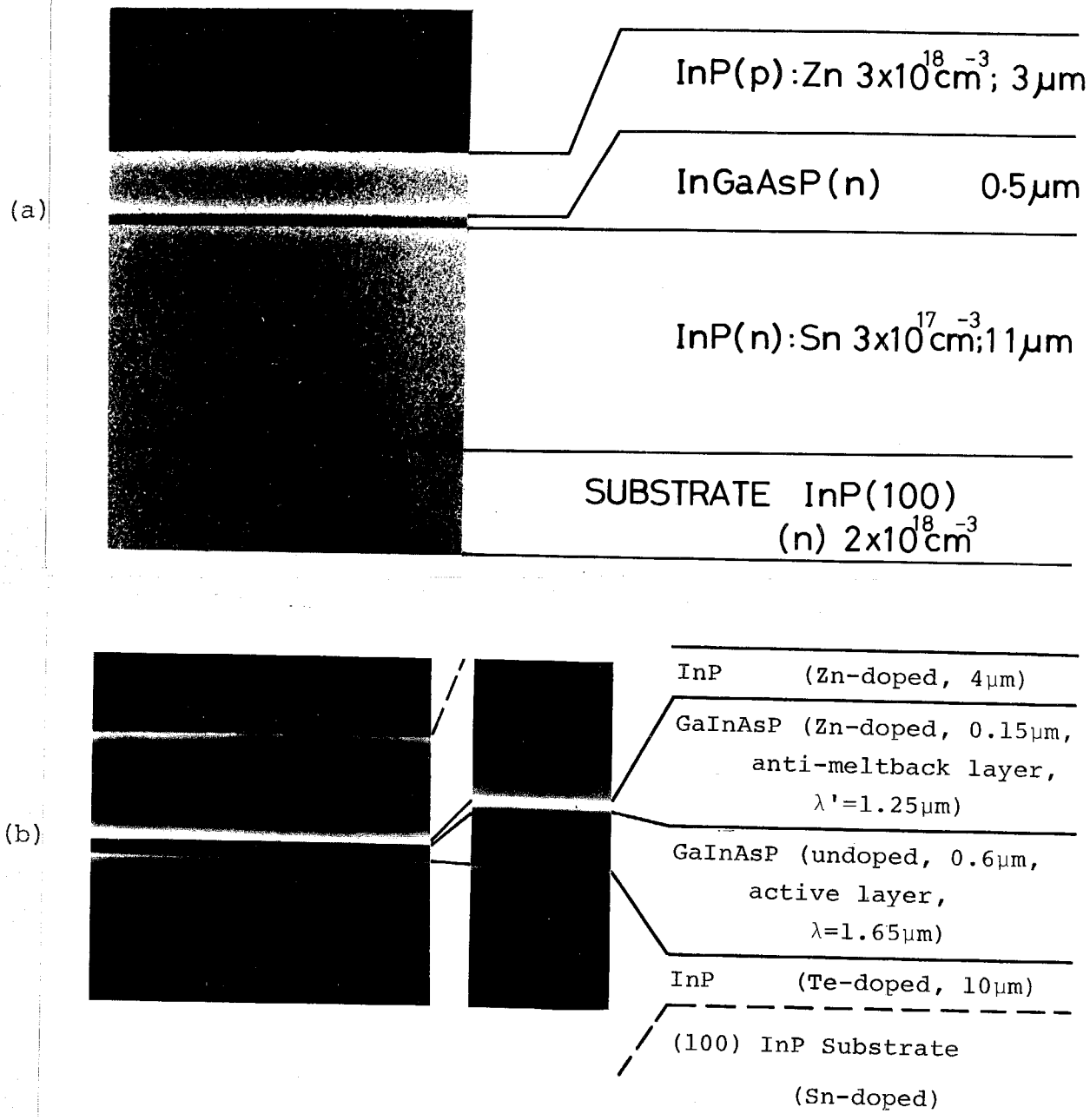

Fig.3-21 SEM photographs of cleaved and etched cross sections of DH wafers, (a) ordinary three layer structure with the lasing wavelength of 1.35μm, (b) four layer structure with the lasing wavelength of 1.65μm and the corresponding wavelength of the anti-melt-back(AMB) layer of 1.25μm.

3.7 Conclusion

A new structure GaInAsP/InP longer wavelength laser with an additional quaternary layer called "anti-melt-back(AMB)" layer was proposed to prevent the meltback problem during the liquid phase epitaxial growth.

The growth conditions of GaInAsP lattice matched to (100) oriented InP substrate were clarified for the almost complete wavelength range by use of the two-phase solution technique.

The growth temperature dependences of the growth conditions and the growth speed was clarified.

CHAPTER 4 1.5 - 1.6 μm WAVELENGTH GaInAsP/InP DH LASERS WITH ANTI-MELT-BACK (AMB) LAYER

4.1 Introduction

In this chapter the lasing properties of the GaInAsP/InP DH lasers grown by the two-phase solution technique are given. The threshold current densities of 1.5-1.6μm wavelength GaInAsP/InP DH lasers with an additional "anti-melt-back(AMB) layer" structure are given in comparison with the ordinary structure GaInAsP/InP lasers. The temperature dependences of the threshold current, the lasing wavelength, and the spontaneous emission spectrum are given for the various wavelength lasers. Finally, room temperature CW operations of 1.5-1.6μm wavelength GaInAsP/InP DH lasers with SiO_2 defined stripe structure are presented.

4.2 Fabrication of laser diode

After the growth of GaInAsP/InP DH wafer, injection lasers were fabricated with a broad area contact structure and an SiO_2 defined stripe structure. Fabrication processes of the oxide stripe lasers are given as follows.

[1] The grown wafer was put into Hg to remove Indium left over. Both upper and down surfaces were wiped by absorbent cotton damped with methanol.

[2] Cleaning the wafer surface by the same manner in [1] with acetone, methanol, and trichloroethylene, successively.

[3] Depositing SiO_2 on the surface with the thickness of

200-300nm by chemical vapor deposition technique.

[4] Cleaning the wafer by the same manner in [1] with acetone and methanol.

[5] Drying for 30-40min at 100°C.

[6] Spreading the photoresist of AZ-1350 on the wafer with the spinner condition of 4000rpm for 30sec.

[7] Prebaking for 30min at 90-100°C.

[8] Mask alignement and exposure. Exposure time of 1-2sec was used for 10-30μm wide stripe windows by the light source of mercury lamp.

[9] Development was done for 2sec in AZ-1350 developer. Washing in pure water and blowing the water drops off.

[10] Post baking for 30min at 120-140°C.

[11] Etching of SiO_2 film by the solution of NH_4F(40g)+HF (14cc)+H_2O(100cc) for 50-60sec. Washing in pure water.

[12] Removing the photoresist by AZ-1350 remover at 60-70°C. Washing in pure water.

[13] Zn diffusion by use of vacuum closed quartz ample. The diameter and the length of the ample were 10mm and 10cm, respectively. 10mg of ZnP_2 and 10mg of $ZnAs_2$ were used as the diffusion sources. This ample was inserted into the diffusion furnace for 2-3min and pushed into water.

[14] Polishing the substrate side of the wafer to a thickness of about 100-150μm.

[15] Evaporations of Au(80mg)/Zn(15mg) and Au(80mg)/Sn(15mg) to the p and n type sides, respectively.

[16] Alloying in high pure hydrogen atmosphere for 2min at 410-420°C.

[17] Evaporations of Au(40mg) and In(60mg) to the p type side.

[18] Cleavage to form facet mirrors.

In the case of the fabrication of the broad area contact lasers, the processes of [3]-[13] and [17] were avoided.

4.3 Threshold current density

Laser diodes were cut out by cleavage with the cavity length of 200-400μm. For broad contact lasers the width was chosen to be about a half of the cavity length. Then the laser diode was mounted on an Indium bed on an Au-plated copper block, with p side down, as shown in Fig.4-1. These lasers were operated under pulsed condition, at first, with the pulse repetition rate and the width of 1KHz and 200-400nsec, respectively. Figure 4-2 shows (a) the photograph and (b) the schematic diagram of the pulse driving circuit. In the measurement of the injected current versus the light output characteristic, Ge-APD was used as a detector. The size of a laser diode was measured by a surface end type microscope with the accuracy of 2μm. In the measurement of the lasing wavelength, Ge solar cell of one inch diameter combined to a low noise amplifier circuit was used because there was no other detector material available for the wavelength region of 1.5-1.6μm and it was very difficult to use Ge-APD for this measurement due to the small size. Figure 4-3 shows the schematic diagram of the detection circuit together with the outlook of it.

Threshold current density J_{th} normalized by the active layer thickness d is a convenient parameter for evaluating the quality of the grown crystal, the resonator structure, and the

smoothness of the active layer. J_{th} of various wavelength lasers were measured under above mentioned pulsed condition and the results are shown in Table 4-1 with the thickness of the active layer and that of the AMB layer. In this Table, the samples of wafer No.3 were SiO_2 defined stripe lasers with the stripe width of 25μm, others were broad contact type lasers. J_{th}/d of these lasers were approximately 5-6KA/cm^2/μm in the wavelength range of 1.45-1.65μm. It is almost comparable to the value 5.3KA/cm^2/μm of $Ga_{0.47}In_{0.53}As/InP$ ordinary structure laser obtained by the molecular beam epitaxial growth technique [176] and also to the value 4-5KA/cm^2/μm of 1.52μm wavelength ordinary structure GaInAsP/InP lasers obtained by the two-phase solution technique with lower growth temperature of T_g=623°C. Normalized threshold current density and the threshold current density of both ordinary structure laser and the four layer structure with AMB layer are shown in Fig. 4-4 as a function of the lasing wavelength averaged in the wafer. Slightly higher value of J_{th}/d of the four layer structure laser was caused by the thinner active layer thickness (for the lasing wavelength λ of more than 1.5μm), and for the lasers with the lasing wavelength of 1.45μm, it was due to the lack of the barrier height between the active layer and AMB layer. At the lasing wavelength of 1.1μm, J_{th}/d was 1.5times higher than that of longer wavelength lasers of λ>1.2 μm, where the leakage current flowing over the hetero barrier is dominant although the barrier height is estimated to be 0.23eV. Assuming that the active layer is thick enough and the loss of external cladding region can be neglected, and the

(a)

(b)

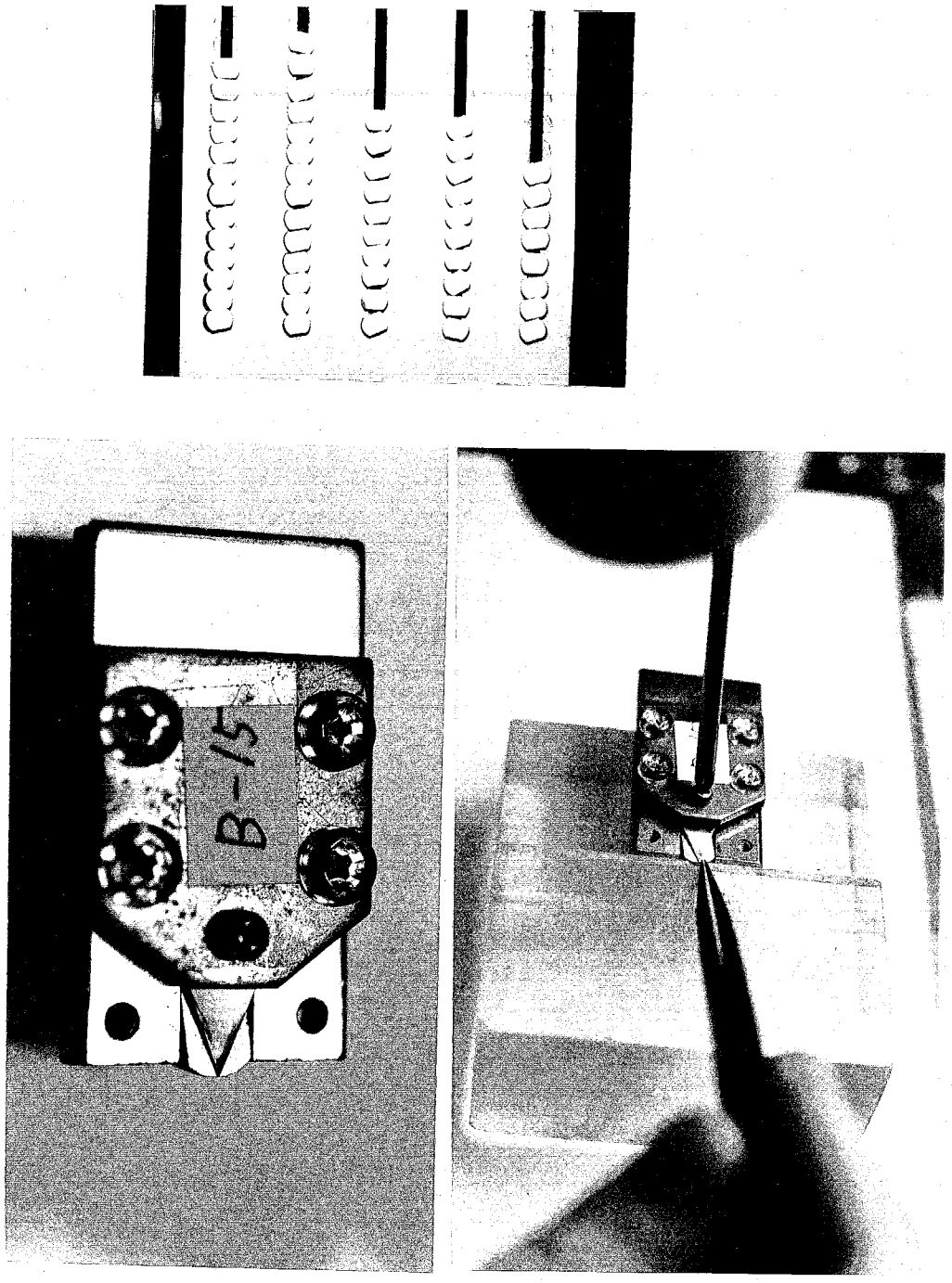

Fig.4-1 Photographs of the laser mount. Laser diode was set on (a) an Indium bed on an Au-plated copper block and fixed by (b) an Au-plated pin. The screw seen in the center of the mount was used to press the diode down. (Designed by S.Akiba)

(a)

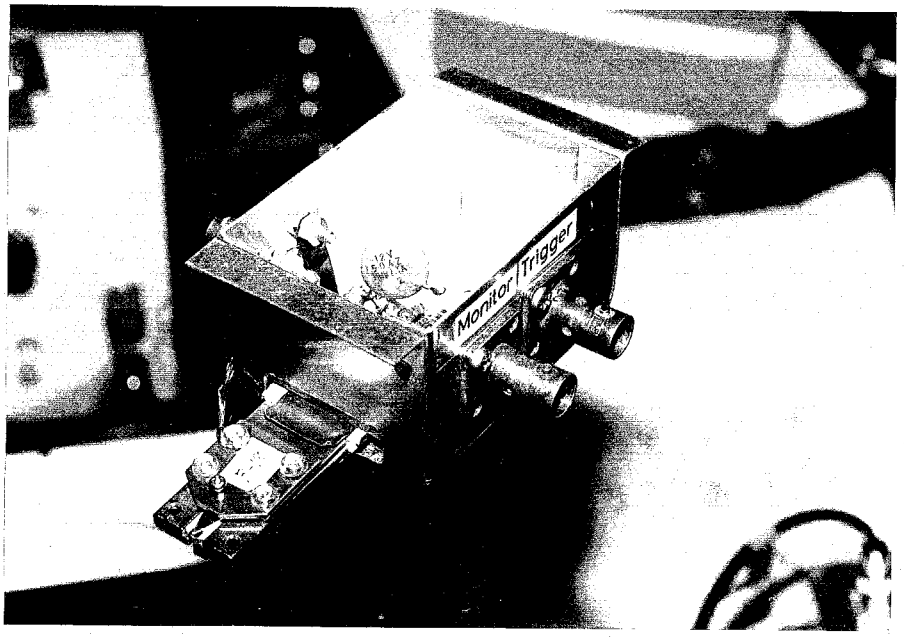

(b)

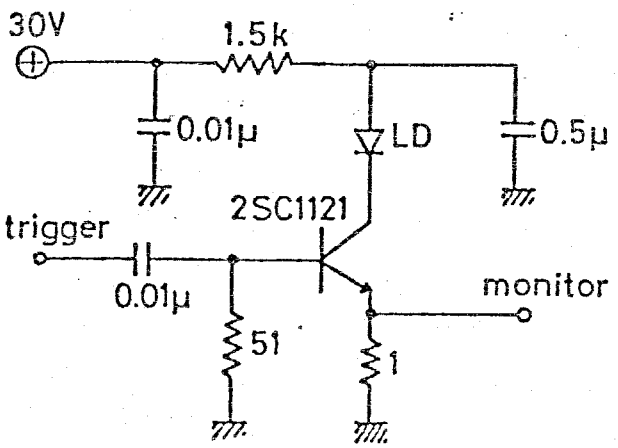

Fig.4-2 (a) Photograph of the pulse current driving circuit.
(b) Schematic diagram of the driving circuit.

(a)

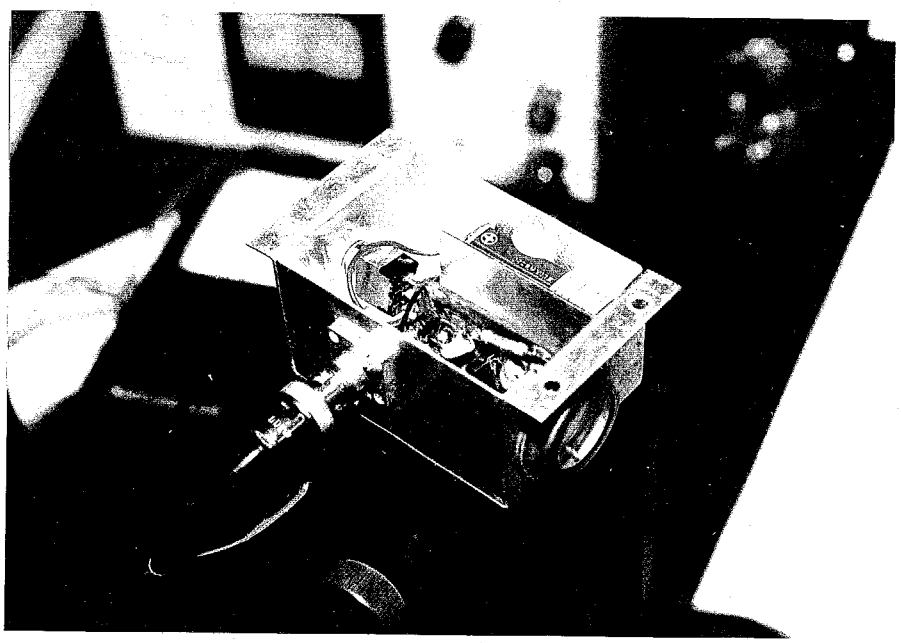

(b)

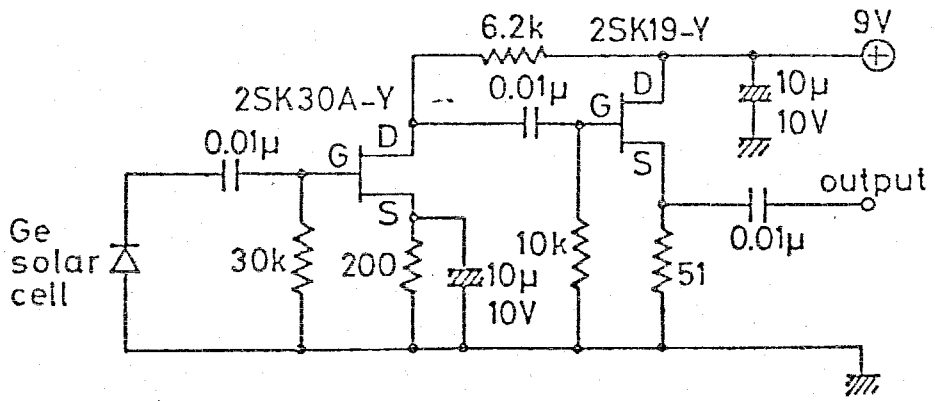

Fig.4-3 (a) Photograph of the detection circuit used for pulse operating measurement.
(b) Schematic diagram of the detection circuit. Bias voltage was supplied by a dry battery cell packed in the unit.
(Designed by H.Kawanishi)

Table 4-1 Active layer thickness and threshold current density of four layer structure lasers with AMB layer. d and d' are thickness of active and AMB layers, respectively.

Waf. No.	λ (μm)	d (μm)	d' (μm)	J_{th} (KA/cm^2)
1	1.45	0.30	0.05	1.7~2.2
2	1.50	0.60	0.17	3.0~3.6
3	1.51	0.40	0.10	2.0~3.0
4	1.53	0.30	0.20	1.5~1.9
5	1.59	0.25	0.15	1.6~2.0
6	1.60	0.15	0.10	1.2~1.8
7	1.62	0.30	0.10	1.7~2.0
8	1.65	0.60	0.15	2.5~3.6

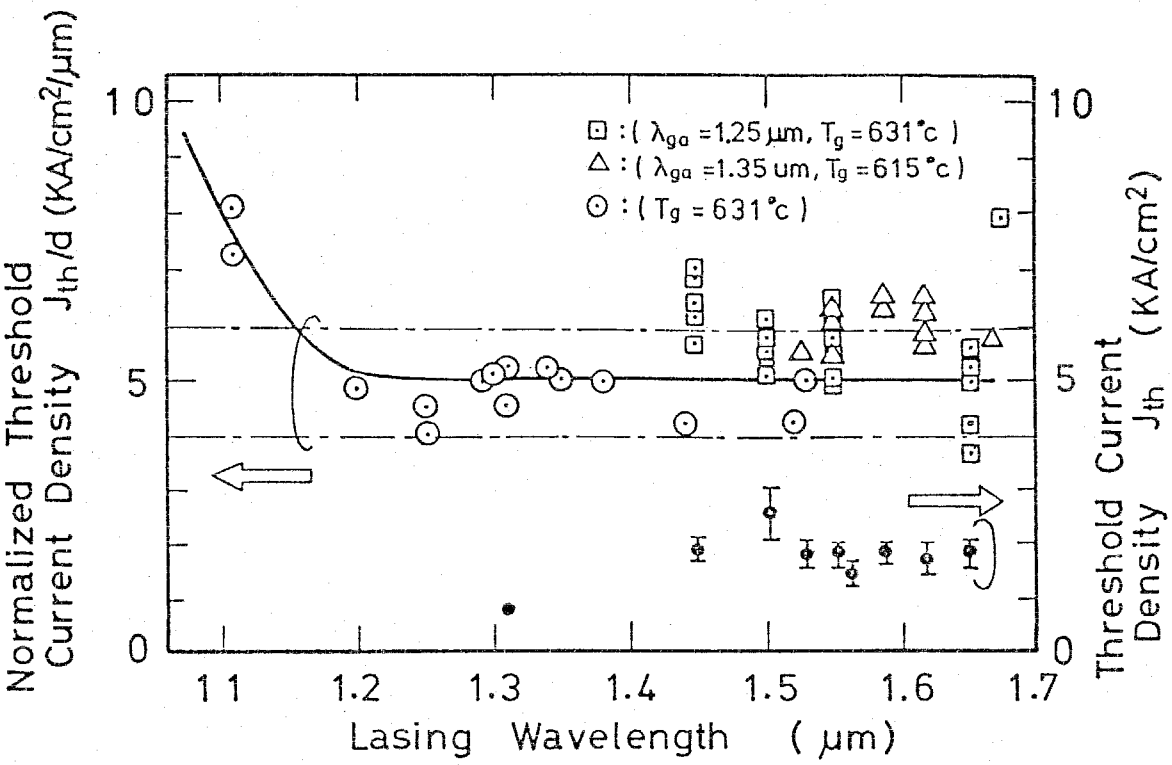

Fig.4-4 Normalized threshold current density J_{th}/d and the threshold current density J_{th} as a function of the lasing wavelength.

Dotted open circle data were obtained by ordinary structure lasers. Data indicated by the square and the triangle were obtained by four layer structure.

threshold carrier density of GaInAsP laser is almost constant for the wavelength range of 1.1-1.65μm, then the ratio of the leakage current to the effective current will go up at the longer wavelength because the quasi Fermi level of injected carriers will be higher than that of shorter wavelength laser due to the smaller effective mass of an electron. Therefore, the barrier height of more than 0.25eV was considered to be necessary for the longer wavelength GaInAsP lasers. In the visible light emitting AlGaAs/GaAs lasers, the required barrier height is smaller because the effective mass of an electron is much larger.

4.4 Temperature dependences of threshold current density and lasing wavelength

The threshold current density J_{th} is approximated by exponential dependence against the temperature T as follows,

$$J_{th}(T)=J_0\exp(T/T_0) \qquad (4\text{-}1)$$

where T_0 is the temperature parameter with 100-150K for GaInAsP/InP DH lasers at low temperature, and is similar to that of AlGaAs/GaAs DH lasers, however, it decreases at around room temperature, which remains as a serious problem for practical use [175][304].

The temperature dependences of the threshold current and the lasing wavelength were measured for the various wavelength GaInAsP/InP DH lasers at the same time. Figure 4-5 shows (a) the schematic diagram of the experimental set up and (b) the photograph of the dewar used for this measurement. The laser mount described in the previous section 4.3 was set on the

copper plate(2mm thick) which was contacted to the bottom of the dewar through sufficiently thick and large copper block. A part of the copper plate was rounded by Ni-Cr heating wire isolated by thin mica plates. For the detection of the temperature, thermocouple was set on the copper plate near to the laser diode. The temperature was controlled by using liquid nitrogen and the heater from 110K to more than 100°C. With this set up, the threshold current was measured through the monochromator with the resolution of about 4nm, next the lasing wavelength was measured at the injection current of 1.2times the threshold current with the resolution of 0.4-0.6 nm.

As a result, a breakpoint was usually observed in the threshold-temperature characteristics for any wavelength laser investigated, although there was no such breakpoint in the lasing wavelength property. Examples of experimental results are shown in Table 4-2, where λ is the lasing wavelength at room temperature(23°C), and T_0 is the temperature coefficient of threshold, defined by eq.(4-1), below the breakpoint temperature T_B, and T_1 is that above T_B. Sample No. of B1-B11 and S1-S12 correspond to the broad contact type lasers and the SiO_2 stripe geometry lasers, respectively. Longer wavelength lasers with AMB layer are denoted by open circles for B11 and S7-S12. Figure 4-6 shows typical examples of the temperature dependences of threshold and lasing wavelength for ordinary structure lasers. Figure 4-7 shows the examples of them for four layer structure lasers with AMB layer. For most lasers, T_0 were 100-150K and independent of lasing wavelength. For stripe geometry lasers(S9-S11), T_0 is relatively small. This

fact is considered to be due to the carrier leakage from the stripe edge because T_0 of broad contact type lasers prepared from the same wafer (J_{th}/d=5KA/cm^2/μm) is relatively larger (T_0=100-150K). The ratio $J_{th}(T=300K)/J_{th}(T=150K)$ was 5-6 for the ordinary structure lasers with the breakpoint, but it was 8-13 for the lasers of smaller T_0 without the breakpoint. Taking account of J_{th}/d=4-5KA/cm^2/μm for ordinary structure lasers and J_{th}/d=5-6KA/cm^2/μm for the four layer structure lasers, $J_{th}(T=150K)/d$ should be less than 1KA/cm^2/μm with the cavity length of 200-400μm.

The temperature dependence of the threshold current has been studied intensively related to the Auger recombination, non radiative recombination at the hetero interface, carrier leakage flowing over the hetero barrier, and the absorption due to transitions between the split off band and heavy hole valence band [304]-[319]. It will be discussed in the next chapter in section 5.5.

The lasing wavelength of the peak mode was measured at $I=1.2I_{th}$. It increased almost linearly with the temperature. Figure 4-8 shows the incremental lasing wavelength-temperature ratio $\Delta\lambda/\Delta T$ as a function of lasing wavelength at room temperature. The ratio $\Delta\lambda/\Delta T$ increased with λ. It is interisting to say that $\Delta\lambda/\Delta T$ of the SiO_2 stripe laser with stripe width of 20-30μm is about 10 percent smaller than that of broad contact laser. However, this fact is not fully understood.

Next the spectrum width of spontaneous emission was measured with PbS detector at various temperatures. SiO_2

(a)

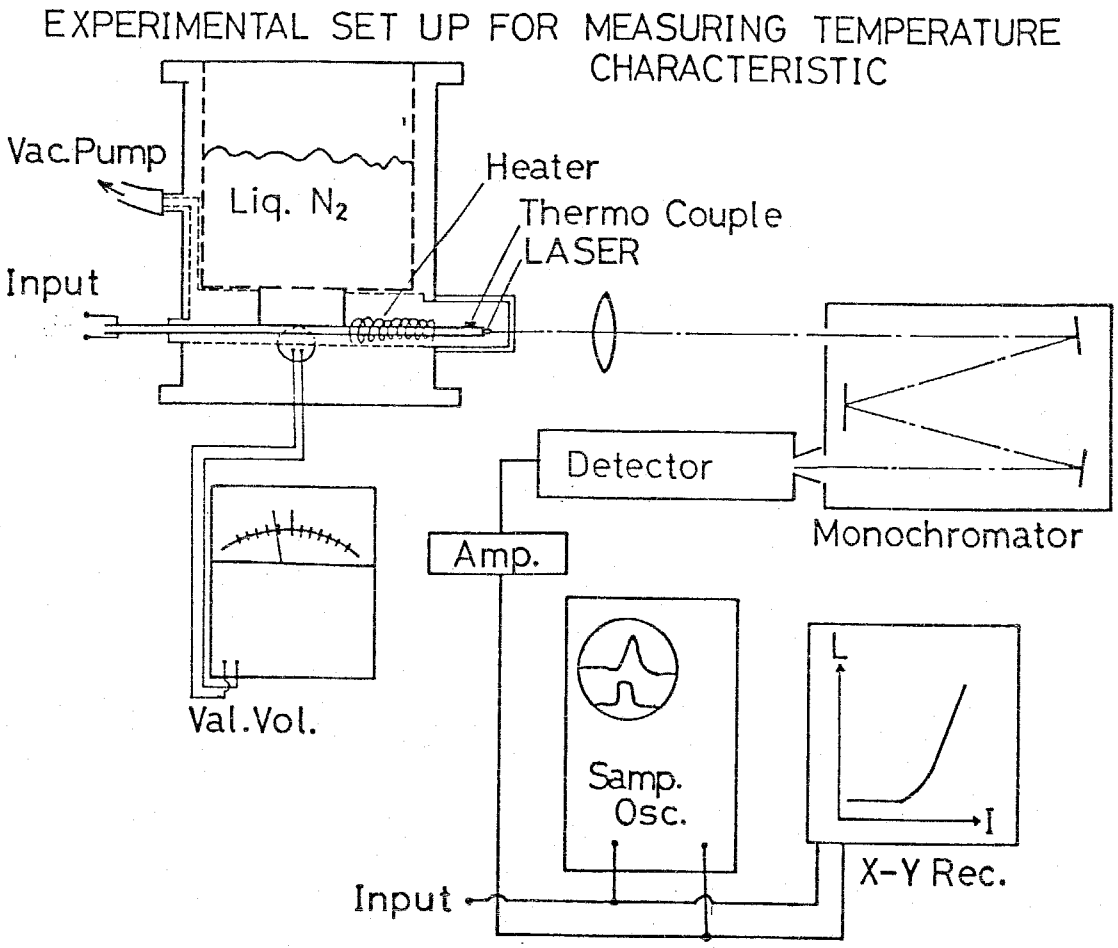

(b)

Fig.4-5 (a) Schematic diagram of the experimental set up used for the measurement of the temperature dependences.

(b) Photograph of the liquid nitrogen dewar

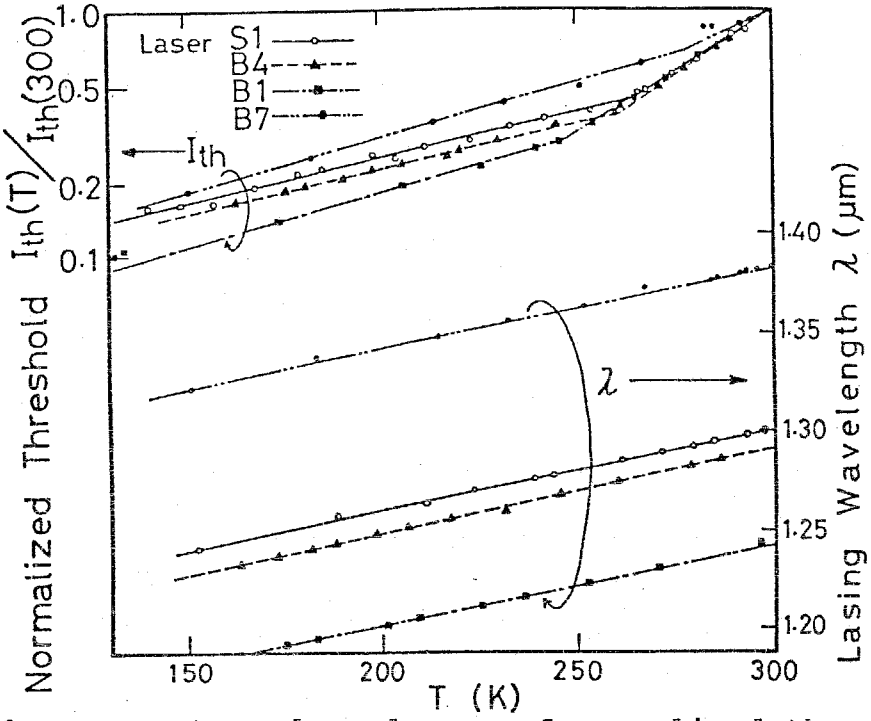

Fig.4-6 Temperature dependences of normalized threshold current and the lasing wavelength for ordinary structure GaInAsP/InP lasers.

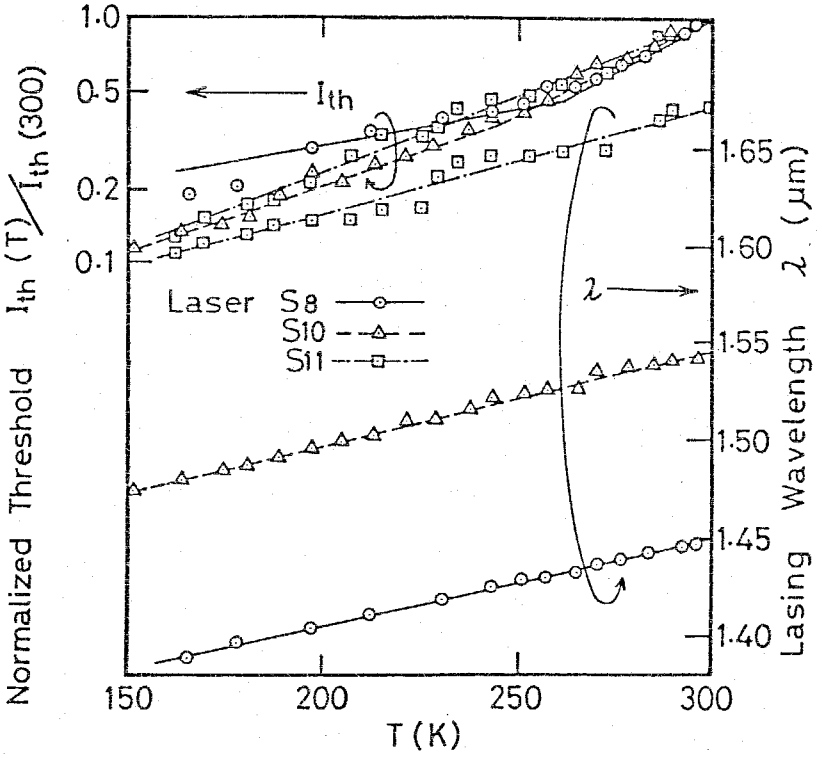

Fig.4-7 Temperature dependences of normalized threshold current and the lasing wavelength for four layer structure GaInAsP/InP lasers with AMB layer.

Table 4-2 Temperature characteristics of various wavelength GaInAsP/InP lasers.

Wavelength λ(μm)	Sample No.	T_0(K)	T_1(K)	T_B(K)	$\frac{J_{th}(300K)}{J_{th}(250K)}$	Δλ/ΔT (nm/deg.)
1.24	B1	96.0	43.9	248	3.14	0.38
	B2	137	52.3	245	2.69	0.36
1.28	B3	117	42.1	261	2.76	0.44
	B4	119	41.1	260	2.86	0.44
1.29	B5	154	48.5	248	2.32	0.42
	B6	109	50.9	278	1.98	0.40
1.38	B7	98.1	50.5	278	2.05	0.43
	B8	108	54.7	266	2.13	0.41
1.52	B9	102	40.8	274	2.42	0.53
	B10	149	42.3	257	2.91	0.53
o 1.67	B11	108	50.6	223	2.76	0.59
1.30	S1	112	43.0	266	2.63	/
	S2	154	42.4	265	2.56	0.38
1.32	S3	133	63.6	238	2.18	0.30
	S4	109	67.6	242	1.94	0.40
	S5	130	57.8	247	2.30	0.36
1.35	S6	102	57.2	246	2.41	0.44
o 1.45	S7	90.0	60.5	267	2.10	0.39
	S8	147	51.2	261	2.31	0.44
o 1.55	S9	61.8	45.3	267	2.73	0.44
	S10	74.7	56.5	245	2.43	0.48
o 1.67	S11	62.6	/	/	2.23	0.54
	S12	100	43.0	263	2.63	/

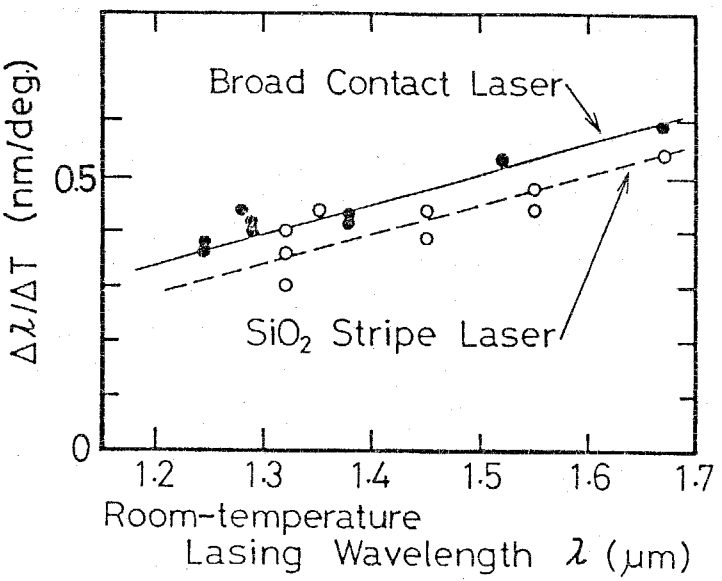

Fig.4-8 Incremental lasing wavelength-temperature ratio as a function of room temperature lasing wavelength. The slope of both extrapolated lines is 0.56nm/deg/μm.

stripe lasers of 20μm width were used at low CW current level of about 200A/cm^2. Figure 4-9 shows spontaneous spectrum profile as a function of the temperature for (a) 1.30μm wavelength and (b) 1.55μm wavelength lasers. Emission intensity was normalized by the total intensity. The temperature dependence of peak wavelength $\Delta\lambda/\Delta T$ was consistent with that of the broad contact laser. In the case of 1.55μm laser, there was no emission peak near 1.25μm which corresponds to bandgap wavelength of the AMB layer. Emission intensity at 1.25μm was less than 1 percent of the peak emission intensity at 1.555μm at room temperature. Spectral width increased exponentially with the temperature for both lasers as shown in Fig.4-10, but there was no such breakpoint temperature as seen in threshold characteristic. The half maximum spectral width was 100nm or 73meV at λ=1.3μm and 140nm or 75meV at λ=1.55μm, respectively, at room temperature, but the energy spread was quite similar in each wavelength [174][179].

4.5 Room temperature CW operation and the lasing properties

Quite low threshold current density of less than 2KA/cm^2 was obtained at the wavelength of 1.5-1.6μm by use of the AMB layer as listed in Table 4-1. From these low threshold wafers, the low threshold currents of of less than 200mA were obtained for the SiO_2 defined stripe lasers with the stripe width of 10-25μm as shown in Fig.4-11. The low threshold current lasers with the threshold current less than 250mA were bonded with the copper heatsink by Indium solder in order to get low thermal resistance.

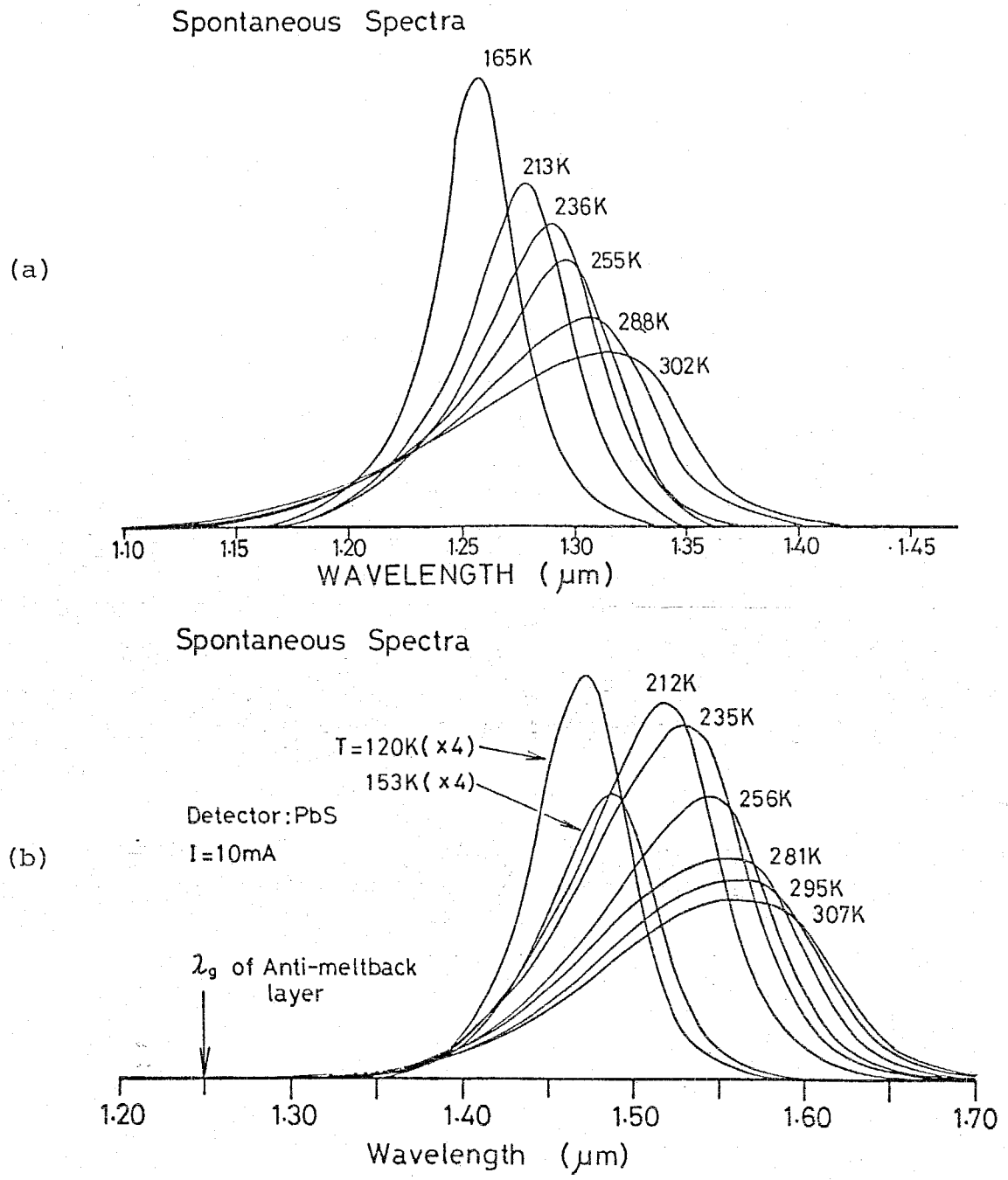

Fig.4-9 Spontaneous emission pattern from the edge emission of SiO_2 stripe laser as a function of the temperature. Stripe width was 20μm and the measurement was performed at low CW current level of 200A/cm^2.

(a) Ordinary structure laser with λ=1.30μm.

(b) Four layer structure laser with λ=1.55μm. The corresponding wavelength of AMB layer was 1.25μm.

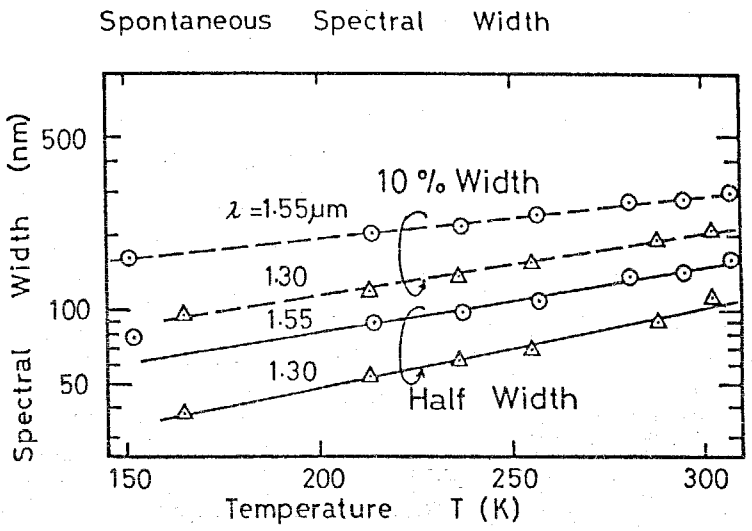

Fig.4-10 Temperature dependence of spontaneous spectral width for two different wavelength lasers with λ=1.30μm and λ=1.55μm.

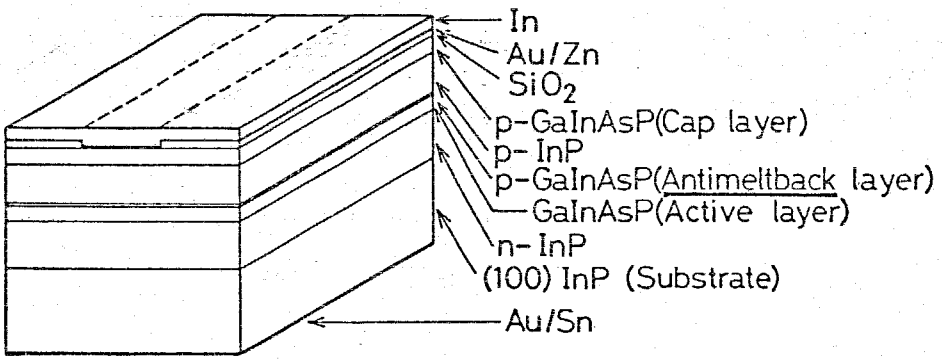

1.45-1.65μm GaInAsP/InP Laser with Anti-meltback Layer

Fig.4-11 Schematic diagram of SiO_2 stripe laser with the AMB layer.

(a)

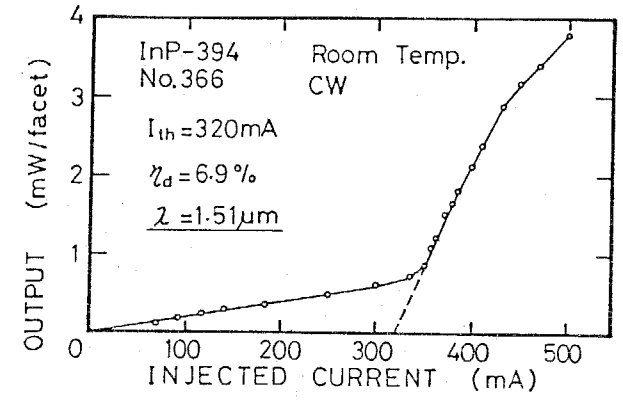

(b)

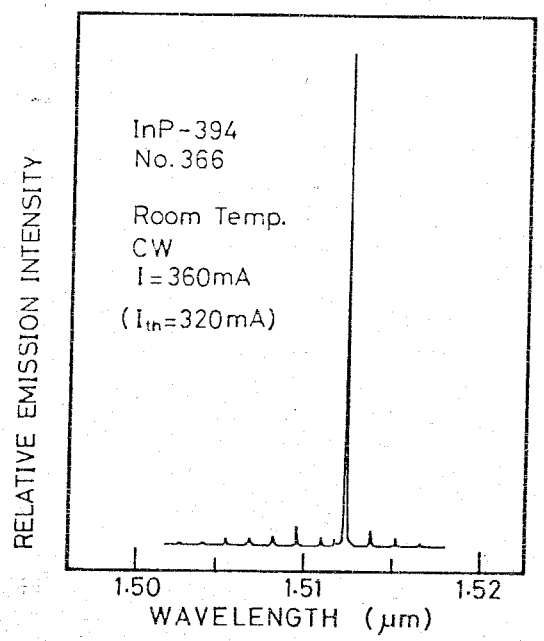

Fig.4-12

Lasing properties of 1.51μm wavelength GaInAsP /InP laser under room temperature CW operation.

(a) I-L characteristic

(b) Lasing spectrum at $I=1.11I_{th}$.

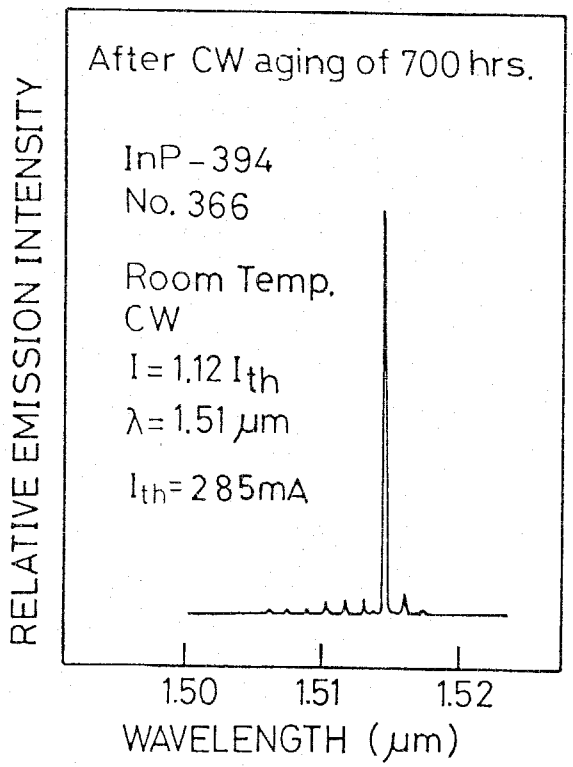

Fig.4-13

Lasing spectrum after aging of 700hours at room temperature.

(a)

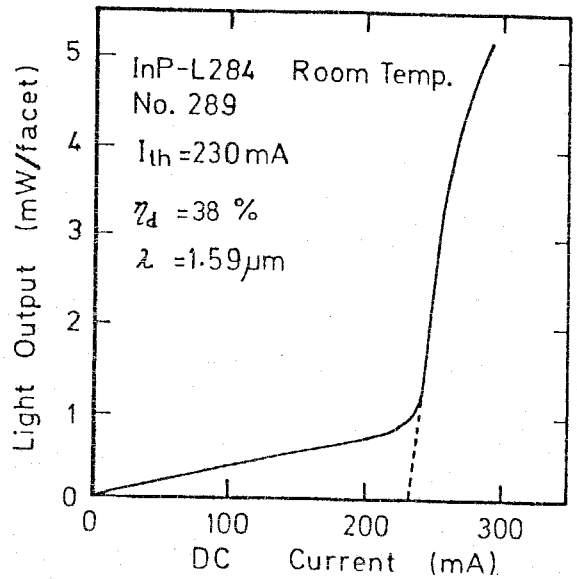

(b)

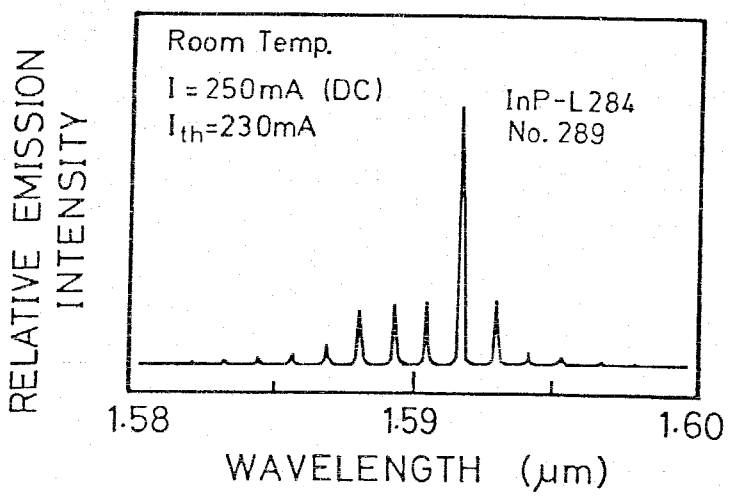

Fig.4-14 Lasing properties of 1.59μm wavelength GaInAsP/InP laser under room temperature CW operation.

(a) I-L characteristic

(b) Lasing spectrum at $I=1.09I_{th}$.

CW operations of these longer wavelength GaInAsP/InP lasers were obtained at room temperature with the lasing wavelength of 1.5-1.6μm. Figure 4-12 shows (a) the I-L characteristic and (b) the lasing spectrum of CW operated laser with the stripe width of 25μm and the cavity length of 300μm. This laser operated more than 700hours under room temperature CW condition with the constant output of 1.5mW/facet. No significant change of lasing spectrum was observed after that aging, the threshold current after 700hours' aging became smaller than that of initial condition as shown in Fig. 4-13. This instability in the threshold current and the quite low differential quantum efficiency were due to the poor bonding technique. After several trials, the room temperature CW operation of 1.59μm wavelength GaInAsP/InP laser with the stripe width of 13μm was obtained with the lower threshold current and the higher differential quantum efficiency of 230mA and 38 percent, respectively. Figure 4-14 shows (a) the I-L characteristic and (b) the lasing spectrum of 1.59μm GaInAsP/InP laser under room temperature CW operation.

4.6 Conclusion

Room temperature CW operations of 1.5-1.6μm wavelength GaInAsP/InP DH lasers were obtained by use of an anti-melt-back (AMB) layer with the threshold current of 230mA and the differential quantum efficiency of 38 percent. Reliability of this longer wavelength GaInAsP/InP laser was confirmed to be more than 700hours under room temperature CW operation. The normalized threshold current density of 5-6KA/cm^2/μm and the

threshold current density of less than 2KA/cm^2 were obtained. The temperature coefficient of the threshold current was 100-150K and 40-70K at the temperature below 250K and at around room temperature. These values were independent of the lasing wavelength of the lasing wavelength. Incremental ratio of the lasing wavelength to the temperature was 0.4nm/deg for 1.3μm wavelength laser and 0.5nm/deg for 1.55μm wavelength laser.

CHAPTER 5 1.6 μm WAVELENGTH GaInAsP/InP BURIED HETEROSTRUCTURE (BH) LASERS

5.1 Introduction

GaInAsP/InP DH lasers have received considerable attention as light sources for optical communication especially for long distance communication using ultra low-loss silica optical fiber [20]. Room temperature CW operations of 1.5-1.6μm wavelength were achieved by LPE growth technique through some special techniques and by VPE growth technique. Reliability of these longer wavelength GaInAsP/InP lasers were confirmed to be more than 10000hours in 1981 by Noda, Sakai, Matsushima, and Akiba [244]. These CW operated lasers reported in earlier time were all SiO_2 defined stripe lasers with the stripe width of 10-25μm which caused the high threshold current and low limit temperature of CW operation.

However for practical use, it is important to develop lasers with good lasing properties, such as a transverse fundamental mode operation, low threshold current, higher efficiency, single longitudinal mode operation under high frequency direct modulation, etc. Therefore several kinds of GaInAsP/InP stripe lasers have been investigated mainly in the 1.3μm wavelength region, such as a buried heterostructure (BH) laser, an MSB laser, an RW laser, an SA laser, a Ridge W laser, a BC laser, a PCW laser, a CCM laser, a PBH laser, an SML laser, an EMS laser, a VGSB laser, and an LSW laser, which are denoted in section 1.3.

In this chapter, a BH laser was selected from the view

point of its high performances and was fabricated at the wavelength of 1.6μm. Fabrication technique and the lasing properties of the BH lasers are given. Room temperature CW operation with quite low threshold current and stable transverse single mode operation were obtained. The temperature dependences of the threshold current and the differential quantum efficiency are measured and discussed.

5.2 Merits of BH laser

For practical use of the long distance optical fiber communications, the following superior properties are required to the light sources,

[1] Lasing wavelength of 1.5-1.6μm

[2] High differential quantum efficiency

[3] High optical output power

[4] High coupling efficiency to the single-mode optical fiber

[5] Fairly long life time

[6] High temperature CW operation

[7] High speed direct modulation

[8] Narrow spectral width.

The item [1] is achieved by use of GaInAsP/InP laser, the other candidate of AlGaAsSb/GaSb lasers have not been known so well as GaInAsP/InP lasers. The items [2]-[4] are devoted to the increase of the transmission distance limited by the minimum detectable optical power of the light detector. From the item [4], a transverse single mode operation of the laser is preferable. The item [5] is desired to all devices and it is estimated from the accelerated life test under high

temperature CW operation denoted in the item [6], for which the low threshold current operation is required. The item [7] is achieved by the direct modulation of the injection current with the frequency up to a few GHz with the bias current of 1.2-1.5 times the threshold current, and this frequency will be increased by the increase of the bias current, for which the low threshold current operation is preferable. The item [8] is essential for the long distance optical fiber communication as discussed in section 1.1. However, if there is any other modulation technique preferable to the direct modulation of injection current, the item [8] will attach very severe condition to the laser. In other words, there are two types of lasers which are applicable for the practical long distance optical fiber communications. One is the laser with a high speed external modulator and the other is the longitudinal single mode operating laser under high speed direct modulation of injection current.

On the other hand, a buried heterostructure (BH) laser has the following advantages inherently,

[1] Low threshold current

[2] High temperature CW operation

[3] Built-in index guiding

[4] Linear output characteristic

[5] Simple structure.

Most attractive merit of the BH laser is denoted by the item [1], it will make high temperature CW operation possible and the reliability will be confirmed in a relatively short time, which leads to faster realization of the optical fiber

communication system. Not only that, it also leads to the possibility of the monolithic integration of a large number of lasers with additional electronic devices. The item [3] is necessary for the stable transverse single mode operation under high speed modulation and it also gives the good linearity in the output characteristic denoted in the item [4], it also leads to a possibility of a optical integrated circuit using three dimensional optical waveguide. Simple structure would be preferable when other electronic devices and other functions are added. Items [7] and [8] mentioned in the requirements for the light sources can be achieved by the introduction of periodic structures of the distributed Bragg reflector (DBR) and the distributed feed back (DFB). Only the disadvantage could be the smaller optical output due to a narrow active region width, but it is not so significant from the viewpoint of the long distance optical fiber communication because it can be overcome by a improvement of the coupling coefficient to the fiber and 6dB reduction of the optical output power reduces the transmission distance only about 12Km.

From above mentioned points, BH laser, which has the fundamental structure of the practical light source for the optical fiber communication, is considered to be one of the most attractive and promising devices.

5.3 Fabrication of BH lasers

First the five layer structure DH wafer consisting of (i) **n type InP cladding layer(Te-doped, 10μm thick)**, (ii) GaInAsP active layer(undoped, 0.2-0.3μm thick), (iii) p type GaInAsP

AMB layer(Zn-doped, 0.1μm thick), (iv) p type InP cladding layer(Zn-doped, 3-4μm thick), and (v) p^+ type GaInAsP cap layer(Zn-doped, 0.5μm thick) was grown on (100) oriented InP substrate by the two-phase solution technique. To obtain good carrier and light confinements, bandgap wavelength λ_{ga} and thickness of AMB layer were set to 1.3μm and 0.1μm, respectively. The light confinement factor of such an asymmetric structure is not strongly dependent on the thickness d' of AMB layer in the range of $0 \leq d' \leq 0.3\mu m$ as detailed in section 2.3. This DH wafer underwent the mesa stripe etching and the regrowth of InP layers for current blocking.

(1) Fabrication processes

After the growth of the DH wafer, SiO_2 was deposited on it with the thickness of 200-300nm by CVD technique and 5-8μm wide stripes were left along the <011> direction as masks for the following mesa etching process. Conventionally, this wafer was etched across the active layer by the solution of Br and methanol and then underwent the regrowth of p and n types InP current blocking layers as shown in Fig.5-1(a). In this study, a new fabrication processes using a selective etching process and a slight meltback method was proposed and demonstrated taking care not to expose the etched InP surface to high temperature atmosphere in order to prevent the thermal damage of InP surface and to get a smooth regrowth of the blocking layers. In this fabrication technique, the DH wafer was first etched by $Br\text{-}CH_3OH$ to the middle of the p type InP cladding layer and then etched by a solution of $4HCl+H_2O$ at about 1°C.

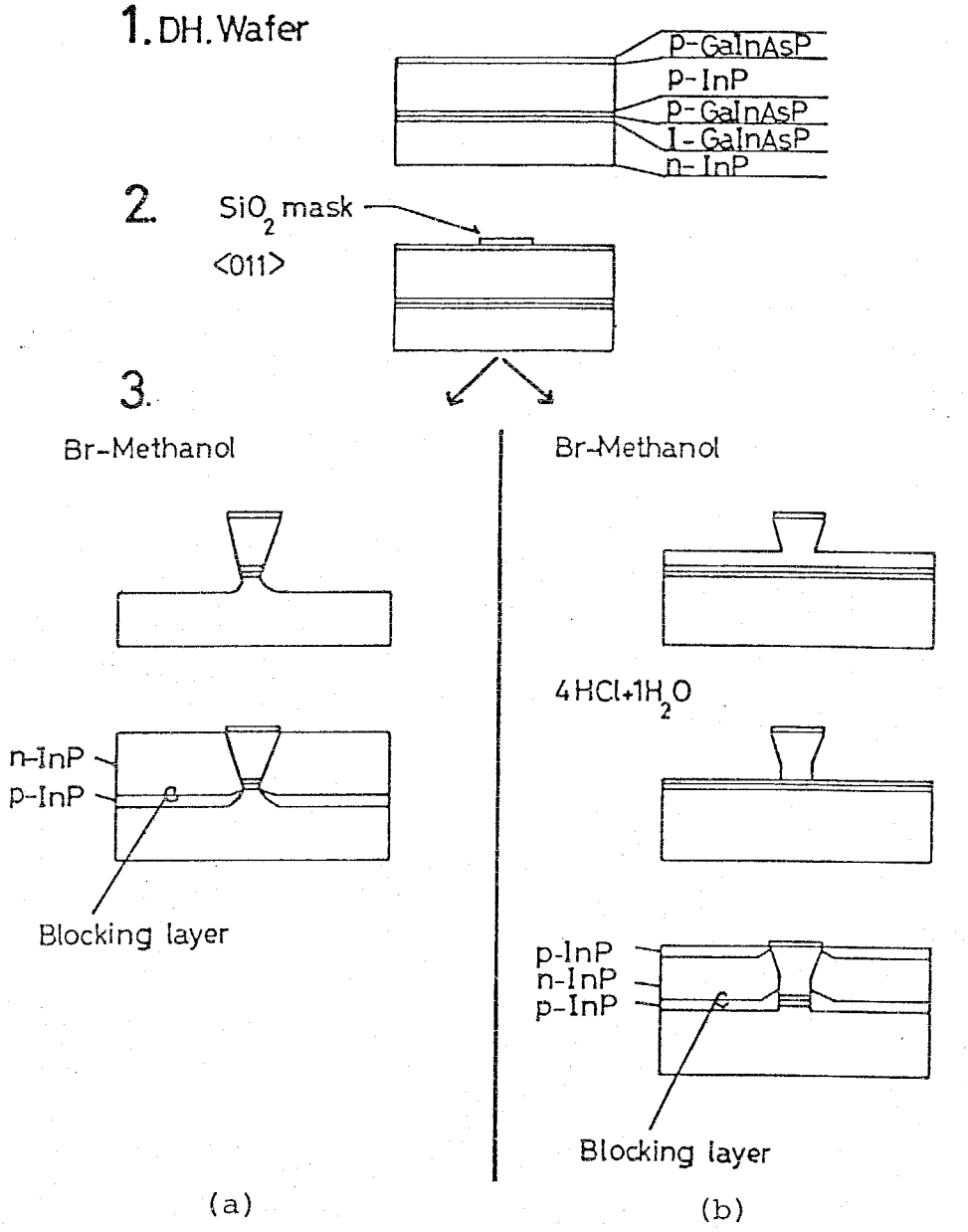

Fig.5-1 Schematic diagrams of two kinds of fabrication processes of BH laser. First, CVD deposited SiO_2 film was formed to narrow stripe mask along the <011> direction by a conventional photolithography technique. Then (a) it was etched across the active layer by Br-CH_3OH and underwent the regrowth of p and n-types InP current blocking layers, or (b) it was etched by Br-CH_3OH and by $4HCl+H_2O$ solution to the surface of GaInAsP AMB layer and underwent the regrowth cycle.

This etching stops automatically just at the AMB layer because this etchant is selective etchant for InP. GaInAsP layers on both the cap layer and the AMB layer work as masks for this etchant, so that the severity of the etching time to get good reproducibility of the stripe width can be relaxed. After those etching the DH wafer underwent a regrowth process using a slight meltback method as shown in Fig.5-1(b). This fabrication technique utilizes the special properties of GaInAsP quaternary crystal as follows,

[1] Thermal damage of GaInAsP crystal is not serious compared with that of InP.

[2] GaInAsP crystal can easily be melted back by the solution of Indium and Phosphorus. Therefore there is proper condition of In-P solution by which only GaInAsP layer is melted back though InP layer is not melted back, that is, in a sense, a selective melt back method.

This fabrication technique, which is a combination of the selective etching process and the selective melt back method, is applicable not only for this type BH laser but also for other types lasers which need the regrowth on InP surface and for flat and smooth growth of the external waveguide adjacent to the active region such as a butt jointed built-in waveguide.

(2) Etching conditions

Figure 5-2 shows (a) the etching characteristics on a DH wafer using 0.2 volume percent Br-CH_3OH at approximately 20°C and (b) an example of the SEM photograph of the cross section. In the Fig.5-2(a), X, Y, and Z show the side etching depth,

etching depth to the mesa neck, and the etching depth to the bottom, respectively. The mesa etched by this etchant has an undercut shape and the etching properties are complicated because the width and the depth of the mesa neck do not vary linearly with the etching time. For example, the speed of the side etching near an etching time of 5min is more than 1.5μm/min, as shown in Fig.5-2(a), so that the width of the neck is changing 3μm/min. Therefore, if the mesa neck is made at the active layer and the same stripe width of the SiO_2 mask is used for all wafers, the width of the neck will vary as much as 1μm from wafer to wafer when the total thickness of p type InP cladding layer and p type GaInAsP cap layer fluctuates within 0.5μm. To put it another way, stripe width of SiO_2 mask should be set to an appropriate value for each DH wafer in order to get the required stripe width of the BH laser.

On the other hand, the mesa neck width can be controlled by using the above mentioned two step etching process because the selective etchant of such a solution reshapes the mesa to a rectangular type by both etch stop layers of GaInAsP. In this etching process, the mesa neck width can be controlled by the first $Br\text{-}CH_3OH$ etching time; it is not necessary to change the stripe width of the SiO_2 mask, even though the total thickness of the p type InP cladding layer and the p type GaInAsP cap layer fluctuates in each wafer. Figure 5-3(a) shows the etching speed in InP using the solution of $4HCl+H_2O$ at approximately 1°C and Fig.5-3(b) shows an SEM photograph of the cross section of the DH wafer etched by $Br\text{-}CH_3OH$ for 30sec to remove the top GaInAsP cap layer and then etched by 4HCl+

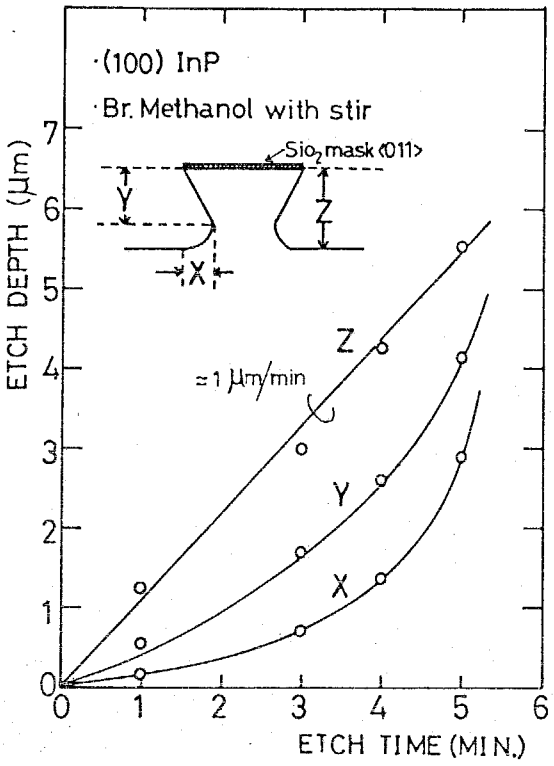

(a)

Fig.5-2

(a) Etching property of 0.2% (volume) Br-CH_3OH at approximately 20°C.

(b)

(b) An example of a cross sectional SEM photograph of a DH wafer etched for 4min.

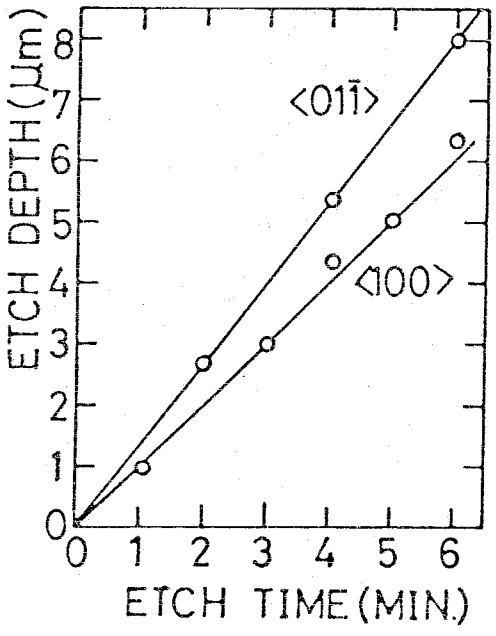

(a)

Fig.5-3

(a) Etching property of $4HCl+H_2O$ solution at approximately 1°C.

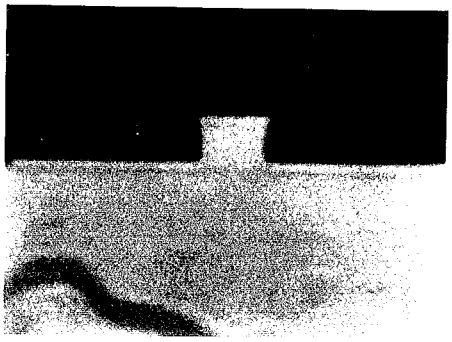

(b)

(b) An example of a cross sectional photograph of a DH wafer etched by the two step etching process as described in the text.

H_2O at 1°C for 3min. Side etching was suppressed by both GaInAsP layers of the cap layer and the AMB layer.

(3) Regrowth condition

After the etching, the DH wafer was cleaned by boiling methanol and trichloroethylene successively, and kept in the vapor of trichloroethylene. Figure 5-4 shows the photograph of the distiller in which etched DH wafers are kept for the regrowth.

Then the DH wafer underwent regrowth to make the blocking layers of p-n-p InP. In this cycle, p-InP, n-InP, and p-InP layers were successively grown on the etched wafer; the top of the mesa was covered with an SiO_2 mask. In this growth, the LPE furnace A and the graphite boat B were used, the etched DH wafer with a size of about 1cmX1cm was surrounded by InP substrate and was covered with InP cover crystal (same as the substrate). After evacuating and flashing hydrogen gas in the reaction tube, the temperature was raised to 563°C in 30min and then slowly to 600°C in 37min. After maintaining this temperature for 30min, it was lowered with a cooling rate of 0.81°C/min. The wafer was slightly melted back at 590°C by an unsaturated In-InP solution for 2sec, then three layers were successively grown for 3, 5, 3min, respectively. For this small meltback, 10mg of InP source material and 5g of Indium were used to make an unsaturated solution. The growth schedule used for this regrowth is shown in Fig.5-5. Figure 5-6 shows an SEM photograph of the cross section of the obtained BH structure. As can be seen, there is no eat into the active

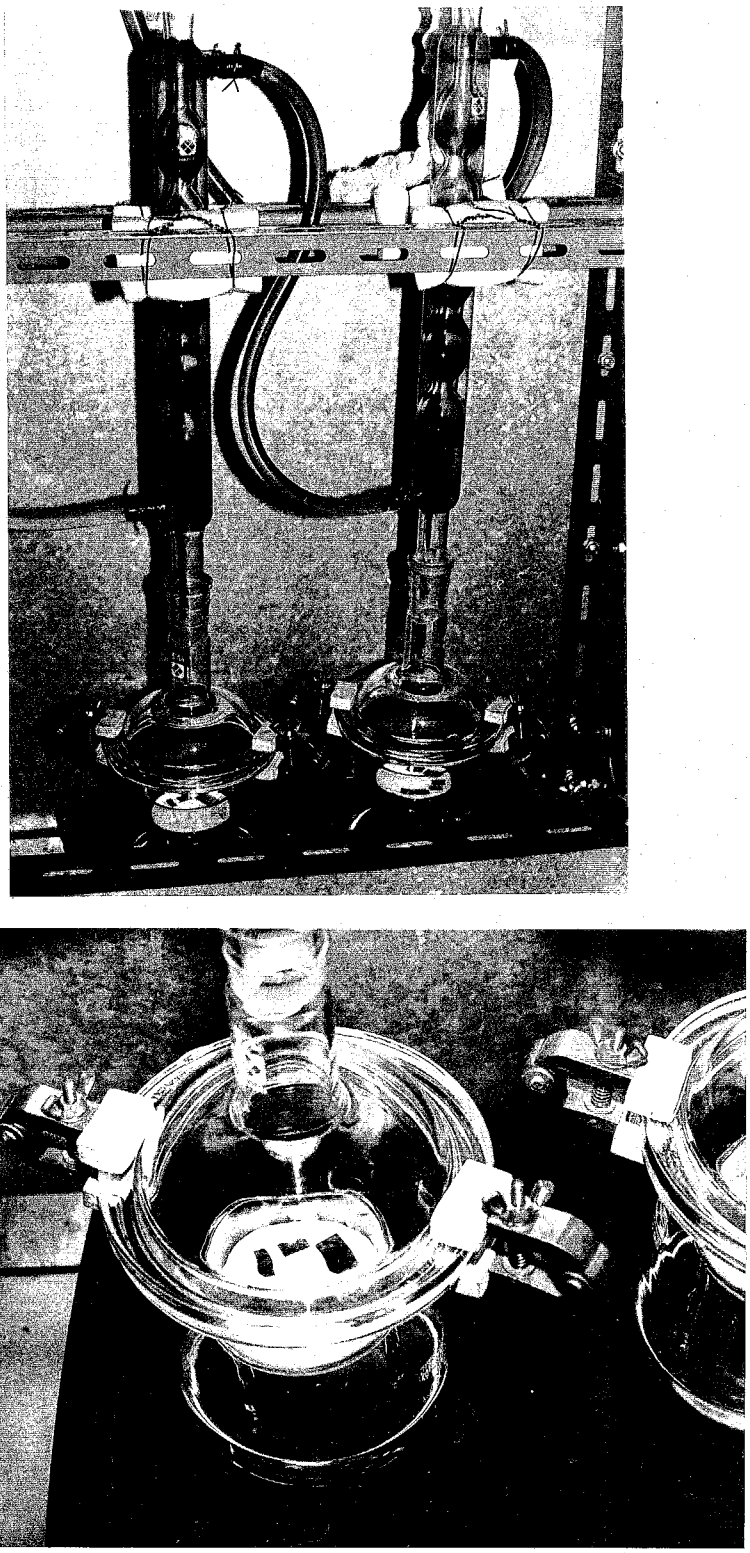

Fig.5-4 The photographs of the distiller in which etched DH wafers are kept. Heated trichloroethylene vaporizes and congeals in the upper part of the distiller cooled by water.

(a)

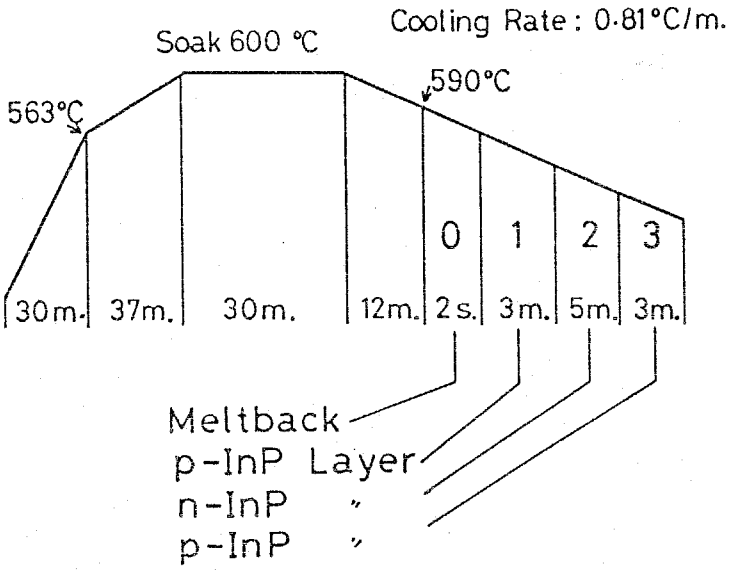

(b)

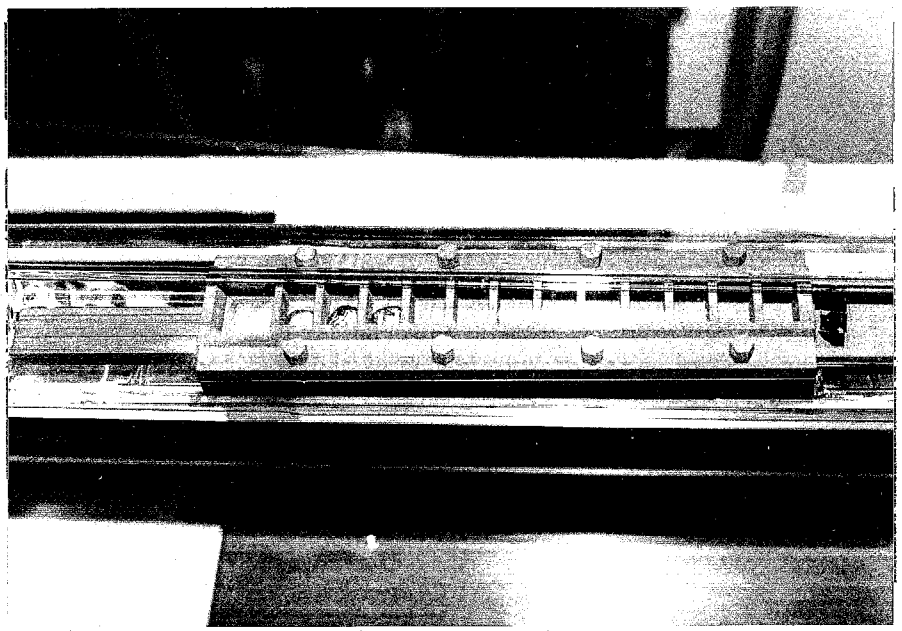

Fig.5-5 (a) Growth schedule used for the regrowth of p, n, and p-types InP current blocking layers. (b) Photograph of an example of the grown wafer just after the regrowth.

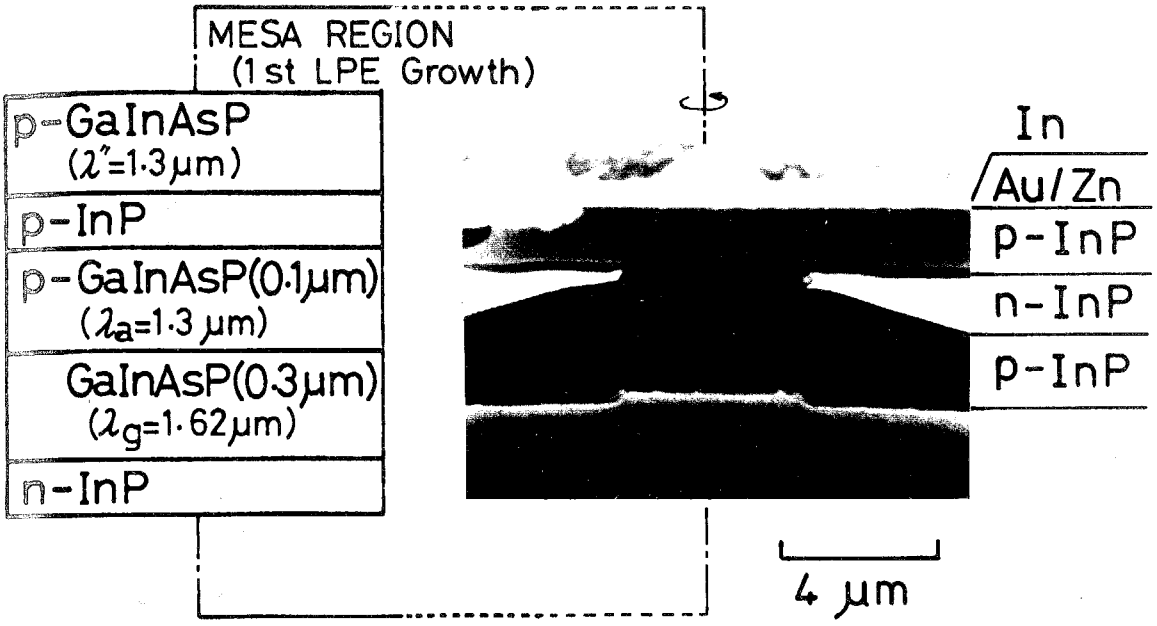

Fig.5-6 SEM photograph of cleaved and etched cross section of the BH laser with the active region width and thickness of 4μm and 0.3μm, respectively.

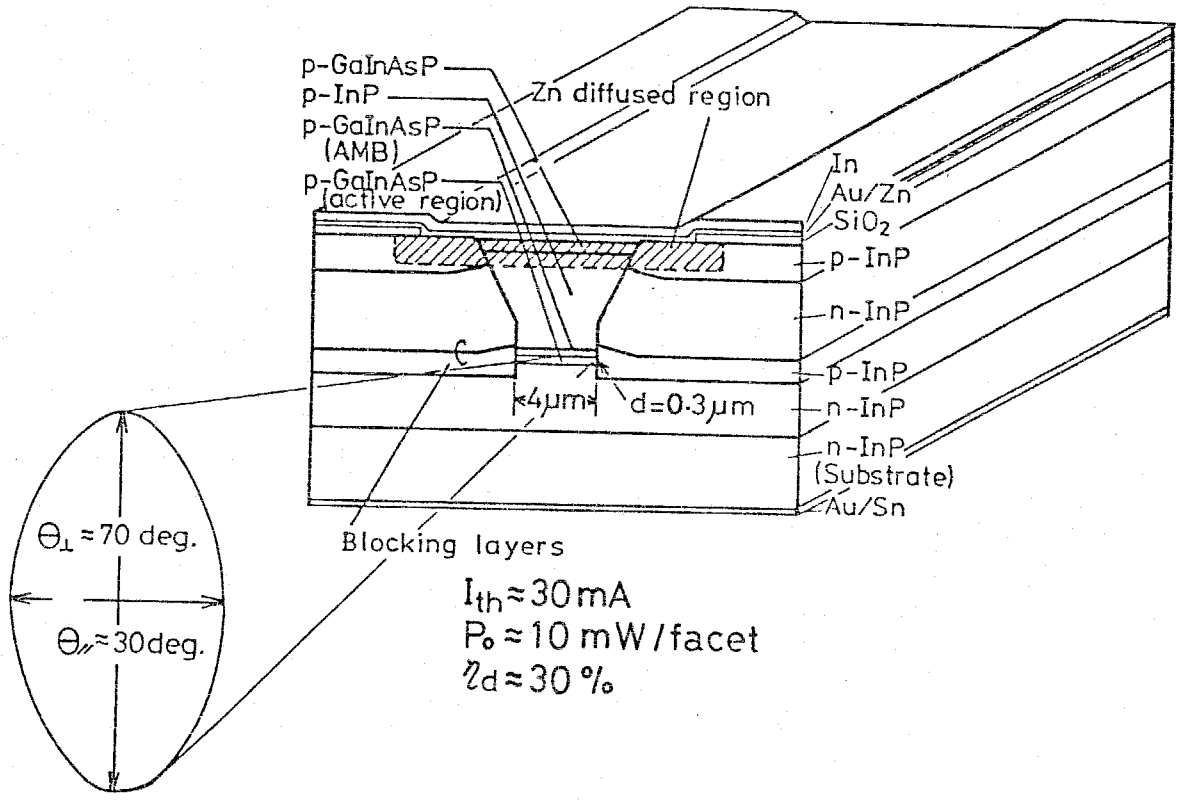

Fig.5-7 Schematic diagram of 1.6μm wavelength GaInAsP/InP BH laser.

region due to meltback, which is peculiar to InP crystal growth on a longer wavelength quaternary crystal because the n type InP cladding layer and the AMB layer worked as stop layers for the meltback and a quite low growth temperature was used.

After this regrowth, the wafer was covered with SiO_2 by CVD technique and 10μm wide windows were opened to diffuse Zn for low ohmic resistance contacts. The top p type InP layer in the regrowth cycle was made to account for eventual misalignment of the Zn diffusion region. After polishing the substrate side of the BH wafer to a thickness of approximately 100μm, ohmic contacts were made by Au/Zn and Au/Sn for p and n type sides, respectively. After 2min alloying at 420°C in pure hydrogen gas, Indium was evaporated onto the p type side for soft contacting. A schematic diagram of an example of the obtained BH laser is shown in Fig.5-7.

5.4 Low threshold current operation

The BH wafer was cleaved into chips with the cavity length of 250-350μm and the chip was mounted on an Indium bed on an Au plated copper heatsink with p-side down. First threshold current was measured under pulsed operation. The pulse width and the repetition rate were 400nsec and 1KHz, respectively. Threshold current as low as 23mA and averaged threshold current of 42mA were obtained from 84 samples with a cavity length of about 300μm and an active region width of 3-5μm. Figure 5-8(a) shows the I-L characteristics of samples with a relatively low threshold current. Figure 5-8(b) shows the distribution of the pulsed threshold current of 84 samples of

the BH lasers. Threshold current density of broad contact type lasers from this DH wafer was about 2KA/cm^2. Therefore threshold current should be less than 30mA for the lasers with the above mentioned size of the active region if there is no leakage current nor additional loss due to roughness of boundary between the active region and regrown InP region. For most samples the light output increased linearly up to twice the threshold current. Transverse single mode operation of this BH laser was obtained up to more than three times the threshold current as shown in Fig.5-9. Room temperature CW operation with the threshold current of 37mA and the differential quantum efficiency of 25 percent was obtained at the wavelength of 1.62μm without thermal bonding only by pushing down to the Indium bed. Figure 5-10 shows the lasing spectrum under CW operation with the output power of 2mW/facet. Then laser chips were thermally bonded on an Au plated copper heatsink using Indium solder evaporated to the heatsink to obtain high efficiency and high power operation. The results are listed in Table 5-1. The lowest threshold current obtained was 28mA and the highest differential quantum efficiency was 43 percent as shown in Fig.5-11. Maximum output power of about 10mW/facet was obtained under room temperature CW operation. Further refinements to get low thermal resistance are still necessary to obtain high power operation.

(a)

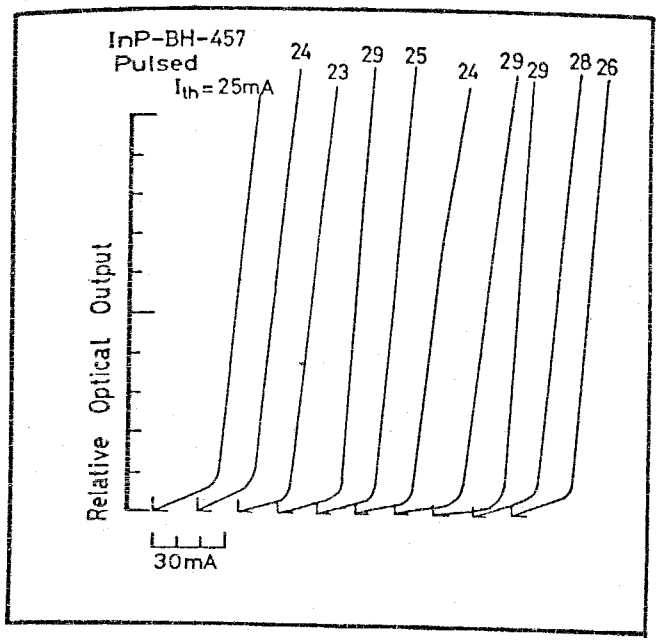

(b)

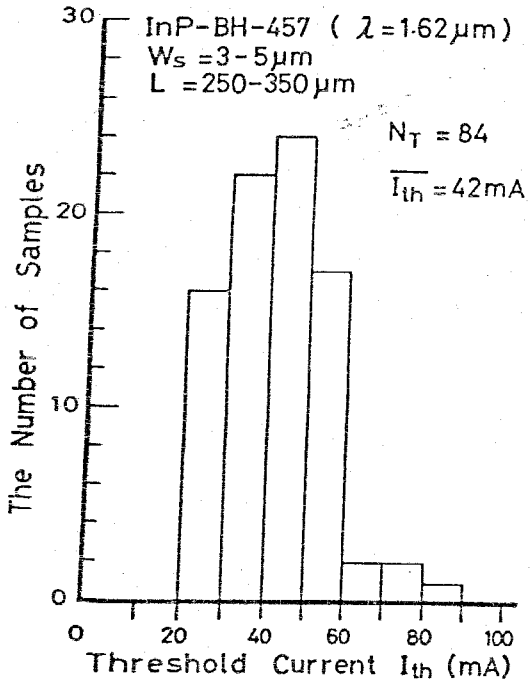

Fig.5-8

(a) I-L characteristics of 1.6μm wavelength GaInAsP/InP BH lasers under pulsed operation.

(b) Distribution of the threshold current of 84 samples.

Averaged threshold current was 42mA.

Fig.5-9

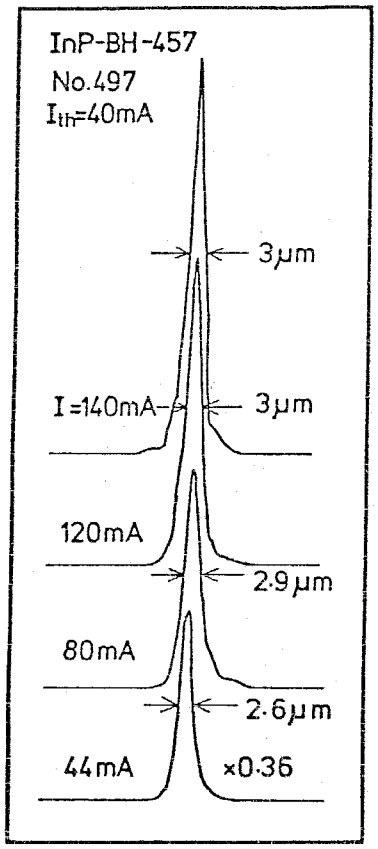

Near field pattern of BH laser as a function of injection current.

Fig.5-10

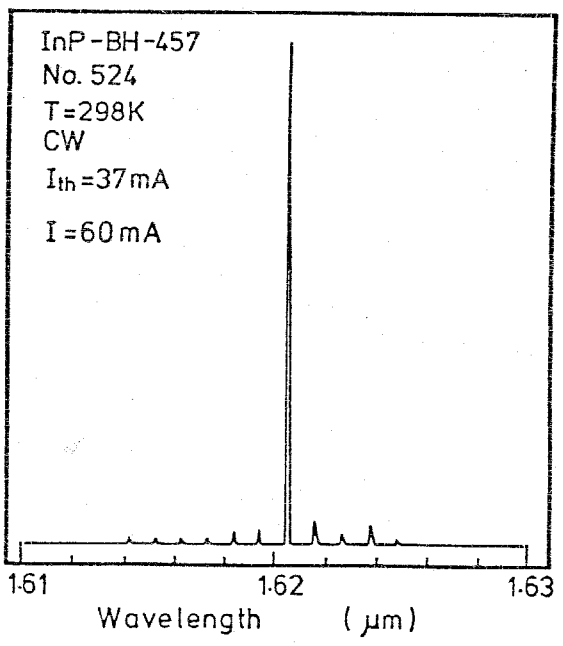

Lasing spectrum under CW operation with the output power of 2mW/facet.

InP-BH-457

λ =1.62μm, W_s =3-5 μm

L =250-350 μm

No.	I_{th} (mA)	η_d (%)
1	28	34
2	30	25
3	37	23
4	38	27
5	43	31
6	46	31
7	54	30
8	55	32
9	55	27
10	59	27
11	71	43

Table 5-1

Threshold current and the differential quantum efficiency of 1.6μm wavelength GaInAsP/InP BH lasers under room temperature CW operation.

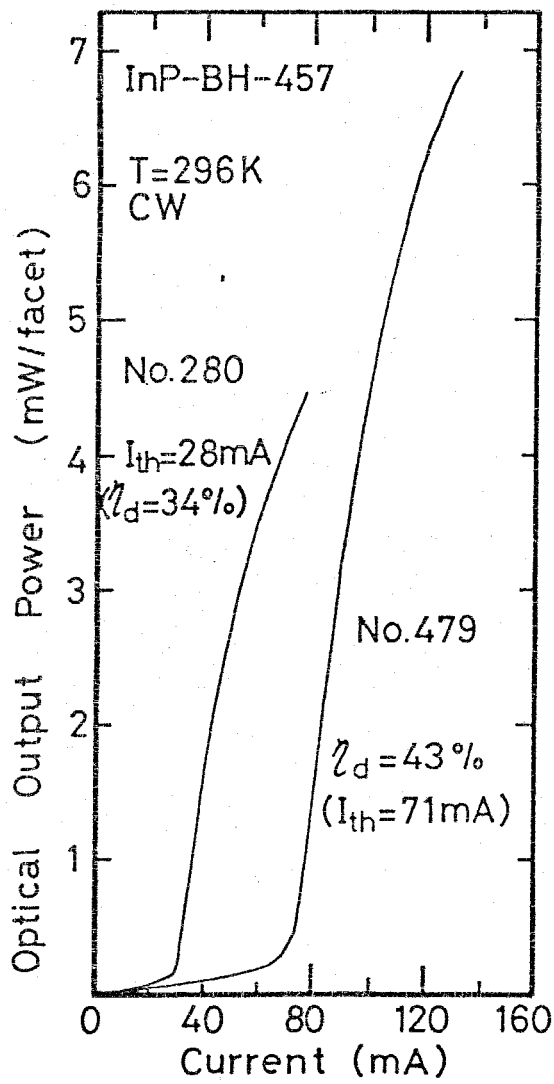

Fig.5-11

I-L characteristics of 1.6μm wavelength GaInAsP/InP BH lasers under room temperature CW operation.

5.5 Temperature dependences of threshold current and differential quantum efficiency

Although a low threshold current operating laser was obtained in 1.6μm wavelength region, there still remains the major problem of temperature dependences of threshold current and differential quantum efficiency. A sharp increase of threshold current was reported by many workers [162][175][205][304][305][314][315]. Phenomena such as non-radiative carrier recombination, carrier recombination at hetero interface, and Auger recombination in active region have been proposed to explain the temperature dependence of the threshold current [306]-[309][312]-[314][317]-[319]. However, those mechanisms can not explain the temperature dependence of the differential quantum efficiency.

The threshold current of GaInAsP/InP laser with the lasing wavelength of 1.6μm increased with the temperature in the same manner as that of 1.3μm wavelength GaInAsP/InP laser though the estimated barrier height between the active layer and InP cladding layer was sufficiently larger, as shown in Fig.5-12. The cause of this phenomenon was studied and tried to be explained related to the temperature dependence of the injected carrier lifetime [304] and that of the spontaneous emission intensity [304][306][312]. However, in the discussion of the laser diodes which have two different transition mechanisms below and above the threshold, not only the carrier loss but also the optical loss should be included. The optical loss of a laser diode is estimated from the differential quantum efficiency.

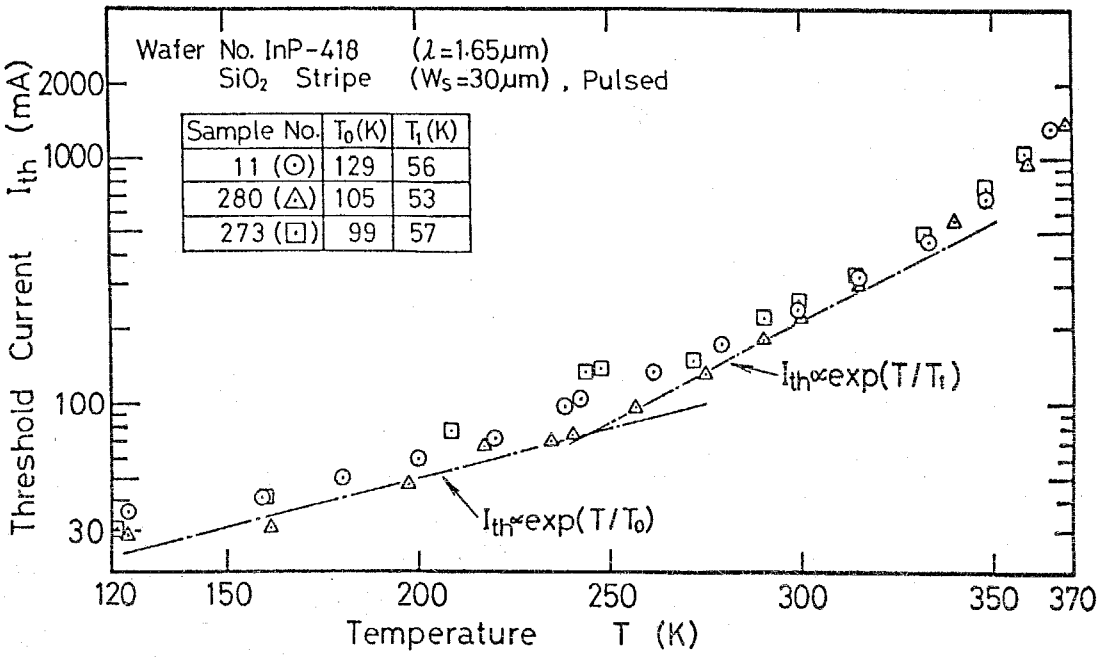

Fig.5-12 Temperature dependence of threshold current of SiO_2 stripe GaInAsP/InP lasers. Lasing wavelength at room temperature was 1.65μm and the stripe width was 30μm.

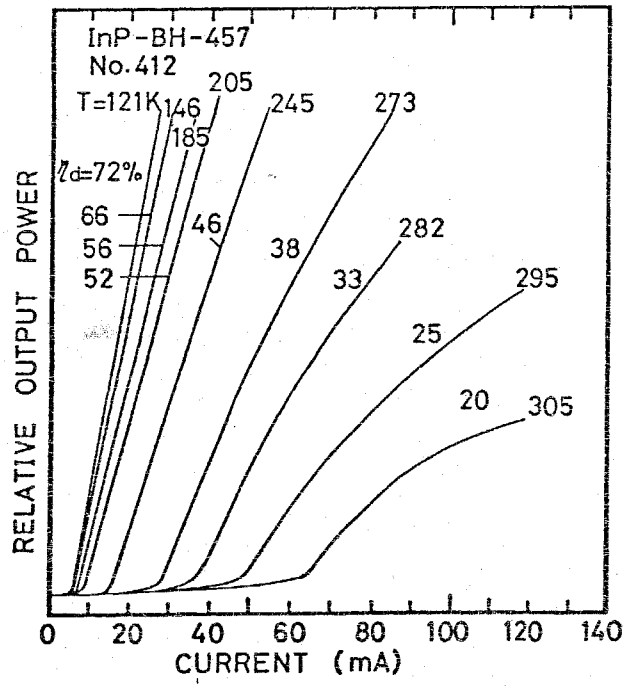

Fig.5-13 I-L characteristics of BH laser under CW operation for various temperatures.

Therefore the temperature dependences of the differential quantum efficiency η_d and the threshold current I_{th} were measured at the same time on 1.6μm wavelength GaInAsP/InP BH lasers. Measurements were carried out under CW condition to avoid misleading I-L characteristic due to poor light output and poor SNR of Ge solar cell. A sharp decrease in the differential quantum efficiency was observed with increasing temperature, which is consistent with the sharp increase of the threshold current. The observed I-L characteristics for one sample are shown in Fig.5-13. As can be seen, above 250K, I_{th} increased quickly with increasing temperature while η_d decreased. The variation of η_d and I_{th} are plotted for several samples as shown in Fig.5-14. Here the length, width, and thickness of active region were about 300μm, 4μm, and 0.3μm, respectively. The devices were bonded with Indium solder to an Au plated copper heatsink and the CW output power was measured using Ge solar cell. The highest CW operation temperature obtained in this measurement was 51°C.

The differential quantum efficiency is given by the following equation,

$$\eta_d = \frac{\ln(1/R)}{\alpha\ell + \ln(1/R)} \eta_i \qquad (5\text{-}1)$$

where R is the reflectivity of the end mirrors, α is the effective absorption loss coefficient along the laser, ℓ is the cavity length of the laser, and η_i is the internal quantum efficiency above the threshold.

The internal quantum efficiency η_i may be written as follows,

$$\eta_i = \frac{1}{1+\tau_R/\tau_{NR}} \qquad (5\text{-}2)$$

where τ_R and τ_{NR} are the radiative and non-radiative carrier lifetimes, respectively. At the injection current below the threshold, τ_R is limited by the spontaneous carrier lifetime of approximately 2-4nsec at room temperature. At the injection current above the threshold, τ_R which should be called the stimulated carrier lifetime is limited by the carrier intraband relaxation time of approximately 10^{-13}sec. The lower limit of the non-radiative lifetime τ_{NR} is considered to be more than a measured carrier lifetime. Thus η_i can be regarded as unity above the threshold although there may be some causes to reduce η_i below the threshold. Then the eq.(5-1) can be rewritten,

$$\eta_d = \frac{\ln(1/R)}{\alpha\ell+\ln(1/R)} \qquad (5\text{-}1')$$

Therefore the temperature dependence of the differential quantum efficiency must be explained by means of that of the effective absorption loss coefficient α. The effective loss coefficient α is given by the following equation,

$$\alpha = \xi\alpha_{ac} + (1-\xi)\alpha_{ex} \qquad (5\text{-}3)$$

where α_{ac} is the absorption loss coefficient in the active layer, α_{ex} is that in the cladding layer, and ξ is the optical confinement factor of the active layer. To put the eq.(5-3) into eq.(5-1'), α_{ac} was calculated from measured value of η_d and ℓ=300μm, and assuming values R=0.42 for the TE_{00} mode, ξ=0.636, and α_{ex}=20cm^{-1} at the temperature of 300K. The results are shown in Fig.5-15. The value α_{ac} increases swiftly from the

temperature of approximately 250K, and is 100-150cm^{-1} at room temperature.

The cause of the large value of α_{ac} should be explained. Adams pointed out two possible absorption mechanisms which could be applied to explain the experimental results [310]. One is the absorption due to the transition from the split-off band into the heavy hole band, α_1. The other is the absorption due to the transitions from the split-off band into impurity levels, α_2. Other absorption mechanisms, such as a free carrier absorption, a transition from impurity levels into the conduction band, and a transition from the conduction band minimum into higher lying minima, were considered and those effects were concluded to be very small. Figure 5-16 shows the schematic diagram of the band structure of the quaternary active layer indicating photon emission across the bandgap and its reabsorption by the transitions from the split-off band into the heavy hole band (α_1) and into the acceptor level (α_2).

The absorption losses α_1 and α_2 can be written as follows,

$$\alpha_1=B_1/[1+\exp\{(E_1-f_v)/kT\}] \qquad (5\text{-}4)$$

$$\alpha_2=B_2/[1+\tfrac{1}{2}\exp\{(E_A-f_v)/kT\}] \qquad (5\text{-}5)$$

where E_1, E_A, and f_v are the energy of the state the electrons in the split-off band transit into, that of the Zn acceptor level, and that of the hole quasi Fermi level. B_1 and B_2 are the fitting parameters. Putting the values of E_1=0.15eV, E_2=0.03eV, B_1=3.7X10^{5}cm^{-1}, B_2=63cm^{-1}, and the temperature dependence of f_v calculated from the measured injection current into the eqs.(5-4) and (5-5), α_1 and α_2 were calculated as a function of a temperature as indicated by the broken lines

in Fig.5-16. This absorption loss α_l will tend to decrease with increasing photon energy, and will be relatively small in 1.3μm wavelength GaInAsP/InP lasers and AlGaAs/GaAs lasers.

Using the relation between the threshold current density and the differential quantum efficiency given by the following equation, which was derived by combining eqs.(2-29),(5-1'), and (5-3),

$$J_{th}=d/(A_l)^2\{\alpha_{in}+\ln(1/R)/(\xi\ell)/\eta_d\}^2.$$

The temperature dependence of the threshold current was calculated with the theoretical values of η_d given by eqs. (5-1'), (5-3), (5-4), and (5-5), as shown in Fig.5-14. The broken line in Fig.5-14 corresponds to the case of $\eta_d=1$ at any temperature. Remaining gap between the theoretically calculated curve and the measured data, that will be increased when the thermal resistance of the laser is reduced, can be explained by the non-radiative carrier loss of Auger recombination.

It is calculated that the temperature dependences of the threshold current and the differential quantum efficiency can be dominated by both the non-radiative carrier loss due to Auger recombination and the absorption loss due to the transitions from the split-off band into the heavy hole band. Therefore the higher differential quantum efficiency must be obtained by the reduction of the optical confinement factor of the active layer and that of the cavity length.

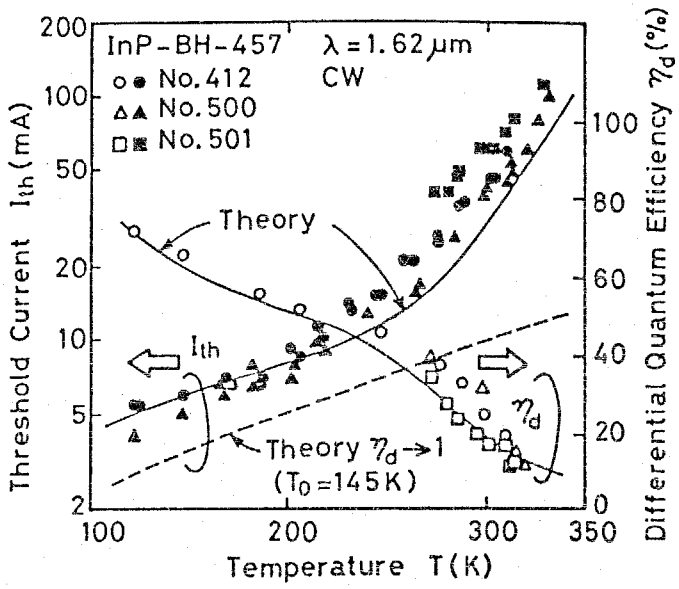

Fig.5-14 Temperature dependences of the threshold current and the differential quantum efficiency for three samples of GaInAsP/InP BH lasers.

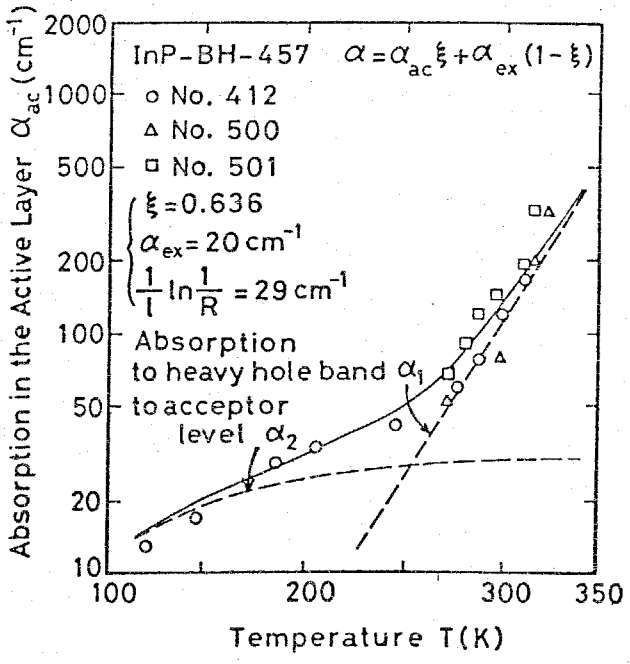

Fig.5-15 Temperature dependence of the absorption loss coefficient in the active layer calculated from the measured values of η_d together with theoretical curves.

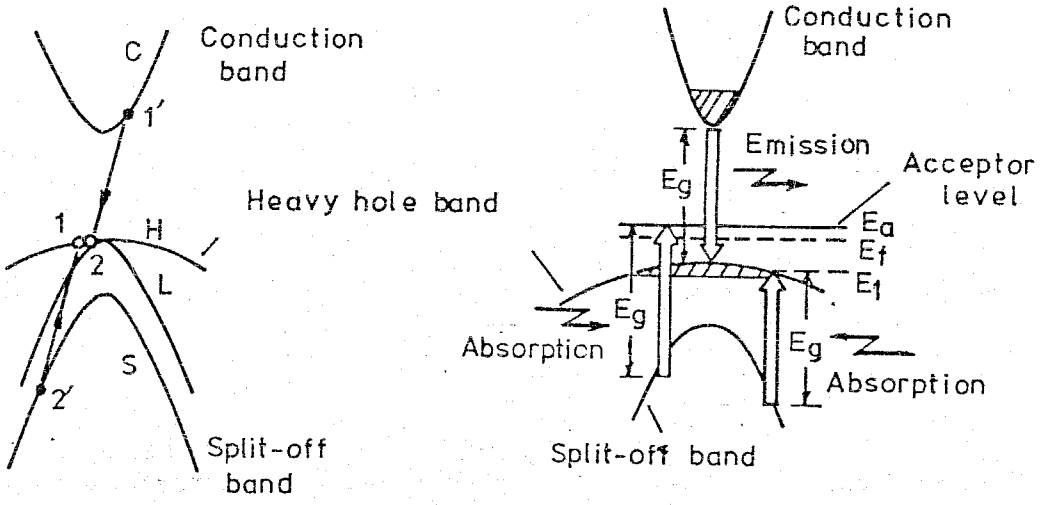

Fig.5-16 Schematic diagram of the band structure of the GaInAsP quaternary active layer indicating photon emission across the bandgap and its reabsorptions due to the transitions from the split-off band.

5.6 Conclusion

1.6μm wavelength GaInAsP/InP BH lasers were fabricated by a new fabrication process using a selective etching and a selective meltback method. Low threshold current of 28mA and the differential quantum efficiency of 43 percent were obtained under room temperature CW operation with the cavity length, the stripe width, and the active region thickness of 250-350μm, 3-5μm, 0.3μm, respectively. Under pulsed operation, the threshold current as low as 23mA and the averaged threshold current of 42mA from 84 samples were obtained.

The transverse single mode operation with the injection current up to more than 3 times the threshold was obtained.

The temperature dependences of the threshold current and the differential quantum efficiency were measured in wide temperature range for the first time. Steep increase of the threshold current in the temperature dependence was related to the temperature dependence of the differential quantum efficiency through the intervalence band absorption due to the transitions from the split-off band into the heavy hole band and the Zn acceptor level.

CHAPTER 6 1.5-1.6 μm WAVELENGTH GaInAsP/InP DISTRIBUTED BRAGG REFLECTOR (DBR) LASERS

6.1 Introduction

In the long distance optical fiber communication, the highest performance is obtained by the single-mode fiber with the minimum loss and the light source with a narrow spectral width as discussed in chapter 1. However the spectral width of the conventional laser will be no more narrow when it is modulated directly, because the spectral broadening due to the lasing mode hopping occurs. Therefore strong selectivity of the lasing mode will be levied on the laser for practical use. Candidates for that purpose are a distributed Bragg reflector (DBR) laser, a distributed feed-back(DFB) laser, and an ultra short cavity laser such as a surface emitting(SE) laser [253].

In this chapter, the fabrication and the lasing properties including the spectral width property under high speed direct modulation of the buried heterostructure distributed Bragg reflector integrated twin guide(BH-DBR-ITG) laser are shown. A stable single mode operation with the modulation frequency up to 3GHz was obtained. This laser is confirmed to be applicable for the long distance optical fiber communication with the transmission bandwidth-transmission distance product BL of 185GHzKm.

6.2 Dynamic spectral width of semiconductor laser

In conventional lasers which have no special selectivity of the lasing wavelength, multi-mode lasing occurs under high

speed direct modulation due to a variation of the injected carrier density. In the stationary operation the injected carrier density would be almost clamped down at the threshold carrier density even in high injection current level when the temperature change due to the injection current was negligible. The schematic diagrams of gain profiles under a stationary operation and a high speed direct modulation are indicated by the solid line and the dashed line in Fig.6-1. As can be seen, several resonant modes have a gain more than the threshold gain under high speed direct modulation, which leads to a multi-mode operation. This phenomenon was reported by Ikegami in 1979 [283] and was called "spectral broadening". The spectral width due to this spectral broadening was measured to be 2.3nm for AlGaAs/GaAs TJS laser and 10nm for 1.6μm wavelength GaInAsP/InP BH laser [289], as shown in Fig.6-2(a) and (b), respectively. This large spectral width leads to a desperate value of the transmission bandwidth-transmission distance product BL of approximately 5GHzKm for the conventional single-mode optical fiber.

On the contrary, a stable single mode operation under high speed direct modulation was obtained by DBR-ITG laser with the lasing wavelength of both 1.3μm and 1.5-1.6μm regions [287] [288]. Figure 6-3 shows the schematic diagram of the gain profile under a stationary operation and a high speed direct modulation as indicated by the solid line and the dashed line, respectively. As can be seen, only a single mode can have a gain more than the threshold gain even in high speed direct modulation. Thus a stable single mode operation in high speed

direct modulation and the very small spectral width, which leads to high value of BL, could be expected. However, there still remains an excess spectral width due to the refractive index variation caused by the variation of the injected carrier density in a high frequency direct modulation.

The contribution to the refractive index variation due to plasma oscillations of free carriers is expressed theoretically by Nash [298] as,

$$\Delta n=-e^2Nn/(2m_c\omega^2\varepsilon) \qquad (6\text{-}1)$$

where e, n, n, m_c, ω, and ε are the electronic charge, the carrier density, the refractive index, the effective mass of an electron, the angular frequency of the light, and the dielectric constant, respectively. The ratio of the refractive index variation to the injected carrier density $dn/(dN)=-7.6X10^{-21}cm^3$ could be obtained by differentiating the eq. (6-1) by N and putting the values of $n=3.62$, $m_c=0.044m_0$ (the mass of an electron), $\omega=2\pi c/\lambda$ (c:light velocity in space), $\lambda=1.6\mu m$, $\varepsilon=12.4\varepsilon_0$ (ε_0:permittivity of vacuum). When the laser is directly modulated with a sinusoidal current, the injected carrier density will be expressed as,

$$N=N_0+N_m(\omega_m)e^{j\omega_m t} \qquad (6\text{-}2)$$

where ω_m is the modulation angular frequency. Then the maximum spectral width under direct modulation will approximately be given as the following equation,

$$\Delta\lambda_m=\{2N_m\xi(dn/dN)/n_{eff}\}\lambda \qquad (6\text{-}3)$$

where ξ, n_{eff}, and λ are the optical confinement factor of the active layer, the effective refractive index of the laser cavity, and the lasing wavelength, respectively. This kind of

an excess spectral width under high speed direct modulation was found by Kishino, Aoki, and Suematsu [289], and called a "dynamic line shift". Schematic diagrams of the variation of the injected carrier density and the corresponding dynamic line shift are shown in Fig.6-4 for a help of the explanation.

The dynamic spectral width, which means the time domain averaged spectral width under a direct modulation, is limited by the spectral broadening for conventional lasers and the dynamic line shift for the special lasers such as a DBR laser, a DFB laser, and an ultra short cavity laser. The former one is usually more than ten times larger than the latter one, the ultimately lower limit of the dynamic spectral width, which leads to the ultimate value BL of the conventional single-mode optical fiber, should be discussed on the dynamic line shift. This dynamic line shift can be reduced by the reduction of N_m and ξ and by an introduction of an unexcited region along the light propagating direction. However, the former two ways can not be applicable under a constant output power condition. In a DBR laser which has an unexcited region of DBR, the dynamic line shift is expressed as,

$$\Delta\lambda_m=\{2N_m\xi(dn/dN)/n_{eff}\}\lambda\ell/(\ell+L_{eff}) \qquad (6-4)$$

where ℓ and L_{eff} are the active region length and the effective length of DBR region denoted in chapter 2, respectively. In a constant output power condition, it is almost proportional to $\Delta\lambda_m \propto 1/\sqrt{(\ell+L_{eff})}$ [289']. The same feature ca be expected for the ultra short cavity laser consisting of an excited region and an unexcited region such as an SE laser.

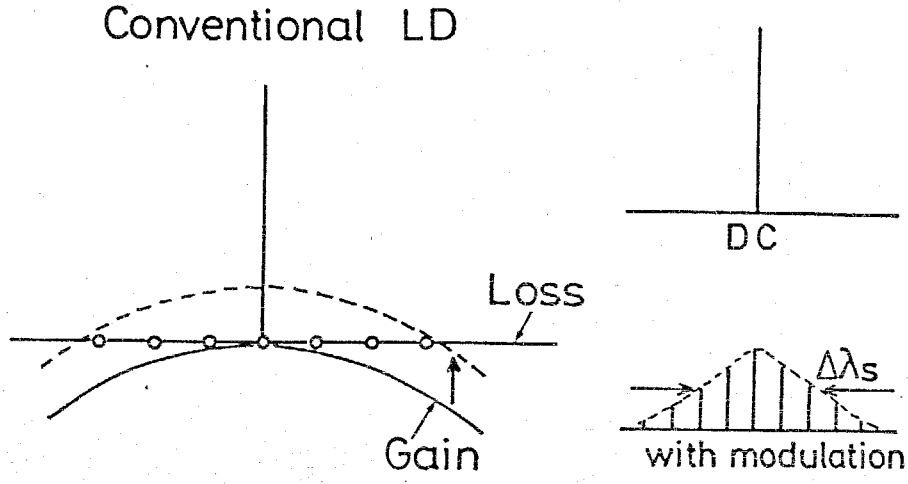

Fig.6-1 Schematic diagram of the gain profile of conventional laser. Solid and dashed lines indicate that under a stationary operation and a high speed direct modulation, respectively.

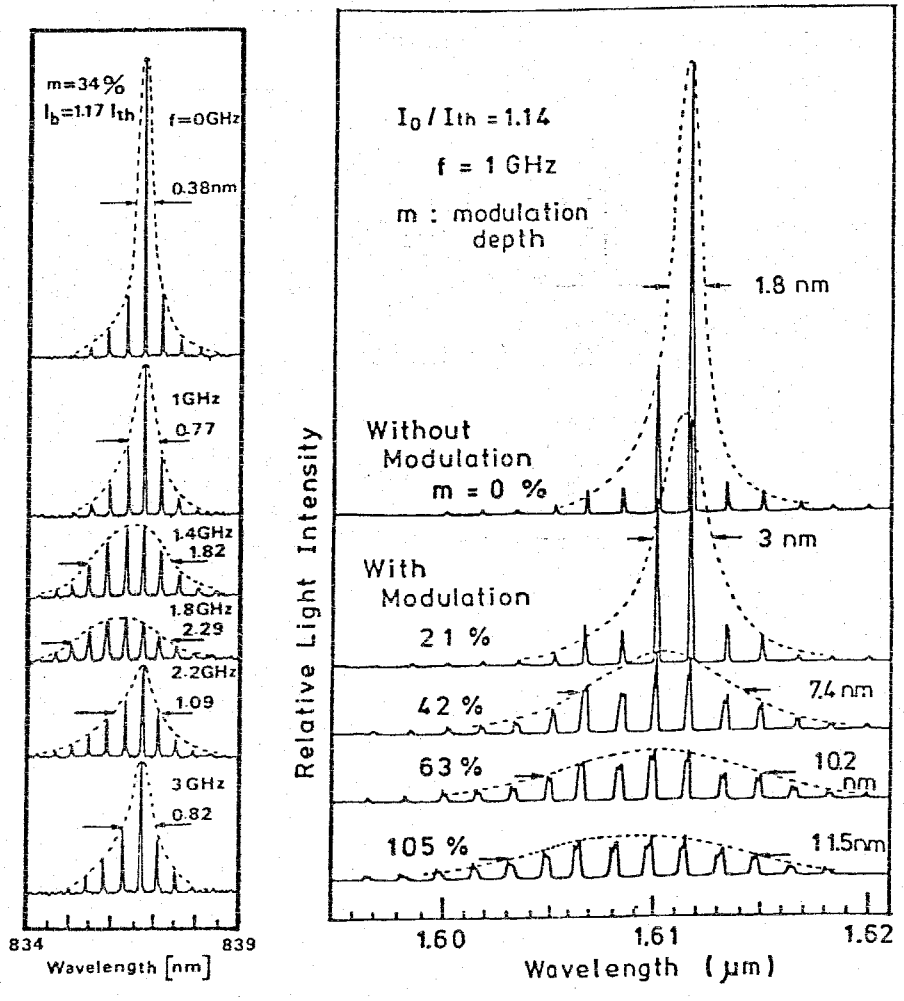

Fig.6-2 Lasing spectrum under high speed direct modulation measured on (a) AlGaAs/GaAs TJS laser and (b) GaInAsP/InP BH laser, after refs.[289][289"].

Fig.6-3

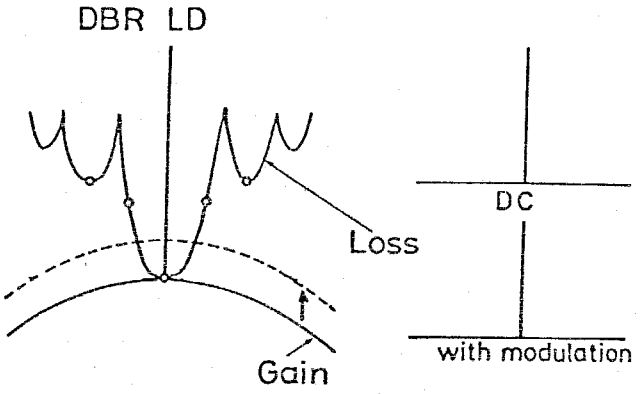

Schematic diagram of gain profile and the loss profile of DBR laser. Solid and dashed lines indicate that under a stationary operation and a high speed direct modulation, respectively.

The threshold gain depends on the profile of the mirror loss due to the wavelength selectivity of DBR.

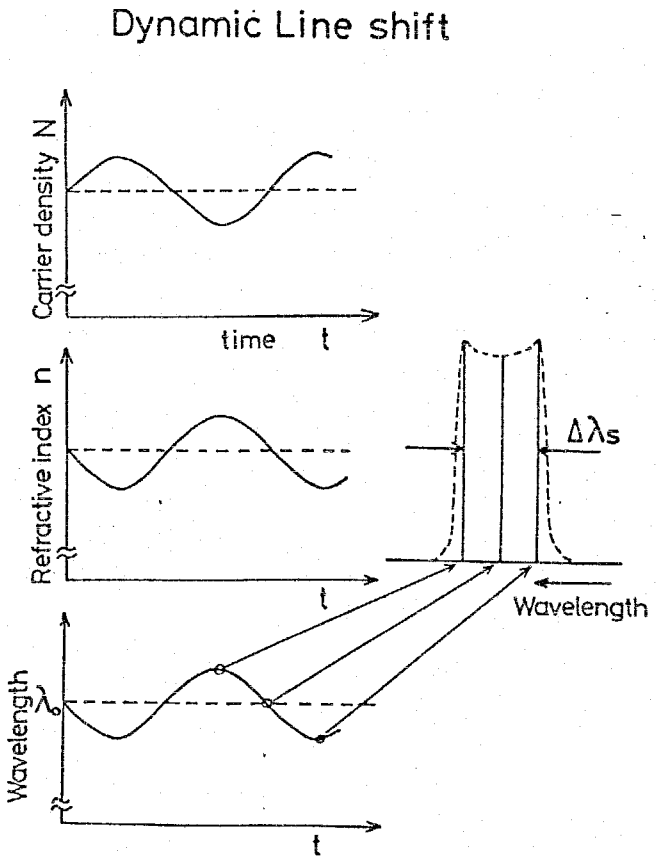

Fig.6-4 Schematic diagrams of the injected carrier density under high speed direct modulation and the corresponding observable lasing spectrum due to the dynamic line shift.

6.3 Fabrication of BH-DBR-ITG laser

In this study, 1.5-1.6μm wavelength DBR lasers were fabricated aiming at a narrow dynamic spectral width. They were fabricated with the integrated twin guide(ITG) structure because of the capability of the application for monolithically integrated light sources. A schematic diagram of DBR-ITG laser is shown in Fig.6-5. The light generated in the active guide layer couples to the output guide within the active region and then couples to the DBR region. The equivalent refractive index of the active guide layer was designed to match to that of the output guide layer for higher coupling efficiencies of C_o and C_{out} defined by Utaka, Kobayashi, and Suematsu [243]. The distributed Bragg reflector was formed on a thin InP layer between the active and output guide layers in order to prevent the increase of a scattering loss. The fabrication of BH-DBR-ITG lasers mainly consists of four processes such as the growth of ITG structure wafer, the regrowth for BH structure, the formation of the DBR, and the formation of electrodes.

First, an ITG structure wafer, which consists of seven layers of (i) n type InP cladding layer(Te-doped, 5-10μm thick), (ii) n type GaInAsP output guide layer(Te-doped, 0.6μm thick), (iii) n type InP separation layer(Te-doped, 0.3μm thick), (iv) undoped GaInAsP active guide layer(0.2μm thick, λ_g=1.59μm), (v) undoped GaInAsP anti-melt-back layer(0.1μm thick, λ_g=1.35 μm), (vi) p type InP cladding layer(Zn-doped, 2μm thick), and (vii) p type GaInAsP cap layer(Zn-doped, 0.5μm thick, λ_g=1.25 μm), was grown on (100) oriented InP using the two-phase

solution technique with the growth conditions of (T_s, T_g)= (670°C, 615°C) as mentioned in chapter 3. Amounts of the source crystals and dopants used for this wafer growth are listed in Table 6-1 with the estimated doping levels. Figure 6-6 shows an example of the growth schedule typically used for the growth of the ITG wafer.

After the growth, the wafer was evaluated by the degree of a lattice mismatch and the thickness of each layer. Then a part of it was cut off and underwent the fabrication process of broad contact type lasers. Threshold current density of 2-3KA/cm^2 and the break down voltage in the V-I characteristic of more than 7 volts were obtained. Lasing wavelengths of these lasers were measured for the design of the corrugation period. The other part of the grown wafer underwent the etching for mesa stripe and the regrowth for BH structure. In this case, the ITG wafer was conventionally etched down to the n type cladding layer with the etchant of Br-CH_3OH and was slightly melted back in the same manner described in chapter 5. Because the GaInAsP output guide layer could not be three dimensional waveguide when the new fabrication process mentioned in chapter 5 was applied. Regrowth conditions were almost the same as those used in chapter 5.

After the regrowth, the corrugation was formed on the InP separation layer according to the following procedures.

[1] After removing the SiO_2 mask, the wafer was cleaned and dried in the same manner as described in section 4.2.

[2] Photoresist of AZ-1350 was spread on the grown wafer with the spinner conditions of 5000rpm and 30sec.

Drying for 5min at 90°C, the same procedure was repeated 5 times to get hard contact of the photoresist because it will be damaged by the following etchings.

[3] Drying for 30min at 90-100°C.

[4] Mask alignment and exposure. Exposure time of 4-5sec was used for 800μm wide stripe windows and the interval of 1200μm perpendicular to the direction of the buried stripes. Then the development was done 4-5sec in AZ-1350 developer.

[5] Post baking for 30min at 120-140°C.

[6] Etching of GaInAsP cap layer with the selective etchant of $3H_2SO_4+H_2O_2+H_2O$ solution at 30°C.

[7] Etching of InP cladding layer with the selective etchant of $4HCl+H_2O$ solution at 1°C.

[8] Etching of the AMB layer and the active layer with the same etchant used in the procedure [6].

[9] Removing the photoresist by AZ remover, the wafer was cleaned in boiling methanol, acetone, and trichloroethylene, and then dried for 30min at 100°C.

[10] Spreading the diluted AZ-1350 photoresist with the same volume of AZ thinner. The spinner conditions of 8500rpm and 20sec were used to get a thin photoresist film(100 nm thick) for the formation of the first order corrugations for DBR with a period of 240-250nm.

[11] Drying for 5min at 90°C.

[12] Exposure of the first order corrugations by conventional holographic photolithography technique using the 325nm wavelength line of He-Cd laser. A schematic diagram of

the experimental set up and the photographs of it are shown in Fig.6-7(a) and (b), respectively.

[13] Development by AZ-1350 developer for 3-5sec.

[14] Checking the period of the exposed corrugation by the measurement of the diffraction angle using the same He-Cd laser as shown in Fig.6-8.

[15] Post baking for 5min at 120°C.

[16] Etching of the corrugations with the solution of HCl+ $CH_3COOH+H_2O$ (named KKI etchant in ref.[273]). Etched corrugation depth of approximately 30-50nm was obtained with the etching time of 2-5sec at 30°C.

[17] Removing the photoresist and cleaning the wafer in boiling methanol, acetone, and trichloroethylene.

[18] Deposition of SiO_2 film with the thickness of 200-300nm for the mask of Zn diffusion and the electric isolation.

[19] Stripe windows were opened on the active region and Zn diffusion was carried out in the same manner as detailed in section 4.2.

[20] Polishing the wafer to a thickness of approximately 150μm, which was relatively thicker than that of conventional lasers because the total length of this laser was approximately more than twice larger than those lasers.

[21] Evaporations of Au(40mg)/Zn(15mg) and Au(80mg)/Sn(15mg) to the p and n type sides, respectively. In the evaporation of Au/Zn, a metal mask, which has stripe windows of 30μm width and 350μm length with a interval of 1200μm, was adjusted on the wafer to make a ohmic

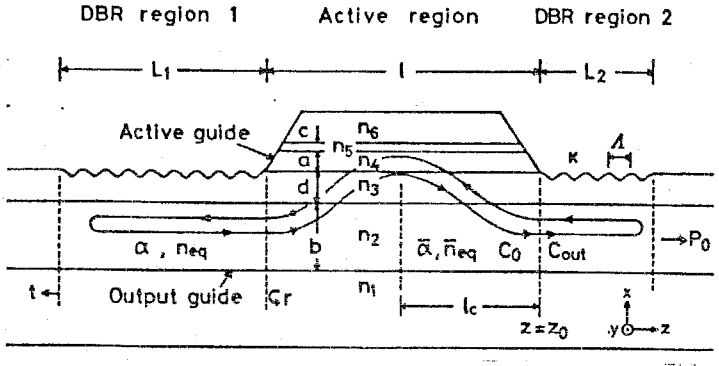

Fig.6-5 Schematic diagram of 1.5-1.6μm wavelength GaInAsP/InP DBR-ITG laser.

Table 6-1 Composition, typical thickness, doping level, and contents of each layer for 1.5-1.6μm ITG wafer.

No.	layer	λ_g (μm)	thickness (μm)	doping level (cm^{-3})	content (mg) 1)				
					InP	GaAs	InAs	Te/In 2)	Zn/In 3)
1	n-InP		5-10	1.2×10^{18}	50			40	
2	n-GaInAsP(O.G.)	1.45	0.55	1.2×10^{18}	50	90	285	40	
3	n-InP(S.L.)		0.4	1.2×10^{18}	50			40	
4	GaInAsP(A.G.)	1.60	0.2	(1×10^{17})	50	165	290		
5	GaInAsP(AMB)	1.35	0.1	(1×10^{17})	50	70	280		
6	p-InP		2-3	1×10^{17}	37				5
7	p-GaInAsP	1.30	0.5	3×10^{18}	50	50	225		40

1) for 5g of Indium solvent, 2) 2.5% Te in Indium, and 3) 1% Zn in Indium.

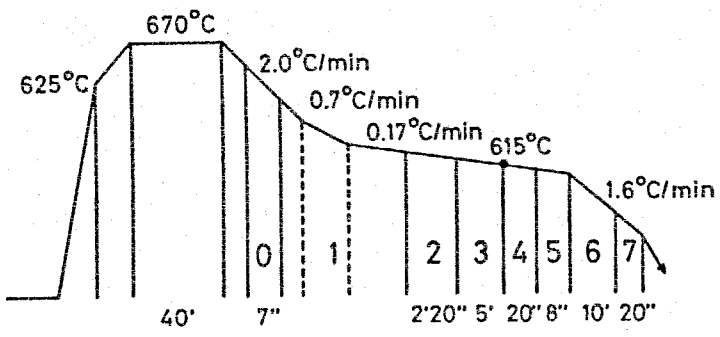

Fig.6-6 A typical growth schedule of the temperature for the ITG wafer.

λ(μm)	Λ (nm)	α(deg)
1.3	190 ~200	55~60
1.5~1.6	220 ~240	40~50

(a)

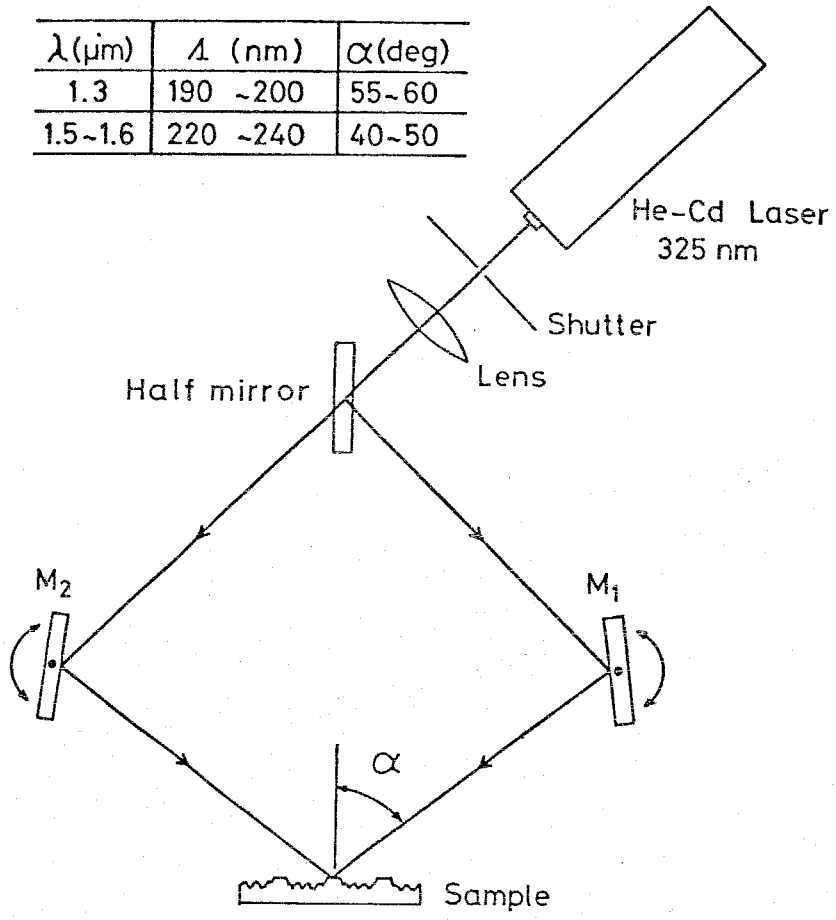

(b)

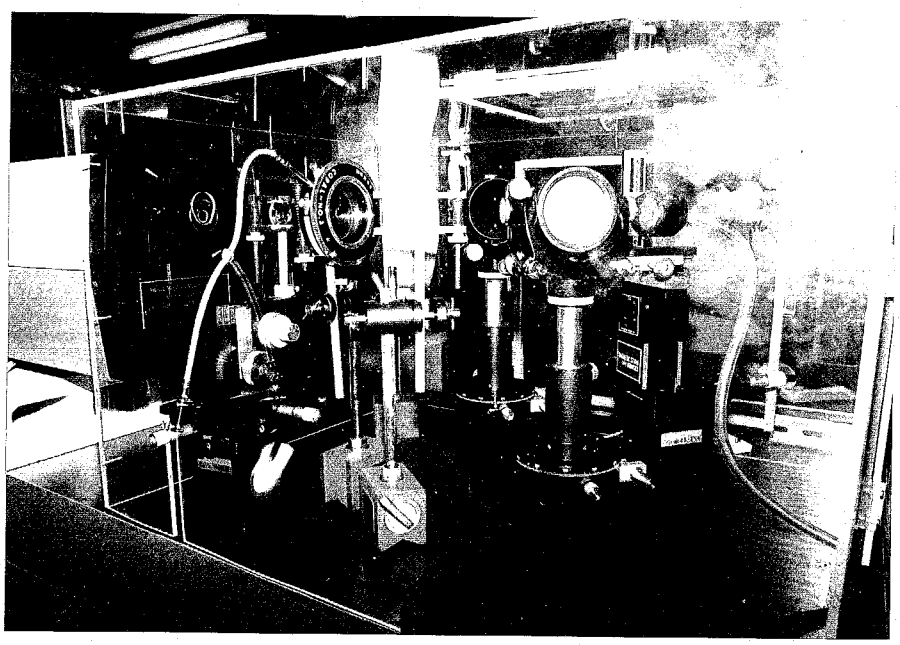

Fig.6-7 (a) Schematic diagram of the experimental set up for the holographic exposure.
(b) Photograph of the holographic exposure system.

(a)

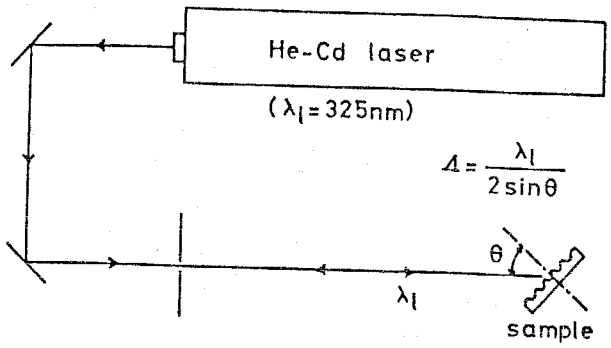

(b)

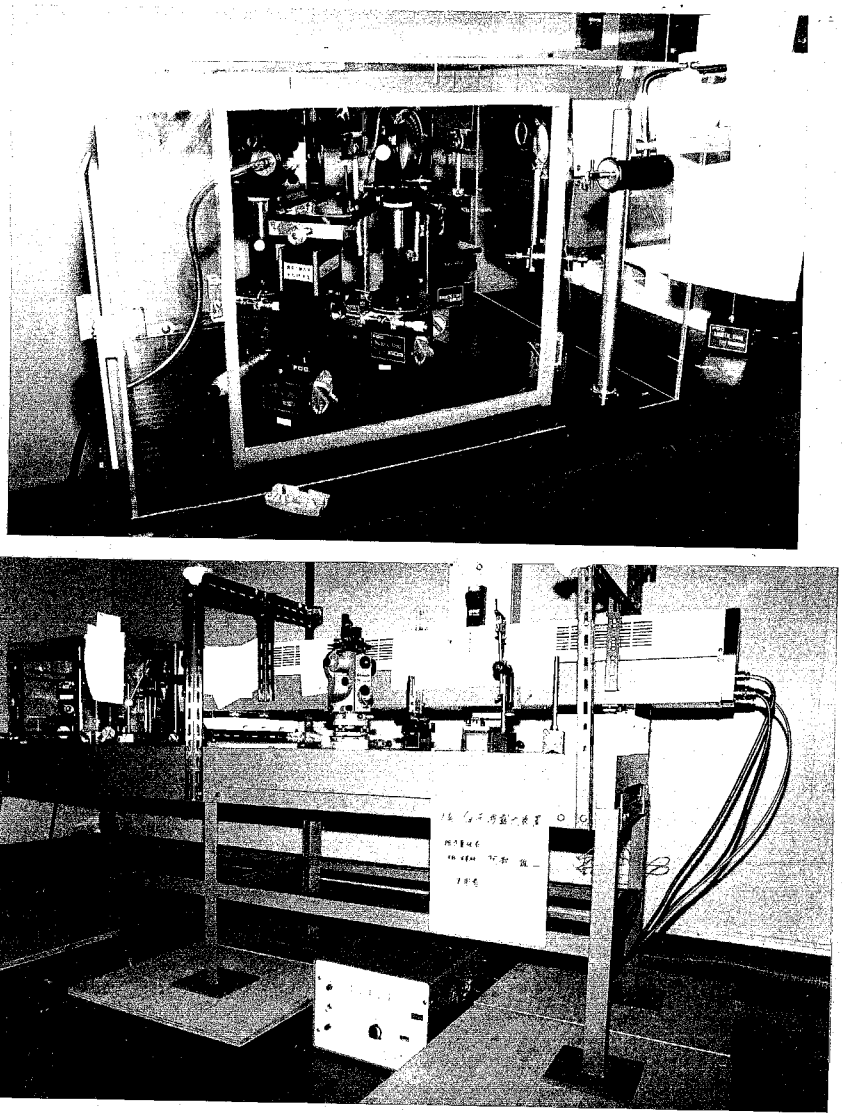

Fig.6-8 (a) Schematic diagram of the measurement system for the period of the first order corrugations.
(b) Photograph of the experimental set up.

Fabrication processes of BH-DBR-ITG lasers

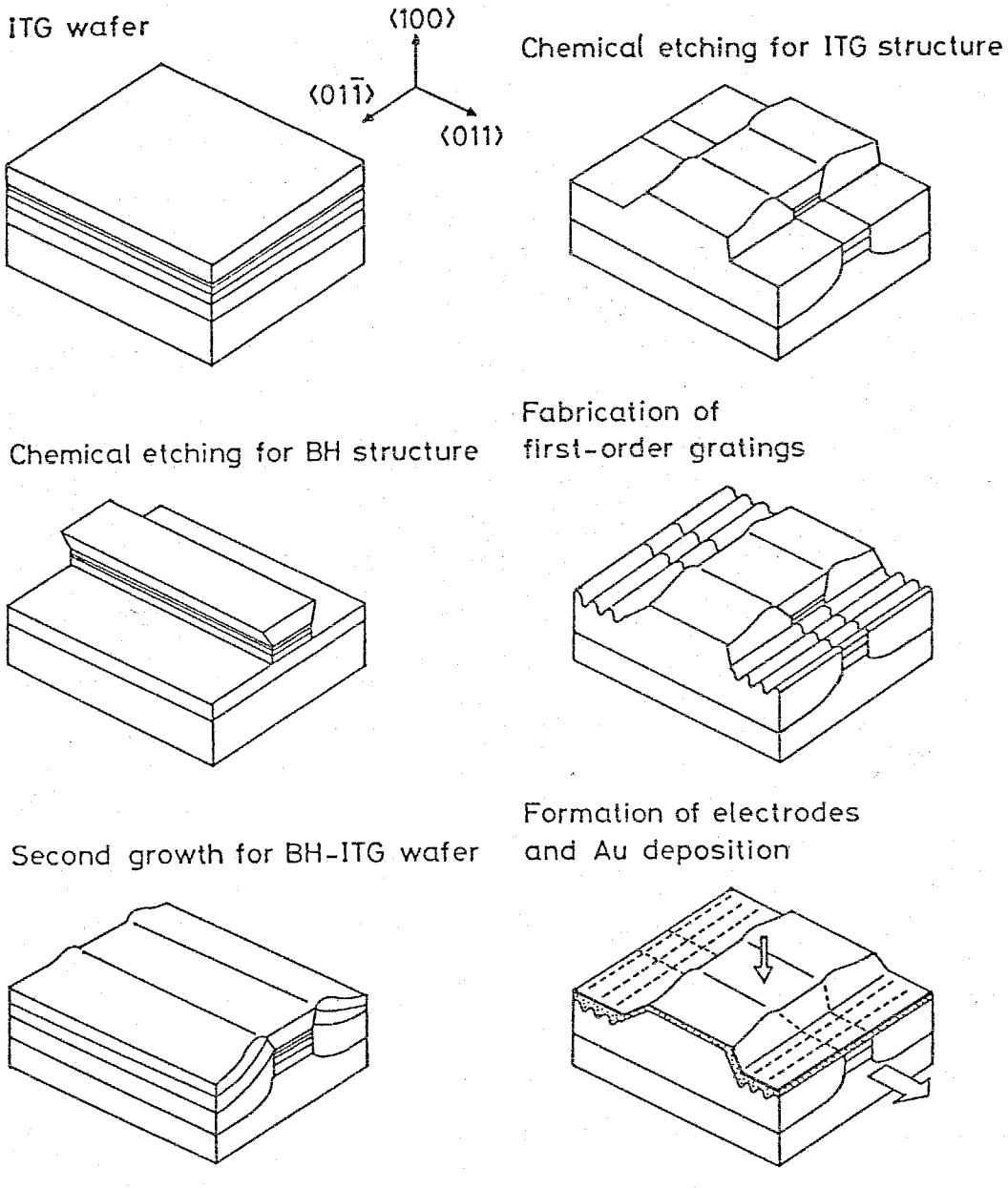

Fig.6-9 Schematic diagram of the fabrication processes for BH-DBR-ITG lasers.

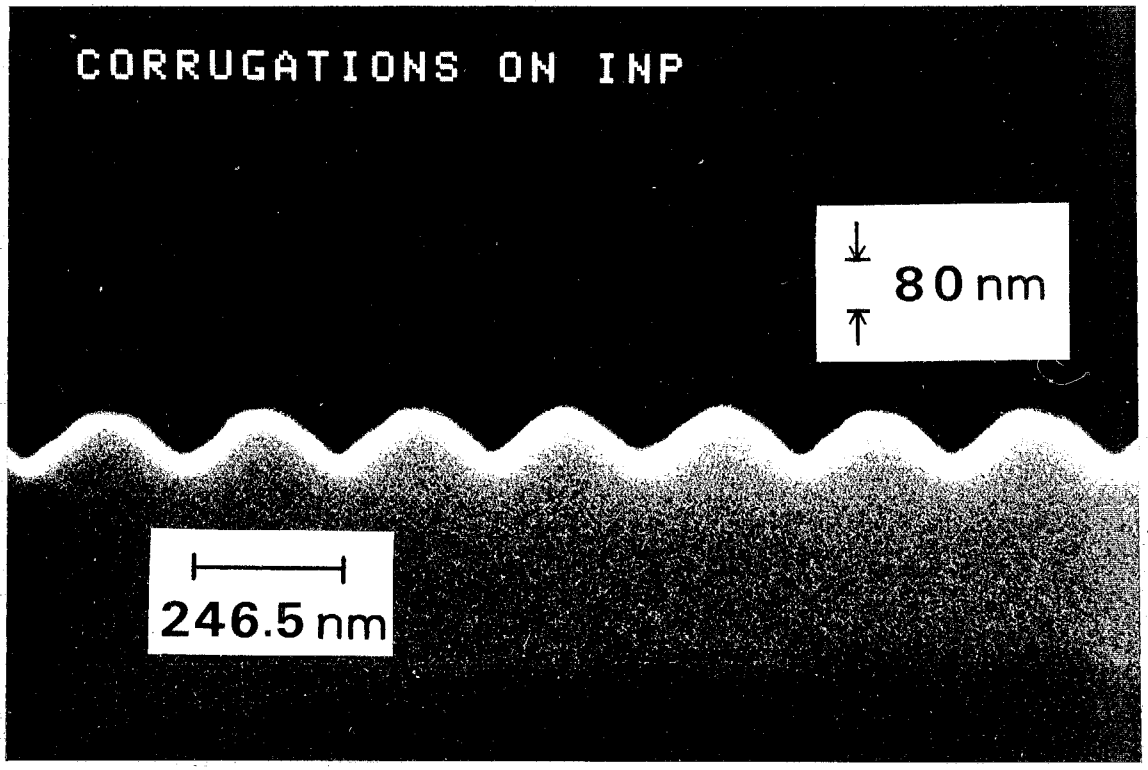

Fig.6-10 SEM photograph of the corrugated surface of InP with the first order corrugations.

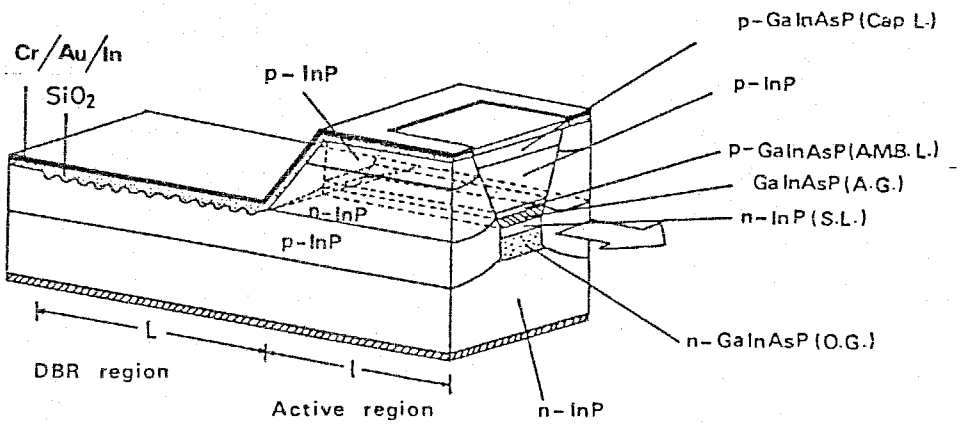

Fig.6-11 Schematic diagram of 1.5-1.6μm wavelength GaInAsP/InP BH-DBR-ITG laser.

contact on the active region.

[22] Alloying in highly pure hydrogen atmosphere for 2min at 410-420°C.

[23] Evaporations of Cr, Au(40mg), and In(40mg) to the ptype side. In this case, they were evaporated to the entire area of the wafer for the formation of TM mode filters and the tight contact of thermal bonding.

[24] Bonding the wafer to a ceramic plate with melting wax and sawing it to long bars by a thin steel wire after cooling the wax. These long bars were preserved in acetone to remove them from the ceramic plate.

[25] Cleaning the bars by fresh acetone several times and drying them by a lamp.

[26] Cleaving the bars into laser chips with a cleaved mirror and a DBR mirror on the opposite side of the chip with the active region length and the DBR region length of 250-350μm and 500-800μm, respectively.

From above mentioned procedures, asymmetric structure BH-DBR-ITG lasers were fabricated as schematically shown in Fig.6-9. Figure 6-10 shows the SEM photograph of the first order corrugations formed on InP substrate crystal.

6.4 Lasing properties of BH-DBR-ITG lasers

(1) Stationary operation

Thus obtained BH-DBR-ITG laser is schematically shown in Fig.6-11. The BH-DBR-ITG lasers which had relatively low threshold current less than 150mA under pulsed operation at

room temperature were bonded to copper heatsinks as mentioned in chapter 4. The pulsed threshold current as low as 80mA was obtained at room temperature with the active region width and length of 3μm and 300μm as shown in Fig.6-12. CW operations of these lasers were obtained with the temperature up to 12°C. Figure 6-13(a) shows the temperature dependences of the threshold current and the lasing wavelength under CW operation. Figure 6-13(b) shows the I-L characteristic and the lasing spectra for various current levels under CW operation at the temperature of 0°C. The incremental lasing wavelength variation of 0.1nm/deg which is 1/5 times that of the conventional lasers was obtained. The threshold current, output power, and the differential quantum efficiency of 78mA, 2.4mW, and 7.6 percent were obtained at 0°C. Stable single longitudinal mode operation was obtained with the injection current level up to more than 1.54 times the threshold current. Another results of those properties are also shown in Fig.6-14(a) and (b). For this laser, the threshold current, output power, and the differential quantum efficiency of 37mA, 6mW, and 16.3 percent were obtained at the temperature of 248K. Single longitudinal mode operation with the injection current level more than 1.54 times the threshold and the incremental lasing wavelength variation of 0.1nm/deg were also obtained for this laser. The large difference of the lasing wavelength of these two lasers was considered to be caused by the non uniformity of the wafer such as the deviation of the thickness of the output guide layer and the incomplete etching of the active layer in the DBR region. For both lasers, the DBR mode operating temperature region of

approximately 25deg was obtained as can be seen in Fig.6-13(a) and Fig.6-14(a), that was caused by a poor reflectivity of the DBR mirror and by a poor coupling coefficient of C_o and C_{out}. The differential quantum efficiency η_d of the asymmetric DBR-ITG laser shown in Fig.6-11 is expressed as

$$\eta_d = \frac{1-R}{[1+\{R/(C_{out}^2 R_c)\}^{1/2}]\{1-(C_{out}^2 RR_c)^{1/2}\}} \times \frac{\ln\{1/(C_{out}^2 RR_c)^{1/2}\}}{\alpha\ell+\ln\{1/(C_{out}^2 RR_c)^{1/2}\}} \qquad (6\text{-}5)$$

where R and R_c are the reflectivities of the cleaved facet and the DBR, C_{out} is the coupling coefficient between the active region and the DBR region. Putting $\alpha=38cm^{-1}$, $\ell=350\mu m$, R=0.42 and $\eta_d=0.163$ into the eq.(6-5), the effective reflectivity of the DBR was calculated to be $C_{out}^2 R_c=0.15$. This low value was due to the phase mismatching between the active guide and the output guide and to the poor reflectivity of the DBR. Further improvements in these factors are required still now. The problem of the phase matching was too severe for the high differential quantum efficiency and the low threshold current, a new structure DBR laser of a butt-jointed built-in (BJB) type was proposed to overcome it [260]. Figure 6-15 shows the schematic diagram of the BJB-DBR laser.

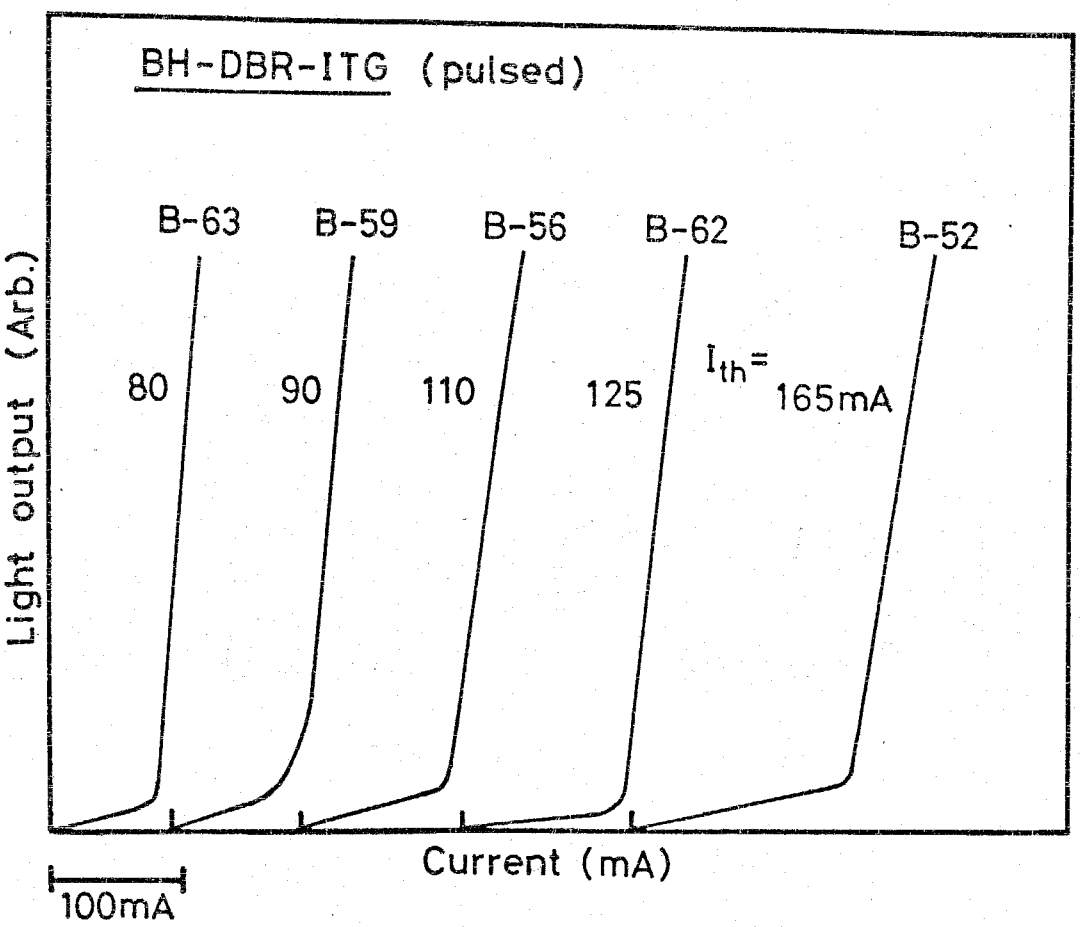

Fig.6-12 I-L characteristics of BH-DBR-ITG lasers under pulsed operation at room temperature. Active region thickness and width were 0.2μm and 3μm, and the lengths of active and DBR regions were 200-350μm and 500-800μm, respectively.

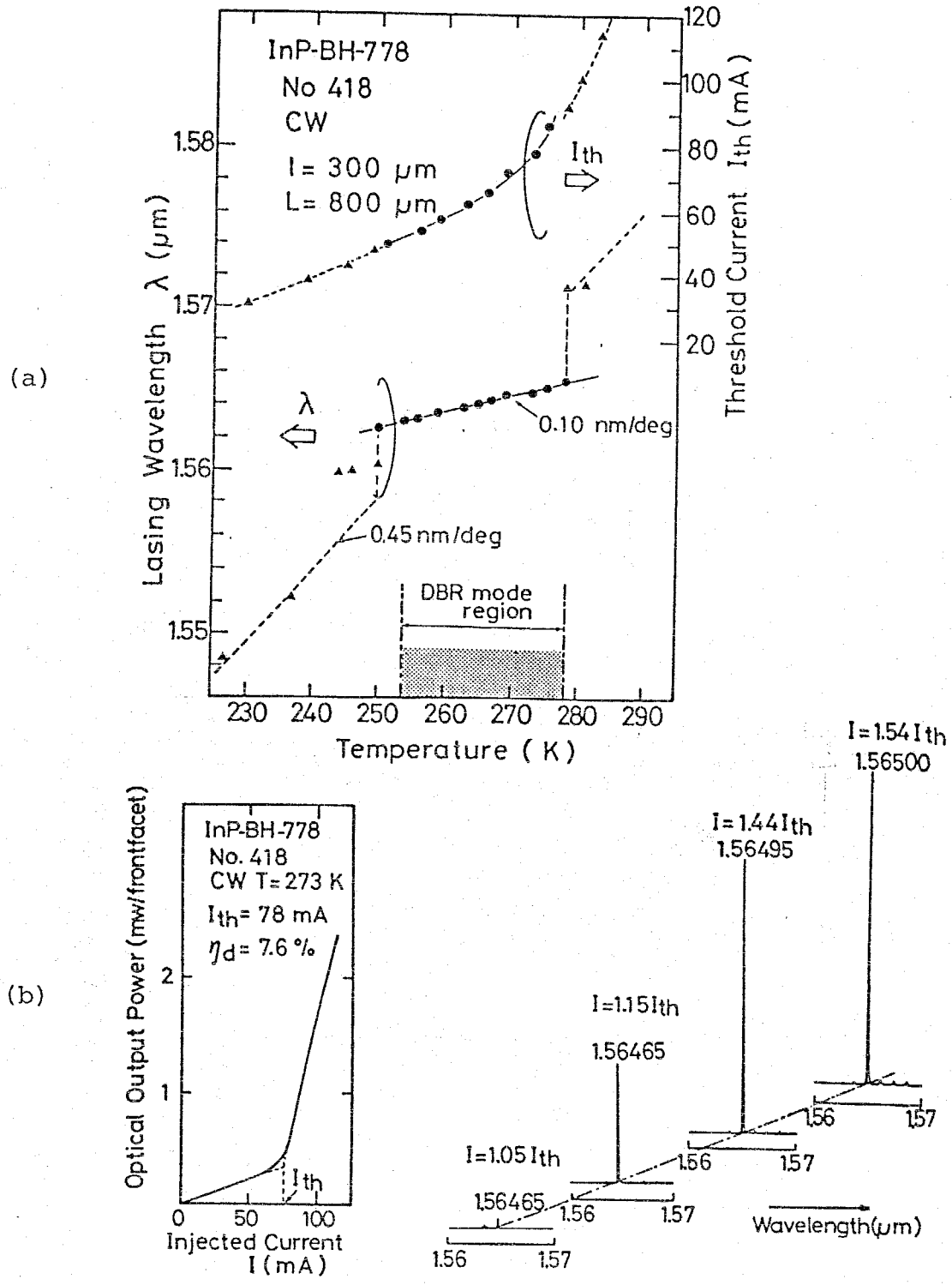

Fig.6-13 (a) Temperature dependences of the threshold current and the lasing wavelength of laser A.
(b) I-L characteristic and the lasing spectra for various injection current levels of laser A.

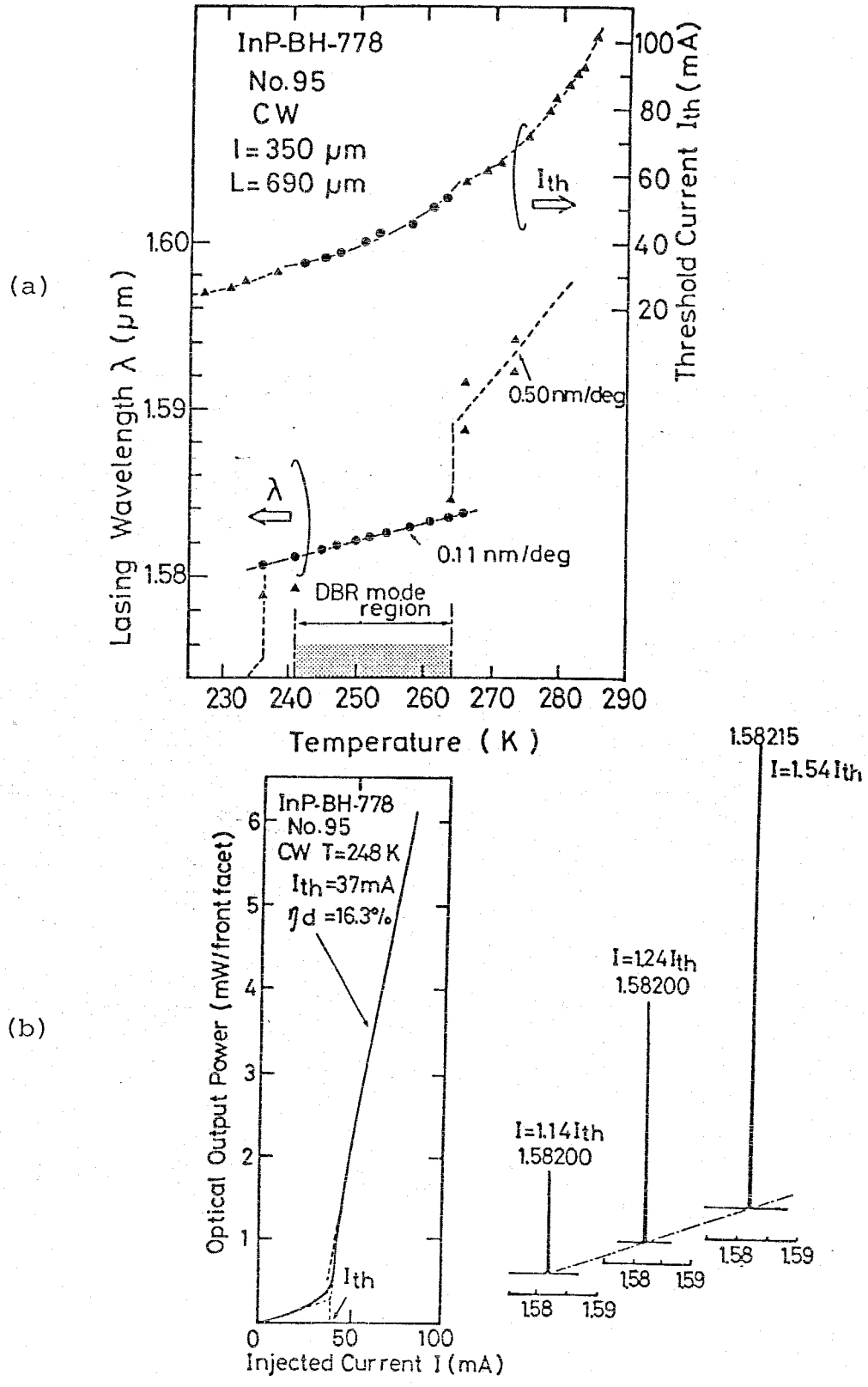

Fig.6-14 (a) Temperature dependences of the threshold current and the lasing wavelength of laser B.
(b) I-L characteristic and the lasing spectra for various injection current levels of laser B.

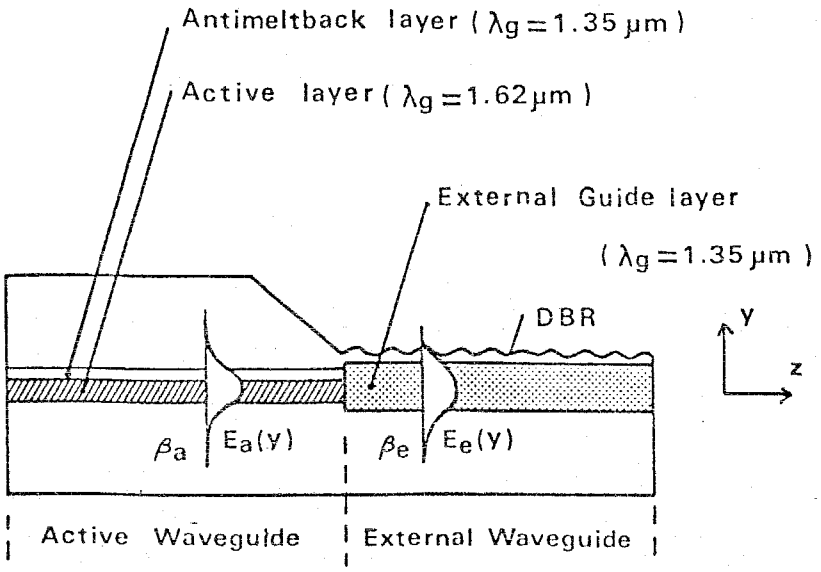

Fig.6-15 A schematic diagram of a 1.6μm wavelength GaInAsP/InP butt-jointed built-in (BJB) DBR laser.

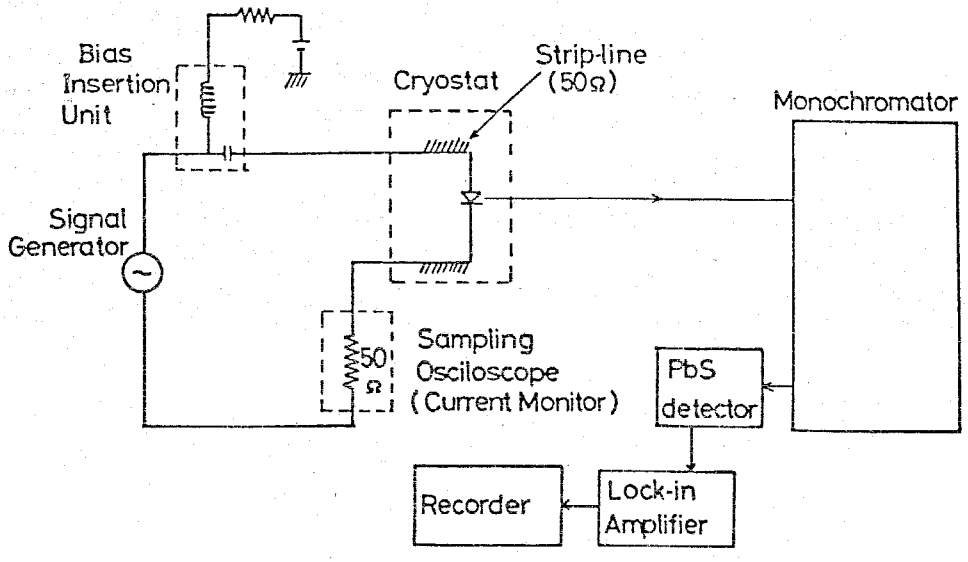

Fig.6-16 Schematic diagram of the measurement system of the high speed direct modulation.

(2) High speed direct modulation

The sample B of BH-DBR-ITG laser was directly modulated by sinusoidal current. DC bias current was fixed at 1.2 times the threshold current. The modulated current was supplied to the laser diode through the feeding coaxial cable and the strip line of 50Ω resistance. The modulated current was monitored by Sampling Oscilloscope. The modulated optical power from the laser diode was detected by PbS detector through the monochromator. The response time of PbS detector was much large, so that the time-averaged spectra were measured. The spectrum resolution was estimated to be about 0.07nm fron the full width of half maximum of the spectrum without modulation. The experimental set up used in this measurement is schematically shown in Fig.6-16.

Figure 6-17 shows the spectra of BH-DBR-ITG laser under high speed direct modulation with the modulation depth of 100 percent. A stable single mode operation was obtained with modulation frequency from 0.25GHz to 3GHz. Only the increase of the spectral width of the lasing mode, so called dynamic line shift , was observed, but the dynamic spectral broadening usually seen in Fabry-Perot type lasers was not observed at any frequency. Dynamic line shift was caused by the refractive index variation of the active layer under direct modulation. The maximum dynamic line shift was 0.27nm at the resonance-like frequency of 1.8GHz. This value was almost as same as the spectral width of only one lasing mode of directly modulated conventional Fabry-Perot type lasers [289]. But because of single mode operation under direct modulation, the

dynamic spectral width of BH-DBR-ITG laser measured was equal to the dynamic line shift and approximately 1/37 times the dynamic spectral width of conventional Fabry-Perot type lasers. Figure 6-18 shows the lasing wavelength of CW operation and the spectra of directly modulated BH-DBR-ITG laser at the resonance-like frequency of 1.8GHz with the modulation depth m of 100 percent as a function of the heatsink temperature. As can be seen, a single mode operation under high speed direct modulation was obtained in the almost whole temperature range at stable CW DBR mode operation.

The dynamic line shift varies with the modulated carrier density which depends on the modulation depth and the frequency. Figure 6-19 shows an example of the modulation depth dependence of the dynamic line shift with the modulation frequency of 1.8GHz. The dynamic line shift increased with the modulation depth. The modulation frequency dependence of the dynamic line shift was measured for the modulation depth of 50 and 100 percent and the results are shown in Fig.6-20. As can be seen, the dynamic line shift has a maximum value at a resonance-like frequency and the results agreed with the theoretical calculation from a large signal analysis as indicated by the solid lines.

Figure 6-21 shows the calculated transmission bandwidth of conventional single-mode optical fiber with the material dispersion of 20psec/nm/Km as a function of the transmission distance with the parameter of the dynamic spectral width of light source. As can be seen, the transmission bandwidth increases to 185GHzKm by using BH-DBR-ITG lasers with such

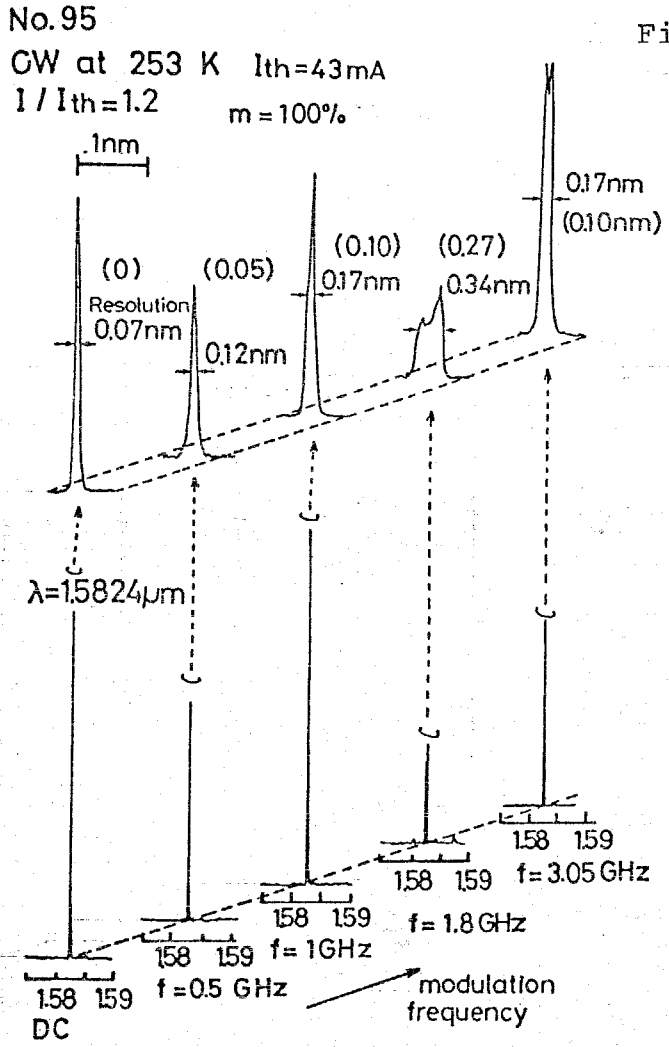

Fig.6-17

Lasing spectra of 1.58μm wavelength BH-DBR-ITG laser under stationary operation and high speed direct modulation with the frequency from 0.5GHz to 3GHz and the modulation depth of m=100%.

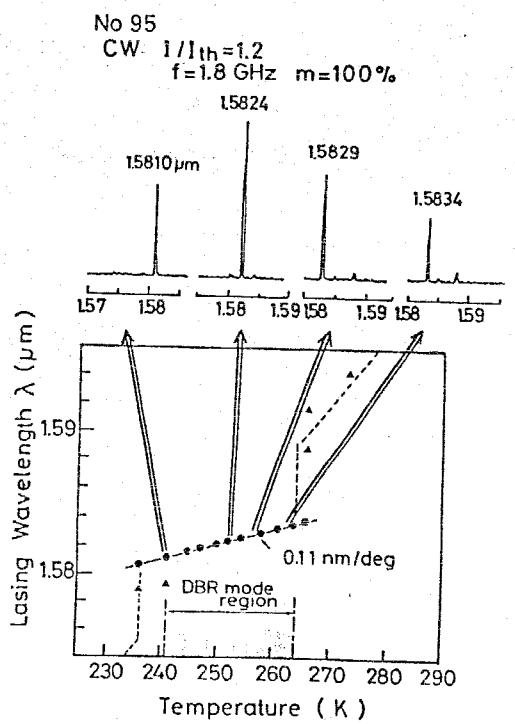

Fig.6-18

Lasing spectra of BH-DBR-ITG laser under high speed direct modulation with various temperatures.

Modulation frequency and the depth were fixed at 1.8GHz and 100%, respectively.

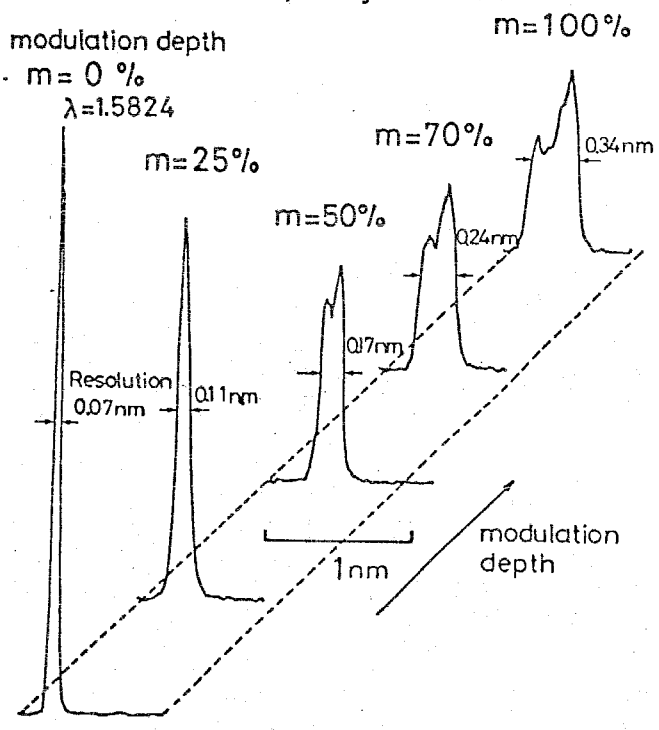

Fig.6-19

Lasing spectra of BH-DBR-ITG laser with various modulation depths.

The modulation frequency was fixed at 1.8GHz which was almost the resonance-like frequency.

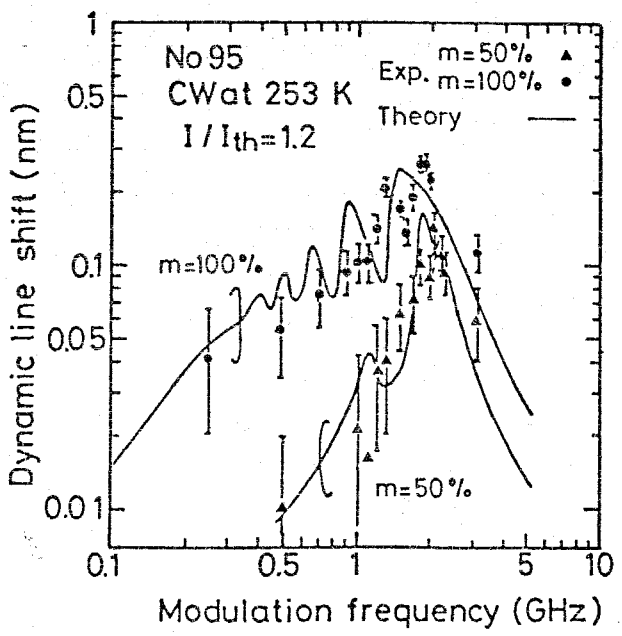

Fig.6-20

Dynamic line shift as a function of the modulation frequency with the modulation depths of 50 and 100%.

Solid lines indicate the calculated results from a large signal analysis.

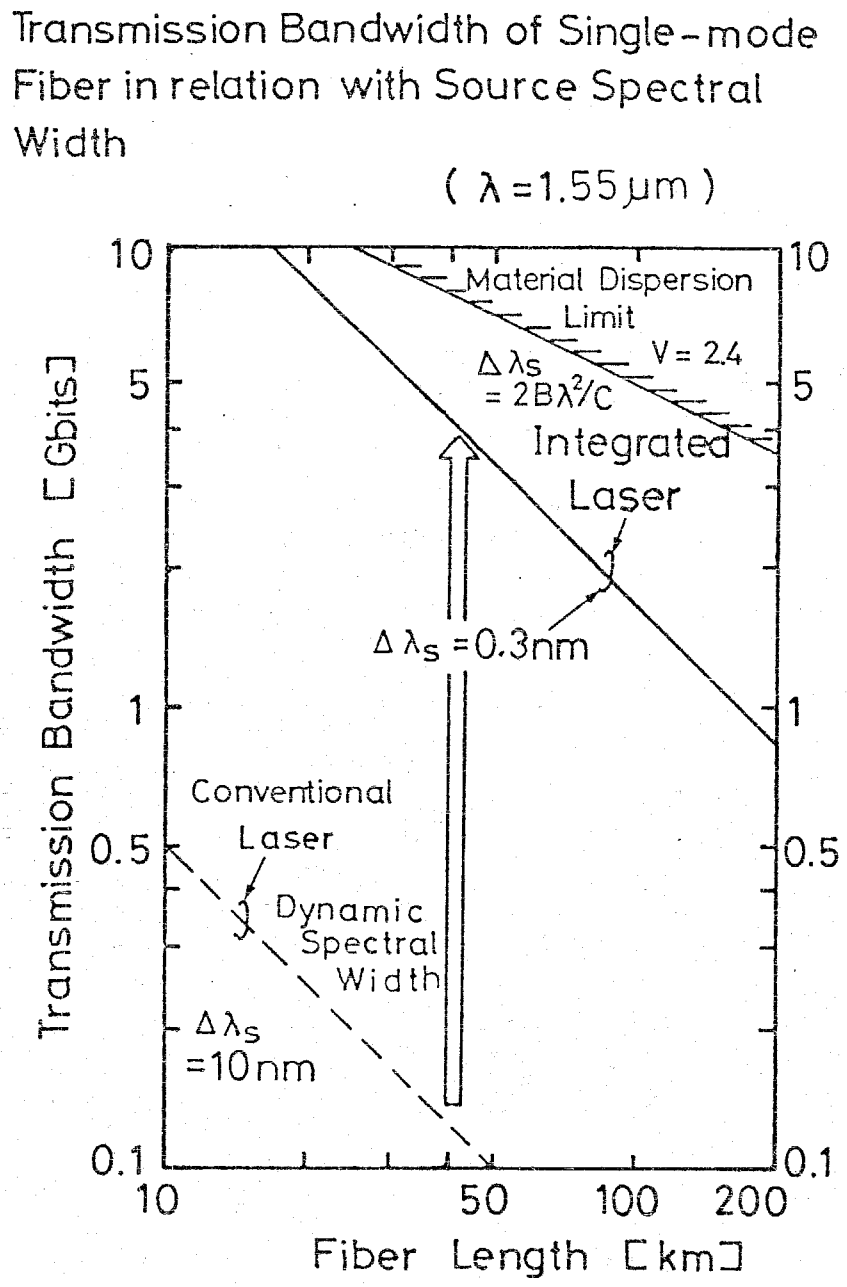

Fig.6-21 Transmission bandwidth of the conventional single-mode optical fiber with a dispersion of 20psec/nm/Km at the wavelength of 1.55μm as a function of the transmission distance.

narrow spectral width of 0.27nm as measured here. The bandwidth is about 37 times larger than that by using conventional Fabry-Perot type lasers. It could be possible to increase the transmission bandwidth to the material dispersion limit still more by optimizing the laser structure as discussed in section 6.2. However, this small value of the dynamic spectral width is fairly enough for the long distance optical fiber communication system using a presently available light detector as discussed in section 1.1.

6.5 Conclusion

The BH-DBR-ITG lasers of low threshold current were fabricated in the wavelength region of 1.5-1.6μm. The CW operation temperature as high as 12°C, the threshold current of 37mA, the differential quantum efficiency of 16.3 percent, and the output power of more than 6mW were obtained at the temperature of 248K. The single mode operation with the injection current more than 1.54 times the threshold current was obtained.

The single longitudinal mode operation under high speed direct modulation was also obtained with the frequency up to 3GHz with the modulation depth of 100 percent at the bias current of 1.2 times the threshold. The dynamic spectral width of 0.27nm was obtained at the resonance-like frequency. From that, the transmission bandwidth-transmission distance product BL of 185GHzKm for the conventional ultimately low-loss single mode optical fiber was obtained and the capability of the BH-DBR-ITG laser for the practical use in the long distance optical fiber communication was proved.

CHAPTER 7 CONCLUSIONS

The purpose of this thesis is to realize a long wavelength GaInAsP/InP laser as a light source for the long distance optical fiber communications using an ultimately low-loss optical fiber which has the minimum transmission loss wavelength of 1.5-1.6μm. According to that, the low threshold current GaInAsP/InP lasers with the wavelength of 1.6μm were developed by introducing an anti-melt-back (AMB) layer structure for the first time, and a buried heterostructure. Next, very narrow dynamic spectral width of less than 0.3nm under high frequency direct modulation up to 3GHz was realized by a buried heterostructure distributed Bragg reflector integrated twin guide (BH-DBR-ITG) laser with the wavelength of 1.5-1.6μm, which is enough for the long distance optical fiber communications using presently available optical fibers and detectors.

The concluding remarks in this study are summarized as follows:

[1] A new structure using an additional "anti-melt-back" layer was proposed to prevent the meltback problem during the liquid phase epitaxial growth of longer wavelength GaInAsP/InP lasers, and the room temperature CW operations of 1.5-1.6μm wavelength GaInAsP/InP lasers were achieved by introducing it.

[2] The growth conditions of GaInAsP quaternary crystals lattice matched to (100) oriented InP substrate were clarified and the fabrication of GaInAsP/InP double

heterostructure lasers of 1.1-1.67μm wavelength region was made possible.

[3] The threshold current density normalized by the active layer thickness of 5-6KA/cm^2/μm was obtained for the anti-melt-back layer structure laser with the wavelength of 1.45-1.65μm, it was almost comparable to that of the ordinary structure laser with the wavelength of 1.2-1.5μm. Thus the increase of threshold current due to the additional anti-melt-back layer was experimentally found to be negligible.

[4] The temperature dependences of the threshold current and the lasing wavelength variation were made clear with the lasers of different compositions of the active layer. For all the lasers investigated, the threshold current was found to increase with the temperature exponentially as given by $I_{th}(T)=I_{tho}\exp(T/T_0)$, the value T_0 of 100-150K and 40-70K was obtained at the temperature below 250K and at around room temperature, respectively. The temperature dependence of the lasing wavelength was found to be 0.4nm/deg for 1.3μm wavelength laser and 0.5nm/deg for 1.55μm wavelength laser.

[5] A new fabrication process using a selective etching and a selective meltback method was proposed to make buried heterostructure lasers of 1.6μm wavelength region taking account of fine crystal growth on the side walls of the etched stripe mesa. By use of this method, the room temperature CW operations of 1.6μm wavelength GaInAsP/InP BH lasers were obtained with a low threshold current of

28mA and a differential quantum efficiency of 43 percent for the cavity length, the stripe width, and the thickness of active region of 250-350μm, 3-5μm, 0.3μm, respectively.

[6] The steep increase of the threshold current versus the temperature was found to be related to the temperature dependence of the differential quantum efficiency from the measurements of the 1.6μm wavelength BH lasers with CW conditions. This fact was concluded to be caused by the intervalence band absorption and non-radiative Auger recombination, the reduction of the optical confining effect was proved to be necessary for the high differential quantum efficiency.

[7] The buried heterostructure distributed Bragg reflector integrated twin guide laser of the low operation current was achieved in 1.5-1.6μm wavelength region. The CW operation temperature as high as 12°C, the low threshold current of 37mA, the differential quantum efficiency of 16.3 percent per front facet, and the output power of 6mW at the temperature of 248K were obtained. The single longitudinal mode operation was kept with the injection current of more than 1.54 times the threshold.

[8] The temperature region of the single longitudinal mode operation of the distributed Bragg reflector laser was discussed theoretically taking account of the effect of the refractive index variation due to the injected carriers. It was proved to be increased by the reductions of the active region length and the optical confinement factor of the active region.

[9] The single longitudinal mode operation under high frequency direct modulation was obtained for the BH-DBR-ITG laser with the frequency from 0.25GHz up to 3GHz and the modulation depth of 100 percent at the bias current of 1.2 times the threshold. Any spectral broadening, which occurs in conventional Fabry-Perot type lasers due to the increase of lasing modes under high frequency direct modulation, was not observed. The dynamic spectral width of this laser was only 0.27nm as the maximum at resonance-like frequency of 1.8GHz and was only 1/37 of that of conventional 1.5-1.6μm wavelength BH lasers. This value corresponds to the transmission bandwidth-distance product of 185GHz·Km for ordinary ultimately low-loss optical fiber, and also gives the prospect of this laser as a light source for the long distance optical fiber communications.

ACKNOWLEDGEMENTS

The author has been greatly indebted to Professor Yasuharu SUEMATSU for his guidance throughout this study and giving him lessons day and night from the views of human life, technology, and histories.

The author would like to acknowledge Associate Professors K.IGA and K.FURUYA of Tokyo Institute of Technology for their fruitful discussions on this study.

The author would like to express his appreciation to Professors K.SUETAKE(presently with Kanagawa University), T.SEKIGUCHI, T.TAKOH, M.KAWAMURA, K.TAKAHASHI, Y.NAITOH, N.GOTOH, Associate Professors M.MATSUMURA, T.MORIIZUMI, and M.KONAGAI of Tokyo Institute of Technology for their fruitful discussions.

The author is grateful to Drs. C.OTA, T.YAMAMOTO, K.SAKAI, S.AKIBA, and Y.MATSUSHIMA of KDD laboratory and the members of Associate Professor K.IGA's laboratory such as Drs. Y.KOKUBUN, K.WAKAO(Fujitsu Co.), and Mr.K.MORIKI for their fruitful discussions and the considerable assistances from the beginning of this study.

The author would like to acknowledge Drs. Y.ITAYA(presently with NTT) and K.UTAKA(KDD) for their kind and continuous support in almost everything in the experiments such as the crystal growth, the fabrication of BH-DBR-ITG lasers.

The author would like to acknowledge Drs. H.KAWANISHI (Kohgakuin University) for his continuous support and advices in fabricating low noise detection circuit for longer wave-

length region and his preceding achievements on DBR-ITG lasers, and K.KISHINO of Tokyo Institute of Technology for his kind and fruitful discussions throughout this study.

The author is very grateful to Drs. A.R.ADAMS(Surrey University in United Kingdom) and K.E.STUBKJAER(now in Denmark) for their encourageous advices, suggestions, and works during their stay in Japan and the kind corrections of my English.

The author is also grateful to Professor M.H.PILKUHN (Stuttgart University in Federal Republic of Germany) for his fruitful discussions and his interesting and enlightening lectures on semiconductor lasers and detectors.

The author would like to acknowledge Associate Professors M.YAMADA(Kanazawa University), T.KAMBAYASHI(Technological University of Nagaoka), and T.HONG(Korea Marchant Marine College) for their fruitful discussions on laser dynamics and the fabrication of the lasers.

The author would like to acknowledge Messers. M.ASADA, T.TANBUN-EK, F.KOYAMA of his colleagues of Professor SUEMATSU and FURUYA's laboratory for their important achievements and their helps beyond expression in prepapring this thesis.

The author also would like to acknowledge Messers. T.MISHIMA,M.KODAIRA(Toshiba Co.), K.ITOH, Y.ABE, A.KOSHIZUKA (Fujitsu Co.), S.YOSHIZAWA for their helpful assistances in the experiments and calculations, Miss K.SUGIYAMA, Mr. S.TAMURA, and Miss K.YOKOTA for their help in the crystal growth.

The author would like to acknowledge Messers. T.OKUMURA (Anritsu Co.), Y.TAKAHASHI(Anritsu Co.) for their help in measuring the dopant concentrations of In/Zn and In/Te

alloys, T.WATANABE(from Unison Co.), and S.SUZAKI(from Fujikura Cabling Co.) for their assistances in the crystal growth and the fabrication.

The author would like to acknowledge Mr. T.TSUDA(NEC Co.) and Associate Professor Y.KIDOH(Toyama Technological High School) for their continuous and kind encouragements.

The author would like to acknowledge Dr. H.TOKIWA(KDD), Messers. S.ISHIKAWA(NEC Co.), M.MIYAMOTO(Fujikura Cabling Co.), S.KATAYAMA(Nippon Sheet Glass Co.), Y.SAITOH(Fujitsu Fanac Co.), H.NISHIMOTO(NEC Co.), Y.SAKAKIBARA(Mitsubishi Co.), M.KUBOTA (NTT), K.KOBAYASHI(NEC Co.), C.CHONG(now in Singapore), and K.KWOK(Nissei Trading Co.) for their encouragements in their student age.

The author also would like to acknowledge all the colleagues of Professor SUEMATSU and FURUYA's laboratory, Dr. O.HIROTA of Tokyo Institute of Technology, Messers. T.SUGOU, K.MATSUMOTO, I.KOMAZAKI, K.KIKUSHIMA, Y.TOHMORI, M.SHINDOH(from JNR), J.TODA (from Dai Nippon Printing Co.), Z.WANG(from China), S.WANG (from China), S.TEJIMA, H.TSUSHIMA, A.KASUKAWA, E.TAKAO, T.MATSUSHITA Miss M.YASUDA, and Miss H.KAWAKAMI for their helpful assistances in preparing this thesis and giving the author pleasant student life.

The author also would like to express appreciation to the members of Professors TAKAHASHI's laboratory, SEKIGUCHI's laboratory, NAITOH's laboratory, NOMURA's laboratory for providing the experimental equipments.

This work was supported by Scientific Research Grant-In-Aid from the Ministry of Education, Science, and Culture, Japan.

The author was financially supported by the Japan Scholarship Society.

Finally, the author would like to express his gratitude to all his family.

APPENDIX

History of GaInAsP/InP lasers

year	Growth Tech. Sub. Orient.	λ(μm)	Remarks	Authors	Ref.No.
1975	LPE (111)B	1.1	pulse	A.P.Bogatov L.M.Dolginov P.G.Eliseev M.G.Milvidsky B.N.Sverdlov E.G.Shevchenko	[162]
1976	LPE (111)B	1.1	pulse	J.J.Hsieh	[163]
	LPE (111)B	1.1	CW	J.J.Hsie J.A.Rossi J.P.Donnelly	[164]
	LPE (111)B	1.15	pulse	K.Oe K.Sugiyama	[165]
	LPE (111)B	1.57	T=77K	H.Nagai Y.Noguchi	[166]
1977	LPE (100)	1.27	pulse	T.Yamamoto K.Sakai S.Akiba Y.Suematsu	[167]
	LPE (100)	1.21 1.25	BH CW, I_{th}=60mA	J.J.Hsieh C.C.Shen	[168]
	LPE (100)	1.13	pulse (T=110K)	Y.Itaya Y.Suematsu K.Iga	[169]
	LPE (100)	1.3	CW	K.Oe S.Ando K.Sugiyama	[170]
	VPE	1.7	pulse	C.J.Nuese R.E.Enstrom J.R.Appert	[171]
	LPE (100)	1.2	pulse vertical furnace	K.Wakao K.Moriki T.Kambayashi K.Iga	[172]
1978	LPE (100)	1.5	pulse	H.Nagai Y.Noguchi	[174]
	LPE (100)	1.3	CW	T.Yamamoto K.Sakai S.Akiba Y.Suematsu	[175]
	MBE (100)	1.65	pulse	B.I.Miller J.H.McFee R.J.Martin P.K.Tien	[176]

1978	LPE (100)	1.25	DBR T=150K pulse	H.Kawanishi Y.Suematsu Y.Itaya S.Arai	[177]
	LPE (100)	1.3	BH CW, I_{th}=60mA	H.Kano K.Oe S.Ando K.Sugiyama	[178]
	LPE (100)	1.67	Quaternary Clad. pulse	S.Akiba K.Sakai T.Yamamoto	[179]
	LPE (100)	1.2-1.5	pulse	S.Arai Y.Itaya Y.Suematsu K.Kishino S.Katayama	[180]
1979	VPE	1.25	CW, I_{th}=85mA η_d=50% Life>4000hrs	G.H.Olsen C.J.Nuese M.Ettenberg	[181]
	LPE (100)	1.3	MSB pulse	K.Kishino Y.Suematsu Y.Itaya	[182]
	LPE (100)	1.3	J_{th}=770A/cm^2	Y.Itaya S.Katayama Y.Suematsu	[183]
	LPE (100)	1.67	AMB pulse	S.Arai Y.Suematsu Y.Itaya	[184]
	LPE (100)	1.15	RW CW	A.Doi N.Chinone K.Aiki R.Itoh	[185]
	LPE (100)	1.5	Opt. Waveguide pulse	N.Kobayashi Y.Horikoshi	[186]
	LPE (100)	1.3	DBR(first order) T=180K pulse	H.Kawanishi Y.Suematsu K.Utaka Y.Itaya S.Arai	[188]
	LPE (100)	1.18	TJS T=100K pulse	D.J.Bull N.B.Patel F.C.Prince Y.Nannichi	[189]
	LPE (100)	1.3	SA CW	H.Nishi M.Yano Y.Nishitani Y.Akita M.Takusagawa	[190]
	LPE (100)	1.3	CW Life>10000hrs	T.Yamamoto K.Sakai S.Akiba	[191]

1979	LPE (100)	1.2-1.3	CW Zn-diffused	J.J.Hsieh	[192]
	LPE (100)	1.3	CW	Y.Itaya Y.Suematsu S.Katayama K.Kishino S.Arai	[193]
	LPE (100)	1.1	DFB T=170K	A.Doi T.Fukuzawa M.Nakamura R.Itoh K.Aiki	[194]
	LPE (100)	1.56	AMB CW, I_{th}=300mA	S.Akiba K.Sakai Y.Matsushima T.Yamamoto	[195]
	LPE (100)	1.55	pulse J_{th}=2.1KA/cm^2	G.D.Henshall P.D.Greene	[196]
	LPE (100)	1.55	CW I_{th}=250mA	H.Kawaguchi K.Takahei Y.Toyoshima H.Nagai G.Iwane	[197]
	LPE (100)	1.3	EMS pulse	F.C.Prince N.B.Patel D.J.Bull	[198]
	LPE (100)	1.55	Ridge Waveguide CW	I.P.Kaminow R.E.Nahory M.A.Pollack L.W.Stulz J.C.DeWinter	[200]
	LPE (100)	1.35	J_{th}=670A/cm^2	R.J.Nelson	[201]
	LPE (100)	1.2	SEL T=77K	H.Soda K.Iga C.Kitahara Y.Suematsu	[203]
	LPE (100)	1.51	AMB CW	S.Arai M.Asada Y.Suematsu Y.Itaya	[204]
1980	LPE (100)	1.3	DBR-ITG (first order) pulse	K.Utaka Y.Suematsu K.Kobayashi H.Kawanishi	[206]
	VPE (100)	1.3	CW (dual chamber)	T.Mizutani M.Yoshida A.Usui H.Watanabe T.Yuasa I.Hayashi	[207]

1980	LPE (100)	1.62	BH (AMB) CW I_{th}=110mA	Y.Itaya T.Tanbun-Ek K.Kishino S.Arai Y.Suematsu	[208]
	LPE (100)	1.3	Strip-BH CW I_{th}=170mA	R.J.Nelson P.D.Wright P.A.Barnes R.L.Brown T.Cella R.G.Sobers	[209]
	LPE (100)	1.3	Etched Mirror I_{th}=300mA	K.Iga B.I.Miller	[210]
	LPE (100)	1.5	BH CW I_{th}=25mA	H.Nagai Y.Noguchi K.Takahei Y.Toyoshima G.Iwane	[212]
	LP-MOCVD (100)	1.15	pulse	J.P.Hirtz J.P.Duchemin P.Hirtz B.DeCremoux T.Pearsall M.Bonnet	[213]
	LPE (100)	1.16	Quantum well	E.A.Rezek N.Holonyak,Jr. B.K.Fuller	[214]
	LPE (100)	1.62	BH (AMB) CW I_{th}=37mA	S.Arai M.Asada Y.Suematsu Y.Itaya T.Tanbun-Ek K.Kishino	[215]
	LPE (100)	1.5-1.6	DBR-ITG (AMB) (first order) pulse	K.Utaka K.Kobayashi K.Kishino Y.Suematsu	[216]
	VPE (100)	1.55 1.65	CW	G.H.Olsen T.J.Zamerowski N.J.DiGiuseppe	[217]
	VPE (100)	1.5-1.55	CW	W.D.Johnston,Jr K.E.Strege	[218]
	LPE (100)	1.3	BC CW I_{th}=28mA	T.Murotani E.Oomura H.Higuchi H.Namizaki W.Susaki	[219]
	LPE (100)	1.5	CW	J.J.Hsieh	[220]
	LPE (100)	1.3	Wet-etched Mirror, pulse	B.I.Miller K.Iga	[221]

1980	LPE (100)	1.3	BH CW I_{th}=10mA	M.Hirao S.Tsuji K.Mizushima A.Doi M.Nakamura	[223]
	LPE (100)	1.5	PCW CW	N.Matsumoto K.Onabe T.Yuasa Y.Matsumoto T.Furuse I.Sakuma	[224]
	LPE (100)	1.3	Etched Mirror CW, I_{th}=190mA	K.Iga B.I.Miller	[225]
	LPE (100)	1.5	BH (p-InP Sub.) CW I_{th}=40mA	Y.Nakano K.Takahei Y.Noguchi M.Tokunaga H.Nagai K.Nawata M.Fujimoto	[227]
	LPE (100)	1.3	TS CW	K.Moriki K.Wakao M.Kitamura K.Iga Y.Suematsu	[228]
	LPE (100)	1.65	BH CW I_{th}=33mA	Y.Noguchi K.Takahei Y.Suzuki H.Nagai	[229]
	LPE (100)	1.2	T-laser (on semi-insul. Sub.) pulse	P.C.Chen K.L.Yu S.Margalit A.Yariv	[230]
1981	LPE (100)	1.3 1.5	PBH CW I_{th}=15mA	I.Mito K.Kaede M.Kitamura Y.Odagiri M.Seki K.Kobayashi	[231]
	LPE (100)	1.5	BH (semi-insul. Sub.) CW, I_{th}=38mA	T.Matsuoka K.Takahei Y.Noguchi H.Nagai	[232]
	LPE (100)	1.5	SML CW I_{th}=82mA	H.Imai H.Ishikawa T.Tanahashi M.Takusagawa	[233]
	LPE (100)	1.3	BC CW I_{th}=12mA	E.Oomura H.Higuchi R.Hirao H.Namizaki T.Murotani W.Susaki	[234]

1981	LP-MOCVD (100)	1.3	pulse	J.P.Hirtz M.Razeghi J.P.Larivain S.Hersee J.P.Duchemin	[235]
	LPE (100)	1.5	PCW CW	Y.Noda K.Sakai Y.Matsushima	[236]
	MBE (100)	1.70	CW T=6°C	H.Asahi Y.Kawamura M.Ikeda H.Okamoto	[237]
	LPE (100)	1.5	BH-LD array (4) CW I_{th}=50mA	Y.Suzuki Y.Noguchi K.Takahei H.Nagai G.Iwane	[238]
	LPE (100)	1.3	EMS I_{th}=45mA	P.C.Chen K.L.Yu S.Margalit A.Yariv	[240]
	LPE (110)	1.3	J_{th}=1KA/cm^2	F.Z.Hawrylo	[241]
	LPE (100)	1.5-1.6	BH-DBR-ITG CW (T=250K)	K.Kobayashi K.Utaka Y.Abe Y.Suematsu	[242]
	LPE (100)	1.5-1.6	BH-DBR-ITG Single mode f=1GHz	K.Utaka K.Kobayashi Y.Suematsu	[243]
	LPE (100)	1.5	(AMB) CW Life>10000hrs	Y.Noda K.Sakai Y.Matsushima S.Akiba	[244]
	LPE (100)	1.3	VGSB CW I_{th}=10mA	H.Ishikawa H.Imai T.Tanahashi Y.Nishitani M.Takusagawa	[245]
	LPE (100)	1.3	Shottky-barrier stripe, CW	J.C.Bouley G.Chaminant J.Charil P.Devoldere M.Gilleron	[246]
	LPE (100)	1.55	DFB, pulse	O.Mikami	[249]
	LP-MOCVD (100)	1.23	CW I_{th}=250mA	M.Razeghi J.P.Hirtz P.Hirtz J.P.Larivain R.Bondeau B.DeCremoux J.P.Duchemin	[250]

1981	LPE (100)	1.3	Etched Mirror Lens-like strip waveguide I_{th}=160mA	K.Moriki K.Iga M.Uchida K.Wakao T.Kunikane	[252]
	LPE (100)	1.2	BH-SE T=77K	H.Okuda H.Soda K.Moriki Y.Motegi K.Iga	[253]
	LPE + MOCVD (100)	1.3	BH (MO-CVD over growth) CW, I_{th}=57mA	W.Ng C.S.Hong H.Manasevit P.D.Dapkus	[254]
	LP-MOCVD (100)	1.5	pulse J_{th}=2.5KA/cm^2	M.Razeghi P.Hirtz J.P.Larivain R.Blondeau B.DeCremoux J.P.Duchemin	[255]
	LPE (100)	1.55	BH (p-InP Sub.) CW I_{th}=30mA	Y.Nakano K.Takahei Y.Noguchi H.Nagai K.Nawata M.Tokunaga	[256]
	LPE (100)	1.54	BC CW I_{th}=45mA	W.J.Delvin R.H.Walling P.J.Fiddyment R.E.Hobbs D.Murrell R.E.Spillett A.G.Steventon	[257]
	LPE (100)	1.3 1.58	CCM CW, I_{th}=15mA	H.Nomura M.Sugimoto A.Suzuki	[258]
	LPE (100)	1.58	BH-DBR-ITG (first order) CW (T=250K, I_{th}=37mA)	T.Tanbun-Ek S.Arai F.Koyama K.Kishino S.Yoshizawa T.Watanabe Y.Suematsu	[259]
	LPE (100)	1.58	BH-DBR-ITG Single mode 0.5GHz<f<3GHz	F.Koyama S.Arai Y.Suematsu K.Kishino	[259']
	LPE (100)	1.55	BJB-DBR (first order) pulse	Y.Abe K.Kishino Y.Suematsu S.Arai	[260]

1981	LPE (100)	1.5-1.6	BH-DFB (second order) CW, I_{th}=60mA Single mode	NTT group	[261]
	LPE (100)	1.57	BH-DFB (first order) CW, I_{th}=250mA Single mode f=500Mbit/s	K.Utaka S.Akiba K.Sakai Y.Matsushima	[262]

REFERENCES

[1] K.C.Kao and G.A.Hockman, "Dielectric-fiber surface waveguides for optical frequencies", Proc. Inst. Electron. Engineers, vol.113, 7, pp.1151-1158, July 1966.

[2] F.P.Kapron, D.B.Keck and R.D.Maurer, "Radiation losses in glass optical waveguides", Appl.Phys.Lett., vol.17, 10, pp.423-425, Nov 1970.

[3] D.B.Keck, P.C.Schultz and F.Zimar, "Attenuation of multimode glass optical waveguides", Appl.Phys.Lett., vol.21, pp.215-217, Sept. 1972.

[4].D.B.Keck, R.D.Maurer and P.C.Schultz, "On the ultimate lower limit of attenuation in glass optical waveguides", Appl.Phys.Lett., vol.22, pp.307-309, April 1973.

[5] L.G.Cohen, P.Kaiser, J.B.MacChesney, P.B.O'Connor and H.M.Presby, "Tranmission porperties of a low-loss near-parabolic-index fiber", Appl.Phys.Lett,. vol.26, pp.472-474, April 1975.

[6] J.B.MacChesney, P.B.O'Connor, and J.R.Simpson, "A new technique for the preparation of low-loss and graded-index optical Fibers," Proc.IEEE, vol.62, 9, pp.1280-1281, Sept 1974.

[7] J.B.MacChesney, P.B.O'Connor, F.V.DiMarcello, J.R.Simpson and P.D.Lazay, "Preparation of low loss optical fibers using simultaneous vapor phase deposition and fusion." Tenth International Congress on Glass, July 1974, Kyoto, Japan.

[8] M.Horiguchi and H.Osanai, "Spectral losses of low-OH-content optical fibers," Electron.Lett., vol.12, pp.310-311, June 1976.

[9] T.Izawa, N.Shibata and A.Takeda, "Optical attenuation in pure and doped fused silica in the IR wavelength region," Appl.Phys.Lett., vol.31, 1, pp.33-35, July 1977.

[10] Yasuji Ohmori, Hisaaki Okazaki, Iwao Hatakeyama and Hisao Tanaka, "Very low OH content P_2O_5-doped silica fibres," Electron.Lett., vol.15, 20, pp.616-618, Sept. 1979

[11] K.Chida, F.Hanawa, M.Nakahara and N.Inagaki, "Simultaneous dehydration with consolidation for VAD method," Electron.Lett., vol.15, pp.835-836, 1979.

[12] T.Moriyama, O.Fukuda, K.Sanada and K.Inada; "Ultimately low OH content V.A.D. optical fiberes," Electron.Lett., vol.16, 18, pp.698-699, Aug. 1980.

[13] F.Hanawa, S.Sudo, M.Kawachi and M.Nakahara, "Fabrication of completely OH-free V.A.D. fibre," Electron.Lett., vol.16, 18, pp.699-700, August.1980,

[14] S.Kawakami and J.Nishizawa, "An optical waveguide with optiumum distribution of the refractive index with reference to waveform distortion," IEEE Trans.Microwave Theory and Techniques, MTT-16, 10, pp.114, Oct.1968

[15] K.Furuya, M.Miyamoto and Y.Suematsu, "Bandwidth of single mode optical fibers," Trans.IECE Jpn., vol.E-62, 5, pp.305-310, May 1979.

[16] M. Nakahara, K.Chida, F. Hanawa, S. Sand Masaharu Horiguchi, "Fabrication of low-loss and wide-bandwidth V.A.D. optical fibres at 1.3μm wavelength," Electron.Lett., vol.16, 3, pp.102-103, Jan. 1980

[17] C.Lin, P.L.Liu, T.P.Lee, C.A.Burrus, F.T.Stone, A.J.Ritger, "Measuring high-bandwidth fibres in the 1.3μm region with picosecond InGaAsP injection lasers and ultrafast InGaAs detectors," Electron.Lett., vol.17, 13, pp.438-440, Jun.1981

[18] M.Nakahara, S.Sudo, N.Inagaki, K.Yoshida, S.Shibuya, K.Kokura and T.Kuroha, "Ultra wide bandwidth V.A.D. fibre," Electron.Lett., vol.16, 10, pp.391-392, May 1980.

[19] M.Kawachi, A.Kawana and T.Miyashita, "Low-loss single-mode fiber at the material-dispersion-free wavelength of 1.27μm," Electron.Lett., vol.13, pp.442-443, July 1977.

[20] T.Miya, Y.Terunuma, T.Hosaka and T.Miyashita, "An ultimately low-loss single-mode fiber at 1.55μm," Electron.Lett., vol.15, 4, pp.106-108, Feb.1979.

[21] T.Miya, A.Kawana, Y.Terunuma, and T.Hosaka, "Fabrication of Single-Mode Fiber for 1.5μm Wavelength Region," Trans.IECE, Japan, vol.E63, 7, pp.514-519, July 1980.

[22] S.Tomaru, M.Yasu, M.Kawachi, and T.Edahiro, "VAD single mode fibre with 0.2 dB/km loss," Electron. Lett., vol.17, 2, pp.92-93, Jan. 1981.

[23] H.Murata and N.Inagaki, "Low-loss Single-Mode Fiber Development and splicing Research in Japan," IEEE J., vol.QE-17, 6, pp.835-849, June 1981.

[24] D.N.Payne and W.A.Gambling, "Zero material dispersion in optical fibers," Elect.Lett., vol.11, pp8-9, April 1975.

[25] H.Tsuchiya and N.Imoto, "Single mode fiber delay equalization and baseband response," IECE of Japan, Eng.Res.Rep., OQE79-22, May 1979.

[26] K.I.White and B.P.Nelson, "Zero total dispersion in step-index monomode fibers at 1.30 and 1.55μm," Electron. Lett., vol.15, no.13, pp396-397, June 1979.

[27] L.G.Cohen, C.Lin and W.G.French, "Tailoring zero chromatic dispersion into the 1.5-1.6μm low loss spectral region of single mode fibers," Electron. Lett., vol.15, pp334-335, June 1979.

[28] W.A.Gambling H.Matsumura, and C.M.Ragdale, "Zero total dispersion in graded-index single-mode fibres," Electron. Lett., vol.15, 15, pp.474-476, July 1979.

[29] H.Tsuchiya, and N.Imoto, "Dispersion-free single-mode fibre in 1.5 μm wavelength region," Electron. Lett., vol.15, 15, pp.476-478, July 1979.

[30] L.Jeunhomme, "Dispersion minimisation in single-mode fibres between 1.3 μm and 1.7 μm," Electron. Lett., vol.15, 15, pp.478-479, July 1979.

[31] K.Okamoto, T.Edahiro, A.Kawana, and T.Miya, "Dispersion minimisation in single-mode fibres over a wide spectral range," Electron. Lett., vol.15, 22, pp.729-731, Oct. 1979.

[32] C.T.Chang, "Minimum dispersion at 1.55μm for single-mode step-index fibers," Electron. Lett., vol.15, 23, pp.765-767, Nov.1979.

[33] N.Imoto, A.Kawana, S.Machida, and H.Tsuchiya, "Characteristics of Dispersion free single-mode fiber in the 1.μm wavelength region," IEEE J.of Quantum Electron., vol.QE-16, 10, pp.1052-1058, Oct. 1980.

[34] T.Miya, A.Kawana, Y.Terunuma, T.Hosaka and Y.Ohmori, "Low Loss Zero-Dispersion Single-Mode Fibers in the 1.5μm Wavelength Region," Trans. of the IECE of Japan, vol.E 64, 1, pp.32-33, 1981.

[35] R.Olshansky and G.Scherer, "High GeO_2 optical waveguides," Opt. Comm. Conf., Conf. Proc. 12.5, Amsterdam, Sept. 1979.

[36] K.Petermann, "Theory of microbending loss in monomode fibers with arbitrary refractive index profile," Acta Elektron. Ubertragung, vol.30, pp.337-342, Sept. 1976.

[37] J.Sakai and T.Kimura, "Practical microbending loss formula for single-mode optical fibers," IEEE J. Quantum Electron., vol. QE-15, pp.497-500, June 1979.

[38] K.Furuya and Y.Suematsu, "Random-bend loss in single-mode and parabolic-index multimode optical fiber cables," Appl.Opt., vol.19, 9, pp.1493-1500, May 1980.

[39] M.Kubota, K.Furuya and Y.Suematsu, "Random-bend loss-evaluation in single-mode optical fiber with various index profiles," Trans. IECE. Japan. vol.E-63, 10, pp.723-730, Oct.1980.

[40] I.Hatakeyama and H.Tsuchiya, "Fusion splices for single-mode optical fibers," IEEE J. vol.QE-14, 8, pp.614-619, Aug.1978.

[41] Y.Toda, O.Watanabe, M.Ogai, and S.Seikai, "Low-Loss Fusion Splice of Single mode fiber" Int. Conf. on Comm., Denver, Colorado, Con. Rec. vol.1 of 4, pp.27.7.1-27.7.6, June 14-18, 1981.

[42] R.Ulrich, "Polarization stabilization on single-mode fiber," Appl. Phys. Lett., vol.35, 11, pp.840-842, Dec. 1979.

[43] M.Kubota, T.Olhara, K.Furuya, and Y.Suematsu, "Electro-optical polarisation control on single-mode optical fibres," Electron. Lett., vol.16, 15, pp.573, July 1980.

[44] H.C.Lefvre, "Single-mode fibre fractional wave devices and polarisation controllers," Electron. Lett., vol.16, 20, pp.778-780, Sept.1980.

[45] Y.Kidoh, Y.Suematsu, and K.Furuya, "Polarization Control on Output of Single-Mode Optical Fibers," IEEE J. of Quantum Electron., vol.QE-17, 6, pp.991-994, June 1981.

[46] R.H.Stolen, V.Ramaswamy, P.Kaiser, and W.Pleibel, "Linear polarization in birefringent single-mode fibers," Appl. Phys. Lett., vol.33, pp.699-701, Oct. 1978.

[47] H.Matsumura, T.Katsuyama, and T.Suganuma, "Fundamental study of single polarization fibers," in Proc. 6th European Conf. Opt. Comm., York, England, Sept. pp.49-52, 1980.

[48] K.Okamoto, Y.Sasaki, T.Miya, T.Miya, M.Kawachi and T.Edahiro, "Polarisation characteristics in long length V.A.D. single-mode fibers," Electron. Lett., vol.16, 20, pp.768-769, Sept. 1980.

[49] N.Imoto, and M.Ikeda, "Polarization Dispersion Measurement in Long Single-Mode Fibers with Zero Dispersion Wavelength at 1.5μm," IEEE J. of Quantum Electron., vol.QE-17, 4, pp.542-545, April 1981.

[50] T.Okoshi, "Single-Porarization single-mode optical fibers," IEEE J., vol.QE-17, 6, pp.879-885, June 1981.

[51] K.Kitayama, H.Seikai, and N.Uchida, "Polarisation-maintaining single-mode fibre with azimuthally inhomogeneous index profile," Electron. Lett., vol.17, 12, pp.419-420, June 1981.

[52] T.Katsuyama, H.Matsumura, and T.Suganuma, "Low-loss single-polarisation fibres," Electron. Lett., vol.17, 13, pp.473-474, June 1981.

[53] S.Machida, J.Sakai, and T.Kimura, "Polarisation conservation in single-mode fibres," Electron. Lett., vol.17, 14, pp.494-495, July 1981.

[54] T.Hosaka, K.Okamoto, T.Miya Y.Sasaki, and T.Edahiro, "Low-loss single polarisation fibres with asymmetrical strain birefringence," Electron. Lett., vol.17, 15, July 1981.

[55] N.Shibata, M.Takeda, S.Seikai, and N.Uchida, "Wavelength dependence of polarisation mode dispersion in elliptical-core single-mode fibres," Electron. Lett., vol.17, 16, Aug. 1981.

[56] R.J.McIntyre, "Multiplication noise in uniform avalanche diodes," IEEE Trans. Electron. Devices, vol.ED-13, pp166-168, jan. 1966.

[57] R.J.McIntyre, "The distribution of gains in uniformly multiplying avalanche photodiodes: Theory," IEEE Trans. Electron Devices, vol. ED-19, pp.703-713, June 1972.

[58] J.Conradi, "The distribution of gains in uniformly multiplying avalanche photodiodes: Experimental," IEEE Trans. Electron. Devices, vol.ED-19, pp.713-718, June 1972.

[59] C.E.Hurwitz and J.J.Hsieh, "GaInAsP/InP avalanche photodiodes," Apply. Phys. Lett., vol.32, 8, pp.487-489, April 1978.

[60] T.Takanashi and Y.Horikoshi, "InGaAsP/InP avalanche photo-diode," Japan. J. Appl. Phys., vol.17, 11, pp.2065-2066, Nov.1978.

[61] G.H.Olsen and H.Kressel, "Vapor-grown 1.3μm InGaAsP/InP avalanche photodiodes," Electron. Lett., vol.15, pp.141-142, Mar. 1979.

[62] M.Feng, J.D.Oberstar, T.H.Windhorn, L.W.Cook, G.E.Stillman, and G.G.Streetman, "Be-implanted 1.3-μm InGaAsP avalanche photodetectors," Appl. Phys. Lett., vol.34, 9, pp.591-593, May 1979.

[63] K.Taguchi, Y.Matsumoto, and K.Nishida, "InP-InGaAsP planar avalanche photodiodes with self-guard-ring effect," Electron. Lett., vol.15, 15, pp.453-455, July 1979.

[64] K.Nishida, K.Taguchi and Y.Matsumoto, "InGaAsP Heterostructure

Avalanche Photodiodes with High Avalanche Gain," Appl. Phys. Lett., vol.35, 3, pp.251-253, Aug. 1979.

[65] R.Yeats and S.H.Chiao, "Leakage current in InGaAsP avalanche photodiodes," Appl. Phys. Lett., vol.35, 2, pp.167-170, Jan.1980.

[66] Y.Takanashi and Y.Horikoshi, "Noise Performance of 1.3μm InGaAsP/InP Avalanche Photodiode at -190°C," J.J.A.P., vol.19, 3, pp.L163-L166, March 1981.

[67] Y.Takanashi, M.Kawashima and Y.Horikoshi, "Required Donor Concentration of Epitaxial Layers for Efficient InGaAsP Avalanche Photodiodes," J.J.A.P., vol.19, 4, pp.693-701, April 1980.

[68] F.Osaka, K.Nakazima, T.Kaneda and T.Sakurai, "InP/InGaAsP Avalanche Photodiodes with New Guard Ring Structure," Electron. Lett., vol.16, 18, pp.716-717, Aug. 1980.

[69] H.Ando, N.Susa and H.Manbe,"Planar InP Avalanche Photodiode with Zn-Diffused Guard Ring," Electron.Lett., vol.17, 8, pp.292-294, April 1981.

[70] T.Shirai, F.Osaka, S.Yamasaki T.Kaneda and N.Susa, "Multiplication noise of InP avalanche photodiodes," Appl.Phys.Lett., vol.39, 2, pp.168-169, July 1981.

[71] T.P.Pearsall and M.Papuchon, "The $Ga_{0.47}In_{0.53}As$ homo-junction photodiode--A new avalanche photodetector in the near infrared between 1.0 and 1.6μm," Appl.Pnys.Lett., vol.33, 7, pp.640-642, Oct.1978.

[72] Y.Matsushima, K.Sakai, S.Akiba and T.Yamamoto, "Zn-diffused $In_{0.53}Ga_{0.47}As$/InP avalanche photodetector," Appl.Phys.Lett., vol.35, 6, pp.466-468, Sept. 1979.

[73] H.Kambe, N.Susa, H.Nakagome and H.Ando, "InGaAs Avalache photodiode with InP p-n Junction," Electron., vol.16, 5, pp.163-165, Feb.1980.

[74] Y.Matsushima, K.Sakai, S.Akiba and T.Yamamoto, "Dark-Current of $In_{0.53}Ga_{0.47}As$/InP Mesa-Type Avalanche Photodetector," J.J.A.P., vol.19, 3, pp.573-574, 1980.

[75] H.Ando, H.Kambe, M.Ito and T.Kaneda, "Tunneling Current in InGaAs and Optimum Design for InGaAs/InP Avalanche Photodiode," J.J.A.P., vol.19, 6, pp.L227-L280, June 1980.

[76] Y.Matsushima, K.Sakai, S.Akiba and T.Yamamoto, "Planner $In_{0.53}Ga_{0,47}As$ Avalanche Photodiodes with Guard-Ring Structure," J.J.A.P., vol.19, 7, pp.1441-1442, 1980.

[77] N.Susa, H.Nakagome, O.Mikami, H.Ando and H.Kanbe, "New InGaAs/InP Avalanceh Photodiode Structure for the 1-1.6μm Wavelength Region," IEEE of Jour. of Quantum Electron., vol.QE-16, 8, pp.864-870, Aug.1980.

[78] Y.Matsushima, K.Sakai, S.Akiba and T.Yamamoto, "High multipulication gain $In_{0.53}Ga_{0.47}As$/InP heterostructure avalanche photodiode (HAPD) fabricated by diffusion technique," in 6th European Conf. on Opt. Com., York, England, Sept. 1980, pp.226-229.

[79] N.Susa, H.Nakagome, H.Ando and H.Kanbe, "Characteristics in InGaAs/InP Avalanche Photodiodes with Separated Absorption and Multiplication Regions," IEEE J. Quantum Electron., vol.QE-17, 2, pp.243-250, Feb.1981.

[80] H.Ando, Y.Yamauchi, H.Nakagome, N.Susa and H.Kanbe, "InGaAs/InP Separated Absorption and Multiplication Regions Avalanche Photodiode Using Liquid- and Vapor-Phase Epitaxies," IEEE Jour. of QE., vol.QE-17, 2, pp.250-254, Feb.1981.

[81] V.Diadiuk, S.H.Groves, C.E.Hurwitz and G.W.Iseler, "Low Dark-Current, High Gain GaInAs/InP Avalanche Photodetectors," IEEE Quantum Electron., vol.QE-17, 2, pp.260-264, Feb. 1981.

[82] Y.Takanashi and Y.Horikoshi, "InGaAs/InGaAsP Avalanche Photodiodes and Analysis of Internal Quantum Efficiency," J.J.A.P., vol.20, 7, pp.1271-1278, July 1981.

[83] O.K.Kim, S.R.Forrest, W.A.Bonner and R.G.Smith, "A high gain $In_{0.53}Ga_{0.47}As$/InP avalanche photodiode with no tunneling leakage current," Appl.Phys.Lett., vol.39, 5, pp.402-404, Sept.1981.

[84] J.A.Copeland, A.G.Dentai, and T.P.Lee, "P-n-p-n optical detector and lihgt-emitting diodes," IEEE J.Quantum Electron., vol.QE-41, pp.810-813, Nov. 1978.

[85] M.A.Washington, R.E.Nahory, M.A.Pollack and E.D.Beebe, "High-efficiency $In_{1-x}Ga_xAs_yP_{1-y}$/InP photodetectors with selective wavelength response between 0.9 and 1.7μm," Appl.Phys.Lett., vol.33, 10, pp.854-856, Nov.1978.

[86] C.A.Burrus, A.G.Dentai, and T.P.Lee, "InGaAsP p-i-n Photodiodes with Low Dark Current and Small Capacitance," Electron.Lett., vol.15, 20, pp.655-657, Spet. 1979.

[87] R.F.Leheny, R.E.Nahory and M.A.Pollack, "$In_{0.53}Ga_{0.47}As$ p-i-n Photodiodes for Long-Wavelength Fibre-Optic Systems," Electron.Lett., vol.15, 22, pp.713-715, Oct. 1979.

[88] T.P.Lee, C.A.Burrus, A.G.Dentai and K.Ogawa, "Small Area InGaAs/InP p-i-n Photodiodes: Fabrication Characteristics and Performance of Devices in 274 Mb/s and 45 Mb/s Lightwave Receives at 1.31μm Wavelength," Electron. Lett., vol.16, 4, pp.155-156, Feb. 1980.

[89] Thomas P.Pearsall, "$Ga_{0.53}In_{0.47}As$: A Tenary Semiconductor for Photodetector Applications," IEEE.Jour. of Quantum Electron., vol.QE-16, 7, pp.709-720, Julay 1980.

[90] M.Tobe and Y.Amemiya, "High-sensitivity InGaAsP/InP phototransistors," Appl.Phys.Lett., vol.37, 1, pp.73-75, July 1980.

[91] P.D.Wright, R.J.Nelson, and T.Cella, "High-gain InGaAsP-InP heterojuction phototransistors," Appl. Phys.Lett., vol.37, 2, pp.192-194, July 1980.

[92] J.C.Campbell, A.G.Dentai, C.A.Burrus and J.F.Ferguson, "High Sensitivity InP/InGaAs Heterojunction Phototransistor," Electron.Lett., vol.16, 18, pp.713-714, Aug. 1980.

[93] F.Capasso, R.A.Logan, A.Hutchison and D.D.Manchon, "InGaAsP/InGaAs Heterojunction p-i-n Detectors with Low Dark Current and Small Capacitance for 1.3-1.6μm Fibre Optic Systems," Electron.Lett., vol.16, 23, pp.893-895, Nov.1980.

[94] R.F.Leheny, R.E.Nahory, M.A.Pollack, E.Beebe and J.C.de Winter, "Characterization of $In_{0.53}Ga_{0.47}As$ Photodiodes Exhibiting Low Dark Current and Low Junction Capacitance," IEEE Jour. of Quantum Electron., vol.QE-17, 2, pp.227-231, Feb.1981.

[95] Tien-Pei Lee, C.A.Burrus,Jr, and A.G.Dentai, "InGaAs/InP p-i-n Photodioses for Lightwave Communications at the 0.95-1.65μm Wavelength," IEEE J.Quantum Electron., vol.QE-17, 2, pp.232-238, Feb. 1981.

[96] K.Takahashi, T.Murotani, M.Ishi, W.Susaki and S.Takamiya, "A Monolithic 1×10 Array of InGaAsP/InP Photodiodes with Small Dark Current and Uniform Responsivities," IEEE J. Quantum Electron., vol.QE-17, 2, pp.239-242, Feb. 1981.

[97] T.P.Pearsall, M.Piskorski, A.Brochet and J.Chevrier, "A $Ga_{0.47}In_{0.53}As$/InP Heterophotodiode with Reduced Dark Current," IEEE J.Quantum Electron., vol.QE-17, 2, pp.255-259, Feb.1981.

[98] J.C.Campbell, A.G.Dentai, C.A.Burrus,Jr., and J.F.Ferguson, "InP/InGaAs Heterojunction Phototransistors," IEEE J. Quantum Electron., vol.QE-17, 2, pp.264-269, Feb.1981.

[99] J.C.Gammer, H.Ohno and J.M.Ballantyne, "High-Speed Photoconductive Detectors Using GaInAs," IEEE J.Quantum Electron., vol.QE-17, 2, pp.269-272, Feb.1981.

[100]D.Fritzsch, E.Kuphal and R.Aulbach, "Fast Response InP/InGaAsP Heterojunction Phototransistors," Electron.Lett., vol.17, 5, pp.178-180, March 1981.

[101]A.Sasaki and M.Kuzuhara, "InGaAsP-InP Heterojunction Phototransistors and Light Amplifiers," J.J.A.P., vol.40, 4, pp.L283-L286, April 1981.

[102]T.P.Pearsall, "Photodetectors for optical communication," J.Optical Communications, vol.2, pp.42-48, June 1981.

[103]H.J.Klein, R.Kaumanns and H.Beneking, "High-Speed $Ga_{0.47}In_{0.53}As$ Photoconductive Detector for Picosecond Light Pulses," Electron.Lett., vol.17 , pp.421-422, June 1981.

[104]T.P.Lee, C.A.Burrus, K.Ogawa and A.G.Dentai, "Very-High-Speed Back-Illuminated InGaAs/InP PIN Punch-Through Photodiodes," Electron.Lett., vol.17, 12, pp.431-432, June 1981.

[105]R.G.Smith, "Photodetectors for Fiber Transmission Systems," Proc. IEEE., vol.68, 10, pp.1247-1253, Oct.1981.

[106]F.Capasso, R.A.Logan, P.W.Foy and S.Sumski, "Low Leakage Current and Saturated Reverse Characteristic in Broad-Area InGaAsP Diodes," Electron.Lett., vol.16, 7, pp.241-242, March 1980.

[107]T.P.Lee and C.A.Burrus, "Dark current and breakdown characteristics of dislocation-free InP photodiodes," Appl.Phys.Lett., vol.36, 7, pp.587-589, April 1980.

[108]S.R.Forrest, M.DiDomenico,Jr., R.G.Smith and H.J.Stocker, "Evidence for tunneling in reverse-biased III-V photodetector diodes," Appl.Phys.Lett., vol.36, 7, pp.580-582, April 1980.

[109]S.R.Forrest, "$In_{0.53}Ga_{0.47}As$ photodiodes with dark current limited by generation-recombination and tunneling," Appl.Phys.Lett., vol.37, 3, pp.322-325, Aug. 1980.

[110]Stephen R.Fofrrest, "Perfoemance of $In_xGa_{1-x}As_yP_{1-y}$ Photodiodes with Dark Current Limited by Diffusion, Generation Recombination, and Tunneling," IEEE J. Quantum Electron., vol.QE-17, 2, pp.217-226, Feb. 1981.

[111]R.F.Leheny, R.E.Nahory, M.A.Pollack and E.D.Beebe, "$In_{0.53}Ga_{0.47}$ As PIN-FET photo-receiver for 1.0-1.7μm wavelength fiber optic systems," in Tech. Dig. Integrated and Guided Wave Optics Meet. (Incline Village, NV), Paper WC4, Jan.1980.

[112]D.R.Smith, R.C.Hooper, K.Ahmad, D.Jenkins, A.W.Mabbit and R.Nicklin, "p-i-n/F.E.T. Hybrid Optical Receiver for Linger-Wavelength Optical Communication Systems," Electron.Lett., vol.16, 2, pp.69-71, Jan. 1980.

[113]R.F.Leheny, R.E.Nahory, M.A.Pollack, A.A.Ballman, E.D.Beebe, J.C.DeWinter, R.J.Martin, "Integrated $In_{0.53}Ga_{0.47}As$ p-i-n F.E.T. Photoreceiver," Electron.Lett., vol.16, 10, pp.353-355, May 1980.

[114]D.R.Smith, A.K.Chatterjee, M.A.Z.Rejman, D.Wake, and B.R.White, "p-i-n F.E.T. Hybrid Optical Receiver for 1.1-1.6μm Optical Communicaiton Systems," Electron.Lett., vol.16, 19, pp.750-751, Sept.1980.

[115]S.Sakai, M.Umeno and Y.Amemiya, "InGaAsP/InP double-heterostructure photodiodes," J.J.A.P., vol.17, 9, pp.1701-1972, Sept.1978.

[116]J.C.Campbell, A.G.Dentai, T.P.Lee and C.A.Burrus, "Improved TwoWavelength Demultiplexing InGaAsP Photodetector ," IEEE Jour. of Quantum Electron., vol.QE-16, 6, pp.601-603, June 1980.

[117]H.Melchior and W.T.Lynth, "Signal and Noise response of high speed germanium avalanche photo-diode," IEEE Trans. Electron Devices, vol.ED-13, 12, pp.729-838, Dec. 1966.

[118]H.Ando, H.Kanbe, T.Kimura, T.Yamaoka and T.Kaneda, "Characteristics of germanium avalanche photodiodes in the wavelength region of 1-1.6μ," IEEE J., vol.QE-14, 11, pp.804-809, Nov. 1978.

[119]M.C.Brain, "Responsivity and noise characterisation of Ge avalanche photodiode throughout wavelength range 1.1-1.7μm," Electron.Lett., vol.15, 25, pp.821-823, Dec. 1979.

[120]T.Kaneda, S.Kagawa. T.Mikawa, Y.Toyama and H.Ando, "An n^+-n-p germanium avalanhe photodiode," Apply.Phys.Lett., vol.35, 7, pp.572-574, April. 1980.

[121]Osamu Mikami, Hiroaki Ando, Hiroshi Kanbe, Takashi Mikawa, Takao Kaneda and Yoshikazu Toyama, "Improved Germanium Avalanche Photodiodes," IEEE J. of Quantum Electron., vol.QE-16, 9, pp.1002-1007, Sept. 1980.

[122]T.Mikawa, S.Kagawa, T.Kaneda, T.Sakurai, H.Ando, and O.Mikami, "A Low-Noise n^+np Gemanium Avalanceh Photodiode," IEEE J. of Quantum

Electron., vol. QE-17 2, pp.210-216, Feb. 1981.

[123]H.Kanbe, G.Grosskopf, O.Mikami and S.Machida, "Dark Current Noise Characteristics and Their Temperature Dependence in Germanium Avalanche Photodiodes," IEEE. J. of Quantum Electron., vol.QE-17, 8, pp.1534-1539, Aug. 1981

[124]T.Kagawa and G.Motosugi, "AlGaAsSb Avalanche Photodiodes for 1.0-1.3μm Wavelength Region," J.J.A.P., vol.18, 12, pp.2317-2318, 1979.

[125]F.Capasso, M.B.Panish, S.Sumski and P.W.Foy, "Very high quantum efficiency GaSb mesa photodetectors between 1.3 and 1.6μm," Appl.Phys.Lett., vol.36, 2, pp.165-167, Jan. 1980.

[126]R.Chin, H.D.Law, K.Nakano and R.A.Milano, :Schottky barrier $Ga_{1-x}Al_xAs_{1-y}Sb_y$ alloy avalanche photodetectors," Appl. Phys. Lett., vol.37, 6, pp.550-551, Spet. 1980.

[127]F.Capasso, M.B. Panish and S.Sumski, "The Liquid-Phase Epitaxial Growth of Low Net Donor Concentration (5×10^{14}-5×10^{15}/cm^3) GaSb for Detector Applications in the 1.3-1.6μm Region," IEEE J. of Quantum Electron., vol.QE-17, 2, pp.273-274, Feb. 1981.

[128]O.Hildebrand, W.Kuebart, K.W.Benz and M.H.Pilkuhn, "$Ga_{1-x}As_xSb$ Avalanche Photodiodes: Resonant Impact Ionization with Very High Ratio of Ionization Coefficients," IEEE J. of Quantum Electron., vol.QE-17, 2, pp.284-288, Feb. 1981.

[129]H.D.Law, R.Chin, K.Nakano and R.A.Milano, "The GaAlAsSb Quaternary and GaAlSb Ternary Alloy and Their Application to Infrared Detectors," IEEE J. of Quantum Electron., vol.QE-17, 2, pp.275-283, Feb. 1981.

[130]F.Capasso, W.T.Tsang and Hutchinson, "The Graded Band Gap Avalanche Diode: A New Molecular Beam Epitaxial with a Large Ionization Rates Ratio," Internat. Symposium. on Gallium Arsenide and Related Compounds, Oiso, Japan, V-3, Spet. 1981.

[131]J.Heslage, T.N.Duy, G.Pichard, M.Royer, "Fast, high gain 1.3μm HgCdTe Photodiode," 7th ECOC, 11.4, Copenhagen, Denmark, Sept. 1981.

[132]T.P.Pearsall: "Photodetectors for optical communication", J.Opt.Commu., vol.2, pp.42-48, Jun.1981

[133]Y.Suematsu, "Long Wavelength Optical Fiber Communication, " to be published in IEEE J. of Quantum Electron.

[134]R.N.Hall, G.E.Fenner, J.D.Kingsley, T.J.Soltys, and R.O.Carlson, "Coherent light emission from GaAs junctions," Phys. Rev. Lett., vol.9, 9, pp.366-368 , Nov.1962.

[135]M.I.Nathan, W.P.Dumkem G.Buuns, F.H.Dill, and G.J.Lasher, "Stimulated emission of radiation from GaAsp-n junctions," Appl.Phys. Lett., vol.1, 3, pp.62-64, Nov. 1962.

[136]T.M.Quist, R.J.Keyes, W.E.Krag, B.Lax, A.L.McWhorter, R.H.Rediker, and H.J.Zeiger, "Semiconductor maser of GaAs ," Appl.Phys.Lett., vol.1, 4, pp.91-92, Dec. 1962.

[137]H.Kroemer; "A Proposed Glass of Heterojunction Injection Lasers," Proc. IEEE, vol.51 12, pp.1782-1783, Dec. 1963.

[138]H.Rupprecht, J.M.Woodall and G.D.Pettit, "Effective visible electroluminescence at 300°K from $Ga_{1-x}Al_xAs$ p-n junctions grown by liquid-phase epitaxy," Appl. Phys. Lett., vol.11. 3. pp.81-83, Aug. 1967.

[139]H.Rupprech J.M.Woodall, G.D.Pettit, J.W.Crowe and H.F.Quinn, "Stimulated Emission from $Ga_{1-x}As_xAs$ Diodes", IEEE Semicon. Laser Conf., Las Vegas, Session V, Nov. 1967.

[140]I.Hayashi, M.B.Panishi, P.W.Foy and S.Sumski, "Junction lasers, which operate contiuously at room temperature," Appl. Phys. Lett., vol.17, 3, pp.109-111, Aug. 1970.

[141]T.Yamamoto and Y.Suematsu, "GaInAsP/InP injection semiconductor laser for optical communication," J. Oyo Butsuri (in Japanese) pp.918-923, Sept. 1977.

[142]E.K.Mueller and J.J.Richards, "Miscibility of III-V Semiconductors studied by flash evaporation," J. Appl.Phys. vol.35, pp.1233-1241, Apr. 1964.

[143]A.Sasaki, M.Nishiuma and Y.Takeda, "Energy Band Structure and Lattice Constant Chart of III-V Mixed Semiconductors, and AlGaSb/AlGaAsSb Semiconductor Lasers on GaSb Substrates," J.J.A.P., vol.19, 9, pp.1695-1702, Sept.1980.

[144]C.J.Nuese and R.E.Enstrom, "Efficient 1.06μm emission from $In_xGa_{1-x}As$ electroluminescent diodes," IEEE. Trans., Electron. Devices, vol.ED-19, pp.1067-1069, Sept. 1972.

[145]A.W.Mabbitt and C.D.Mobsby, " High-speed high-power 1.06μm Gallium-Indium-Arsenide light-emitting diodes," Electron. Lett., vol.11, pp.157-158, Apr. 1975.

[146]C.J.Nuese and G.H.Olsen, "Room-temperature heterojunction laser diodes of $In_xGa_{1-x}As/In_yGa_{1-y}P$ with emission wavelength between 0.9μm and 1.15μm," Appl.Phys.Lett., vol.26, pp.528-531, May 1975.

[147]C.J.Nuese, G.H.Olsen, M.Ettenberg, J.J.Gannon and T.J.Zamerowski, "CW room-temperature $In_xGa_{1-x}As/In_yGa_{1-y}P$ 1.06μm lasers," Appl. Phys. Lett., vol.29, pp.807-809, Dec. 1976.

[148]A.W.Mabbitt and R.C.Goodfellow, "High-radiance small area gallium-indium-arsenide 1.06μm light-emitting diodes," Electron. Lett., vol.11, pp.274-275, Jun. 1975.

[149]T.Ota, M.Yamaguchi, Y.Mizushima, T.Urisu, H.Kijima and K.Oe, "$In_xGa_{1-x}As$ Injection Lasers," J.J.A.P., vol.14, 7, pp.1073-1074, Jul. 1975.

[150]K.Sugiyama and H.Saito, "GaAsSb-AlGaAsSb double heterojunction lasers," J.J.A.P., vol.11, pp.1057-1058, 1972.

[151]R.E.Nahory and M.A.Pollack, "Low-threshold room-temperature double-heterostructure $GaAs_{1-X}Sb_x/Al_yGa_{1-y}As_{1-x}Sb_x$ injection lasers at 1-μm wavelengths," Appl. Phys. Lett., vol.25 pp.562-564, Nov. 1975.

[152]R.E.Nahory, M.A.Pollack, E.D.Beebe, J.C.DeWinter and R.E.Dixon, "Continuous operation of 1.0-μm-wavelength $GaAs_{1-x}Sb_x/Al_yGa_{1-y}As_{1-x}Sb_x$ double-heterosturcture injection lasers at room temperature," Appl. Phys. Lett., vol.28, pp.19-21, Jan. 1976.

[153]R.E.Nahory, M.A.Pollack and J.K.Abrokwah, "Threshold Characteristics and extended wavelength operation of $GaAs_{1-x}Sb_x/Al_yGa_{1-y}As_{1-x}Sb_x$ double-heterosturcture lasers," J.J.A.P., vol.48, 9, pp.3988-3990, Sept. 1977.

[154]C.Chaminant, J.Charil, J.C.Bouley and E.V.K.Rao, "Growth and properties of GaAsSb/GaAlAsSb double heterostructure lasers," Solid-State Electron Devices, vol.3, 6, pp.196-200, Nov. 1979.

[155]A.P.Bogatov, L.M.Dolginov, L.V.Druzhinina, P.G.Eliseev, B.N.Sverdlov and E.G.Shevchenko, "Heterojunction lasers made of $Ga_xIn_{1-x}As_yP_{1-y}$ solid solutions," Sov. J. Quantum Electron., vol.4, p.1281, Apr. 1975.

[156]G.Motosugi and T.Kagawa, "Temperature dependence of the threshold current of AlGaAsSb/GaSb DH lasers," Jpn. J. Appl. Phys., vol.19, 11, pp.2303-2304, Nov. 1980.

[157]L.M.Dolginov, A.E.Drakin, L.V.Druzhinina, P.G.Eliseev, M.G.Milvidsky, V.A.Skripkin and B.N.Sverdlov, "Low threshold heterojunction AlGaAsSb/GaSb lasers in the wavelength range of 1.5-1.8μm," IEEE J. of Quantum Electron., vol.QE-17, 5, pp.593-597, May 1981.

[158]N.Kobayashi, Y.Horikoshi and C.Uemura,"Room temperature operation of the InGaAsSb/AlGaAsSb DH laser at 1.8μm wavelength," Jpn. J. Appl. Phys., vol.19, 1, pp.L30-32, Jan. 1980.

[159]H.Kano and K.Sugiyama, "2.0μm C.W. operation of GaInAsSb/GaSb D.H. lasers at 80K," Electron. Lett., vol.16, 4, pp.146-147, Feb. 1980.

[160]N.Kobayashi and Y.Horikoshi, "DH lasers fabricated by new III-V semiconductor material InAsPSb," Jpn. J. Appl. Phys., vol.19, 10, pp.L641-L644, Oct. 1980.

[161]M.Kawashima, S.Saito and Y.Horikoshi, "Lattice matched PbSeSnTe DH laser," Nat. Conv. Rec. of Japan Soc. of Appl. Phys., 29p-H-17, Mar. 1981.

[162]A.P.Bogatov, L.M.Dolginov, P.G.Eliseev, M.G.Milvidskii, B.N.Sverdlov and E.G.Shevchenko, "Radiative characteristics of InP-GaInPAs laser heterostructures," Sov. Phys. Semicond., vol.9, 10, pp.1282-1285, Oct. 1975.

[163]J.J.Hsieh, "Room-temperature operation of GaInAsP/InP double-heterostructure diode lasers emitting at 1.1μm," Appl. Phys. Lett., vol.28, pp.283-285, Mar. 1976.

[164]J.J.Hsieh, J.A.Rossi and J.P.Donnelly, "Room-temperature cw operation of GaInAsP/InP double-heterostructure diode lasers emitting at 1.1μm," Appl. Phys. Lett., vol.28, pp.709-711, Jun. 1976.

[165]K.Oe and K.Sugiyama, "GaInAsP/InP double-hetero structure lasers prepared by a new LPE apparatus," Jpn. J. Appl. Phys., vol.15, 12, pp.740-741, Dec. 1976.

[166]H.Nagai and Y.Noguchi, "Crack formation in InP-$Ga_xIn_{1-x}As$-InP double heterostructure fabrication," Appl. Phys. Lett., vol.29, pp.740-742, Dec. 1976.

[167]T.Yamamoto, K.Sakai, S.Akiba and Y.Suematsu, "Fast pulse behaviour of InGaAsP/InP double-heterostructure lasers emitting at 1.27μm," Electron. Lett., vol.13, pp.142-143, Mar. 1977.

[168]J.J.Hsieh and C.C.Shen, "Room-temperature CW operation of buried-stripe double-heterostructure GaInAsP/InP diode lasers," Appl. Phys. Lett., vol.30, pp.429-431, Apr. 1977.

[169]Y.Itaya, Y.Suematsu and K.Iga, "Carrier lifetime measurement of GaInAsP/InP double-heterostructure lasers," Jpn. J. Appl. Phys., vol.16, pp.1057-1058, Jun. 1977.

[170]K.Oe, S.Ando and K.Sugiyama, "1.3μm cw operation of GaInAsP/InP DH diode lasers at room temperature," Jpn. J. Appl. Phys., vol.16, pp.1273-1274, Jul. 1977.

[171]C.J.Nuese, R.E.Enstrom and J.R.Appert, "1.7μm hetero-junction lasers and photodiodes of $In_{0.53}Ga_{0.47}As/InP$," IEEE Trans. Electron. Devices, vol.ED-24, pp. , Sept. 1977.

[172]K.Wakao, K.Moriki, T.Kambayashi and K.Iga, "GaInAsP/InP DH laser grown by newly designed vertical LPE furnace," Jpn. J. Appl. Phys., vol.16, 11, pp.2073-2076, Nov. 1977.

[173]Zh.I.Alferov, A.T.Gorelenok, P.Kopiev, V.N.Mdivani and V.K.Tibilov, "Low-threshold lasers based on InGaAsP system heterostructures," Pisma Zh. Tekh. Fiz., vol.3, 22, pp.1169-1171, 1977.

[174]H.Nagai and Y.Noguchi, "InP-$Ga_xIn_{1-x}As_yP_{1-y}$ double-heterostructure for 1.5μm wavelength," Appl. Phys. Lett., vol.32, pp.243-246, Feb. 1978.

[175]T.Yamamoto, K.Sakai, S.Akiba and Y.Suematsu, "$In_{1-x}Ga_xAs_yP_{1-y}$ DH lasers fabricated on InP (100) substrate," IEEE J. Quantum Electron., vol.QE-14, 2, pp.95-98, Feb. 1978.

[176]B.I.Miller, J.H.McFee, R.J.Martin and P.K.Tien, "Room-temperature operation of lattice-matched InP/$Ga_{0.47}In_{0.53}As$/InP double-heterostructure lasers grown by MBE," Appl. Phys. Lett., vol.33, 1, pp.44-47, Jul. 1978.

[177]H.Kawanishi, Y.Suematsu, Y.Itaya and S.Arai, "$Ga_xIn_{1-x}As_yP_{1-y}$-InP injection laser partially loaded with distributed Bragg reflectors," Jpn. J. Appl. Phys., vol.17, 8, pp.1439-1440, Aug. 1978.

[178]H.Kano, K.Oe, S.Ando and K.Sugiyama, "Buried stripe GaInAsP/InP DH laser prepared by using meltback method," Jpn. J. Appl. Phys., vol.17, 10, pp.1887-1888, Oct. 1978.

[179]S.Akiba, K.Sakai and T.Yamamoto, "$In_{0.53}Ga_{0.47}As/In_{1-x}Ga_xAs_yP_{1-y}$ double heterostructure lasers with emission wavelength of 1.67μm at room temperature," Jpn. J. Appl. Phys., vol.17, 10, pp.1899-1900, Oct. 1978.

[180]S.Arai, Y.Itaya, Y.Suematsu, K.Kishino and S.Katayama, "Condition of LPE growth for lattice matched GaInAsP/InP DH lasers with (100) substrate in the range of 1.2-1.5μm," Jpn. J. Appl. Phys., vol.17, 11, pp.2067-2068, Nov. 1978.

[181]G.H.Olsen, C.J.Nuese and M.Ettenberg, "Low-threshold 1.25μm vapor-grown InGaAsP cw lasers," Appl. Phys. Lett., vol.34, 4, pp.262-264, Feb. 1979.

[182]K.Kishino, Y.Suematsu and Y.Itaya, "Mesa-substrate buried-hetero-structure GaInAsP/InP injection lasers," Electron. Lett., vol.15, pp.134-136, Feb. 1979.

[183]Y.Itaya, S.Katayama and Y.Suematsu, "Narrow-beam divergence of the emission from low-threshold GaInAsP/InP double-heterostructure lasers," Electron. Lett., vol.15, pp.123-124, Feb. 1979.

[184]S.Arai, Y.Suematsu and Y.Itaya, "1.67μm $Ga_{0.47}In_{0.53}As$/InP DH lasers double cladded with InP by LPE technique," Jpn. J. Appl. Phys., vol.18, 3, pp.709-710, Mar. 1979.

[185]A.Doi, N.Chinone, K.Aiki and R.Ito, "$Ga_xIn_{1-x}As_yP_{1-y}$/InP rib-waveguide injection lasers made by one-step LPE," Appl. Phys. Lett., vol.34, 6, pp.393-395, Mar. 1979.

[186]N.Kobayashi and Y.Horikoshi, "1.5μm InGaAsP/InP d.h. laser with optical waveguide structure," Jpn. J. Appl. Phys., vol.18, 5, May 1979.

[187]G.H.Olsen, C.J.Nuese and M.Ettenberg, "Reliability of vapor-grown InGaAs and InGaAsP heterojunction laser structures," IEEE J. Quantum Electron., vol.QE-15, pp.688-693, Aug. 1979.

[188]H.Kawanishi, Y.Suematsu, K.Utaka, Y.Itaya and S.Arai, "$Ga_xIn_{1-x}As_yP_{1-y}$/InP injection laser partially loaded with first-order distributed Bragg reflector," IEEE J. Quantum Electron., vol.QE-15, pp.701-706, Aug. 1979.

[189]D.J.Bull, N.B.Patel, F.C.Prince and Y.Nannichi, "Oxide defined TJS lasers in InGaAsP/InP DH structures," IEEE. J. Quantum Electron., vol.QE-15, pp.710-7 , Aug. 1979.

[190]H.Nishi, M.Yano, Y.Nishitani, Y.Akita and M.Takusagawa, "Self-aligned structure InGaAsP/InP DH lasers," Appl. Phys. Lett., vol35, pp.232-234, Aug. 1979.

[191]T.Yamamoto, K.Sakai and S.Akiba, "10000 h continuous CW operation of $In_{1-x}Ga_xAs_yP_{1-y}$/InP DH lasers at room temperature," IEEE J. Quantum Electron., vol.QE-15, pp.684-687, Aug. 1979.

[192]J.J.Hsieh, "Zn-diffused stripe-geometry double-heterostructure GaInAsP/InP diode lasers," IEEE J. Quantum Electron., vol.QE-15, pp.694- , Aug. 1979.

[193]Y.Itaya, Y.Suematsu, S.Katayama, K.Kishino and S.Arai, "Low-threshold current density (100) GaInAsP/InP double-heterostructure lasers for wavelength 1.3μm," Jpn. J. Appl. Phys., vol.18, 9, pp.1795-1807, Sept. 1979.

[194]A.Doi, T.Fukuzawa, M.Nakamura, R.Ito and K.Aiki, "InGaAsP/InP distributed-feedback injection lasers fabricated by one-step liquid phase epitaxy," Appl. Phys. Lett., vol.35, 6, pp.441-443, Sept. 1979.

[195]S.Akiba, K.Sakai, Y.Matsushima and T.Yamamoto, "Room temperature C.W. operation of InGaAsP/InP heterostructure lasers emitting at 1.56μm," Electron. Lett., vol.15, 19, pp.606-607, Sept. 1979.

[196]G.D.Henshall and P.D.Greene, "Low-threshold (Ga,In) (As,P) D.H. lasers emitting at 1.55μm grown by L.P.E.," Electron. Lett., vol.15, 20, pp.621-622, Sept. 1979.

[197]H.Kawaguchi, K.Takahei, Y.Toyoshima, H.Nagai and G.Iwane, "Room-temperature C.W. operation of InP/InGaAsP/InP double heterostructure diode lasers emitting at 1.55μm," Electron. Lett., vol.15, 21, pp.669-670, Oct. 1979.

[198]F.C.Prince, N.B.Patel and D.J.Bull, "(InGa)(AsP)/InP embedded mesa stripe lasers," Appl. Phys. Lett., vol.35, 8, pp.577-580, Oct. 1979.

[199]F.C.Prince, N.B.Patel and D.J.Bull, "InP-$In_{1-x}Ga_xAs_yP_{1-y}$ embedded mesa stripe lasers," IEEE J. Quantum Electron., vol.QE-16, 10, pp.1034-1038, Oct. 1979.

[200]I.P.Kaminow, R.E.Nahory, M.A.Pollack, L.W.Stulz and J.C.DeWinter, "Single-mode C.W. ridge-waveguide laser emitting at 1.55μm," Electron. Lett., vol.15, 23, pp.763-765, Nov. 1979.

[201]R.J.Nelson, "Near-equilibrium LPE growth of low threshold current density $In_{1-x}Ga_xAs_yP_{1-y}$(λ=1.35μm) DH lasers," Appl. Phys. Lett., vol.35, 9, pp.654-656, Nov. 1979.

[202]S.D.Hersee, A.C.Carter, R.C.Goodfellow, G.Hawkins and I.Griffith, "Growth and characterization of GaInAsP/InP double heterostructure material for stripe geometry lasers emitting near 1.3μm," Solid-State Electron Devices, vol.3, 6, pp.179-186, Nov. 1979.

[203]H.Soda, K.Iga, C.Kitahara and Y.Suematsu, "GaInAsP/InP surface emitting injection lasers," Jpn. J. Appl. Phys., vol.18, 12, pp.2329-2330, Dec. 1979.

[204]S.Arai, M.Asada, Y.Suematsu and Y.Itaya, "Room temperature CW operation of GaInAsP/InP DH laser emitting at 1.51μm," Jpn. J. Appl. Phys., vol.18, 12, pp.2333-2334, Dec. 1979.

[205]S.Arai, Y.Suematsu and Y.Itaya, "1.11-1.67μm (100) GaInAsP/InP injection lasers prepared by liquid phase epitaxy," IEEE J. Quantum Electron., vol.QE-16, 2, pp.197-205, Feb. 1980.

[206]K.Utaka, Y.Suematsu, K.Kobayashi and H.Kawanishi, "GaInAsP/InP integrated twin-guide lasers with first-order distributed Bragg reflectors at 1.3μm wavelength," Jpn. J. Appl. Phys., vol.19, 2, pp.L137-L140, Feb. 1980.

[207]T.Mizutani, M.Yoshida, A.Usui, H.Watanabe, T.Yuasa and I.Hayashi, "Vapor phase growth InGaAsP/InP DH structures by the dual-growth-chamber method," Jpn. J. Appl. Phys., vol.19, 2, pp.L113-L116, Feb. 1980.

[208]Y.Itaya, T.Tanbun-Ek, K.Kishino, S.Arai and Y.Suematsu, "1.6μm wavelength buried heterostructure GaInAsP/InP lasers," Jpn. J. Appl. Phys., vol.19, 3, pp.L141-L144, Mar. 1980.

[209]R.J.Nelson, P.D.Wright, P.A.Barnes, R.L.Brown, T.Cella and R.G.Sobers, "High-output power InGaAsP(λ=1.3μm) strip-buried heterostructure lasers," Appl. Phys. Lett., vol.36, 5, pp.358-360, Mar. 1980.

[210]K.Iga and B.I.Miller, "GaInAsP/InP laser with monolithically integrated monitoring detector," Electron. Lett., vol.16, 9, pp.342-343, Apr. 1980.

[211]P.D.Wright, R.J.Nelson and T.Cella, "InGaAsP double heterostructure lasers(λ=1.3μm) with etched reflector," Appl. Phys. Lett., vol.36, 7, pp.518-520, Apr. 1980.

[212]H.Nagai, Y.Noguchi, K.Takahei, Y.Toyoshima and G.Iwane, "InP/GaInAsP buried heterostructure lasers of 1.5μm region," Jpn. J. Appl. Phys., vol.19, 4, pp.L218-L220, Apr. 1980.

[213]J.P.Hirtz, J.P.Duchemin, P.Hirtz, B.DeCremoux, T.Pearsall and M.Bonnet, "$Ga_xIn_{1-x}As_yP_{1-y}$/InP D.H. laser emitting at 1.15μm grown by low-pressure metalorganic C.V.D.," Electron. Lett., vol.16, pp.275-277, Apr. 1980.

[214]E.A.Rezek, N.Holonyak, Jr. and B.K.Fuller, "Temperature dependence of threshold current for coupled multiple quantum-well $In_{1-x}Ga_xP_{1-z}As_z$-InP heterostructure laser diodes," J. Appl. Phys., vol.51, pp.2402-2405, May 1980.

[215]S.Arai, M.Asada, Y.Suematsu, Y.Itaya, T.Tanbun-Ek and K.Kishino, "New 1.6μm wavelength GaInAsP/InP buried heterostructure lasers," Electron. Lett., vol.16, 10,pp.349-350, May 1980.

[216]K.Utaka, K.Kobayashi, K.Kishino and Y.Suematsu, "1.5-1.6μm GaInAsP/InP integrated twin-guide lasers with first-order distributed Bragg reflectors," Electron. Lett., vol.16, 12, pp.455-456, Jun. 1980.

[217]G.H.Olsen, T.J.Zamerowski and N.J.Digiuseppe, "1.5-1.7μm V.P.E. InGaAsP/InP C.W. lasers," Electron. Lett., vol.16, 13, pp.515-518, Jun. 1980.

[218]W.D.Johnston, Jr. and K.E.Strege, "Uniformly low-threshold diode lasers at 1.5-1.55μm from VPE $In_xGa_{1-x}As_yP_{1-y}$ material," 38th Annual Device Research Conf., Ithaca, NY, Jun. 1980.

[219]T.Murotani, E.Oomura, H.Higuchi, H.Namizaki and W.Susaki, "InGaAsP/InP buried crescent laser emitting at 1.3μm with very low threshold current," Electron. Lett., vol.16, 14, pp.566-568, Jul. 1980.

[220]J.J.Hsieh, "High-temperature cw operation of GaInAsP/InP lasers emitting at 1.5μm," Appl. Phys. Lett., vol.37, 1, pp.25-27, Jul. 1980.

[221]B.I.Miller and K.Iga, "GaInAsP/InP stripe lasers with etched mirrors fabricated by a wet chemical etch," Appl. Phys. Lett., vol.37, 4, pp.339-341, Aug. 1980.

[222]M.Hirao, A.Doi, S.Tsuji, M.Nakamura and K.Aiki, "Fabrication and characterization of narrow stripe InGaAsP/InP buried heterostructure lasers," J. Appl. Phys., vol.51, pp.4539-4540, Aug. 1980.

[223]M.Hirao, S.Tsuji, K.Mizushima, A.Doi and M.Nakamura, "Long wavelength InGaAsP/InP lasers for optical fiber communication systems," J. Opt. Comm., vol.1, 1, pp.10-14, Sept. 1980.

[224]N.Matsumoto, K.Onabe, T.Yuasa, M.Ueno, Y.Matsumoto, T.Furuse and I.Sakuma, "1.5μm wavelength InGaAsP/InP plano-convex waveguide (PCW) lasers," Nat. Conv. Rec. of Japan Soc. of Appl. Phys., 17a-Q-6, Oct. 1980.

[225]K.Iga and B.I.Miller, "C.W. operation of GaInAsP/InP laser with chemically etched mirror," Electron. Lett., vol.16, 22, pp.830-832, Oct. 1980.

[226]K.Iga, M.A.Pollack, B.I.Miller and R.J.Martin, "GaInAsP/InP DH lasers with a chemically etched facet," IEEE J. Quantum Electron., vol.QE-16, 10, pp.1044-1047, Oct. 1980.

[227]Y.Nakano, K.Takahei, Y.Noguchi, M.Tokunaga, H.Nagai, K.Nawata and M.Fujimoto, "1.5μm InGaAsP/InP BH lasers on p-type InP substrates," Jpn. J. Appl. Phys., vol.19, 10, pp.L612-L614, Oct. 1980.

[228]K.Moriki, K.Wakao, M.Kitamura, K.Iga and Y.Suematsu, "Single transverse mode operation of terraced substrate GaInAsP/InP lasers at 1.3μm wavelength," Jpn. J. Appl. Phys., vol.19, 11, pp.2191-2196, Nov. 1980.

[229]Y.Noguchi, K.Takahei, Y.Suzuki and H.Nagai, "Low threshold current CW operation of InP/GaInAs buried heterostructure lasers," Jpn. J. Appl. Phys., vol.19, 12, pp.L759-L762, Dec. 1980.

[230]P.C.Chen, K.L.Yu, S.Margalit and A.Yariv, "A new GaInAsP/InP T-laser at 1.2μm fabricated on semi-insulating substrate," Jpn. J. Appl. Phys., vol.19, 12, pp.L775-L776, Dec. 1980.

[231]I.Mito, K.Kaede, M.Kitamura, Y.Odagiri, M.Seki and K.Kobayashi, "InGaAsP planar buried heterostructure laser diode," Paper of Technical Group of IECE of Japan, Optical and Quantum Electron.(in Japanese), OQE80-116, Jan. 1981.

[232]T.Matsuoka, K.Takahei, Y.Noguchi and H.Nagai, "1.5μm region InP/GaInAsP buried heterostructure lasers on semi-insulating substrates," Electron. Lett., vol.17, 1, pp.12-14, Jan. 1981.

[233]H.Imai, H.Ishikawa, T.Tanahashi and M.Takusagawa, "InGaAsP/InP separated multiclad layer stripe geometry lasers emitting at 1.5μm, " Electron, Lett., vol.17, 1, pp.17-19, Jan. 1981.

[234]E.Oomura, H.Higuchi, R.Hirao, H.Namizaki, T.Murotani and W.Susaki, "Transverse mode control in InGaAsP/InP buried crescent diode lasers," Electron. Lett., vol.17, 2, pp.83-84, Jan. 1981.

[235]J.P.Hirtz, M.Razeghi, J.P.Larivain, S.Hersee and J.P.Duchemin, "Low threshold GaInAsP/InP lasers with good temperature dependence grown by low pressure MOVPE," Electron. Lett., vol.17, 3, pp.113-114, Feb. 1981.

[236]Y.Noda, K.Sakai and Y.Matsushima, "High temperature CW operation of 1.5μm InGaAsP/InP buffer-layer loaded planoconvex waveguide lasers," Electron. Lett., vol.17, 6, pp.226-227, Mar. 1981.

[237]H.Asahi, Y.Kawamura, M.Ikeda and H.Okamoto, "Near room temperature CW operation at 1.70μm of MBE grown InGaAs/InP DH lasers," Jpn. J. Appl. Phys., vol.20, 3, pp.L187-L190, Mar. 1981.

[238]Y.Suzuki, Y.Noguchi, K.Takahei, H.Nagai and G.Iwane, "1.5μm region BH laser array," Jpn. J. Appl. Phys., vol.20, 3, pp.L229-L232, Mar. 1981.

[239]L.A.Coldren, B.I.Miller, K.Iga and J.A.Rentschler, "Monolithic two-section GaInAsP/InP active-optical-resonator devices formed by reactive ion etching," Appl. Phys. Lett., vol.38, 5, pp.315-317, Mar. 1981

[240]P.C.Chen, K.L.Yu, S.Margalit and A.Yariv, "Embedded epitaxial growth of low-threshold GaInAsP/InP injection lasers," Appl. Phys. Lett., vol.38, 5, pp.301-303, Mar. 1981.

[241]F.Z.Hawrylo, "LPE growth of 1.3μm InGaAsP CW lasers on (110) InP substrates," Electron. Lett., vol.17, 8, pp.282-283, Apr. 1981.

[242]K.Kobayashi, K.Utaka, Y.Abe and Y.Suematsu, "CW operation of 1.5-1.6μm wavelength GaInAsP/InP buried-heterostructure integrated twin-guide laser with distributed Bragg reflector," Electron. Lett., vol.17, 11, pp.366-368, May 1981.

[243]K.Utaka, K.Kobayashi and Y.Suematsu, "Lasing characteristics of 1.5-1.6μm GaInAsP/InP integrated twin-guide lasers with first-order distributed Bragg reflectors," IEEE J. Quantum Electron., vol.QE-17, 5, pp.651-658, May 1981.

[244]Y.Noda, K.Sakai, Y.Matsushima and S.Akiba, "10000-hour continuous CW operation of InGaAsP/InP heterostructure lasers with a buffer layer at room temperature," Jpn. J. Appl. Phys., vol.20, 5, pp.997-998, May 1981.

[245]H.Ishikawa, H.Imai, T.Tanahashi, Y.Nishitani and M.Takusagawa, "V-grooved substrate buried heterostructure InGaAsP/InP laser," Electron. Lett., vol.17, 13, pp.465-467, Jun. 1981.

[246]J.C.Bouley, G.Chaminant, J.Charil, P.Devoldere and M.Gilleron, "A Schottky-barrier-delineated stripe structure for a GaInAsP-InP cw laser," Appl. Phys. Lett., vol138, 11, pp.845-847, Jun. 1981.

[247]K.Wakao, K.Moriki, M.Kitamura, K.Iga and Y.Suematsu, "$Ga_xIn_{1-x}As_yP_{1-y}$/InP terraced substrate single-mode laser," IEEE J. Quantum Electron., vol.QE-17, 6, Jun. 1981.

[248]K.Sakai, F.Tanaka, Y.Noda, Y.Matsushima, S.Akiba and T.Yamamoto, "Transverse mode controlled InGaAsP/InP lasers at 1.5μm range with buffer-layer loaded plano-convex waveguide (BL-PCW) structures," IEEE J. Quantum Electron., vol.QE-17, 7, pp.1245-1250, Jul. 1981.

[249]O.Mikami, "1.55μm GaInAsP/InP distributed feedback lasers," Jpn. J. Appl. Phys., vol.20, 7, pp.L488-L490, Jul. 1981.

[250]M.Razeghi, J.P.Hirtz, P.Hirtz, J.P.Larivain, R.Bondeau, B.DeCremoux and J.P.Duchemin, "Room temperature CW operation of GaInAsP/InP double-heterostructure diode lasers emitting at 1.23μm grown by low-pressure metalorganic chemical vapour deposition, " Electron. Lett., vol.17, 17, pp.597-598, Aug. 1981.

[251]K.Furuya, L.A.Coldren, B.I.Miller and J.A.Rentschler, "Crystallographic facets chemically etched in GaInAsP/InP for integrated optics," Electron. Lett., vol.17, 17, pp.582-583, Aug. 1981.

[252]K.Moriki, K.Iga, M.Uchida, K.Wakao and T.Kunikane, "1.3μm-wavelength mode controlled GaInAsP/InP etched laser," Electron. Lett., vol.17, 16, pp.559-560, Aug. 1981.

[253]H.Okuda, H.Soda, K.Moriki, Y.Motegi and K.Iga, "GaInAsP/InP surface emitting injection laser with buried heterostructures," Jpn. J. Appl. Phys., vol.20, 8, pp.L563-L566, Aug. 1981.

[254]W.Ng, C.S.Hong, H.Manasevit and P.D.Dapkus, "Low-threshold 1.3-μm GaInAsP/InP buried heterostructure lasers by liquid phase epitaxy and metalorganic chemical vapor deposition," Appl. Phys. Lett., vol.39, 3, pp.188-189, Aug. 1981.

[255]M.Razeghi, P.Hirtz, J.P.Larivain, R.Blondeau, B.DeCremoux and J.P.Duchemin, "1.5μm room-temperature pulsed operation of GaInAsP/InP double heterostructure grown by LP MOCVD," Electron Lett., vol.17, 18, pp.643-644, Sept. 1981.

[256]Y.Nakano, K.Takahei, Y.Noguchi, H.Nagai, K.Nawata and M.Tokunaga, "InGaAsP/InP BH lasers on p-type InP substrates," Electron. Lett., vol.17, 18, pp.645-646, Sept. 1981.

[257]W.J.Devlin, R.H.Walling, P.J.Fiddyment, R.E.Hobbs, D.Murrell, R.E.Spillett and A.G.Steventon, "Low threshold channelled-substrate buried crescent InGaAsP lasers emitting at 1.54μm," Electron. Lett., vol.17, 18, pp.651-653, Sept. 1981.

[258]H.Nomura, M.Sugimoto and A.Suzuki, "InGaAsP current confinement mesa substrate buried heterostructure laser diodes fabricated by one LPE process," Paper of Technical Group of IECE of Japan(in Japanese), Optical and Quantum Electron., OQE80-117, 1981.

[259]T.Tanbun-Ek, S.Arai, F.Koyama, K.Kishino, S.Yoshizawa, T.Watanabe and Y.Suematsu, "Low threshold current CW operation of GaInAsP/InP buried heterostructure distributed-Bragg-reflector integrated-twin-guide laser emitting at 1.5-1.6μm," Electron. Lett., vol.17, 25/26, pp.967-968, Dec. 1981.

[259']F.Koyama, S.Arai, Y.Suematsu and K.Kishino, "Dynamic spectral width of rapidly modulated 1.58μm GaInAsP/InP buried-heterostructure distributed-Bragg-reflector integrated-twin-guide lasers," Electron. Lett., vol.17, 25/26, pp.938-940, Dec. 1981.

[260]Y.Abe, K.Kishino, Y.Suematsu and S.Arai, "GaInAsP/InP integrated laser with butt-jointed built-in distributed-Bragg-reflection waveguide," Electron. Lett., vol.17, 25/26, pp.945-947, Dec. 1981.

[261]T.Matsuoka, H.Nagai, Y.Itaya, Y.Noguchi, Y.Suzuki, and T.Ikegami, "CW operation of DFB-BH GaInAsP/InP lasers in 1.5μm wavelength region," Electron. Lett., vol.18, 1, pp.27-28, Jan. 1982

[262]K.Utaka, S.Akiba, K.Sakai and Y.Matsushima, "Room-temperature CW operation of distributed-feedback buried-heterostructure InGaAsP/InP lasers emitting at 1.57μm," Electron. Lett., vol.17, 25/26, pp.961-963, Dec. 1981.

[263]R.E.Nahory, M.A.Pollack and J.C.DeWinter, "Efficient LPE-grown $In_xGa_{1-x}As$ LEDs at 1.0-1.1μm wavelengths," Appl. Phys. Lett., vol.25, pp.146-148, Aug. 1974.

[264]T.P.Pearsall, B.I.Miller, R.J.Capik and K.J.Bachmann, "Efficient lattice-matched double-heterostructure LEDs at 1.1μm from $Ga_xIn_{1-x}As_yP_{1-y}$," Appl. Phys. Lett., vol.28, pp.499-501, May 1976.

[265]S.Horiuchi, K.Ikeda, T.Tanaka and W.Susaki, "A new LED structure with a self-aligned sphere lens for efficient coupling to optical fibers," IEEE Trans. Electron Devices, vol.ED-24, pp.986-990, Jul. 1977.

[266]H.Nagai and Y.Noguchi, "InP/GaInAsP double heterostructure LED's in the 1.5μm wavelength region," IOOC'77 , Tokyo, B2-2, Jul. 1977.

[267]A.G.Dentai, T.P.Lee, C.A.Burrus and E.Buehler, "Small-area high-radiance CW InGaAsP LEDs emitting at 1.2 to 1.3μm," Electron. Lett., vol.13, 16, pp.484-485, Aug. 1977.

[268]K.Oe, S.Ando and K.Sugiyama, "Surface emitting LEDs for the 1.2-1.3μm wavelength with GaInAsP/InP double hetero-structures," Jpn. J. Appl. Phys., vol.16, 9, pp.1693-1694, Sept. 1977.

[269]P.D.Wright, Y.H.Chai, H.Morkoc and G.A.Antypas, "InGaAsP/InP double heterojunction high radiance LEDs," 3rd IEEE Specialist Conf. on the Technology of Electroluminescent Devices, San Francisco, C6, Nov. 1978.

[270]L.M.Dolginov, A.E.Drakin, P.G.Eliseev, T.V.Berdnikova, M.G.Milvidsky, V.P.Orlov, Y.K.Panteleev, B.N.Sverdlov and E.G.Shevchenko, "High efficiency GaInPAs/InP light-emitting diodes," Sov. J. Quantum Electron., vol.8, 11, pp.1404-1405, Nov. 1978.

[271]S.Machida, H.Nagai and T.Kimura, "Modulation characteristics og InGaAsP/InP LEDs at 1.5μm wavelength," Electron. Lett., vol.15, 6, pp.175-177, Mar. 1979.

[272]R.C.Goodfellow, A.C.Carter, I.Griffith and R.R.Bradley, "GaInAsP/InP fast, high-radiance, 1.05-1.3μm wavelength LEDs with efficient lens coupling to small numerical aperture silica optical fibres," IEEE Trans. Electron Devices, vol.ED-26, pp.1215-1220, Aug. 1979.

[273]K.Iga, T.Kambayashi, K.Wakao, C.Kitahara and K.Moriki, "GaInAsP/InP double-heterostructure planar LED's," IEEE Trans. Electron Devices, vol.ED-26, pp.1227-1230, Aug. 1979.

[274]H.Grothe, W.Proebster and W.Harth, "Mg-doped InGaAsP/InP L.E.D.s for high-bit-rate optical-communication systems," Electron. Lett., vol.15, 22, pp.702-703, Oct. 1979.

[275]S.Sakai, T.Aoki, Y.Amemiya and M.Umeno, "A new InGaAsP/InP dual-wavelength LED," Appl. Phys. Lett., vol.35, 8, pp.588-589, Oct. 1979.

[276]R.H.Burton, H.Temkin and V.G.Keramidas, "Plasma separation of InGaAsP/InP light-emitting diodes," Appl. Phys. Lett., vol.37, 4, pp.411-412, Aug. 1980.

[277]T.P.Lee, C.A.Burrus and A.G.Dentai, "Dual wavelength surface emitting InGaAsP L.E.D.s," Electron. Lett., vol.16, 28, pp.845-846, Oct. 1980.

[278]O.Wada, S.Yamakoshi, M.Abe, Y.Nishitani and T.Sakurai, "High radiance InGaAsP/InP lensed LED's for optical communication systems at 1.2-1.3μm," IEEE J. Quantum Electron., vol.QE-17, 2, pp.174-178, Feb. 1981.

[279]S.Yamakoshi, M.Abe, O.Wada, S.Komiya and T.Sakurai, "Reliability of high radiance InGaAsP/InP LED's operating in the 1.2-1.3μm wavelength," IEEE J. Quantum Electron., vol.QE-17, 2, pp.167-173, Feb. 1981.

[280]S.Sakai, T.Aoki, M.Tobe and M.Umeno, "Simplified dual channel optical transmission using integrated light emitters and photodetectors," Jpn. J. Appl. Phys., vol.20, 3, pp.L205-L207, Mar. 1981.

[281]G.H.Olsen, F.Z.Hawrylo, D.J.Channin, D.Botez and M.Ettenberg, "1.3μm LPE- and VPE-grown InGaAsP edge-emitting LED's," IEEE J. Quantum Electron., vol.17, 10, pp.2130-2134, Oct. 1981.

[282]H.Temkin, A.K.Chin, M.A.DiGiuseppe and G.Keramidas, "Light-current characteristics of InGaAsP light emitting diodes," Appl. Phys. Lett., vol.39, 6, pp.405-407, Sept. 1981.

[283]T.Ikegami, "Spectral broadening and tailing effect in directly modulated injection lasers," 1st European Conf. on Opt. Fiber Comm., London, p.111, Sept. 1975.

[284]S.Akiba, K.Sakai and T.Yamamoto, "Direct modulation of InGaAsP/InP double heterostructure lasers," Electron. Lett., vol.14, 6, pp.197-198, Mar. 1978.

[285]S.Akiba, Y.Itaya, K.Sakai, T.Yamamoto and Y.Suematsu, "Measurement of carrier lifetime in InGaAsP/InP double heterostructure lasers," Trans. IECE of Japan, vol.E-61, 3, pp.124-128, Mar. 1978.

[286]Y.Sakakibara, K.Furuya, Y.Suematsu and Y.Itaya, "Direct modulation characteristics of GaInAsP/InP D.H. lasers with various stripe widths measured by sharp-pulse method," Electron. Lett., vol.15, pp.594-596, Sept. 1979.

[287]Y.Sakakibara, K.Furuya, K.Utaka and Y.Suematsu, "Single-mode oscillation under high-speed direct modulation in GaInAsP/InP integrated twin-guide lasers with distributed Bragg reflectors," Electron. Lett., vol.16, 12, pp.456-458, Jun. 1980.

[288]K.Utaka, K.Kobayashi, F.Koyama, Y.Abe and Y.Suematsu, "Single-wavelength operation of 1.53μm GaInAsP buried-heterostrucutre integrated twin-guide laser with distributed Bragg reflector under direct modulation up to 1GHz," Electron. Lett., vol.17, 11, pp.368-369, May 1981.

[289]K.Kishino, S.Aoki and Y.Suematsu, "Wavelength variation of 1.6μm wavelength buried heterostructure GaInAsP/InP lasers due to direct modulation," to be appeared in IEEE J. Quantum Electron., 1982.

[289']F.Koyama, S.Arai, T.Tanbun-Ek, Y.Suematsu, K.Kishino, Y.Abe, S.Yoshizawa and T.Watanabe, "Dynamic spectral width of directly modulated 1.5μm distributed Bragg reflector integrated twin guide lasers," Papers of Technical Group of IECE of Japan(in Japanese), Microwave, MW81-82, Dec. 1981.

[289"]Z.Wang, K.Kishino, and Y.Suematsu, "Specral broadening in semi-conductor laser due to direct modulation," to be presented in Nat. Conv. Rec. of IECE of Japan(in Japanese), Mar. 1982.

[290]E.Oomura, T.Murotani, M.Ishii and W.Susaki, "Optical damage limit of InP/InGaAsP DH lasers," Nat. Conv. Rec. of Japan Soc. of Appl. Phys. (in Japanese), 27p-w-13, Mar. 1979.

[291]Y.Horikoshi, T.Kobayashi and Y.Furukawa, "Lifetime of InGaAsP-InP and AlGaAs-GaAs DH lasers estimated by the point defect generation model," Jpn. J. Appl. Phys., vol.18, 12, pp.2237-2244, Dec. 1979.

[292]K.Mizuishi, M.Hirao, S.Tsuji, H.Sato and M.Nakamura, "Accelerated aging characteristics of InGaAsP/InP buried heterostructure lasers emitting at 1.3μm," Jpn. J. Appl. Phys., vol.19, 7, pp.L429-L432, Jul. 1980.

[293]J.B.Restorff, B.Houston, J.R.Burke, and R.E.Hayes, "Measurement of effective mass in $In_{0.9}Ga_{0.1}As_{0.22}P_{0.78}$ by Shubnikov-de Haas oscillations," Appl. Phys. Lett., vol.32, 3, pp.189-190, Feb. 1978.

[294]R.J.Nicholas, J.C.Portal, C.Houlbert, P.Perrier and T.P.Pearsall, "An experimental determination of the effective masses for $Ga_xIn_{1-x}As_yP_{1-y}$ alloys grown on InP," Appl. Phys. Lett., vol.34, 8, pp.492-494, Apr. 1979.

[295]C.Hermann and T.P.Pearsall, "Optical pumping and the valence-band light-hole effective mass in $Ga_xIn_{1-x}As_yP_{1-y}$ ($y\simeq 2.2x$)," Appl. Phys. Lett., vol.38, 6, pp.450-452, Mar. 1981.

[296]T.Takagi, "Refractive index of $Ga_{1-x}In_xAs$ prepared by vapor-phase epitaxy," Jpn. J. Appl. Phys., vol.17, 10, pp.1813-1817, Oct. 1978.

[297]E.Oomura, T.Murotani, M.Ishii and W.Susaki, "Refractive index of $In_{0.84}Ga_{0.16}As_{0.46}P_{0.54}$ at its laser oscillating wavelength of 1.2μm," Jpn. J. Appl. Phys., vol.18, 4, pp.855-856, Apr. 1979.

[298]K.Stubkjaer, Y.Suematsu, M.Asada, S.Arai and A.R.Adams, "Measurements of refractive-index variation with free carrier density and temperature for 1.6μm GaInAsP/InP lasers," Electron. Lett., vol.16, 23, pp.895-896, Nov. 1980.

[298']F.R.Nash, "Mode guidance parallel to the junction plane of double-heterostructure GaAs lasers," J. Appl. Phys., vol.44, pp.4696-4707, 1973.

[299]A.Olsson and C.L.Tang, "Injected-carrier induced refractive-index change in semiconductor lasers," Appl. Phys. Lett., vol.39, 1, pp.24-26, Jul. 1981.

[300]R.E.Nahory and M.A.Pollack, "Threshold dependence on active layer thickness in InGaAsP/InP DH lasers," Electron. Lett., vol.14, pp.727-729, Nov. 1978.

[301]D.Botez, "InGaAsP/InP double-heterostructure lasers: Simple expressions for wave confinement, beamwidth, and threshold current over wide ranges in wavelength(1.1-1.65μm)," IEEE J. Quantum Electron., vol.17, 2, pp.178-186, Feb. 1981.

[302]M.Tokunaga, Y.Nakano, K.Takahei, Y.Noguchi, H.Nagai and K.Nawata, "Effect of cavity length on 1.55μm buried-heterostructure DH laser characteristics," Electron. Lett., vol.17, 6, pp.234-236, Mar. 1981.

[303]M.Asada, K.Itoh, Y.Suematsu and S.Arai, "Cavity length dependence of differential quantum efficiency of GaInAsP/InP lasers," Electron. Lett., vol.17, 14, pp.486-487, Jul. 1981.

[304]Y.Horikoshi and Y.Furukawa, "Temperature sensitive threshold current of InGaAsP-InP double heterostructure lasers," Jpn. J. Appl. Phys., vol.18, 4, pp.809-815, Apr. 1979.

[305]R.E.Nahory, M.A.Pollack and J.C.DeWinter, "Temperature dependence of InGaAsP double-heterostructure laser characteristics," Electron. Lett., vol.15, 21, pp.695-696, Oct. 1979.

[306]G.H.B.Thompson and G.D.Henshall, "Nonradiative carrier loss and temperature sensitivity of threshold in 1.27μm (GaIn)(AsP)/InP D.H. lasers," Electron. Lett., vol.16, 1, pp.42-44, Jan. 1980.

[307]M.Yano, H.Nishi and M.Takusagawa, "Influence of interfacial recombination on oscillation characteristics of InGaAsP/InP DH lasers," IEEE J. Quantum Electron., vol.QE-16, 6, pp.661-667, Jun. 1980.

[308]N.K.Dutta, R.J.Nelson and P.A.Barnes, "Temperature dependence of threshold and electrical characteristics of InGaAsP-InP D.H. lasers," Electron. Lett., vol.16, 17, pp.653-654, Aug. 1980.

[309]M.Yano, H.Nishi and M.Takusagawa, "Temperature characteristics of threshold current in InGaAsP/InP heterostructure lasers," J. Appl. Phys., vol.51, pp.4022-4028, 1980.

[310]A.R.Adams, M.Asada, Y.Suematsu and S.Arai, "The temperature dependence of the efficiency and threshold current of $In_{1-x}Ga_xAs_yP_{1-y}$ lasers related to intervalence band absorption," jpn. J. Appl. Phys., vol.19, 10, pp.L621-L624, Oct. 1980.

[311]J.N.Walpole, T.A.Lind, J.J.Hsieh and J.P.Donnelly, "Gain spectra in GaInAsP/InP proton-bomberded stripe-geometry DH lasers," IEEE J. Quantum Electron., vol.QE-17, 2, pp.186-192, Feb. 1981.

[312]T.Uji, K.Iwamoto and R.Lang, "Nonradiative recombination in InGaAsP/InP light sources causing light emitting diode outputzsaturation and strong laser-threshold-current temperature sensitivity," Appl. Phys. Lett., vol.38, 4, pp.193-195, Feb. 1981.

[313]N.K.Dutta and R.J.Nelson, "Temperature dependence of threshold of InGaAsP/InP double-heterostructure lasers and Auger recombination," Appl. Phys. Lett., vol.38, 6, pp.407-409, Mar. 1981.

[314]G.H.B.Thompson, "Temperature dependence of threshold current in (GaIn)(AsP) DH lasers at 1.3 and 1.5μm wavelength," IEEE Proc., vol.128, 2, pp.37-43, Apr. 1981.

[315]M.A.Pollack, J.R.Pawlik, R.E.Nahory and P.J.Anthony, "Comparison of electrical characteristics and threshold temperature dependences of $\lambda \sim 1.3\mu m$ and $\lambda \sim 1.6\mu m$ stripe-geometry InGaAsP DH lasers," IEEE J. Quantum Electron., vol.17, 4, pp.450-453, Apr. 1981.

[316]M.Asada, A.R.Adams, K.Stubkjaer, Y.Suematsu and S.Arai, "The temperature dependence of the threshold current of GaInAsP/InP DH lasers," IEEE J. Quantum Electron., vol.QE-17, 5, pp.611-619, May 1981.

[317]M.Yano, H.Imai, K.Hori and M.Takusagawa, "High temperature characteristics of stripe-geometry InGaAsP/InP double-heterostructure lasers," IEEE J. Quantum Electron., vol.QE-17, 5, pp.619-626, May 1981.

[318]A.Sugimura, "Band-to-band Auger recombination effect on InGaAsP laser threshold," IEEE J. Quantum Electron., vol.QE-17, 5, pp.627-635, May 1981.

[319]A.Sugimura, "Band-to-band Auger recombination in InGaAsP lasers," Appl. Phys. Lett., vol.39, 1, pp.21-23, Jul. 1981.

[320]R.L.Moon, G.A.Antypas and L.W.James, "Bandgap and lattice constant of GaInAsP as a function of alloy composition," J. Electron. Mater., vol.13, 3, pp.635-644, Aug. 1974.

[321]J.J.Hsieh, "Thickness and surface morphology of GaAs LPE lasers grown by supercooling, step-cooling, equilibrium-cooling, and two-phase solution techniques," J. Cryst. Growth, vol.27, pp.49-61, 1974.

[322]J.J.Hsieh, M.C.Finn and J.A.Rossi, "Conditions for lattice matching in LPE growth of GaInAsP layers on InP substrates," Proc. 6th Int. Symp. Gallium Arsenide Related Compounds, vol.336, p.37, 1977.

[323]J.J.Hsieh, "Measured compositions and laser emission wavelength of $Ga_xIn_{1-x}As_yP_{1-y}$ LPE layers lattice-matched to InP substrate," J. Electron. Mater., vol.7, pp.31-37, Jan. 1978.

[324]H.Nagai and Y.Noguchi, "InP-$Ga_xIn_{1-x}As_yP_{1-y}$ double heterostructure for 1.5μm wavelength," Appl. Phys. Lett., vol.32, 4, pp.234-236, Feb. 1978.

[325]J.J.Coleman, "Arsenic and gallium distribution coefficients in liquid-phase epitaxial $Ga_xIn_{1-x}P_yAs_{1-y}$," Appl. Phys. Lett., vol.32, 6, pp.388-390, Mar. 1978.

[326]T.P.Pearsall, R.Bisaro, R.Ansel and P.Merenda, "The growth of $Ga_xIn_{1-x}As$ on (100) InP by liquid-phase epitaxy," Appl. Phys. Lett., vol.32, 8, pp.497-499, Apr. 1978.

[327]M.Feng, T.H.Windhorn, M.M.Tashima and G.E.Stillman, "Liquid-phase epitaxial growth of lattice-matched InGaAsP on (100)-InP for the 1.15-1.31-μm spectral region," Appl. Phys. Lett., vol.32, 11, pp.758-761, Jun. 1978.

[328]M.A.Pollack, R.E.Nahory, J.C.DeWinter and A.A.Ballman, "Liquid phase epitaxial $In_{1-x}Ga_xAs_yP_{1-y}$ lattice matched to <100> InP over the complete wavelength range $0.92<\lambda<1.65\mu m$," Appl. Phys. Lett., vol.33, 4, pp.314-316, Aug. 1978.

[329]K.Oe and K.Sugiyama, "Orientation effects in the LPE growth of GaInAsP quaternary alloys," Appl. Phys. Lett., vol.33, 5, pp.449-451, Sept. 1978.

[330]M.Feng, M.M.Tashima, T.H.Windhorn and G.E.Stillman, "Composition dependence of the influence of lattice mismatch on surface morphology in LPE growth of InGaAsP on (100)-InP[a)]," Appl. Phys. Lett., vol.33, 6, pp.533-535, Sept. 1978.

[331]R.E.Nahory, M.A.Pollack, W.D.Johnston,Jr. and R.L.Barns, "Band gap versus composition and demonstration of Vegard's law for $In_{1-x}Ga_xAs_yP_{1-y}$ lattice matched to InP," Appl. Phys. Lett., vol.33, 7, pp.659-661, Oct. 1978.

[332]M.Feng, L.W.Cook, M.M.Tashima, T.H.Windhorn and G.E.Stillman, "The influence of LPE growth techniques on the alloy composition of InGaAsP," Appl. Phys. Lett., vol.34, 4, pp.292-295, Feb. 1979.

[333]K.Takahei, H.Nagai and H.Kawaguchi, "Low temperature liquid phase epitaxy growth for room-temperature cw operation of 1.55-μm InGaAsP/InP double-heterostructure laser," Appl. Phys. Lett., vol.36, 4, pp.309-310, Feb. 1980.

[334]J.J.Hsieh, "Phase diagram for LPE growth of GaInAsP layers lattice matched to InP substrates," IEEE J. Quantum Electron., vol.QE-17, 2, pp.118-122, Feb. 1981.

[335]G.A.Antypas and R.L.Moon, "Growth and characterization of InP-InGaAsP lattice matched heterostructures," J. Electrochem. Soc., vol.120, pp.1574-1577, 1973.

[336]K.Takahei and H.Nagai, "Instability of In-Ga-As-P liquid solution during low temperature LPE growth of $In_{1-x}Ga_xAs_{1-y}P_y$ on InP," Jpn. J. Appl. Phys., vol.20, 4, pp.L313-L316, Apr. 1981.

[337]M.G.Astles, F.G.H.Smith and E.W.Williams, "Indium Phosphide, II. Liquid epitaxial growth," J. Electrochem. Soc., vol.120, pp.1750-1757, 1973.

[338]A.Rosental, Y.Itaya and Y.Suematsu, "Measurement of Zn doping level in InGaAsP/InP DH lasers," Jpn. J. Appl. Phys., vol.17, 8, pp.1655-1656, Aug. 1979.

[339]H.C.Casey,Jr., "Room-temperature threshold current dependence of GaAs-$Al_xGa_{1-x}As$ double-heterostructure lasers on x and active layer thickness," J. Appl. Phys., vol.49, pp.3684-3692, Jul. 1978.

[340]K.Stubkjaer, M.Asada, S.Arai and Y.Suematsu, "Spontaneous recombination, gain and refractive index variation for 1.6μm wavelength InGaAsP/InP lasers," Jpn. J. Appl. Phys., vol.20, 8, pp.1499-1505, Aug. 1981.

[341]M.Yamada and Y.Suematsu, "Theory of single mode injection lasers taking into account of electronic intraband relaxation, " Jpn. J. Appl. Phys., vol.18, Suppl.18-1, pp.347-354, 1978.

PUBLICATION LIST

I. Papers and Letters

(1) S.ARAI, Y.ITAYA, Y.SUEMATSU, K.KISHINO, and S.KATAYAMA: "Conditions of LPE Growth for Lattice Matched GaInAsP/InP DH Lasers with (100) Substrate in the Range of 1.2-1.5μm," Jpn.J.Appl.Phys.,(S),Vol.17,No.11,pp.2067-2068,Nov.1978

(2) S.ARAI, Y.SUEMATSU, and Y.ITAYA:"1.67μm $Ga_{0.47}In_{0.53}As$/InP DH Lasers Double Cladded with InP by LPE Technique," Jpn.J.Appl.Phys.,(S),Vol.18,No.3,pp.709-710,Mar.1979

(3) S.ARAI, M.ASADA, Y.SUEMATSU, and Y.ITAYA:"Room Temperature CW Operation of (100) GaInAsP/InP DH Laser Emitting at 1.51μm," Jpn.J.Appl.Phys.,(S),Vol.18,No.12,pp.2333-2334 Dec.1979

(4) S.ARAI, Y.ITAYA, Y.SUEMATSU, and K.KISHINO:"1.5-1.6μm Wavelength (100) GaInAsP/InP DH Lasers," Jpn.J.Appl.Phys., Vol.19,Suppl.19-1,pp.411-414,1980

(5) S.ARAI, Y.SUEMATSU, and Y.ITAYA:"1.11-1.67μm (100) GaInAsP/InP Injection Lasers Prepared by Liquid Phase Epitaxy," IEEE J. of Quantum Electron.,Vol.QE-16,No.2, pp.197-205,Feb.1980

(6) S.ARAI, M.ASADA, Y.SUEMATSU, Y.ITAYA, T.TANBUN-EK, and K.KISHINO:"New 1.6μm Wavelength GaInAsP/InP Buried Heterostructure Lasers," Electron.Lett.,Vol.16,No.10, pp.349-350,May 1980

(7) S.ARAI, M,ASADA, T.TANBUN-EK, Y.SUEMATSU, Y.ITAYA, and K.KISHINO:"1.6μm Wavelength GaInAsP/InP BH Lasers," IEEE J. of Quantum Electron.,Vol.QE-17,No.5,pp.640-645, May 1981

(8) Y.ITAYA, S.ARAI, K.KISHINO, M.ASADA, and Y.SUEMATSU:" 1.6μm Wavelength GaInAsP/InP Lasers Prepared by Two Phase Solution Technique," IEEE J. of Quantum Electron., Vol.QE-17,No.5,pp.635-640,May 1981

(9) T.TANBUN-EK, S.ARAI, F.KOYAMA, K.KISHINO, S.YOSHIZAWA, T.WATANABE, and Y.SUEMATSU:"Low Threshold Current CW Operation of GaInAsP/InP Buried Heterostructure Distributed Bragg Reflector Integrated Twin Guide Laser Emitting at 1.5-1.6μm," Electron.Lett.,Vol.17,No.25, pp.967-968,Dec.1981

(10) F.KOYAMA, S.ARAI, Y.SUEMATSU, and K.KISHINO:"Dynamic Spectral Width of Rapidly Modulated 1.58μm GaInAsP/InP Buried-Heterostructure Distributed-Bragg-Reflector Integrated-Twin-Guide Lasers," Electron.Lett.,Vol.17, No.25,pp.938-940,Dec.1981

II. Related Papers and Letters

(1) H.KAWANISHI, Y.SUEMATSU, Y.ITAYA, and S.ARAI:"$Ga_xIn_{1-x}As_yP_{1-y}$-InP Injection Laser Partially Loaded with Distributed Bragg Reflector," Jpn.J.Appl.Phys.,(S), Vol.17,No.8,pp.1439-1440,Aug.1978

(2) Y.ITAYA, Y.SUEMATSU, S.KATAYAMA, K.KISHINO, and S.ARAI: "Low Threshold Current Density (100) GaInAsP Double Heterostructure Lasers for Wavelength 1.3μm," Jpn.J.Appl. Phys.,Vol.18,No.9,pp.1795-1805,Sept.1979

(3) H.KAWANISHI, Y.SUEMATSU, K.UTAKA, Y.ITAYA, and S.ARAI:" $Ga_xIn_{1-x}As_yP_{1-y}$/InP Injection Laser Partially Loaded with First-Order Distributed Bragg Reflector," IEEE J. of Quantum Electron.,Vol.QE-15,No.8,pp.701-706,Aug.1979

(4) Y.ITAYA, T.TANBUN-EK, K.KISHINO, S.ARAI, and Y.SUEMATSU: "1.6μm Wavelength Buried Heterostructure GaInAsP/InP Lasers," Jpn.J.Appl.Phys.,Vol.19,No.3,pp.L141-L144, Mar.1980

(5) A.R.ADAMS, M.ASADA, Y.SUEMATSU, and S.ARAI:"The Temperature Dependence of the Efficiency and Threshold Current of $In_{1-x}Ga_xAs_yP_{1-y}$ Lasers Related to Intervalence Band Absorption," Jpn.J.Appl.Phys.,Vol.19,No.10, pp.L621-L624,Oct.1980

(6) K.STUBKJAER, Y.SUEMATSU, M.ASADA, S.ARAI, and A.R.ADAMS: "Measurement of Refractive Index Variation with Free Carrier Density and Temperature for 1.6μm GaInAsP/InP Lasers," Electron.Lett.,Vol.16,No.2,pp.895-896,Nov.1980

(7) M.ASADA, A.R.ADAMS, K.STUBKJAER, Y.SUEMATSU, Y.ITAYA, and S.ARAI:"The Temperature Dependence of the Threshold Current of GaInAsP/InP DH Lasers," IEEE J. of Quantum Electron.,Vol.QE-17,No.5,pp.611-619,May 1981

(8) K.STUBKJAER, M.ASADA, S.ARAI, and Y.SUEMATSU:"Spontaneous Recombination, Gain, and Refractive Index Variation for 1.6μm Wavelength GaInAsP/InP Lasers," Jpn.J.Appl.Phys., Vol.20,No.8,pp.1499-1505,Aug.1981

(9) M.ASADA, K.ITOH, Y.SUEMATSU, and S.ARAI:"Cavity Length Dependence of Differential Quantum Efficiency of GaInAsP/InP Lasers," Electron.Lett.,Vol.17,No.4,pp.486-487, Jul.1981

(10) Y.ABE, K.KISHINO, Y.SUEMATSU, and S.ARAI:"GaInAsP/InP Integrated Laser with Butt-Jointed Built-in Distributed-Bragg-Reflection Waveguide," Electron.Lett.,Vol.17,No.25, pp.945-947,Dec.1981

III. International Conferences

(1) S.ARAI, Y.ITAYA, Y.SUEMATSU, K.KISHINO, and S.KATAYAMA: "Crystal Growth and Lasing Threshold of Lattice Matched GaInAsP/InP DH Lasers Grown on (100) Substrate in the Range of 1.2-1.5μm," 4th European Conf. on Optical Comm., Genova,Italy,(Postdeadline Paper) PD7,Sept.1978

(2) S.ARAI, Y.ITAYA, Y.SUEMATSU, and K.KISHINO:"1.5-1.6μm Wavelength (100) GaInAsP/InP DH Lasers," The 11th Conf. on Solid State Devices,Tokyo,B-3-4,Aug.1979

(3) S.ARAI, K.KISHINO, Y.ITAYA, M.ASADA, T.TANBUN-EK, and Y.SUEMATSU:"Room Temperature CW Operation of 1.5-1.6μm Wavelength Range GaInAsP/InP Lasers," The 5th Topical Meeting on Integ. and Guided Wave Optics,Lake Tahoe, Nevada,U.S.A.,MD6-1,Jan.1980

(4) S.ARAI, M.ASADA, Y.ITAYA, T.TANBUN-EK, K.KISHINO, and Y.SUEMATSU:"1.6μm Wavelength GaInAsP/InP BH Lasers," 38th Annual Device Research Conf.,Ithaca,NY,U.S.A., IVB-4,Jun.1980

(5) S.ARAI, M.ASADA, Y.ITAYA, T.TANBUN-EK, K.KISHINO, and Y.SUEMATSU:"1.6μm Wavelength GaInAsP/InP BH Lasers Fabricated by New Process," 6th European Conf. on Optical Comm.,York,U.K.,Conf.Publication,Vol.190, pp.180-183,Sept.1980

(6) F.KOYAMA, S.ARAI, T.TANBUN-EK, K.KISHINO, and Y.SUEMATSU: "Low Threshold Current GaInAsP/InP Integrated Twin Guide Lasers with Distributed Bragg Reflector Emitting at 1.55μm," 6th Topical Meeting on Integ. and Guided-Wave optics,Pacific Grove,CA,U.S.A.,WB-5,Jan.1982

IV. Domestic Conferences

(1) S.ARAI, Y.ITAYA, Y.SUEMATSU, K.KISHINO, S.KATAYAMA, and M.KODAIRA:"Crystal Growth Conditions of 1.2-1.65μm (100) GaInAsP/InP DH Lasers," Papers of Technical Group of IECE, Optical and Quantum Electronics, OQE78-113, Dec.1978

(2) S.ARAI, M.ASADA, T.TANBUN-EK, Y.SUEMATSU, Y.ITAYA, and K.KISHINO:"1.6μm Wavelength GaInAsP/InP BH Lasers," Papers of Technical Group of IECE, Optical and Quantum Electronics, OQE80-107, Dec.1980

V. National Convention Records

(1) S.ARAI, Y.ITAYA, T.MISHIMA, and Y.SUEMATSU:"Temperature Dependence of the Threshold Current of GaInAsP/InP DH Lasers," Nat. Conv. Rec. of IECE, 791, Mar.1978

(2) S.ARAI, Y.ITAYA, and Y.SUEMATSU:"Lattice Matched GaInAsP/InP DH Lasers in the Wavelength of 1.2-1.5μm," Nat. Cov. Rec. of Appl. Phys.,5p-Z-11, Nov.1978

(3) S.ARAI, M.KODAIRA, Y.SUEMATSU, and Y.ITAYA:"Room Temperature Operation of InP/GaInAs/GaInAsP/InP DH Lasers Emitting at 1.65μm," Nat. Conv. Rec. of IECE, 836, Mar.1979

(4) S.ARAI, M.ASADA, K.KISHINO, Y.ITAYA, A.KOSHIZUKA, and Y.SUEMATSU:"Room Temperature CW Operations of 1.5-1.6μm Wavelength GaInAsP/InP DH Lasers," Nat. Conv. Rec. of IECE, 785, Mar.1980

(5) S.ARAI and Y.SUEMATSU:"Single Mode Operation Temperature Range of Distributed Bragg Reflector Lasers," Nat. Conv. Rec. of IECE, 326, Oct.1981

(6) S.ARAI, S.YOSHIZAWA, and Y.SUEMATSU:"Temperature Dependences of Lasing Properties of Distributed Bragg Reflector Lasers," Nat. Conv. Rec. of IECE, to be presented in Mar.1982

V. Patent

(1) Y.SUEMATSU and S.ARAI:"Fabrication Method of Stripe Semiconductor Lasers by Selective Meltback," Application No.029317,1979

(2) Y.SUEMATSU, S.ARAI, and K.KISHINO:"Buried Structure Semiconductor Lasers," Application No.086798,1980